

Table of contents

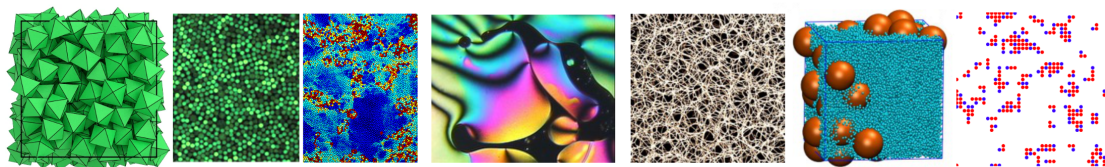
Welcome to the Complex Disordered Matter Course!	5
Overview	5
Delivery and format	6
Intended learning outcomes	6
Contact details	7
Questions and comments	7
Recommended texts and literature	8
Colloids	8
Polymers and surfactants	9
Glasses	9
I Unifying concepts	10
1 Introduction to phase behaviour and enhanced fluctuations	11
2 Key concepts for phase transitions	14
2.1 Observables and expectation values	14
2.2 Correlations	15
2.2.1 Spatial correlations	15
2.2.2 Temporal correlations	17
3 The approach to criticality	19
4 The Ising model: the prototype model for a phase transition	21
4.1 The 2D Ising model	21
4.2 Exact solutions: the one dimensional Ising chain	22
4.2.1 More general 1D spins systems: transfer matrix method	25
5 Mean field theory and perturbation schemes	27
5.1 Mean field solution of the Ising model	27
5.2 Spontaneous symmetry breaking	28
5.3 Phase diagram	29
5.4 A closer look: critical exponents	31
5.4.1 Zero H solution and the order parameter exponent	31
5.4.2 Finite (but small) field solution: the susceptibility exponent	32
5.5 Landau theory	33
5.6 Shortcomings of mean field theory	36
6 The Lattice Gas model	38
6.1 Mapping between Ising model and lattice gas	38

6.2 Phase diagram	39
6.3 Real Fluids	39
7 The Static Scaling Hypothesis	41
7.1 Experimental Verification of Scaling	42
7.2 Computer simulation	44
8 Universality and the Renormalisation Group Theory of Critical Phenomena	45
8.1 The critical point: A many length scale problem	45
8.2 Methodology of the RG	46
8.3 Universality and Scaling	48
8.3.1 Fluid-magnet universality	50
8.4 Near critical scaling	50
8.5 Universality classes	51
8.6 Critical exponents	52
8.7 Finite-size scaling	53
8.8 Summary of main points	54
8.9 Addendum: The effective coupling viewpoint of the renormalization group (non examinable)	55
8.9.1 A simple example	56
8.9.2 Universality and scaling	59
9 The renormalisation group: effective coupling viewpoint	62
9.1 A simple example	63
9.2 Universality and scaling	66
10 Dynamics of first order phase transitions: nucleation, growth and spinodal de- composition	69
10.1 Introduction to nucleation	69
10.2 Classical Nucleation Theory: Homogeneous Nucleation	70
10.2.1 Interpretation and Scaling Behavior	71
10.3 Domain growth	71
10.4 Spinodal decomposition	72
10.4.1 Non-Conserved Order Parameter Dynamics (Model A)	72
10.4.2 Conserved Order Parameter Dynamics (Model B)	73
10.4.3 Schematic of Domain Growth in 2D Ising model	74
10.4.4 Dynamics Scaling Hypothesis	74
10.4.5 Summary of Growth Laws	75
11 Introduction to stochastic processes	76
11.1 The Master Equation	76
11.2 From the Master Equation to the Diffusion Equation	77
11.3 Consequences of time reversal symmetry	80
11.3.1 Detailed balance	80
11.3.2 Computer simulation	81
12 The Langevin Approach	83
12.1 The Random Walk and the Langevin equation	83
12.2 Brownian Motion	84
12.2.1 Noise Properties	85
12.2.2 Solving the Langevin Equation (velocity)	85
12.2.3 Mean-square velocity	86
12.2.4 Mean-square displacement	86
12.2.5 External Forces and Mobility	87

12.2.6 Molecular Dynamics simulation of Brownian motion for a colloid particle in a liquid suspension	88
13 Dynamics of Fluctuations	92
13.1 Linear Response Theory and the Fluctuation-Dissipation Theorem	92
13.2 Onsager's Theorem	93
II Complex disordered systems	95
14 Entropy matters	96
14.1 Systems and definitions	97
14.1.1 Elementary constituents and energy scales	97
14.1.2 Classes of systems	98
15 Colloids	101
15.1 Kinds of colloids	101
15.2 Stability of colloids and colloid-colloid interactions	103
15.2.1 Fundamental and effective forces	104
15.2.2 Van der Waals interaction	104
15.2.3 Double-layer interaction	106
15.2.4 Steric interactions and depletion interactions	108
15.2.5 Asakura-Oosawa depletion potential	110
15.3 Colloids as big atoms	114
15.3.1 The archetype: hard-spheres	114
15.3.2 Beyond hard-spheres: simple liquids	120
15.4 Characterisation of colloidal systems	122
15.4.1 Structural properties: the radial distribution function	122
15.4.2 Dynamics: single vs collective displacements	126
15.4.3 Stokes-Einstein relation	129
References	135
16 Polymers	136
16.1 General molecular properties	136
16.1.1 Example structures	137
16.2 Models for the conformation of polymers	137
16.2.1 Freely-jointed chain	137
16.2.2 Freely-rotating chain	141
16.2.3 Excluded volume effects	146
16.3 Good, poor and theta solvents	148
16.4 Concentrated polymer solutions	150
References	151
17 Liquid crystals	152
17.1 Anisotropic particles	152
17.2 Liquid crystal phases	153
17.3 Orientational correlations and the isotropic/nematic transition	154
17.4 Landau-de Gennes mean field theory	156
17.5 Maier-Saupe theory	158
17.5.1 Lattice model: the Lebwohl-Lasher model	159
17.6 Splay, twist and bend	161
17.7 Topological defects	162
References	162

18 Surfactants	163
18.1 Hydrophobicity and amphiphiles	163
18.2 Self-assembled structures	164
18.2.1 Aggregation: general case	165
18.2.2 Aggregation: the surfactant case	166
18.2.3 Shape of surfactant assemblies	167
18.3 A simple on-lattice model for micelle formation	169
References	172
19 Arrested states	173
19.1 Energy landscapes	174
19.2 Glasses	176
19.2.1 Glass formation	176
19.3 Viscosity and relaxation times	178
19.3.1 Connection between VFT and configurational entropy: the Adam-Gibbs model	180
19.3.2 Alternative perspective: Dynamical facilitation and the parabolic law	180
19.4 Physical gels	181
19.4.1 Colloid-polymer mixtures as an example	184
19.4.2 Arrested spinodal scenario	187
20 Active matter	189
20.1 Beyond thermal systems	189
20.2 Life-inspired motion: <i>run and tumble</i>	190
20.3 Coloured noise	194
20.4 Active Brownian particle and motility-induced phase separation	194
20.4.1 Mean squared displacement of Active Brownian Particles	195
20.4.2 Interacting ABPs and motility induced phase separation	198
21 Problems	199
21.1 Relaxation time in atomic fluids	199
21.2 Equipartition	199
21.3 Gravitational length	199
21.4 Peclet number	200
21.5 Diffusion equation	200
21.6 Mean square displacement	200
21.7 Relaxation time in colloidal suspensions	200
21.8 Colloidal crystals	200
21.9 Lagrange's expression for the radius of gyration	201
21.10 Mean length	201
21.11 Real data	201
21.12 Micelles	202
21.13 Viscosity	202
21.14 The glass transition	202
III Experimental techniques	203
Appendices	204
A Revision guide	204
B Mindmaps - Linking concept and methods	206

Welcome to the Complex Disordered Matter Course!



Overview

This course introduces you to the theoretical, computational and experimental aspects of the physics of complex disordered matter.

Complex disordered matter is the study of wide range of systems like **polymers**, **colloids**, **glasses**, **gels**, and **emulsions**, which lack long-range order but exhibit intricate behaviour. Colloids, suspensions of microscopic particles in a fluid, are useful for studying disordered structures due to their observable dynamics. Similarly, polymer systems can form amorphous solids or glasses when densely packed or cooled, showing solid-like rigidity despite their disordered structure. These materials often undergo phase transitions, such as demixing and crystallisation, and near these transitions, they can display critical phenomena with extensive fluctuations and correlations.

These various are examples of **soft matter**. In soft matter systems, the interplay between disorder, softness, and phase behavior leads to rich physical phenomena, particularly near critical points where even small changes in external conditions can trigger large-scale reorganizations and universal behaviour. Glasses, for instance, exhibit slow relaxation and memory effects, while colloidal systems may crystallize, phase separate, or become jammed depending on particle interactions and concentration. Understanding such behaviors involves studying how microscopic interactions and thermal fluctuations influence macroscopic properties, especially in non-equilibrium conditions. Through techniques like scattering, microscopy, rheology, and simulation, one can explore how disordered soft materials respond to stress, age, or undergo transitions—insights that are vital for applications in materials design, biotechnology, and beyond.

This course is organized into three interconnected parts, each offering a distinct perspective on the study of complex disordered matter.

- **Part 1: Unifying concepts** (Nigel Wilding) introduces the theoretical framework for rationalising complex disordered matter which is grounded in statistical mechanics and thermodynamics. We emphasize the theory of phase transitions, thermal fluctuations, critical phenomena, and stochastic dynamics—providing the essential theoretical tools

needed to describe and predict the behavior of soft and disordered systems.

- **Part 2: Complex disordered matter** (Francesco Turci) explores the phenomenology of key examples of complex disordered soft matter systems, including colloids, polymers, liquid crystals, glasses, gels, and active matter. These systems will be analyzed using the theoretical concepts introduced in Part 1, highlighting how disorder, interactions, and fluctuations shape their macroscopic behavior.
- **Part 3: Experimental techniques** (Adrian Barnes) focuses on the methods of microscopy, and scattering via x-rays, neutrons and light that are used to study complex disordered matter, offering insight into how their properties are measured and understood in real-world contexts.

In addition to theory and experiment, computer simulation plays a central role in soft matter research. This course includes a substantial coursework component consisting of two computational projects. These exercises will allow you to apply state-of-the-art simulation techniques to investigate the complex behavior of disordered systems, bridging theory and observation through hands-on exploration.

Delivery and format

- Detailed e-notes (accessible via Blackboard) can be viewed on a variety of devices. Pdf is also available.
- We will give ‘traditional’ lectures (Tuesdays, Wednesdays, Fridays) in which we use slides to summarise and explain the lecture content. Questions are welcome (within reason...)
- Try to read ahead in the notes, then come to lectures, listen to the explanations and then reread the notes.
- Rewriting the notes or slides to express your own thoughts and understanding, or annotating a pdf copy can help wire the material into your own way of thinking.
- There are problem classes (Thursdays) where you can try problem sheets and seek help. Lecturers may go over some problems with the class.
- The navigation bar on the left will allow you to access the lecture notes and problem sets.

Intended learning outcomes

The course will

- Introduce you to the qualitative features of a range of complex and disordered systems and the experimental techniques used to study them.
- Introduce you to a range of model systems and theoretical techniques used to elucidate the physics of complex disordered matter.
- Provide you with elementary computational tools to model complex disordered systems numerically and predict their properties.
- Allow you to apply your physics background to understand a variety of systems of interdisciplinary relevance.
- Connect with the most recent advances in the research on complex disordered matter.

Contact details

The course will be taught by

- Prof Nigel B. Wilding (unit director): nigel.wilding@bristol.ac.uk
- Dr Francesco Turci: F.Turci@bristol.ac.uk
- Dr Adrian Barnes: a.c.barnes@bristol.ac.uk

Questions and comments

If you have any questions about the course, please don't hesitate to contact the relevant lecturer, either by email (see above) or in a problems class.

Finally, this is a new course for 2025/26. If you find any errors or mistakes or something which isn't clear, please let us know by email, or fill in this anonymous form:

[Submit an error/mistake/query](#)

Recommended texts and literature

Needs to be tidied and unified.

Experimental textbooks?

One motivation for supplying you with detailed notes for this course course is the absence of a wholly ideal text book. However, it should be stressed that while these notes approach (in places) the detail of a book, the notes are not fully comprehensive and should be regarded as the ‘bare bones’ of the course, to be fleshed out via your own reading and supplementary note taking. To this end perhaps the most appropriate textbooks are:

A good book at the right level for the phase transitions and critical phenomena part of the course is

- **J.M. Yeomans: Statistical Mechanics of Phase Transitions**

A good book covering all aspects of this part of the course including non-equilibrium systems is

- **D. Chandler: Introduction to Modern Statistical Mechanics**

You might also wish to dip into the introductory chapters of the following more advanced texts

- **N Goldenfeld: Lectures on Phase Transitions and the Renormalization Group**
- **J.J. Binney, N.J. Dowrick, A.J.Fisher and M.E.J. Newman: The Theory of Critical Phenomena**

For revision on thermodynamics and statistical mechanics

- **F. Mandl: Statistical Physics.**

For Stochastic dynamics

- **N.G. van Kampen: Stochastic processes in Physics and Chemistry**

The best overall text for part 2 of the course is: R.A.L Jones, Soft Condensed Matter, Oxford University Press.

Additionally, the following more specialised texts should also be useful. They can be found in the University Library under the stated shelfmark.

Colloids

- (1) D.F.Evans, H.Wennerström: The Colloidal Domain - Where Physics, Chemistry, Biology, and Technology Meet. VCH Publishers (1994).
- (2) R.J.Hunter: Introduction to Modern Colloid Science. Oxford University Press (1993).
- (3) W.B.Russel, D.A.Saville, W.R.Schowalter: Colloidal Dispersions Cambridge University Press (1989).
- (4) D.H.Everett: Basic Principles of Colloid Science.

Royal Society of Chemistry Paperbacks (1988)

Polymers and surfactants

- (1) R.J. Young and P.A. Lovell: Introduction to polymers .
- (2) M. Doi: Introduction to polymer physics
- (3) J.Israelachvili, Intermolecular and Surface Forces, Academic Press (1992), Chs. 16 and 17

Glasses

- (1) J. Zarzycki; Glasses and the vitreous state. Cambridge University Press (1991).

Part I

Unifying concepts

Chapter 1

Introduction to phase behaviour and enhanced fluctuations

A phase transition can be defined as a macroscopic rearrangement of the internal constituents of a system in response to a change in the thermodynamic conditions to which they are subject. A wide variety of physical systems undergo such transitions. Understanding the properties of phase transitions is fundamental to the study of soft and complex matter, as these systems often exhibit rich and subtle transformations between different states of organization. Whether in colloidal suspensions, polymer blends, liquid crystals, or biological materials, phase transitions underpin a wide range of physical behaviours, from self-assembly and pattern formation to critical phenomena and dynamical arrest. By analysing how macroscopic phases emerge from microscopic interactions and external conditions, one gains crucial insight into the principles that govern structure, stability, and functionality in these intricate systems. As such, an understanding of phase transitions not only enriches theoretical understanding but also informs practical applications across materials science, biophysics, and nanotechnology. For these reasons we will devote a large proportion of this course to the study of phase transitions.

Two classic examples of systems displaying phase transitions are the ferromagnet and fluid systems. For the magnet, a key observable is the magnetisation defined as the magnetic moment per spin, given by $m = M/N$, with N the number of spins. m can be positive or negative, dependent on whether the spins are aligned ‘up’ or ‘down’. As the temperature of a ferromagnet is increased, its net magnetisation $|m|$ is observed to decrease smoothly, until at a certain temperature known as the critical temperature, T_c , it vanishes altogether (see left part of Figure 1.1). We define the magnetisation to be the *order parameter* of this phase transition.

One can also envisage applying a magnetic field H to the system which, depending on its sign (i.e. whether it is aligned (positive) or anti-aligned (negative) relative to the magnetisation axis), favours up or down spin states respectively, as shown schematically in Figure 1.1 (right part). Changing the sign of the magnetic field H for $T < T_c$ leads to a phase transition characterised by a discontinuous jump in m . We shall explore this behaviour in more detail in section 6.

Similarly, a change of state from liquid to gas can be induced in a fluid system (though not in an ideal gas) simply by raising the temperature. Typically the liquid-vapour transition is abrupt, reflecting the large number density difference between the states either side of the transition. However the abruptness of this transition can be reduced by applying pressure. At one particular pressure and temperature the discontinuity in the density difference between the two states vanishes and the two phases coalesce. These conditions of pressure and temperature serve to locate the critical point for the fluid. We define the density difference $\rho_{\text{liq}} - \rho_{\text{vap}}$ to be the order parameter for the liquid-gas phase transition. We shall meet order parameters for other,

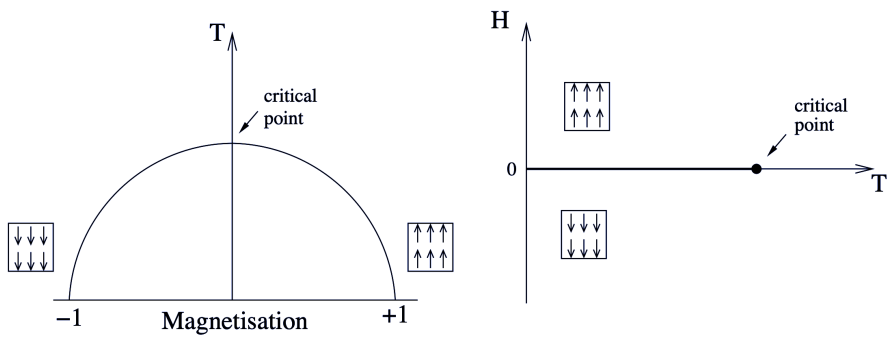


Figure 1.1: Phase diagram of a simple magnet (schematic). Left: magnetisation as a function of temperature for zero applied magnetic field, $H = 0$. Right: Applying a magnetic field that is aligned or antialigned with the direction of the magnetisation leads to a phase transition. The $H = 0$ axis at $T < T_c$ is the coexistence curve for which positive and negative magnetisations are equally likely.

more complex, systems in Section 5.5,

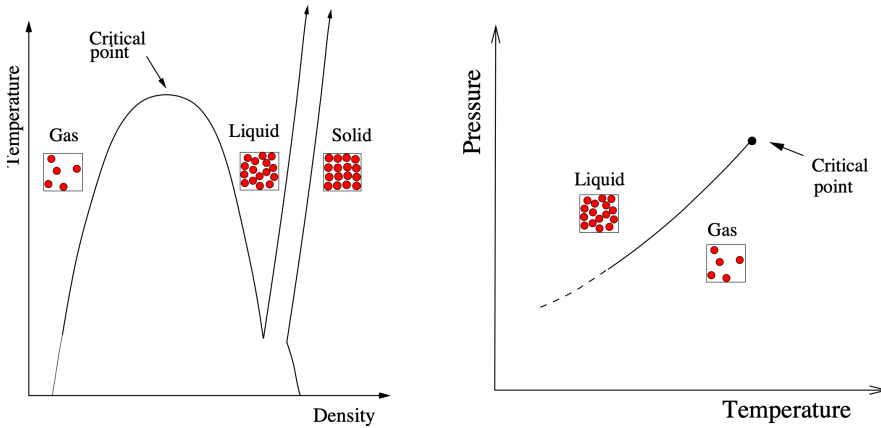


Figure 1.2: Phase diagram of a simple fluid (schematic)

In the vicinity of a critical point, a system displays a host of remarkable behaviors known as *critical phenomena*. Chief among these is the divergence of thermal response functions—such as specific heat, compressibility, or magnetic susceptibility—which signal an enhanced sensitivity to external perturbations. These singularities arise from the emergence of large-scale cooperative interactions among the system's microscopic constituents, as measured by a diverging *correlation length* (see Chapter 2). One visually striking manifestation of this is *critical opalescence*, particularly observed in fluids like CO_2 . As carbon dioxide nears its critical temperature and pressure, the distinction between its liquid and gas phases vanishes, giving rise to huge fluctuations in density. These fluctuations scatter visible light, rendering the fluid milky or opalescent. This scattering effect directly reflects the long-range correlations developing within the fluid. The movie below illustrates the effect as the critical temperature of CO_2 is approached from above. Note the appearance of a liquid-vapour interface (meniscus) as the system enters the two-phase region.

[Movies/critical_point_1.mp4](#)

The recalcitrant problem posed by the critical region is how best to incorporate such collective effects within the framework of a rigorous mathematical theory that affords both physical insight and quantitative explanation of the observed phenomena. This matter has been (and still is!)

the subject of intense theoretical activity.

The importance of the critical point stems largely from the fact that many of the phenomena observed in its vicinity are believed to be common to a whole range of apparently quite disparate physical systems. Systems such as liquid mixtures, superconductors, liquid crystals, ferromagnets, antiferromagnets and molecular crystals may display identical behaviour near criticality. This observation implies a profound underlying similarity among physical systems at criticality, regardless of many aspects of their distinctive microscopic nature. These ideas have found formal expression in the so-called ‘universality hypothesis’ which, since its inception in the 1970s, has enjoyed considerable success.

In the next few lectures, principal aspects of the contemporary theoretical viewpoint of phase transitions and critical phenomena will be reviewed. Mean field theories of phase transitions will be discussed and their inadequacies in the critical region will be exposed. The phenomenology of the critical region will be described including power laws, critical exponents and their relationship to scaling phenomena. These will be set within the context of the powerful renormalisation group technique. The notion of universality as a phenomenological hypothesis will be introduced and its implications for real and model systems will be explored. Finally, the utility of finite-size scaling methods for computer studies of critical phenomena will be discussed, culminating in the introduction of a specific technique suitable for exposing universality in model systems. Thereafter we will consider some foundational concepts in the dynamics of complex disordered matters. We shall look at the processes by which one phase transform into another and introduce differential equations that allow us to deal with the inherent stochasticity of thermal systems. The wider applicability of these unifying concepts to complex disordered systems such as colloids, polymers, liquid crystals and glasses will be covered in part 2 of the course.

Chapter 2

Key concepts for phase transitions

2.1 Observables and expectation values

In seeking to describe phase transition and critical phenomena, it is useful to have a quantitative measure of the difference between the phases: this is the role of the *order parameter*, Q . In the case of the fluid, the order parameter is taken as the difference between the densities of the liquid and vapour phases. In the ferromagnet it is taken as the magnetisation. As its name suggests, the order parameter serves as a measure of the kind of orderliness that sets in when the temperature is cooled below a critical temperature.

Our first task is to give some feeling for the principles which underlie the ordering process. Referring back to [?@sec-canonical](#), the probability p_a that a physical system at temperature T will have a particular microscopic arrangement (alternatively referred to as a ‘configuration’ or ‘state’), labelled a , of energy E_a is

$$p_a = \frac{1}{Z} e^{-E_a/k_B T} \quad (2.1)$$

The prefactor Z^{-1} is the *partition function*: since the system must always have *some* specific arrangement, the sum of the probabilities p_a must be unity, implying that

$$Z = \sum_a e^{-E_a/k_B T} \quad (2.2)$$

where the sum extends over all possible microscopic arrangements.

These equations assume that physical system evolves rapidly (on the timescale of typical observations) amongst all its allowed arrangements, sampling them with the probabilities Equation 2.1 the expectation value of any physical observable O will thus be given by averaging O over all the arrangements a , weighting each contribution by the appropriate probability:

$$\bar{O} = \frac{1}{Z} \sum_a O_a e^{-E_a/k_B T} \quad (2.3)$$

Sums like Equation 2.3 are not easily evaluated. Nevertheless, some important insights follow painlessly. Consider the case where the observable of interest is the order parameter, or more specifically the magnetisation of a ferromagnet.

$$Q = \frac{1}{Z} \sum_a Q_a e^{-E_a/k_B T} \quad (2.4)$$

It is clear from Equation 2.1 that at very low temperature the system will be overwhelmingly likely to be found in its minimum energy arrangements (ground states). For the ferromagnet, these are the fully ordered spin arrangements having magnetisation +1, or -1.

Now consider the high temperature limit. The enhanced weight that the fully ordered arrangement carries in the sum of Equation 2.4 by virtue of its low energy, is now no longer sufficient to offset the fact that arrangements in which Q_a has some intermediate value, though each carry a smaller weight, are vastly greater in number. A little thought shows that the arrangements which have essentially zero magnetisation (equal populations of up and down spins) are by far the most numerous. At high temperature, these disordered arrangements dominate the sum in Equation 2.4 and the order parameter is zero.

The competition between energy-of-arrangements weighting (or simply ‘energy’) and the ‘number of arrangements’ weighting (or ‘entropy’) is then the key principle at work here. The distinctive feature of a system with a critical point is that, in the course of this competition, the system is forced to choose amongst a number of macroscopically different sets of microscopic arrangements.

Finally in this section, we note that the probabilistic (statistical mechanics) approach to thermal systems outlined above is completely compatible with classical thermodynamics. Specifically, the bridge between the two disciplines is provided by the following equation

$$F = -k_B T \ln Z \quad (2.5)$$

where F is the “Helmholtz free energy”. All thermodynamic observables, for example the order parameter Q , and response functions such as the specific heat or magnetic susceptibility are obtainable as appropriate derivatives of the free energy. For instance, utilizing Equation 2.2, one can readily verify (try it as an exercise!) that the average internal energy is given by

$$\bar{E} = -\frac{\partial \ln Z}{\partial \beta},$$

where $\beta = (k_B T)^{-1}$.

The relationship between other thermodynamic quantities and derivatives of the free energy are given in fig. Figure 2.1

2.2 Correlations

2.2.1 Spatial correlations

The two-point connected correlation function measures how fluctuations at two spatial points are statistically related. For a scalar field $\phi(\vec{R})$, which could represent eg. the local magnetisation m in a magnet at position vector \vec{R} , or the local particle number density ρ in a fluid, it is defined as:

$$C(r) = \langle \phi(\vec{R})\phi(\vec{R} + \vec{r}) \rangle - \langle \phi(\vec{R}) \rangle^2,$$

$$\begin{array}{c}
Z = \sum_a e^{-E_a/k_B T} \\
\downarrow \\
F = -k_B T \ln Z \\
\swarrow \quad \searrow \\
\bar{E} = - \left(\frac{\partial(\beta F)}{\partial \beta} \right)_H \quad \bar{M} = - \left(\frac{\partial F}{\partial H} \right)_T \quad (M = mN) \\
\downarrow \quad \downarrow \\
C_H = \left(\frac{\partial \bar{E}}{\partial T} \right)_H \quad \chi_T = \left(\frac{\partial m}{\partial H} \right)_T
\end{array}$$

Figure 2.1: Relationships between the partition function and thermodynamic observables

where $\langle \cdot \rangle$ denotes an ensemble or spatial average over all \vec{R} , and $r = |\vec{r}|$ is the spatial separation between the two points.

$C(r)$ quantifies the spatial extent over which field values are correlated and in homogeneous and isotropic systems, it depends only on the separation r .

If $C(r)$ decays quickly, we say that correlations are short-ranged. Typically this occurs well away from criticality and takes the form of exponential decay

$$C(r) \sim e^{-r/\xi}$$

where the correlation length ξ is the characteristic scale over which correlations decay.

Near a critical point $C(r)$ decays more slowly - in a power-law fashion - and correlations are long-ranged.

$$C(r) \sim r^{-(d-2+\eta)}$$

where d is the spatial dimension and η is a critical exponent.

In isotropic fluids and particle systems, a closely related and more directly measurable quantity (particularly in simulations) is the **radial distribution function** $g(r)$, which describes how particle density varies as a function of distance from a reference particle. For such systems, the two-point correlation function of the number density field $\rho(\vec{r})$ is related to $g(r)$ as follows:

$$g(r) = 1 + \frac{C(r)}{\rho^2},$$

where ρ is the average number density. This relation shows that $g(r)$ encodes the same spatial correlations as $C(r)$, but in a form that is more natural for discrete particle systems. Note that

by definition $g(r) \rightarrow 1$ in the absence of correlations ie. when $C(r) = 0$. This is typically the case for $r \gg \xi$.

Experimentally one doesn't typically have direct access to $C(r)$, but rather its Fourier transform known as the **structure factor**

$$S(k) = \int d^d r e^{-i\vec{k} \cdot \vec{r}} C(r),$$

where k is the scattering wavevector.

In equilibrium:

- For short-range correlations (finite ξ), $S(k)$ typically has a Lorentzian form:

$$S(k) \sim \frac{1}{k^2 + \xi^{-2}}.$$

- At criticality (where $\xi \rightarrow \infty$), $S(k)$ follows a power law:

$$S(k) \sim k^{-2+\eta}.$$

This relation enables the extraction of ξ from experimental or simulation data, especially via scattering techniques.

2.2.2 Temporal correlations

Consider a thermodynamic variable x with zero mean that fluctuates over time. Examples include the local magnetization in a magnetic system or the local density in a fluid. Here, x represents a deviation from the average value — a fluctuation.

We're interested in how such fluctuations are correlated over time when the system is in thermal equilibrium. For instance, if x is positive at some time t , it's more likely to remain positive shortly after.

These temporal correlations are characterized by the two-time correlation function (also known as an auto-correlation function):

$$\langle x(\tau)x(\tau+t) \rangle$$

In equilibrium, the correlation function must be independent of the starting time τ . Therefore, we define:

$$\langle x(\tau)x(\tau+t) \rangle = M_{xx}(t)$$

That is, $M_{xx}(t)$ depends only on the time difference t .

We typically expect $M_{xx}(t)$ to decay exponentially over a characteristic correlation time t_c :

$$M_{xx}(t) \sim \exp(-t/t_c)$$

This exponential decay reflects how the memory of fluctuations fades with time.

Now consider two different fluctuating variables, x and y (e.g., local magnetizations at different positions). Their cross-correlation function is defined as:

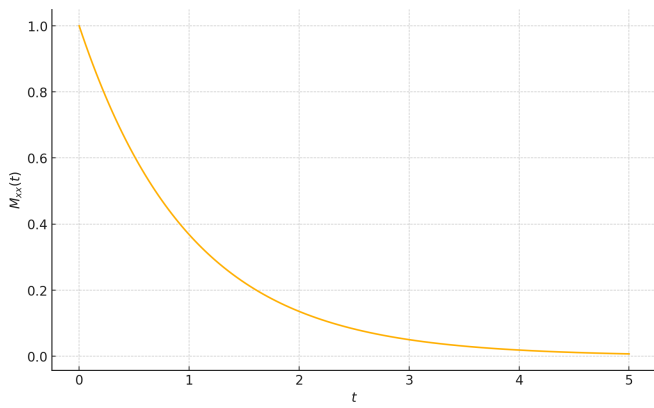


Figure 2.2: Sketch of $M_{xx}(t)$ against t

$$\langle x(\tau)y(\tau+t) \rangle = M_{xy}(t)$$

This defines the elements of a dynamic correlation matrix, of which $M_{xx}(t)$ is the diagonal.

Chapter 3

The approach to criticality

It is a matter of experimental fact that the approach to criticality in a given system is characterized by the divergence of various thermodynamic observables. Let us remain with the archetypal example of a critical system, the ferromagnet, whose critical temperature will be denoted as T_c . For temperatures close to T_c , the magnetic response functions (the magnetic susceptibility χ and the specific heat) are found to be singular functions, diverging as a *power* of the reduced (dimensionless) temperature $t \equiv (T - T_c)/T_c$:

$$\chi \equiv \frac{\partial M}{\partial H} \propto t^{-\gamma} \quad (H = 0) \quad (3.1)$$

(where $M = mN$),

$$C_H \equiv \frac{\partial E}{\partial T} \propto t^{-\alpha} \quad (H = \text{constant}) \quad (3.2)$$

Another key quantity is the correlation length ξ , which measures the distance over which fluctuations of the magnetic moments are correlated. This is observed to diverge near the critical point with an exponent ν .

$$\xi \propto t^{-\nu} \quad (T > T_c, H = 0) \quad (3.3)$$

Similar power law behaviour is found for the order parameter Q (in this case the magnetisation) which vanishes in a singular fashion (it has infinite gradient) as the critical point is approached as a function of temperature:

$$m \propto t^\beta \quad (T < T_c, H = 0) \quad (3.4)$$

(here the symbol β , is not to be confused with $\beta = 1/k_B T$ – this unfortunately is the standard notation.)

Finally, as a function of magnetic field:

$$m \propto h^{1/\delta} \quad (T = T_c, H > 0). \quad (3.5)$$

with $h = (H - H_c)/H_c$, the reduced magnetic field.

As examples, the behaviour of the magnetisation and correlation length are plotted in Figure 3.1 as a function of t .

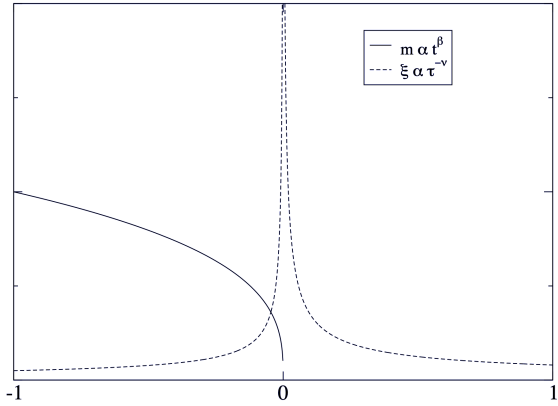


Figure 3.1: Singular behaviour of the correlation length and order parameter in the vicinity of the critical point as a function of the reduced temperature t .

The quantities $\gamma, \alpha, \nu, \beta$ in the above equations are known as critical exponents. They serve to control the rate at which the various thermodynamic quantities change on the approach to criticality.

Remarkably, the form of singular behaviour observed at criticality for the example ferromagnet also occurs in qualitatively quite different systems such as the fluid. All that is required to obtain the corresponding power law relationships for the fluid is to substitute the analogous thermodynamic quantities in to the above equations. Accordingly the magnetisation order parameter is replaced by the density difference $\rho_{liq} - \rho_{gas}$ while the susceptibility is replaced by the isothermal compressibility and the specific heat capacity at constant field is replaced by the specific heat capacity at constant volume. The approach to criticality in a variety of qualitatively quite different systems can therefore be expressed in terms of a set of critical exponents describing the power law behaviour for that system (see the book by Yeomans for examples).

Even more remarkable is the experimental observation that the values of the critical exponents for a whole range of fluids and magnets (and indeed many other systems with critical points) are *identical*. This is the phenomenon of *universality*. It implies a deep underlying physical similarity between ostensibly disparate critical systems. The principal aim of theories of critical point phenomena is to provide a sound theoretical basis for the existence of power law behaviour, the factors governing the observed values of critical exponents and the universality phenomenon. Ultimately this basis is provided by the Renormalisation Group (RG) theory, for which K.G. Wilson was awarded the Nobel Prize in Physics in 1982.

More about the scientists mentioned in this chapter:

[Kenneth Wilson](#)

Chapter 4

The Ising model: the prototype model for a phase transition

In order to probe the properties of the critical region, it is common to appeal to simplified model systems whose behaviour parallels that of real materials. The sophistication of any particular model depends on the properties of the system it is supposed to represent. The simplest model to exhibit critical phenomena is the two-dimensional Ising model of a ferromagnet. Actual physical realizations of 2-d magnetic systems do exist in the form of layered ferromagnets such as K_2CoF_4 , so the 2-d Ising model is of more than just technical relevance.

4.1 The 2D Ising model

The 2-d spin- $\frac{1}{2}$ Ising model envisages a regular arrangement of magnetic moments or ‘spins’ on an infinite plane. Each spin can take two values, $+1$ (‘up’ spins) or -1 (‘down’ spins) and is assumed to interact with its nearest neighbours according to the Hamiltonian

$$H_I = -J \sum_{\langle ij \rangle} s_i s_j - H \sum_i s_i \quad (4.1)$$

where $J > 0$ measures the strength of the coupling between spins and the sum extends over nearest neighbour spins s_i and s_j , i.e it is a sum of the bonds of the lattice. H is a magnetic field term which can be positive or negative (although for the time being we will set it equal to zero). The order parameter is simply the average magnetisation:

$$m = \frac{1}{N} \left\langle \sum_i s_i \right\rangle ,$$

where $\langle \cdot \rangle$ means an average over typical configurations corresponding to the prescribed value of $J/k_B T$.

The fact that the Ising model displays a phase transition was argued in Chapter 2. Thus at low temperatures for which there is little thermal disorder, there is a preponderance of aligned spins and hence a net spontaneous magnetic moment (ie. the system is ferromagnetic). As the temperature is raised, thermal disorder increases until at a certain temperature T_c , entropy drives the system through a continuous phase transition to a disordered spin arrangement with zero

net magnetisation (ie. the system is paramagnetic). These trends are visible in configurational snapshots from computer simulations of the 2D Ising model (see Figure 4.1). Although each spin interacts only with its nearest neighbours, the phase transition occurs due to cooperative effects among a large number of spins.

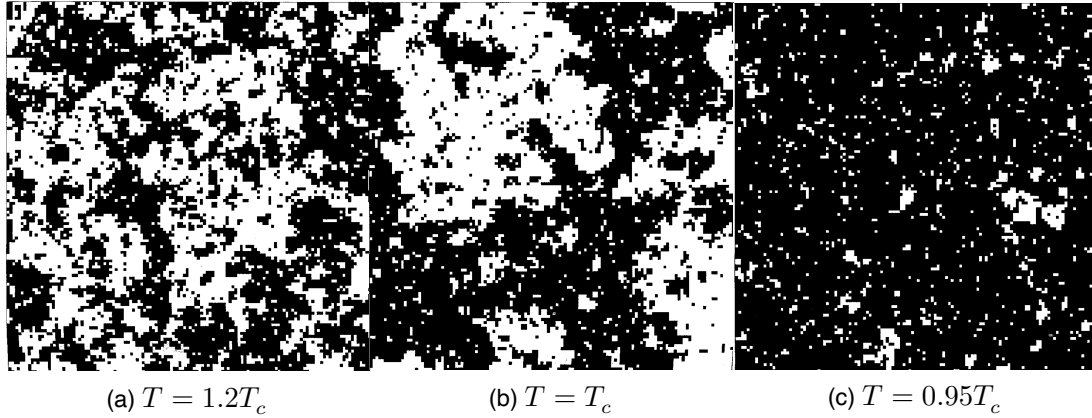


Figure 4.1: Configurations of the 2d Ising model. The patterns depict typical arrangements of the spins (white=+1, black=-1) generated in a computer simulation of the Ising model on a square lattice of $N = 512$ sites, at temperatures (from left to right) of $T = 1.2T_c$, $T = T_c$, and $T = 0.95T_c$. In each case only a portion of the system containing 128 sites is shown. The typical island size is a measure of the correlation length ξ : the excess of black over white (below T_c) is a measure of the order parameter.

[An interactive Monte Carlo simulation of the Ising model](#) demonstrates the phenomenology. By altering the temperature you will be able to observe for yourself how the typical spin arrangements change as one traverses the critical region. Pay particular attention to the configurations near the critical point. They have very interesting properties. We will return to them later!

Although the 2-d Ising model may appear at first sight to be an excessively simplistic portrayal of a real magnetic system, critical point universality implies that many physical observables such as critical exponents are not materially influenced by the actual nature of the microscopic interactions. The Ising model therefore provides a simple, yet *quantitatively* accurate representation of the critical properties of a whole range of real magnetic (and indeed fluid) systems. This universal feature of the model is largely responsible for its ubiquity in the field of critical phenomena. We shall explore these ideas in more detail later in the course.

4.2 Exact solutions: the one dimensional Ising chain

One might well ask why the 2D Ising model is the simplest model to exhibit a phase transition. What about the one-dimensional Ising model (ie. spins on a line)? In fact in one dimension, the Ising model can be solved exactly. It turns out that the system is paramagnetic for all $T > 0$, so there is no phase transition at any finite temperature. To see this, consider the ground state of the system in zero external field. This will have all spins aligned the same way (say up), and hence be ferromagnetic. Now consider a configuration with a various “domain walls” dividing spin up and spin down regions:

Instead of considering the underlying spin configurations, we shall describe the system in terms of the statistics of its domain walls. The energy cost of a wall is $\Delta = 2J$, independent of position. Domain walls can occupy the bonds of the lattice, of which there are $N - 1$. Moreover, the walls are noninteracting, except that you cannot have two of them on the same bond. (Check through these ideas if you are unsure.)

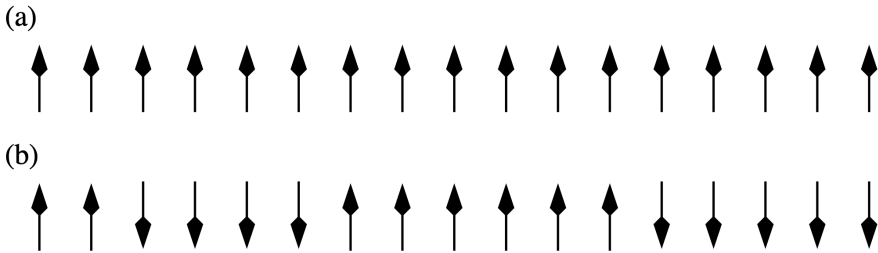


Figure 4.2: (a) Schematic of an Ising chain at $T = 0$. (b) At a small finite temperature the chain is split into domains of spins ordered in the same direction. Domains are separated by notional domain “walls”, which cost energy $\Delta = 2J$. Periodic boundary conditions are assumed.

In this representation, the partition function involves a count over all possible domain wall arrangements. Since the domain walls are non interacting (eg it doesn't cost energy for one to move along the chain) we can calculate Z by considering the partition function associated with a single domain wall being present or absent on some given bond, and then simply raise to the power of the number of bonds:

$$Z = Z_1^{N-1}$$

where

$$Z_1 = e^{\beta J} + e^{\beta(J-\Delta)} = e^{\beta J}(1 + e^{-\beta\Delta})$$

is the domain wall partition function for a single bond and represent the sum over the two possible states: domain wall absent or present. Then the free energy per bond of the system is

$$\beta f \equiv \beta F/(N - 1) = -\ln Z_1 = -\beta J - \ln(1 + e^{-\beta\Delta})$$

The first term on the RHS is simply the energy per spin of the ferromagnetic (ordered) phase, while the second term arises from the free energy of domain walls. Clearly for any finite temperature (ie. for $\beta < \infty$), this second term is finite and negative. Hence the free energy will always be lowered by having a finite concentration of domain walls in the system. Since these domain walls disorder the system, leading to a zero average magnetisation, the 1D system is paramagnetic for all finite temperatures. *Exercise:* Explain why this argument works only in 1D.

The animation below lets you see qualitatively how the typical number of domain walls varies with temperature. If you'd like to explore more quantitatively, a python code performing a Monte Carlo simulation is available. You will learn about Monte Carlo simulation in the coursework and in later parts of the course.

```
#Monte Carlo simulation of the 1d Ising chain with periodic boundary conditions
import numpy as np
import matplotlib.pyplot as plt
from matplotlib.animation import FuncAnimation
from matplotlib.widgets import Slider

# Number of spins
N = 20

# Initialize spins (+1 or -1)
spins = np.random.choice([-1, 1], size=N)
```

```

# Initial temperature
T = 2.0

# Set up figure and axis for the spins
fig, ax = plt.subplots(figsize=(10, 2))
plt.subplots_adjust(bottom=0.25) # make room for slider
ax.set_xlim(-0.5, N - 0.5)
ax.set_ylim(-1, 1)
ax.axis('off')

# Create text objects for each spin
texts = []
for i in range(N):
    arrow = '↑' if spins[i] == 1 else '↓'
    t = ax.text(i, 0, arrow, fontsize=24, ha='center', va='center')
    texts.append(t)

def update(frame):
    """Perform Metropolis updates over all spins, then refresh display."""
    global spins, T
    for _ in range(N):
        i = np.random.randint(N)
        left = spins[(i - 1) % N]
        right = spins[(i + 1) % N]
        deltaE = 2 * spins[i] * (left + right)
        # Metropolis criterion ensures configurations appear with the correct Boltzmann probability
        if deltaE < 0 or np.random.rand() < np.exp(-deltaE / T):
            spins[i] *= -1
    # Update arrows on screen
    for idx, t in enumerate(texts):
        t.set_text('↑' if spins[idx] == 1 else '↓')
    return texts

# Create the animation with caching disabled and blit turned off
ani = FuncAnimation(
    fig,
    update,
    interval=200,
    blit=False,
    cache_frame_data=False
)

# Add a temperature slider
ax_T = plt.axes([0.2, 0.1, 0.6, 0.03], facecolor='lightgray')
slider_T = Slider(ax_T, 'Temperature T', 0.1, 5.0, valinit=T)

def on_T_change(val):
    """Callback to update T when the slider changes."""
    global T
    T = val

slider_T.on_changed(on_T_change)

```

```
# Show the plot (ani is kept in scope so it won't be deleted)
plt.show()
```

Temperature T =

2.0

4.2.1 More general 1D spins systems: transfer matrix method

Generally speaking one-dimensional systems lend themselves to a degree of analytic tractability not found in most higher dimensional models. Indeed for the case of a 1-d assembly of N spins each having m discrete energy states, and in the presence of a magnetic field, it is possible to reduce the evaluation of the partition function to the calculation of the eigenvalues of a matrix—the so called transfer matrix.

Let us start by assuming that the assembly has cyclic boundary conditions, then the total energy of configuration $\{s\}$ is

$$\begin{aligned} H(\{s\}) &= - \sum_{i=1}^N (J s_i s_{i+1} + H s_i) \\ &= - \sum_{i=1}^N (J s_i s_{i+1} + H(s_i + s_{i+1})/2) \\ &= \sum_{i=1}^N E(s_i, s_{i+1}) \end{aligned}$$

where we have defined $E(s_i, s_{i+1}) = -J s_i s_{i+1} - H(s_i + s_{i+1})/2$.

Now the partition function may be written

$$\begin{aligned} Z_N &= \sum_{\{s\}} \exp(-\beta H(\{s\})) \\ &= \sum_{\{s\}} \exp(-\beta [E(s_1, s_2) + E(s_2, s_3) + \dots + E(s_N, s_1)]) \\ &= \sum_{\{s\}} \exp(-\beta E(s_1, s_2)) \exp(-\beta E(s_2, s_3)) \dots \exp(-\beta E(s_N, s_1)) \\ &= \sum_{i,j,\dots,l=1}^m V_{ij} V_{jk} \dots V_{li} \end{aligned}$$

where the $V_{ij} = \exp(-\beta E_{ij})$ are elements of an $m \times m$ matrix \mathbf{V} , known as the transfer matrix (i, j, k etc are dummy indices that run over the matrix elements). You should see that the sum over the product of matrix elements picks up all the terms in the partition function and therefore Equation 4.2 is an alternative way of writing the partition function.

The reason it is useful to transform to a matrix representation is that it transpires that the sum over the product of matrix elements in Equation 4.2 is simply just the trace of \mathbf{V}^N (check this yourself for a short periodic chain), given by the sum of its eigenvalues:-

$$Z_N = \lambda_1^N + \lambda_2^N + \dots \lambda_m^N$$

For very large N , this expression simplifies further because the largest eigenvalue λ_1 dominates the behaviour since $(\lambda_2/\lambda_1)^N$ vanishes as $N \rightarrow \infty$. Consequently in the thermodynamic limit one may put $Z_N = \lambda_1^N$ and the problem reduces to identifying the largest eigenvalue of the transfer matrix.

Specializing to the case of the simple Ising model in the presence of an applied field H , the transfer matrix takes the form

$$\mathbf{V}(H) = \begin{pmatrix} e^{\beta(J+H)} & e^{-\beta J} \\ e^{-\beta J} & e^{\beta(J-H)} \end{pmatrix}$$

This matrix has two eigenvalues which can be readily calculated in the usual fashion as the roots of the characteristic polynomial $|\mathbf{V} - \lambda \mathbf{I}|$. They are

$$\lambda_{\pm} = e^{\beta J} \cosh(\beta H) \pm \sqrt{e^{2\beta J} \sinh^2 \beta H + e^{-2\beta J}}.$$

Hence the free energy per spin $f = -k_B T \ln \lambda_+$ is

$$f = -k_B T \ln \left[e^{\beta J} \cosh(\beta H) + \sqrt{e^{2\beta J} \sinh^2 \beta H + e^{-2\beta J}} \right].$$

The Ising model in 2D can also be solved exactly, as was done by Lars Onsager in 1940. The solution is extremely complicated and is regarded as one of the pinnacles of statistical mechanics. In 3D no exact solution is known.

Chapter 5

Mean field theory and perturbation schemes

Of the wide variety of models of interest to the critical point theorist, the majority have shown themselves intractable to direct analytic (pen and paper) assault. In a very limited number of instances models have been solved exactly, yielding the phase coexistence parameters, critical exponents and the critical temperature. The 2-d spin- $\frac{1}{2}$ Ising model is certainly the most celebrated such example, its principal critical exponents are found to be $\beta = \frac{1}{8}$, $\nu = 1$, $\gamma = \frac{7}{4}$. Its critical temperature is $-2J/\ln(\sqrt{2}-1) \approx 2.269J$. Unfortunately such solutions rarely afford deep insight to the general framework of criticality although they do act as an invaluable test-bed for new and existing theories.

The inability to solve many models exactly often means that one must resort to approximations. One such approximation scheme is mean field theory.

5.1 Mean field solution of the Ising model

Let us look for a mean field expression for the free energy of the Ising model whose Hamiltonian is given in Equation 4.1 . Write

$$s_i = \langle s_i \rangle + (s_i - \langle s_i \rangle) = m + (s_i - m) = m + \delta s_i$$

Then

$$\begin{aligned} H_I &= -J \sum_{\langle i,j \rangle} [m + (s_i - m)][m + (s_j - m)] - H \sum_i s_i \\ &= -J \sum_{\langle i,j \rangle} [m^2 + m(s_i - m) + m(s_j - m) + \delta s_i \delta s_j] - H \sum_i s_i \\ &= -J \sum_i (qms_i - qm^2/2) - H \sum_i s_i - J \sum_{\langle i,j \rangle} \delta s_i \delta s_j \end{aligned}$$

where in the last line we have used the fact that when for each site i we perform the sum $\sum_{\langle i,j \rangle}$ over bonds of a quantity which is independent of s_j , then the result is just the number of bonds per site times that quantity. Since the number of bonds on a lattice of N sites of coordination q

is $Nq/2$ (because each bond is shared between two sites), there are therefore $q/2$ bonds per site.

Now the mean field approximation is to ignore the last term in the last line of Equation 5.1 giving the configurational energy as

$$H_{mf} = - \sum_i H_{mf} s_i + NqJm^2/2$$

with $H_{mf} \equiv qJm + H$ the “mean field” seen by spin s_i . As all the spins are decoupled (independent) in this approximation we can write down the partition function, which follows by taking the partition function for a single spin (by summing the Boltzmann factor for $s_i = \pm 1$) and raising to the power N to find

$$Z = e^{-\beta qJm^2N/2} [2 \cosh(\beta(qJm + H))]^N$$

The free energy follows as

$$F(m) = NJqm^2/2 - Nk_B T \ln[2 \cosh(\beta(qJm + H))].$$

and the magnetisation as

$$m = -\frac{1}{N} \frac{\partial F}{\partial H} = \tanh(\beta(qJm + H))$$

To find $m(H, T)$, we must numerically solve this last equation self consistently.

Note that we can obtain m in a different way. Consider some arbitrary spin, s_i say. Then this spin has an energy $H_{mf}(s_i)$. Considering this energy for both cases $s_i = \pm 1$ and the probability $p(s_i) = e^{-\beta H_{mf}(s_i)}/Z$ of each, we have that

$$\langle s_i \rangle = \sum_{s_i=\pm 1} s_i p(s_i)$$

but for consistency, $\langle s_i \rangle = m$. Thus

$$\begin{aligned} m &= \sum_{s_i=\pm 1} s_i p(s_i) \\ &= \frac{e^{\beta(qJm+H)} - e^{-\beta(qJm+H)}}{e^{\beta(qJm+H)} + e^{-\beta(qJm+H)}} \\ &= \tanh(\beta(qJm + H)) \end{aligned}$$

as before.

5.2 Spontaneous symmetry breaking

This mean field analysis reveals what is happening in the Ising model near the critical temperature T_c . Figure 5.1 shows sketches for $\beta F(m)/N$ as a function of temperature, where for simplicity we restrict attention to $H = 0$. In this case $F(m)$ is symmetric in m . Moreover, at high T , the entropy dominates and there is a single minimum in $F(m)$ at $m = 0$. As T is

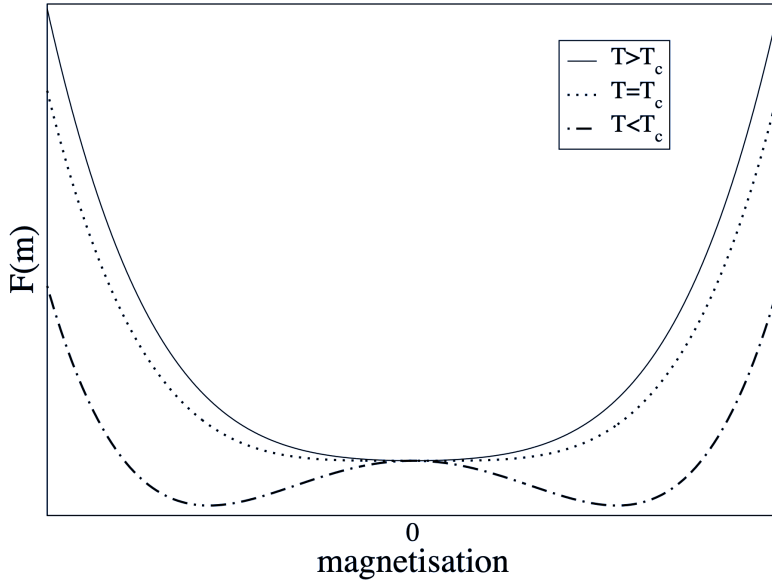


Figure 5.1: Schematic of the form of the free energy for a critical, subcritical and supercritical temperature

lowered, there comes a point ($T = T_c = qJ/k_B$) where the curvature of $F(m)$ at the origin changes sign; precisely at this point

$$\frac{\partial^2 F}{\partial m^2} = 0.$$

At lower temperature, there are instead two minima at nonzero $m = \pm m^*$, where the *equilibrium magnetisation* m^* is the positive root (calculated explicitly below) of

$$m^* = \tanh(\beta J q m^*) = \tanh\left(\frac{m^* T_c}{T}\right)$$

The point $m = 0$ which remains a root of this equation, is clearly an unstable point for $T < T_c$ (since F has a maximum there).

This is an example of spontaneous symmetry breaking. In the absence of an external field, the Hamiltonian (and therefore the free energy) is symmetric under $m \rightarrow -m$. Accordingly, one might expect the actual state of the system to also show this symmetry. This is true at high temperature, but spontaneously breaks down at low ones. Instead there are a pair of ferromagnetic states (spins mostly up, or spins mostly down) which – by symmetry– have the same free energy, lower than the unmagnetized state.

5.3 Phase diagram

The resulting zero-field magnetisation curve $m(T, H = 0)$ looks like Figure 5.2.

This shows the sudden change of behaviour at T_c (phase transition). For $T < T_c$ it is arbitrary which of the two roots $\pm m^*$ is chosen; typically it will be different in different parts of the sample (giving macroscopic “magnetic domains”). But this behaviour with temperature is *qualitatively modified* by the presence of a field H , however small. In that case, there is always a slight magnetization, even far above T_c and the curves becomes smoothed out, as shown. There is

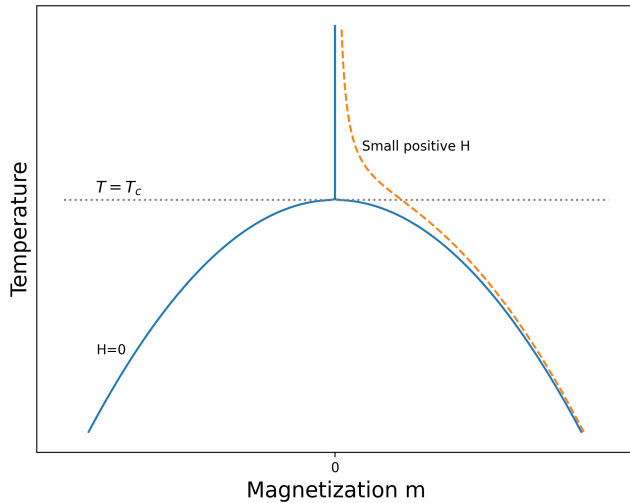


Figure 5.2: Phase diagram of a simple magnet in the m - T plane.

no doubt which root will be chosen, and no sudden change of the behaviour (no phase transition). Spontaneous symmetry breaking does not occur, because the symmetry is already broken by H . (The curve $F(m)$ is lopsided, rather than symmetrical about $m = 0$.)

On the other hand, if we sit below T_c in a positive field (say) and gradually reduce H through zero so that it becomes negative, there is a very sudden change of behaviour at $h = 0$: the equilibrium state jumps discontinuously from $m = m^*$ to $m = -m^*$.

This is called a first order phase transition as opposed to the “second order” or continuous transition that occurs at T_c in zero field. The definitions are:

First order transition: magnetisation (or similar order parameter) depends discontinuously on a field variable (such as h or T).

Continuous transition: Change of functional form, but no discontinuity in m ; typically, however, $(\partial m / \partial T)_h$ (or similar) is either discontinuous, or diverges with an integrable singularity.

In this terminology, we can say that the phase diagram of the magnet in the H , T plane shows a line of first order phase transitions, terminating at a continuous transition, which is the critical point.

🔥 Aside on Quantum Criticality

In some magnetic systems such as $CePd_2Si_2$, one can, by applying pressure or altering the chemical composition, depress the critical temperature all the way to absolute zero! This may seem counterintuitive, after all at $T = 0$ one should expect perfect ordering, not the large fluctuations that accompany criticality. It turns out that the source of the fluctuations that drive the system critical is zero point motion associated with the Heisenberg uncertainty principle. Quantum criticality is a matter of ongoing active research, and open questions concern the nature of the phase diagrams and the relationship to superconductivity. Although the subject goes beyond the scope of this course, there is an accessible article [here](#) if you want to learn more.

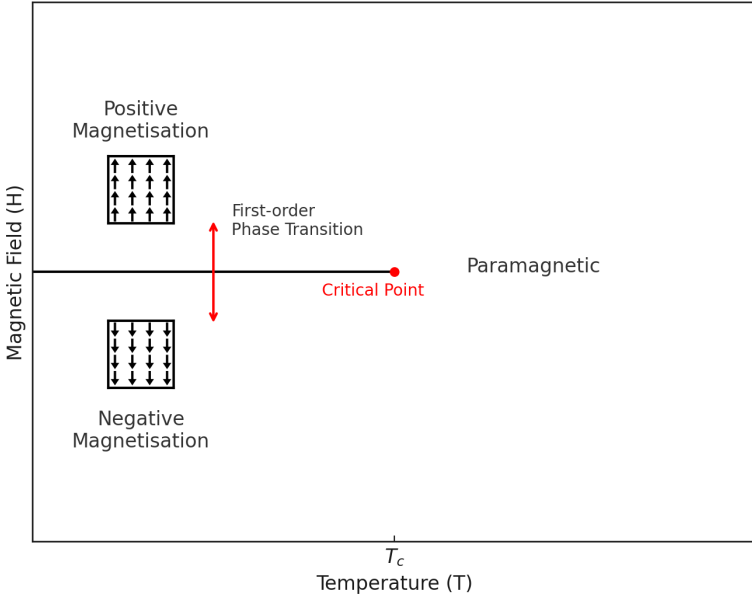


Figure 5.3: Phase diagram of a simple magnet in the H - T plane.

5.4 A closer look: critical exponents

Let us now see how we can calculate critical exponents within the mean field approximation.

5.4.1 Zero H solution and the order parameter exponent

In zero field

$$m = \tanh\left(\frac{mT_c}{T}\right)$$

where $T_c = qJ/k_B$ is the critical temperature at which m first goes to zero.

We look for a solution where m is small ($\ll 1$). Expanding the tanh function and replacing $\beta = (k_B T)^{-1}$ yields

$$m = \frac{mT_c}{T} - \frac{1}{3} \left(\frac{mT_c}{T} \right)^3 + O(m^5).$$

Then $m = 0$ is one solution. The other solution is given by

$$m^2 = 3 \left(\frac{T}{T_c} \right)^3 \left(\frac{T_c}{T} - 1 \right)$$

Now, considering temperatures close to T_c to guarantee small m , and employing the reduced temperature $t = (T - T_c)/T_c$, one finds

$$m^2 \simeq -3t$$

Hence

$$\begin{aligned} m &= 0 \quad \text{for } T > T_c \quad \text{since otherwise } m \text{ imaginary} \\ m &= \pm\sqrt{-3t} \quad \text{for } T < T_c \quad \text{real} \end{aligned}$$

This result implies that (within the mean field approximation) the critical exponent $\beta = 1/2$.

5.4.2 Finite (but small) field solution: the susceptibility exponent

In a finite, but small field we can expand Equation 5.1 thus:

$$m = \frac{mT_c}{T} - \frac{1}{3} \left(\frac{mT_c}{T} \right)^3 + \frac{H}{kT}$$

Consider now the isothermal susceptibility

$$\begin{aligned} \chi &\equiv \left(\frac{\partial m}{\partial H} \right)_T \\ &= \frac{T_c}{T} \chi - \left(\frac{T_c}{T} \right)^3 \chi m^2 + \frac{1}{k_B T} \end{aligned}$$

Then

$$\chi \left[1 - \frac{T_c}{T} + \left(\frac{T_c}{T} \right)^3 m^2 \right] = \frac{1}{k_B T}$$

Hence near T_c

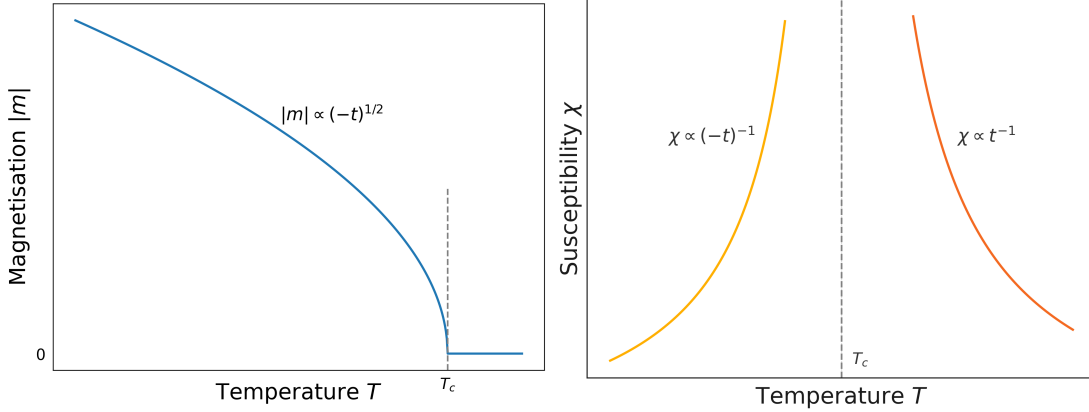
$$\chi = \frac{1}{k_B T_c} \left(\frac{1}{t + m^2} \right)$$

Then using the results of Equation 5.1

$$\begin{aligned} \chi &= (k_B T_c t)^{-1} \quad \text{for } T > T_c \\ \chi &= (-2k_B T_c t)^{-1} \quad \text{for } T \leq T_c \end{aligned}$$

where one has to take the non-zero value for m below T_c to ensure +ve χ , i.e. thermodynamic stability. This result implies that (within the mean field approximation) the critical exponent $\gamma = 1$.

The schematic behaviour of the Ising order parameter and susceptibility are shown in Figure 5.5 (a) and (b) respectively.



(a) Mean field behaviour of the Ising magnetisation (schematic)
(b) Mean field behaviour of the Ising susceptibility (schematic)

5.5 Landau theory

Landau theory is a slightly more general type of mean field theory than that discussed in the previous subsection because it is not based on a particular microscopic model. Its starting point is the Helmholtz free energy, which Landau asserted can be written in terms of power series expansion of the order parameter ϕ :

$$F(\phi) = \sum_{i=0}^{\infty} a_i \phi^i$$

The equilibrium value of ρ is that which minimises the Landau free energy.

🔥 A note on order parameters

We have already seen examples of these in earlier sections, e.g., for the liquid-gas transition this was

$\rho_{liq} - \rho_{gas}$: difference in density of two coexisting phases,

while for the Ising magnet it is the magnetisation m . Both quantities vanish at the critical point. These are examples of *scalar* order parameters – a single number is required to represent the degree of order ($n = 1$).

In the absence of a symmetry-breaking field, the Landau free-energy density f_L must have symmetry $f_L(-\phi) = f_L(\phi)$ (Ising case).

For some other systems, n component vectors are required in order to represent the order:

$$\phi = (\phi_1, \phi_2, \dots, \phi_n)$$

Then $f_L(\phi)$ should be symmetric under $O(n)$ rotations in n -component ϕ -space.

The table below lists examples of order parameters for various physical systems.

Physical System	Order Parameter φ	Symmetry Group
Uniaxial (Ising) ferromagnet	Magnetisation per spin, m	$O(1)$

Fluid (liquid-gas)	Density difference, $\rho - \rho_c$	$O(1)$
Liquid mixtures	Concentration difference, $c - c_c$	$O(1)$
Binary (AB) alloy (e.g., β -brass)	Concentration of one of the species, c	$O(1)$
Isotropic (vector) ferromagnet	n -component magnetisation, $\mathbf{m} = (m_1, m_2, \dots, m_n)$	$O(n)$
	$n = 2$: xy model	$O(2)$
	$n = 3$: Heisenberg model	$O(3)$
Superfluid He ⁴	Macroscopic condensate wavefunction, Ψ	$O(2)$
Superconductor (s-wave)	Macroscopic condensate wavefunction, Ψ	$O(2)$
Nematic liquid crystal	Orientational order, $\langle P_2(\cos \theta) \rangle$	
Smectic A liquid crystal	1-dimensional periodic density	
Crystal	3-dimensional periodic density	

Notes:

- In **superfluid** 4He the order parameter is

$$\Psi = |\Psi| e^{i\theta},$$

the *complex wavefunction* of the macroscopic condensate. Both the amplitude $|\Psi|$ and phase θ must be specified, so this corresponds to $n = 2$.

Superconductors also correspond to $n = 2$.

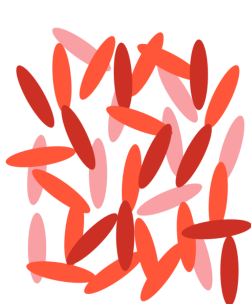
- In a **nematic** liquid crystal, the *orientational* order parameter is

$$\langle P_2(\cos \theta) \rangle \equiv \frac{1}{2} \langle 3 \cos^2 \theta - 1 \rangle,$$

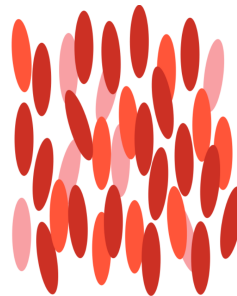
where θ is the angle a molecule makes with the average direction of the long axes of the molecules (known as the *director* \hat{n}). Rotational symmetry is broken. For the case of an n component vector, the free energy should be a function of:

$$\phi^2 \equiv |\phi|^2 = \phi_1^2 + \phi_2^2 + \dots + \phi_n^2 = \sum_{i=1}^n \phi_i^2$$

in the absence of a symmetry breaking field. Rotational symmetry is incorporated into the theory.



(a) Schematic of the isotropic liquid phase of a system of elongated molecules.



(b) Schematic of the nematic liquid phase of a system of elongated molecules. This phase has uniaxial ordering.

Figure 5.5: Isotropic and uniaxially ordered (nematic) phases of liquid crystal molecules.

To exemplify the approach, let us specialise to the case of a ferromagnet where $\phi = m$, the magnetisation and write the Landau free energy as

$$F(m) = F_0 + a_2 m^2 + a_4 m^4 \quad (5.1)$$

Here only the terms compatible with the order parameter symmetry are included in the expansion and we truncate the series at the 4th power because this is all that is necessary to yield the essential phenomenology. On symmetry grounds, the free energy of a ferromagnet should be invariant under a reversal of the sign of the magnetisation. Terms linear and cubic in m are not invariant under $m \rightarrow -m$, and so do not feature.

One can understand how the Landau free energy can give rise to a critical point and coexistence values of the magnetisation, by plotting $F(m)$ for various values of a_2 with a_4 assumed positive (which ensures that the magnetisation remains bounded). This is shown in the following movie:

[Movies/landau_free_energy_evolution.mp4](#)

The situation is qualitatively similar to that discussed in Section 5.2. Thermodynamics tells us that the system adopts the state of lowest free energy. From the movie, we see that for $a_2 > 0$, the system will have $m = 0$, i.e. will be in the disordered (or paramagnetic) phase. For $a_2 < 0$, the minimum in the free energy occurs at a finite value of m , indicating that the ordered (ferromagnetic) phase is the stable one. In fact, the physical (up-down) spin symmetry built into F indicates that there are two equivalent stable states at $m = \pm m^*$. $a_2 = 0$ corresponds to the critical point which marks the border between the ordered and disordered phases. Note that it is an inflexion point, so has $\frac{d^2 F}{dm^2} = 0$.

Clearly a_2 controls the deviation from the critical temperature, and accordingly we may write

$$a_2 = \tilde{a}_2 t$$

where t is the reduced temperature. Thus we see that the trajectory of the minima as a function of $a_2 < 0$ in the above movie effective traces out the coexistence curve in the $m - T$ plane.

We can now attempt to calculate critical exponents. Restricting ourselves first to the magnetisation exponent β defined by $m = t^\beta$, we first find the equilibrium magnetisation, corresponding to the minimum of the Landau free energy:

$$\frac{dF}{dm} = 2\tilde{a}_2 tm + 4a_4 m^3 = 0 \quad (5.2)$$

which implies

$$m \propto (-t)^{1/2},$$

so $\beta = 1/2$, which is again a mean field result.

Likewise we can calculate the effect of a small field H if we sit at the critical temperature T_c . Since $a_2 = 0$, we have

$$F(m) = F_0 + a_4 m^4 - Hm$$

$$\frac{\partial F}{\partial m} = 0 \Rightarrow m(H, T_c) = \left(\frac{H}{4a_4} \right)^{1/3}$$

or

$$H \sim m^\delta \quad \delta = 3$$

which defines a second critical exponent.

Note that at the critical point, a small applied field causes a very big increase in magnetisation; formally, $(\partial m / \partial H)_T$ is infinite at $T = T_c$.

A third critical exponent can be defined from the magnetic susceptibility at zero field

$$\chi = \left(\frac{\partial m}{\partial H} \right)_{T,V} \sim |T - T_c|^{-\gamma}$$

Exercise: Show that the Landau expansion predicts $\gamma = 1$.

Finally we define a fourth critical exponent via the variation of the heat capacity (per site or per unit volume) C_H , in fixed external field $H = 0$:

$$C_H \sim |T - T_c|^{-\alpha}$$

By convention, α is defined to be positive for systems where there is a *divergence* of the heat capacity at the critical point (very often the case). The heat capacity can be calculated from

$$C_H = -T \frac{\partial^2 F}{\partial T^2}$$

From the minimization over m @#eq-minimize one finds (*exercise:* check this)

$$\begin{aligned} F &= 0 \quad T > T_c \\ F &= -a_2^2/4a_4 \quad T < T_c \end{aligned}$$

Using the fact that a_2 varies linearly with T , we have

$$\begin{aligned} C_H &= 0 \quad T \rightarrow T_c^+ \\ C_H &= \frac{T\tilde{a}_2^2}{2a_4} \quad T \rightarrow T_c^- , \end{aligned}$$

which is actually a step discontinuity in specific heat. Since for positive α the heat capacity is divergent, and for negative α it is continuous, this behaviour formally corresponds to $\alpha = 0$

5.6 Shortcomings of mean field theory

While mean field theories provide a useful route to understanding qualitatively the phenomenology of phase transitions, in real ferromagnets, as well as in more sophisticated theories, the critical exponents are not the simple fraction and integers found here. This failure of mean field theory to predict the correct exponents is of course traceable to their neglect of correlations. In later sections we shall start to take the first steps to including the effects of long range correlations.

Table 5.2: Comparison of true Ising critical exponents with their mean field theory predictions in a number of dimensions.

	Mean Field	$d = 1$	$d = 2$	$d = 3$
Critical temperature $k_B T / qJ$	1	0	0.5673	0.754
Order parameter exponent β	$\frac{1}{2}$	-	$\frac{1}{8}$	0.325 ± 0.001
Susceptibility exponent γ	1	∞	$\frac{7}{4}$	1.24 ± 0.001
Correlation length exponent ν	$\frac{1}{2}$	∞	1	0.63 ± 0.001

Chapter 6

The Lattice Gas model

A crude representation of a fluid is the lattice gas model. Here particles can occupy the sites of a hypercubic lattice. The occupancy of a site i is specified by the variable $c_i = 1$ (occupied) or $c_i = 0$ vacant. The complete list of these occupancies $\{c\}$ specifies a microstate. The average particle number density (fraction of occupied sites) is given by

$$c = L^{-d} \sum_i c_i$$

where L is the linear extent of the lattice and d its dimensionality.

The Hamiltonian of the lattice gas model is

$$H_{LG} = -\epsilon \sum_{\langle i,j \rangle} c_i c_j - \mu \sum_i c_i$$

where ϵ is an attraction energy between a pair of particles on adjacent (nearest neighbouring) sites and μ is a field known as the chemical potential, which couples to the particle density which is assumed to fluctuate around a mean value controlled by the prescribed chemical potential. This representation of the model in which the overall density fluctuates is known as the *Grand Canonical ensemble*.

6.1 Mapping between Ising model and lattice gas

The lattice gas model is interesting because whilst being a plausible model for a fluid, it maps onto the Ising model. This extends the applicability of the Ising model. To expose the mapping we write the grand partition function of the lattice gas:

$$\Xi = \sum_{\text{state}} \exp -\beta H_{LG} = \sum_{\{c\}} \exp \left[\beta \epsilon \sum_{\langle i,j \rangle} c_i c_j + \beta \mu \sum_i c_i \right]$$

where the sum is an unrestricted sum over the occupancies of the lattice sites. We now change variables to

$$c_i = (1 + s_i)/2; \quad J = \frac{\epsilon}{4} \quad h = \frac{\epsilon q + 2\mu}{4}$$

Hence

$$H_{LG} = H_1 + \text{constant}$$

Since the last term does not depend on the configuration, it feeds through as an additive constant in the free energy; and since all observables feature as derivatives of the free energy, the constant has no physical implications.

6.2 Phase diagram

Using these translation rules we can plot the phase diagram of the lattice gas in the number density-temperature plane.

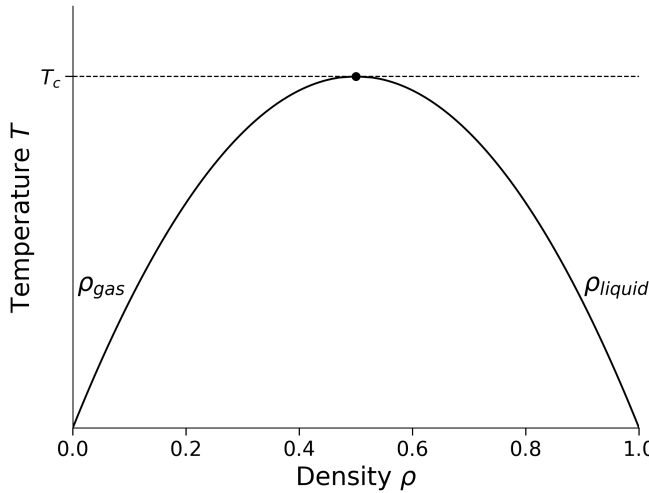


Figure 6.1: Phase diagram of the lattice gas model in the density-temperature plane.

In the $\mu-T$ plane there is a line of first order phase transitions terminating at a critical point. The first order line means that if $T < T_c$ we smoothly increase the chemical potential through the coexistence value of μ , the density of particles on our lattice $\rho = N/L^d$ jumps discontinuously from a low to a high value.

$$\rho_{\text{gas}} = \frac{1 - m^*}{2} \rightarrow \rho_{\text{liquid}} = \frac{1 + m^*}{2}$$

These values merge at T_c , the gas-liquid critical point. At higher temperatures, the distinction between the phases disappears.

6.3 Real Fluids

You may wish to compare this with the results of (say) van der Waals equation (see recommended textbooks for the required phase diagram). The main difference is that the lattice gas has so-called “particle-hole” symmetry, $\rho \rightarrow 1 - \rho$ (inherited from the up-down symmetry of the Ising model) which is not present for a real fluid. Accordingly, the phase diagram in a real fluid looks like a lopsided version of the above picture as shown in Figure 6.2. See [here](#) for some real experimental data showing the asymmetry of the coexistence curve in liquid metals.

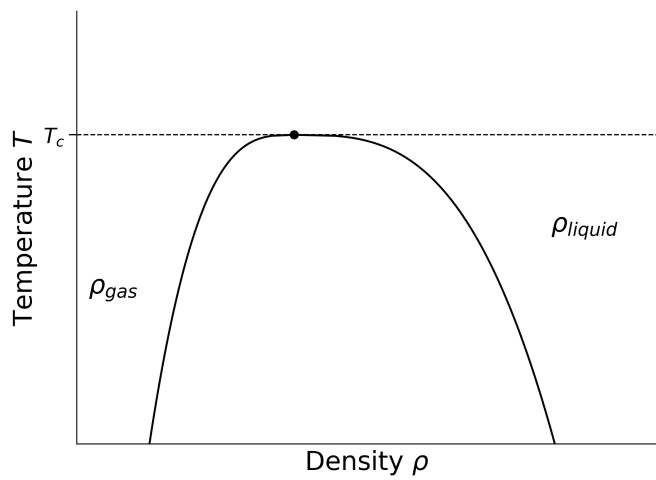


Figure 6.2: Schematic of the liquid-gas phase diagram in the $\rho - T$ plane for a realistic fluid .

Chapter 7

The Static Scaling Hypothesis

Historically, the first step towards properly elucidating near-critical behaviour was taken with the static scaling hypothesis. This is essentially a plausible conjecture concerning the origin of power law behaviour which appears to be consistent with observed phenomena. According to the hypothesis, the basis for power law behaviour (and associated scale invariance or “scaling”) in near-critical systems is expressed in the claim that: in the neighbourhood of a critical point, the basic thermodynamic functions (most notably the free energy) are *generalized homogeneous functions* of their variables. For such functions one can always deduce a scaling law such that by an appropriate change of scale, the dependence on two variables (e.g. the temperature and applied field) can be reduced to dependence on one new variable. This claim may be warranted by the following general argument.

A function of two variables $g(u, v)$ is called a generalized homogeneous function if it has the property

$$g(\lambda^a u, \lambda^b v) = \lambda g(u, v)$$

for all λ , where the parameters a and b (known as scaling parameters) are constants. An example of such a function is $g(u, v) = u^3 + v^2$ with $a = 1/3, b = 1/2$.

Now, the arbitrary scale factor λ can be redefined without loss of generality as $\lambda^a = u^{-1}$ giving

$$g(u, v) = u^{1/a} g(1, \frac{v}{u^{b/a}})$$

A corresponding relation is obtained by choosing the rescaling to be $\lambda^b = v^{-1}$.

$$g(u, v) = v^{1/b} g(\frac{u}{v^{a/b}}, 1)$$

This equation demonstrates that $g(u, v)$ indeed satisfies a simple power law in *one* variable, subject to the constraint that $u/v^{a/b}$ is a constant. It should be stressed, however, that such a scaling relation specifies neither the function g nor the parameters a and b .

Now, the static scaling hypothesis asserts that in the critical region, the free energy F is a generalized homogeneous function of the (reduced) thermodynamic fields $t = (T - T_c)/T_c$ and $h = (H - H_c)$. Remaining with the example ferromagnet, the following scaling assumption can then be made:

$$F(\lambda^a t, \lambda^b h) = \lambda F(t, h).$$

Without loss of generality, we can set $\lambda^a = t^{-1}$, implying $\lambda = t^{-1/a}$ and $\lambda^b = t^{-b/a}$.

Then

$$F(t, h) = t^{1/a} F(1, t^{-b/a} h)$$

where our choice of λ ensures that F on the rhs is now a function of a single variable $t^{-b/a} h$.

Now, as stated in Chapter 2, the free energy provides the route to all thermodynamic functions of interest. An expression for the magnetisation can be obtained simply by taking the field derivative of F (cf. Figure 2.1)

$$m(t, h) = -t^{(1-b)/a} m(1, t^{-b/a} h) \quad (7.1)$$

In zero applied field $h = 0$, this reduces to

$$m(t, 0) = (-t)^{(1-b)/a} m(1, 0)$$

where the r.h.s. is a power law in t . Equation 3.4 then allows identification of the exponent β in terms of the scaling parameters a and b .

$$\beta = \frac{1-b}{a}$$

By taking further appropriate derivatives of the free energy, other relations between scaling parameters and critical exponents may be deduced. Such calculations (*Exercise: try to derive them*) yield the results $\delta = b/(1-b)$, $\gamma = (2b-1)/a$, and $\alpha = (2a-1)/a$. Relationships between the critical exponents themselves can be obtained trivially by eliminating the scaling parameters from these equations. The principal results (known as “scaling laws”) are:-

$$\begin{aligned} \alpha + \beta(\delta + 1) &= 2 \\ \alpha + 2\beta + \gamma &= 2 \end{aligned}$$

Thus, provided all critical exponents can be expressed in terms of the scaling parameters a and b , then only two critical exponents need be specified, for all others to be deduced. Of course these scaling laws are also expected to hold for the appropriate thermodynamic functions of analogous systems such as the liquid-gas critical point.

7.1 Experimental Verification of Scaling

The validity of the scaling hypothesis finds startling verification in experiment. To facilitate contact with experimental data for real systems, consider again Equation 7.1. Eliminating the scaling parameters a and b in favour of the exponents β and δ gives

$$\frac{m(t, h)}{t^\beta} = m\left(1, \frac{h}{t^{\beta\delta}}\right)$$

where the RHS of this last equation can be regarded as a function of the single scaled variable $\tilde{H} \equiv t^{-\beta\delta} h(t, M)$.

For some particular magnetic system, one can perform an experiment in which one measures m vs h for various fixed temperatures. This allows one to draw a set of isotherms, i.e. $m-h$ curves of constant t . These can be used to demonstrate scaling by plotting the data against the scaling variables $M = t^{-\beta}m(t, h)$ and $\tilde{H} = t^{-\beta\delta}h(t, M)$. Under this scale transformation, it is found that all isotherms (for t close to zero) coincide to within experimental error. Reassuringly, similar results are found using the scaled equation of state of simple fluid systems such as He³ or Xe.

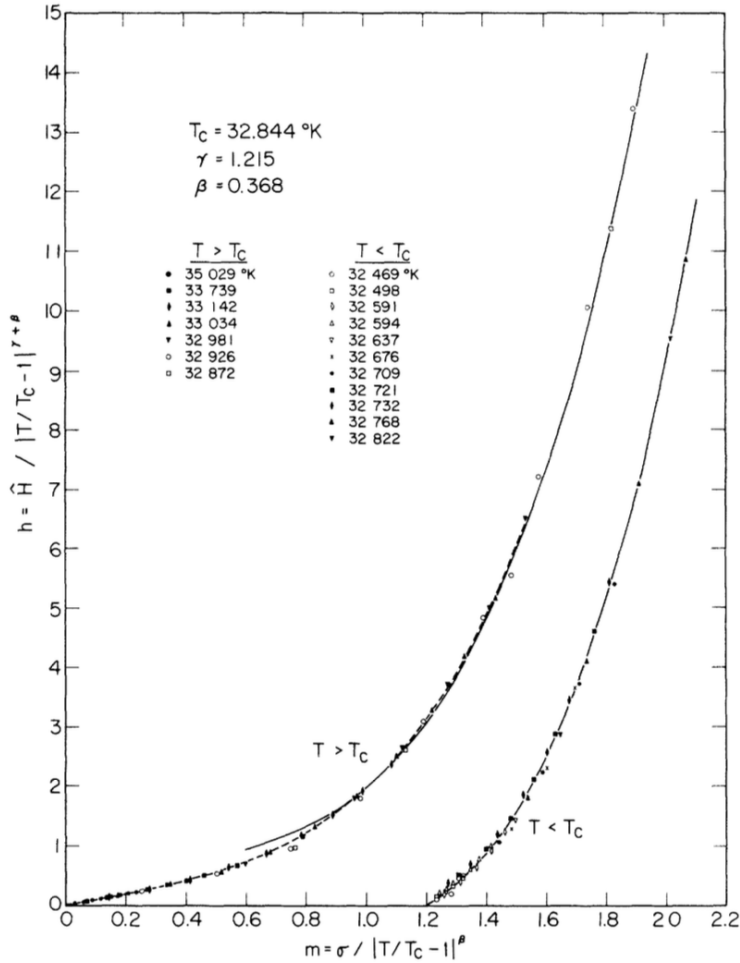


Figure 7.1: Magnetisation of CrBr₃ in the critical region plotted in scaled form (see text). From Ho and Lister (1969).

In summary, the static scaling hypothesis is remarkably successful in providing a foundation for the observation of power laws and scaling phenomena. However, it furnishes little or no guidance regarding the role of co-operative phenomena at the critical point. In particular it provides no means for calculating the values of the critical exponents appropriate to given model systems.

7.2 Computer simulation

In seeking to employ simulation to obtain estimates of bulk critical point properties (such as the location of a critical point and the values of its associated exponents), one is immediately confronted with a difficulty. The problem is that simulations are necessarily restricted to dealing with systems of finite-size and cannot therefore accommodate the truly long ranged fluctuations that characterize the near-critical regime. As a consequence, the critical singularities in C_v , order parameter, etc. appear rounded and shifted in a simulation study. Figure 7.2 shows a schematic example for the susceptibility of a magnet.

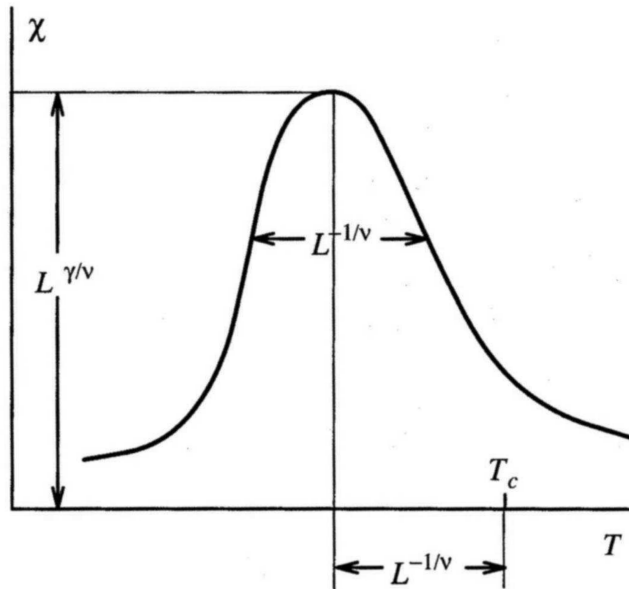


Figure 7.2: Schematic of the near-critical temperature dependence of the magnet susceptibility in a finite-sized system.

Thus the position of the peak in a response function (such as C_v) measured for a finite-sized system does not provide an accurate estimate of the critical temperature. Although the degree of rounding and shifting reduces with system size, it is often the case, that computational constraints prevent access to the largest system sizes which would provide accurate estimates of critical parameters. To help deal with this difficulty, finite-size scaling (FSS) methods have been developed to allow extraction of bulk critical properties from simulations of finite size. FSS will be discussed in Section 8.7

Chapter 8

Universality and the Renormalisation Group Theory of Critical Phenomena

Owing to the absence of a wholly appropriate textbook for the material covered in this section, I have supplied more detailed notes than used in other parts of the unit.

The critical region is characterised by correlated microstructure on *all* length-scales up to and including the correlation length. Such a profusion of degrees of freedom can only be accurately characterized by a very large number of variables. Mean field theories and approximation schemes fail in the critical region because they at best incorporate interactions among only a few spins, while neglecting correlations over larger distances. Similarly, the scaling hypothesis fails to provide more than a qualitative insight into the nature of criticality because it focuses on only one length-scale, namely the correlation length itself. Evidently a fuller understanding of the critical region may only be attained by taking account of the existence of structure on all length-scales. Such a scheme is provided by the renormalisation group method, which stands today as the cornerstone of the modern theory of critical phenomena.

8.1 The critical point: A many length scale problem

A near critical system can be characterized by three important length scales, namely

1. The correlation length, ξ , ie the size of correlated microstructure.
2. Minimum length scale L_{\min} , i.e. the smallest length in the microscopics of the problem, e.g. lattice spacing of a magnet or the particle size in a fluid.
3. Macroscopic size L_{\max} eg. size of the system.

The authentic critical region is defined by a window condition:

$$L_{\max} \gg \xi \gg L_{\min}$$

The physics of this regime is hard to tackle by analytic theory because it is characterized by configurational structure on all scales between L_{\min} and ξ (in fact it turns out that the near critical configurational patterns are *fractal-like*, cf. Figure 4.1b). Moreover different length scales are correlated with one another, giving rise to a profusion of coupled variables in any theoretical

description. The window regime is also not easily accessed by computer simulation because it entails studying very large system sizes L_{\max} , often requiring considerable computing resources.

8.2 Methodology of the RG

The central idea of the renormalisation group (RG) method is a stepwise elimination of the degrees of freedom of the system on successively larger length-scales. To achieve this one introduces a fourth length scale L . In contrast to the other three, which characterize the system itself, L characterises the *description* of the system. It may be thought of as typifying the size of the smallest resolvable detail in a description of the system's microstructure.

Consider the Ising model arrangements displayed in Figure 4.1. These pictures contain *all* the details of each configuration shown: the resolution length L in this case has its smallest possible value, coinciding with the lattice spacing i.e. $L = L_{\min}$. In the present context, the most detailed description is not the most useful: the essential signals with which we are concerned are hidden in a noise of relevant detail. A clue to eliminating this noise lies in the nature of the correlation length, i.e. the size of the largest droplets. The explicit form of the small scale microstructure is irrelevant to the behaviour of ξ . The small scale microstructure is the noise. To eliminate it, we simply select a larger value of the resolution length (or 'coarse-graining' length) L .

There are many ways of implementing this coarse-graining procedure. We adopt a simple strategy in which we divide our sample into blocks of side L , each of which contains L^d sites, with d the space dimensions. The centres of the blocks define a lattice of points indexed by $I = 1, 2, N/L^d$. We associate with each block lattice point centre, I , a coarse-grained or block variable $S_I(L)$ defined as the spatial average of the local variables it contains:

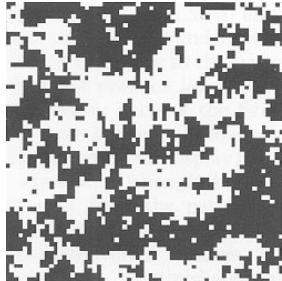
$$S_I(L) = L^{-d} \sum_i^I s_i \quad (8.1)$$

where the sum extends over the L^d sites in the block I . The set of coarse grained coordinates $\{S(L)\}$ are the basic ingredients of a picture of the system having spatial resolution of order L .

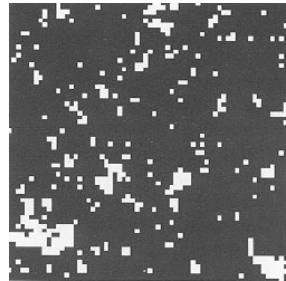
The coarse graining operation is easily implemented on a computer. In so doing one is faced with the fact that while the underlying Ising spins can only take two possible values, the block variables $S_I(L)$ have $L^d + 1$ possible values. Accordingly in displaying the consequences of the blocking procedure, we need a more elaborate colour convention than that used in Figure 4.1. We will associate with each block a shade of grey drawn from a spectrum ranging from black to white.

The results of coarse-graining configurations typical of three different temperatures are shown in Figure 8.1 and Figure 8.2. Two auxiliary operations are implicit in these results. The first operation is a *length scaling*: the lattice spacing on each blocked lattice has been scaled to the same size as that of the original lattice, making possible the display of correspondingly larger portions of the physical system. The second operation is a *variable scaling*: loosely speaking, we have adjusted the scale ('contrast') of the block variable so as to match the spectrum of block variable values to the spectrum of shades at our disposal.

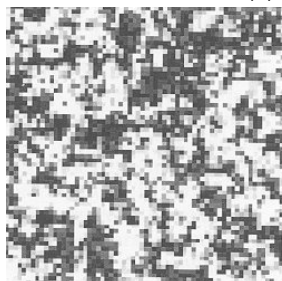
Consider first a system marginally above its critical point at a temperature T chosen so that the correlation length ξ is approximately 6 lattice spacing units. A typical arrangement (without coarse-graining) is shown in Figure 8.1(ai). The succeeding figures, Figure 8.1(aii) and Figure 8.1(aiii), show the result of coarse-graining with block sizes $L = 4$ and $L = 8$, respectively. A clear trend is apparent. The coarse-graining *amplifies* the consequences of the small



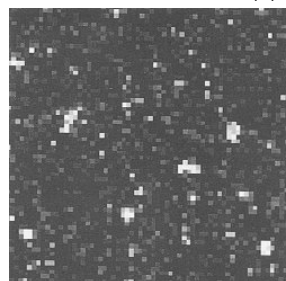
(a) (ai)



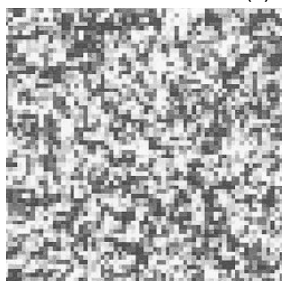
(b) (bi)



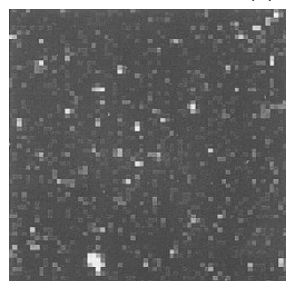
(c) (aii)



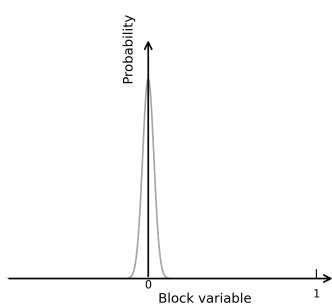
(d) (bii)



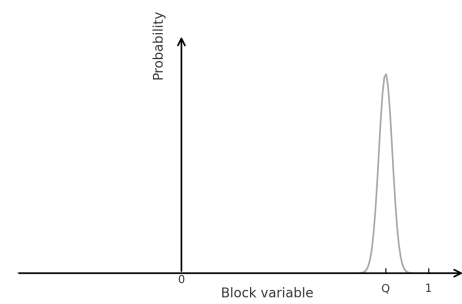
(e) (aiii)



(f) (biii)



(g) (aiv)



(h) (biv)

Figure 8.1: See text for details

deviation of T from T_c . As L is increased, the ratio of the size of the largest configurational features (ξ) to the size of the smallest (L) is reduced. The ratio ξ/L provides a natural measure of how ‘critical’ is a configuration. Thus the coarse-graining operation generates a representation of the system that is effectively less critical the larger the coarse-graining length. The limit point of this trend is the effectively fully disordered arrangement shown in Figure 8.1(aiii) and in an alternative form in Figure 8.1(av), which shows the limiting distribution of the coarse grained variables, averaged over many realizations of the underlying configurations: the distribution is a Gaussian which is narrow (even more so the larger the L value) and centred on zero. This limit is easily understood. When the system is viewed on a scaled L larger than ξ , the correlated microstructure is no longer explicitly apparent; each coarse-grained variable is essentially independent of the others.

A similar trend is apparent below the critical point. Figure 8.1(bi) show a typical arrangement at a temperature $T < T_c$ such that again ξ is approximately 6 lattice spacings. Coarse-graining with $L = 4$ and $L = 8$ again generates representations which are effectively less critical (Figure 8.1(bii) and (biii)). This time the coarse-graining smoothes out the microstructure which makes the order incomplete. The limit point of this procedure is a homogeneously ordered arrangement in which the block variables have a random (Gaussian) distribution centred on the order parameter (Figure 8.1(biv)).

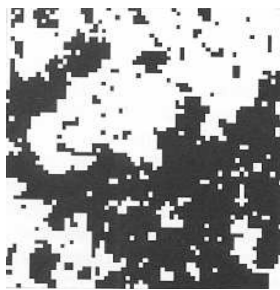
Consider now the situation *at* the critical point. Figure 8.2(ai) shows a typical arrangement; Figure 8.2(aii) and (aiii) show the results of coarse-graining with $L = 4$ and $L = 8$ respectively. Since the ξ is as large as the system itself the coarse graining does not produce less critical representations of the physical system: each of the figures displays structure over *all* length scales between the lower limit set by L and the upper limit set by the size of the display itself. A limiting trend is nevertheless apparent. Although the $L = 4$ pattern is qualitatively quite different from the pattern of the local variables, the $L = 4$ and $L = 8$ patterns display qualitatively similar features. These similarities are more profound than is immediately apparent. A statistical analysis of the spectrum of $L = 4$ configurations (generated as the local variables evolve in time) shows (Figure 8.2(iv)) that it is almost identical to that of the $L = 8$ configurations (given the block variable scaling). The implication of this limiting behaviour is clear: the patterns formed by the ordering variable at criticality look the same (in a statistical sense) when viewed on all sufficiently large length scales.

Let us summarize. Under the coarse-graining operation there is an evolution or *flow* of the system’s configuration spectrum. The flow tends to a limit, or fixed point, such that the pattern spectrum does not change under further coarse-graining. These scale-invariant limits have a trivial character for $T > T_c$, (a perfectly disordered arrangement) and $T < T_c$, (a perfectly ordered arrangement). The hallmark of the critical point is the existence of a scale-invariant limit which is neither fully ordered nor fully disordered but which possesses structure on all length scales. A nice illustration of critical point scale invariance in the Ising model can be viewed [here](#).

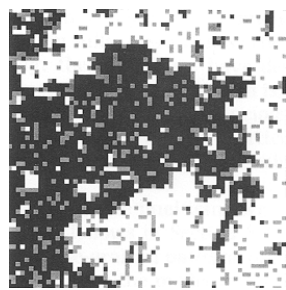
8.3 Universality and Scaling

Equipped with the coarse-graining technique, we now address the universality phenomenon. We aim to understand how it is that systems that are different microscopically can nevertheless display critical point behaviour which (in certain respects) is quantitatively identical.

To obtain initial insight we introduce a spin-1 Ising model in which the spins take on three values ($s_i = 1, 0, -1$), in contrast to the two values ($s_i = 1, -1$) of the spin-1/2 Ising model. The two models have properties which are different: for example, T_c for the three-state model is some 30% lower than that of the two-state model (for the same coupling J). However, there is abundant evidence that the two models have the same universal properties.



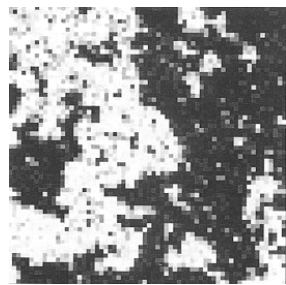
(a) (ai)



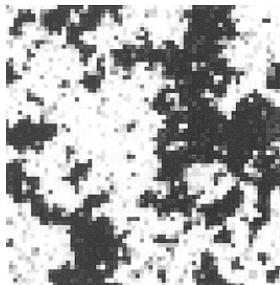
(b) (bi)



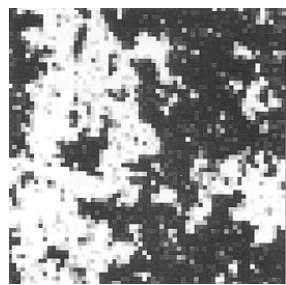
(c) (aii)



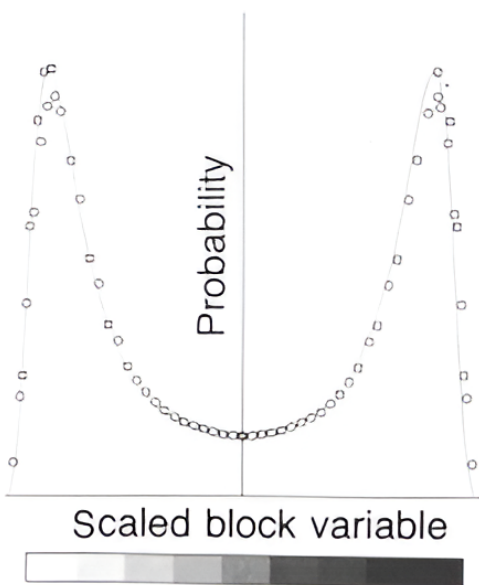
(d) (bii)



(e) (aiii)



(f) (biii)



(g) (iv)

Figure 8.2: See text for details

Let us explore what is the same and what is different in the configurations of the two models at criticality. The configurations of the local variables s_i are clearly qualitatively different for the two models. Now consider the coarse-grained configurations (with $L = 4$ and $L = 8$ respectively) for the three-state model at the critical point. We have already seen that the coarse-graining operation bears the configuration spectrum of the critical two-state Ising model to a non-trivial scale-invariant limit. It is scarcely surprising that the same is true for the three-state model. What is remarkable is that the two limits are the same! This is expressed in Figure 8.2(iv), which shows the near coincidence of the distribution of block variables (grey-levels) for the two different coarse-graining lengths. Thus the coarse-graining erases the physical differences apparent in configurations where the local behaviour is resolvable, and exposes a profound configurational similarity.

8.3.1 Fluid-magnet universality

Let us now turn to fluid-magnet universality. In a magnet, the relevant configurations are those formed by the coarse-grained magnetisation (the magnetic moment averaged over a block of side L). In a fluid, the relevant configurations are those of the coarse-grained density (the mass averaged over a block of side L) or more precisely, its fluctuation from its macroscopic average (Figure 8.3). The patterns in the latter (bubbles of liquid or vapour) may be matched to pattern in the former (microdomains of the magnetisation), given appropriate scaling operations to camouflage the differences between the length scales and the differences between the variable scales.

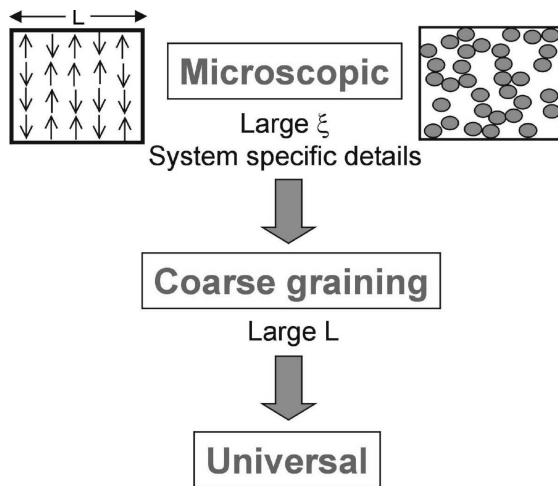


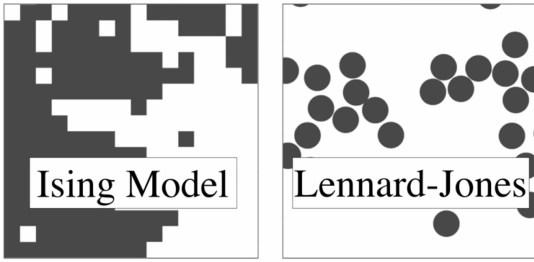
Figure 8.3: Schematic representation of the coarse graining operation via which the universal properties of fluids and magnets may be exposed.

The results is illustrated in Figure 8.4.

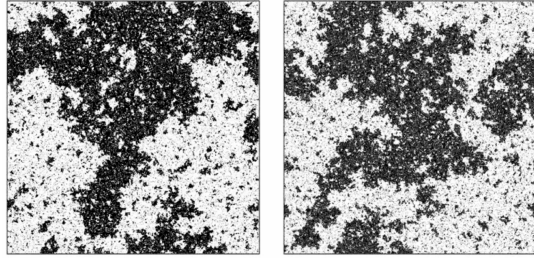
A movie in which we progressively zoom out shows how the loss of microscopic details reveals the large lengthscale universal features. [Movies/universality.mov](#)

8.4 Near critical scaling

The similarity of coarse-grained configurations of different systems is not restricted to the critical temperature itself. Suppose we have a two state spin model and a three state spin model each somewhat above their critical points at reduced temperature t . The two systems will have



(a) 2D critical Ising model and 2d critical Lennard-Jones fluid at small lengthscales



(b) Same models as above, but viewed at large lengthscales

Figure 8.4: Snapshot configurations of the 2D critical Ising model (left) and the 2D critical Lennard-Jones fluid (right). When viewed on sufficiently large length scales the configurational patterns appear universal and self similar.

somewhat different correlation lengths, ξ_1 and ξ_2 say. Suppose however, we choose coarse-graining lengths L_1 for L_2 for the two models such that $\xi_1/L_1 = \xi_2/L_2$. We adjust the scales of the block variables (our grey level control) so that the typical variable value is the same for the two systems. We adjust the length scale of the systems (stretch or shrink our snapshots) so that the sizes of the minimum-length-scale structure (set by L_1 and L_2) looks the same for each system. Precisely what they look like depends upon our choice of ξ/L .

8.5 Universality classes

Coarse graining does not erase all differences between the physical properties of critical systems. Differences in the space dimension d of two critical systems will lead to different universal properties such as critical exponents. Thus, for instance, the critical exponents of the 2D magnet, match those of the 2d fluid, but they are different to those of 3d magnets and fluids.

	$d = 2$	$d = 3$
Critical temperature	0.5673	0.75
Order parameter exponent β	$\frac{1}{8}$	0.325 ± 0.001
Susceptibility exponent γ	$\frac{7}{4}$	1.24 ± 0.001
Correlation length exponent ν	1	0.63 ± 0.001

In fact the space dimension is one of a small set of qualitative features of a critical system which are sufficiently deep-seated to survive coarse graining and which together serve to define the system's universal behaviour, or *universality class*. The constituents of this set are not all identifiable *a priori*. They include the number of components n of the order parameter. Up to

now, we have only considered order parameters which are scalar (for a fluid the density, for a magnet the magnetisation), for which $n = 1$. In some ferromagnets, the order parameter may have components along two axes, or three axes, implying a vector order parameter, with $n = 2$ (the so-called XY model) or $n = 3$ (Heisenberg model), respectively. It is clear that the order-parameter n -value will be reflected in the nature of the coarse-grained configurations, and thus in the universal observables they imply.

A third important feature which can change the universality class of a critical system is the range of the interaction potential between its constituent particles. Clearly for the Ising model, interactions between spins are inherently nearest neighbour in character. Most fluids interact via dispersion forces (such as the Lennard-Jones potential) which is also short ranged owing to the r^{-6} attractive interaction. However some systems have much longer ranged interactions. Notable here are systems of charged particles which interact via a Coulomb potential. The long ranged nature of the Coulomb potential (which decays like r^{-1}) means that charged systems often do not have the same critical exponents as the Ising model and fluid.

8.6 Critical exponents

We consider now how the critical exponents, may be computed via the coarse-graining procedure. In what follows we will refer only to the behaviour of a single typical coarse grained variable, which we shall denote $S(L)$. We suppose that t is sufficiently small that $\xi \gg L_{\min}$. Universality and scaling may be expressed in the claim that, for *any* L and t , scale factors $a(L)$ and $b(L)$ may be found such that the probability distribution $p(S(L), t)$ can be written in the form

$$p(S(L), t) = b(L)\tilde{p}(b(L)S(L), a(L)t) \quad (8.2)$$

where \tilde{p} is a function unique to a universality class. The role of the scale factors a and b is to absorb the basic non-universal scales identified in Section 8.2. The critical exponents are implicit in the L -dependence of these scale factors. Specifically one finds:

$$\begin{aligned} a(L) &= a_0 L^{1/\nu} \\ b(L) &= b_0 L^{\beta/\nu} \end{aligned} \quad (8.3)$$

where the amplitudes a_0 and b_0 are system specific (non-universal) constants.

These results state that the critical exponents (in the form $1/\nu$ and β/ν) characterize the ways in which the configuration spectrum evolves under coarse-graining. Consider, first the exponent ratio β/ν . Precisely at the critical point, there is only one way in which the coarse-grained configurations change with L : the overall scale of the coarse-grained variable (the black-white contrast in our grey scale representation) is eroded with increasing L . Thus the configurations of coarse-graining length L_1 match those of a larger coarse-graining length L_2 only if the variable scale in the latter configurations is amplified. The required amplification follows from Equation 8.2 and Equation 8.3: it is

$$\frac{b(L_2)}{b(L_1)} = \left(\frac{L_2}{L_1} \right)^{\beta/\nu}.$$

The exponent ratio β/ν thus controls the rate at which the scale of the ordering variable decays with increasing coarse-graining length.

Consider now the exponent $1/\nu$. For small but non-zero reduced temperature (large but finite ξ) there is second way in which the configuration spectrum evolves with L . As noted previously, coarse graining reduces the ratio of correlation length to coarse-graining length, and results in configurations with a less critical appearance. More precisely, we see from Equation 8.2 that increasing the coarse graining length from L_1 to L_2 while keeping the reduced temperature constant has the same effect on the configuration spectrum as keeping coarse-graining length constant which amplifying the reduced temperature t by a factor

$$\frac{a(L_2)}{a(L_1)} = \left(\frac{L_2}{L_1}\right)^{1/\nu}.$$

One may think of the combination $a(L)t$ as a measure of the effective reduced temperature of the physical system viewed with resolution length L . The exponent $1/\nu$ controls the rate at which the effective reduced temperature flows with increasing coarse-graining length.

8.7 Finite-size scaling

We can exploit the fact that the scale factors $a(L)$ and $b(L)$ depend on critical exponents to estimate the values of these exponents using computer simulation. Consider the average of the block variable $S(L)$. Consideration of Equation 8.1 shows that this is non other than the value of the order parameter Q , measured over a block of side L . Thus from the definition of an average

$$Q(L, t) = \bar{S}(L, t) = \int S(L)p(S(L), t)dS(L)$$

where $p(S(L))$ is the probability distribution of $S(L)$.

Making use of the representation of Equation 8.2, we then have that

$$Q(L, t) = \int b(L)S(L)\tilde{p}(b(L)S(L), a(L)t)dS(L)$$

To integrate this we need to change the integration variable from $S(L)$ to $b(L)S(L)$. We have $d(b(L)S(L)) = b(L)dS(L)$ since $b(L)$ does not fluctuate. Thus

$$\begin{aligned} Q(L, t) &= b^{-1}(L) \int b(L)S(L)\tilde{p}(b(L)S(L), a(L)t)d(b(L)S(L)) \\ &= b^{-1}(L)f(a(L)t) \\ &= b_0 L^{-\beta/\nu} f(a_0 L^{1/\nu} t) \end{aligned}$$

where f is a universal function (defined as the first moment of $\tilde{p}(x, y)$ with respect to y).

The above results provide a method for determining the critical exponent ratios β/ν and $1/\nu$ via computer simulations of near critical systems. For instance, at the critical point ($t = 0$) and for finite block size, $Q(L, 0)$ will not be zero (the T at which Q vanishes for finite L is above the true T_c , cf. Section 7.2). However, we know that its value must vanish in the limit of infinite L ; it does so like

$$Q(L, 0) = b_0 L^{-\beta/\nu} f(0) \equiv Q_0 L^{-\beta/\nu}$$

Thus by studying the critical point L dependence of Q we can estimate β/ν . A similar approach in which we study two block sizes L , and tune t separately in each case so that the results for $QL^{\beta/\nu}$ are identical provides information on the value of $1/\nu$.

8.8 Summary of main points

As this is quite a long chapter let us summarise the main points:

- **Limitations of conventional theories:** Mean field theories and the scaling hypothesis are insufficient in the critical region due to their neglect of correlations across all relevant length scales.
- **Critical region characteristics:** Near-critical systems exhibit correlated microstructure on all length scales up to the correlation length. The complexity of this structure makes both analytical and computational study challenging.
- **Relevant length scales:**
 1. Correlation length (ξ)
 2. Minimum microscopic scale (L_{\min})
 3. Macroscopic system size (L_{\max})
- **Window Condition for criticality:** The true critical regime satisfies $L_{\max} \gg \xi \gg L_{\min}$, encompassing a broad range of scales where complex, often fractal-like, structures are present.
- **Renormalisation Group (RG) methodology:** RG involves the stepwise elimination of degrees of freedom by coarse-graining the system over increasing length scales. A fourth scale, L , represents the resolution at which the system is described.
- **Effect of coarse-graining:** Coarse-graining changes the effective reduced temperature, captured by the relation $a(L)t$, where $a(L)$ scales with L as $L^{1/\nu}$. This helps describe how critical configurations evolve with resolution.
- **Universality:**
 - Coarse-graining reveals that microscopically different systems can exhibit identical critical behavior when observed at large scales.
 - The concept of universality explains why disparate systems, such as magnets and fluids, can show the same critical exponents and scaling laws.
 - Critical behavior depends primarily on general features like dimensionality and symmetry, rather than microscopic details.
- **Finite-Size scaling:**
 - The average block variable $Q(L, t)$ is related to block size L and reduced temperature t through scaling relations. Computer simulations exploit this to extract scaling functions and the values of critical exponents.

8.9 Addendum: The effective coupling viewpoint of the renormalization group (non examinable)

🔥 Notes for those interested in a different perspective on RG theory.

Let us begin by returning to our fundamental Equation 2.1, which we rewrite as

$$p = Z^{-1} e^{-H}$$

where $H \equiv E/k_B T$.

The first step is then to imagine that we generate, by a computer simulation procedure for example, a sequence of configurations with relative probability $\exp(-H)$. We next adopt some coarse-graining procedure which produces from these original configurations a set of coarse-grained configurations. We then ask the question: what is the energy function H' of the coarse-grained variables which would produce these coarse-grained configurations with the correct relative probability $\exp(-H')$? Clearly the form of H' depends on the form of H thus we can write symbolically

$$H' = R(H)$$

The operation R , which defines the coarse-grained configurational energy in terms of the microscopic configurational energy function is known as a renormalisation group transformation (RG). What it does is to replace a hard problem by a less hard problem. Specifically, suppose that our system is near a critical point and that we wish to calculate its large-distance properties. If we address this task by utilizing the configurational energy and appealing to the basic machinery of statistical mechanics set out in Equation 2.1 and Equation 2.2, the problem is hard. It is hard because the system has fluctuations on all the (many) length scales intermediate between the correlation length ξ and the minimum length scale L_{\min} .

However, the task may instead be addressed by tackling the coarse-grained system described by the energy H' . The large-distance properties of this system are the same as the large-distance properties of the physical system, since coarse-graining operation preserves large-scale configurational structure. In this representation the problem is a little easier: while the ξ associated with H' is the same as the ξ associated with H , the minimum length scale of H' is bigger than that of H . Thus the statistical mechanics of H' poses a not-quite-so-many-length-scale problem, a problem which is effectively a little less critical and is thus a little easier to solve. The benefits accruing from this procedure may be amplified by repeating it. Repeated application of R will eventually result in a coarse-grained energy function describing configurations in which the ξ is no bigger than the minimum length scale. The associated system is far from criticality and its properties may be reliably computed by any of a wide variety of approximation schemes. These properties are the desired large-distance properties of the physical system. As explicit reference to fluctuations of a given scale is eliminated by coarse-graining, their effects are carried forward implicitly in the parameters of the coarse-grained energy.

In order to setup the framework for a simple illustrative example, let us return to the lattice Ising model for which the energy function depended only on the product of nearest neighbour spins. The coefficient of this product in the energy is the exchange coupling, J . In principle, however, other kinds of interactions are also allowed; for example, we may have a product of second neighbour spins with strength J_2 or, perhaps, a product of four spins (at sites forming a square whose side is the lattice spacing), with strength J_3 . Such interactions in a real magnet have their origin in the quantum mechanics of the atoms and electrons and clearly depend upon the details of the system. For generality

therefore we will allow a family of exchange couplings J_1, J_2, J_3, \dots , or $J_a, a = 1, 2, \dots$. In reduced units, the equivalent coupling strengths are $K_a = J_a/k_B T$. Their values determine uniquely the energy for any given configuration.

We note that it is not only useful to allow for arbitrary kinds of interactions: if we wish to repeat the transformation several (indeed many) times, it is also necessary because even if we start with only the nearest neighbour coupling in H the transformation will in general produce others in H' .

Now consider the coarse-graining procedure. Let us suppose that this procedure takes the form of a ‘majority rule’ operation in which the new spins are assigned values +1 or -1 according to the signs of the magnetic moments of the blocks with which they are associated. The new energy function H' will be expressible in terms of some new coupling strengths K' describing the interactions amongst the new spin variables (and thus, in effect, the interactions between blocks of the original spin variables). The RGT simply states that these new couplings depend on the old couplings: K'_1 is some function f_1 of all the original couplings, and generally

$$K'_a = f_a(K_1, K_2, \dots) = f_a(\mathbf{K}), \quad a = 1, 2, \dots \quad (8.4)$$

where \mathbf{K} is shorthand for the set K_1, K_2, \dots

8.9.1 A simple example

This example illustrates how one can perform the RG transformation Equation 9.1 directly, without recourse to a ‘sequence of typical configurations’. The calculation involves a very crude approximation which has the advantage that it simplifies the subsequent analysis.

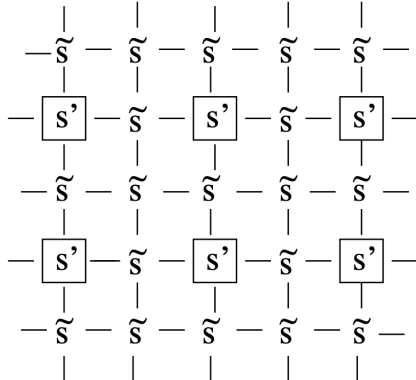


Figure 8.5: Coarse graining by decimation. The spins on the original lattice are divided into two sets $\{s'\}$ and $\{\tilde{s}\}$. The $\{s'\}$ spins occupy a lattice whose spacing is twice that of the original. The effective coupling interaction between the $\{s'\}$ spins is obtained by performing the configurational average over the $\{\tilde{s}\}$

Consider an Ising model in two dimensions, with only nearest neighbour interactions as shown in Figure 9.1. We have divided the spins into two sets, the spins $\{s'\}$ form a square lattice of spacing 2, the others being denoted by $\{\tilde{s}\}$. One then defines an effective energy function H' for the s' spins by performing an average over all the possible arrangements of the \tilde{s} spins

$$\exp(-H') = \sum_{\{\tilde{s}\}} \exp(-H). \quad (8.5)$$

This particular coarse-graining scheme is called ‘decimation’ because a certain fraction (not necessarily one-tenth!) of spins on the lattice is eliminated. This formulation of a new energy function realizes two basic aims of the RG method: the long-distance physics of the ‘original’ system, described by H , is contained in that of the ‘new’ system, described by H' (indeed the partition functions are the same as one can see by summing both sides over s') and the new system is further from critically because the ratio of ξ to lattice spacing (‘minimum length scale’) has been reduced by a factor of $1/2$ (the ratio of the lattice spacings of the two systems). We must now face the question of how to perform the configuration sum in Equation 9.2. This cannot in general be done exactly, so we must resort to some approximation scheme. The particular approximation which we invoke is the high temperature series expansion. In its simplest mathematical form, since H contains a factor $1/k_B T$, it involves the expansion of $\exp(-H)$ as a power series:

$$\exp(-H/k_B T) = 1 - H/k_B T + \frac{1}{2!}(H/k_B T)^2 + \dots$$

We substitute this expansion into the right hand side of Equation 9.2 and proceed to look for terms which depend on the s' spins after the sum over the possible arrangements of the \tilde{s} spins is performed. This sum extends over all the possible (± 1) values of all the \tilde{s} spins. The first term (the 1) in the expansion of the exponential is clearly independent of the values of the s' spins. The second term (H) is a function of the s' spins, but gives zero when the sum over the s' spins is performed because only a single factor of any s' ever appears, and $+1 - 1 = 0$. The third term ($H^2/2$) does contribute. If one writes out explicitly the form of $H^2/2$ one finds terms of the form $K^2 s'_1 \tilde{s} s'_2 = K^2 s'_1 s'_2$, where s'_1 and s'_2 denote two spins at nearest neighbour sites on the lattice of s' spins and \tilde{s} is the spin (in the other set) which lies between them. Now, in the corresponding expansion of the left hand side of Equation 9.2, we find terms of the form $K' s'_1 s'_2$, where K' is the nearest neighbour coupling for the s' spins. We conclude (with a little more thought than we detail here) that

$$K' = K^2 \quad (8.6)$$

Of course many other terms and couplings are generated by the higher orders of the high temperature expansion and it is necessary to include these if one wishes reliable values for the critical temperature and exponents. However, our aim here is to use this simple calculation to illustrate the RG method. Let us therefore close our eyes, forget about the higher order terms and show how the RGT Equation 9.3 can be used to obtain information on the phase transition.

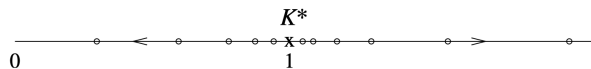


Figure 8.6: Coupling flow under the decimation transformation described in the text.

The first point to note is that that mathematically Equation 9.3 has the fixed point $K^* = 1$; if $K = 1$ then the new effective coupling K' has the same value 1. Further, if K is just larger than 1, then K' is larger than K , i.e. further away from 1. Similarly, if K is less than 1, K' is less than K . We say that the fixed point is unstable: the flow of couplings under repeated iteration of Equation 9.3 is away from the fixed point, as illustrated in Figure 9.2.

The physical significance of this is as follows: suppose that the original system is at its critical point so that the ratio of ξ to lattice spacing is infinite. After one application of the decimation transformation, the effective lattice spacing has increased by a factor of two, but this ratio remains infinite; the new system is therefore also at its critical point. Within the approximations inherent in Equation 9.3, the original system is an Ising model with nearest neighbour coupling K and the new system is an Ising model with nearest neighbour coupling K' . If these two systems are going to be at a common criticality, we must identify $K' = K$. The fixed point $K^* = 1$ is therefore a candidate for the critical point K_c , where the phase transition occurs. This interpretation is reinforced by considering the case where the original system is close to, but not at, criticality. Then ξ is finite and the new system is further from critically because the ratio of ξ to lattice spacing is reduced by a factor of two. This instability of a fixed point to deviations of K from K^* is a further necessary condition for its interpretation as a critical point of the system. In summary then we make the prediction

$$K_c = J/k_B T_c = 1 \quad (8.7)$$

We can obtain further information about the behaviour of the system close to its critical point. In order to do so, we rewrite the transformation (Equation 9.3) in terms of the deviation of the coupling from its fixed point value. A Taylor expansion of the function $K' = K^2$ yields

$$\begin{aligned} K' &= (K^*)^2 + (K - K^*) \left. \frac{\partial K'}{\partial K} \right|_{K=K^*} + \frac{1}{2} (K - K^*)^2 \left. \frac{\partial^2 K'}{\partial K^2} \right|_{K=K^*} + \dots \\ K' - K^* &= 2(K - K^*) + (K - K^*)^2 \end{aligned}$$

where in the second line we have used the fact that the first derivative evaluates to $2K^* = 2$ and $(K^*)^2 = K^*$.

For a system sufficiently close to its critical temperature the final term can be neglected. The deviation of the coupling from its fixed point (critical) value is thus bigger for the new system than it is for the old by a factor of two. This means that the reduced temperature is also bigger by a factor of two:

$$t' = 2t$$

But ξ (in units of the appropriate lattice spacing) is smaller by a factor of $1/2$:

$$\xi' = \xi/2$$

Thus, when we double t , we halve ξ , implying that

$$\xi \propto t^{-1}$$

for T close to T_c . Thus we see that the RGT predicts scaling behaviour with calculable critical exponents. In this simple calculation we estimate the critical exponent $\nu = 1$ for the square lattice Ising model. This prediction is actually in agreement with the exactly established value. The agreement is fortuitous- the prediction in Eq. refeq:Kc for K_c is larger than the exactly established value by a factor of more than two. In order to obtain reliable estimates more sophisticated and systematic methods must be used.

The crude approximation in the calculation above produced a transformation, Equation 9.3, involving only the nearest neighbour coupling, with the subsequent advantages of simple algebra. We pay a penalty for this simplicity in two ways: the results obtained for critical properties are in rather poor agreement with accepted values, and we gain no insight into the origin of universality.

8.9.2 Universality and scaling

In order to expose how universality can arise, we should from the start allow for several different kinds of coupling J_a , and show how the systems with *different* J_a can have the *same* critical behaviour.

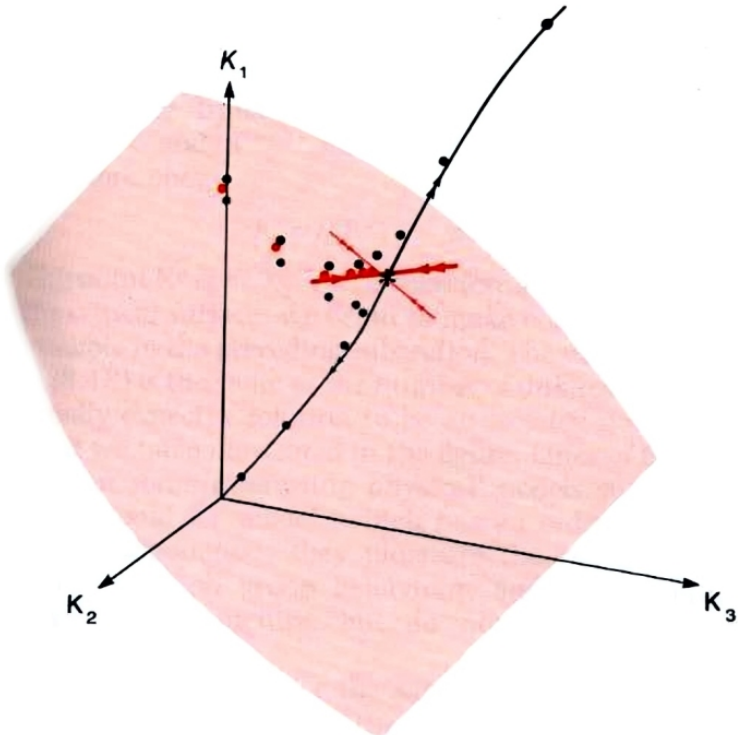


Figure 8.7: General flow in coupling space

Figure 9.3 is a representation of the space of all coupling strengths K_a in the energy function $H/k_B T$. This is of course actually a space of infinite dimension, but representing three of these, as we have done, enables us to illustrate all the important aspects. First let us be clear what the points in this space represent. Suppose we have some magnetic material which is described by a given set of exchange constants J_1, J_2, J_3, \dots . As the temperature T varies, the coupling strengths $K_a = J_a/k_B T$ trace out a straight line, or ray, from the origin of the space in the direction (J_1, J_2, J_3, \dots) . Points on this ray close to the origin represent this magnet at high temperatures, and conversely points far from the origin represent the magnet at low temperatures. The critical point of the magnet is represented by a specific point on this ray, $K_a = J_a/k_B T, a = 1, 2, \dots$. The set of critical points on all of the possible rays forms a *surface*, the critical surface. Formally, it is defined by the set of all possible models (of the Ising type) which have infinite ξ . It is shown schematically as the shaded surface in Figure 9.3. (In the figure it is a two-dimensional surface; more generally it has one dimension less than the full coupling constant space, dividing all models into high and low temperature phases.)

Our immediate goal then is to understand how the RGT can explain why different physical systems near this critical surface have the same behaviour. Let us turn now to the schematic representation of the RG flow in Figure 9.3. Suppose we start with a physical

system, with coupling strengths $K_a, a = 1, 2, \dots$. What the RGT does is generate a new point in the figure, at the coupling strengths $K_a^{(1)} = f_a(\mathbf{K})$; these are the couplings appearing in the effective energy function describing the coarse-grained system. If we repeat the transformation, the new energy function has coupling strengths $K_a^{(2)} = f_a(\mathbf{K})$. Thus repeated application of the transformation generates a flow of points in the figure: $\mathbf{K} \rightarrow \mathbf{K}^{(1)} \rightarrow \dots \rightarrow \mathbf{K}^{(n)}$ where the superscript (n) labels the effective couplings after n coarse-graining steps. If the change in coarse-graining scale is $b (> 1)$ at each step, the total change in coarse-graining scale is b^n after n steps. In the process, therefore, the ratio of ξ to coarse-graining scale is reduced by a factor of b^{-n} . The dots in Figure 9.3 identify three lines of RG flow starting from three systems differing only in their temperature. (The flow lines are schematic but display the essential features revealed in detailed calculations.)

Consider first the red dots which start from the nearest neighbour Ising model at its critical point. The ratio of ξ to coarse-graining scale is reduced by a factor b at each step, but, since it starts infinite, it remains infinite after any finite number of steps. In this case we can in principle generate an unbounded number of dots, $\mathbf{K}^{(1)}, \mathbf{K}^{(2)}, \dots, \mathbf{K}^{(n)}$, all of which lie in the critical surface. The simplest behaviour of such a sequence as n increases is to tend to a limit, K^* , say. In such a case

$$K_a^* = f_a(K^*) \quad a = 1, 2, \dots$$

This point $\mathbf{K}^* \equiv K_1^*, K_2^*, \dots$ is therefore a *fixed point* which lies in the critical surface. By contrast, consider the same magnet as before, now at temperature T just greater than T_c , its couplings K_a , will be close to the first red dot (in fact they will be slightly smaller) and so will the effective couplings $K_a^{(1)}, K_a^{(2)}, \dots$ of the corresponding coarse-grained systems. The new flow will therefore appear initially to follow the red dots towards the same fixed point. However, the flow must eventually move away from the fixed point because each coarse-graining now produces a model further from criticality. The resulting flow is represented schematically by one set of black dots. The other set of black dots shows the expected flow starting from the same magnet slightly below its critical temperature.

We are now in a position to understand both universality and scaling within this framework. We will suppose that there exists a single fixed point in the critical surface which sucks in all flows starting from a point in that surface. Then any system at its critical point will exhibit large-length scale physics (large-block spin behaviour) described by the single set of fixed point coupling constants. The uniqueness of this limiting set of coupling constants is the essence of critical point universality. It is, of course, the algebraic counterpart of the unique limiting spectrum of coarse-grained configurations, discussed in Section 8.5. Similarly the scale-invariance of the critical point configuration spectrum (viewed on large enough length scales) is expressed in the invariance of the couplings under iteration of the transformation (after a number of iterations large enough to secure convergence to the fixed point).

To understand the behaviour of systems near but not precisely at critically we must make a further assumption (again widely justified by explicit studies). The flow line stemming from any such system will, we have argued, be borne towards the fixed point before ultimately deviating from it after a number of iterations large enough to expose the system's noncritical character. We assume that (as indicated schematically in the streams of red and blue lines in Figure 9.3) the deviations lie along a single line through the fixed point, the direction followed along this line differing according to the sign of the temperature deviation $T - T_c$. Since any two sets of coupling constants on the line (on the same side of the fixed point) are related by a suitable coarse-graining operation, this picture implies

that the large-length-scale physics of all near-critical systems differs only in the matter of a length scale. This is the essence of near-critical point universality.

Chapter 9

The renormalisation group: effective coupling viewpoint

Let us begin by returning to our fundamental Equation 2.1, which we rewrite as

$$p = Z^{-1} e^{-H}$$

where $H \equiv E/k_B T$.

The first step is then to imagine that we generate, by a computer simulation procedure for example, a sequence of configurations with relative probability $\exp(-H)$. We next adopt some coarse-graining procedure which produces from these original configurations a set of coarse-grained configurations. We then ask the question: what is the energy function H' of the coarse-grained variables which would produce these coarse-grained configurations with the correct relative probability $\exp(-H')$? Clearly the form of H' depends on the form of H thus we can write symbolically

$$H' = R(H)$$

The operation R , which defines the coarse-grained configurational energy in terms of the microscopic configurational energy function is known as a renormalisation group transformation (RGT). What it does is to replace a hard problem by a less hard problem. Specifically, suppose that our system is near a critical point and that we wish to calculate its large-distance properties. If we address this task by utilizing the configurational energy and appealing to the basic machinery of statistical mechanics set out in Equation 2.1 and Equation 2.2, the problem is hard. It is hard because the system has fluctuations on all the (many) length scales intermediate between the correlation length ξ and the minimum length scale L_{\min} .

However, the task may instead be addressed by tackling the coarse-grained system described by the energy H' . The large-distance properties of this system are the same as the large-distance properties of the physical system, since coarse-graining operation preserves large-scale configurational structure. In this representation the problem is a little easier: while the ξ associated with H' is the same as the ξ associated with H , the minimum length scale of H' is bigger than that of H . Thus the statistical mechanics of H' poses a not-quite-so-many-length-scale problem, a problem which is effectively a little less critical and is thus a little easier to solve. The benefits accruing from this procedure may be amplified by repeating it. Repeated application of R will eventually result in a coarse-grained energy function describing configurations in which the ξ is no bigger than the minimum length scale. The associated system is far

from criticality and its properties may be reliably computed by any of a wide variety of approximation schemes. These properties are the desired large-distance properties of the physical system. As explicit reference to fluctuations of a given scale is eliminated by coarse-graining, their effects are carried forward implicitly in the parameters of the coarse-grained energy.

In order to setup the framework for a simple illustrative example, let us return to the lattice Ising model for which the energy function depended only on the product of nearest neighbour spins. The coefficient of this product in the energy is the exchange coupling, J . In principle, however, other kinds of interactions are also allowed; for example, we may have a product of second neighbour spins with strength J_2 or, perhaps, a product of four spins (at sites forming a square whose side is the lattice spacing), with strength J_3 . Such interactions in a real magnet have their origin in the quantum mechanics of the atoms and electrons and clearly depend upon the details of the system. For generality therefore we will allow a family of exchange couplings J_1, J_2, J_3, \dots , or $J_a, a = 1, 2, \dots$. In reduced units, the equivalent coupling strengths are $K_a = J_a/k_B T$. Their values determine uniquely the energy for any given configuration.

We note that it is not only useful to allow for arbitrary kinds of interactions: if we wish to repeat the transformation several (indeed many) times, it is also necessary because even if we start with only the nearest neighbour coupling in H the transformation will in general produce others in H' .

Now consider the coarse-graining procedure. Let us suppose that this procedure takes the form of a ‘majority rule’ operation in which the new spins are assigned values +1 or -1 according to the signs of the magnetic moments of the blocks with which they are associated. The new energy function H' will be expressible in terms of some new coupling strengths K' describing the interactions amongst the new spin variables (and thus, in effect, the interactions between blocks of the original spin variables). The RGT simply states that these new couplings depend on the old couplings: K'_1 is some function f_1 of all the original couplings, and generally

$$K'_a = f_a(K_1, K_2, \dots) = f_a(\mathbf{K}), \quad a = 1, 2, \dots \quad (9.1)$$

where \mathbf{K} is shorthand for the set K_1, K_2, \dots

9.1 A simple example

This example illustrates how one can perform the RG transformation Equation 9.1 directly, without recourse to a ‘sequence of typical configurations’. The calculation involves a very crude approximation which has the advantage that it simplifies the subsequent analysis.

Consider an Ising model in two dimensions, with only nearest neighbour interactions as shown in Figure 9.1. We have divided the spins into two sets, the spins $\{s'\}$ form a square lattice of spacing 2, the others being denoted by $\{\tilde{s}\}$. One then defines an effective energy function H' for the s' spins by performing an average over all the possible arrangements of the \tilde{s} spins

$$\exp(-H') = \sum_{\{\tilde{s}\}} \exp(-H). \quad (9.2)$$

This particular coarse-graining scheme is called ‘decimation’ because a certain fraction (not necessarily one-tenth!) of spins on the lattice is eliminated. This formulation of a new energy function realizes two basic aims of the RG method: the long-distance physics of the ‘original’ system, described by H , is contained in that of the ‘new’ system, described by H' (indeed the partition functions are the same as one can see by summing both sides over s') and the new system is further from criticality because the ratio of ξ to lattice spacing (‘minimum length

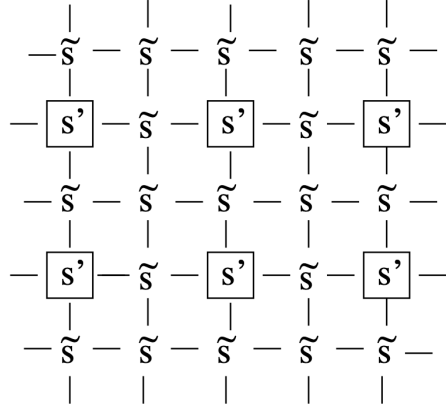


Figure 9.1: Coarse graining by decimation. The spins on the original lattice are divided into two sets $\{s'\}$ and $\{\tilde{s}\}$. The $\{s'\}$ spins occupy a lattice whose spacing is twice that of the original. The effective coupling interaction between the $\{s'\}$ spins is obtained by performing the configurational average over the $\{\tilde{s}\}$

scale') has been reduced by a factor of $1/2$ (the ratio of the lattice spacings of the two systems). We must now face the question of how to perform the configuration sum in Equation 9.2. This cannot in general be done exactly, so we must resort to some approximation scheme. The particular approximation which we invoke is the high temperature series expansion. In its simplest mathematical form, since H contains a factor $1/k_B T$, it involves the expansion of $\exp(-H)$ as a power series:

$$\exp(-H/k_B T) = 1 - H/k_B T + \frac{1}{2!}(H/k_B T)^2 + \dots$$

We substitute this expansion into the right hand side of Equation 9.2 and proceed to look for terms which depend on the s' spins after the sum over the possible arrangements of the \tilde{s} spins is performed. This sum extends over all the possible (± 1) values of all the \tilde{s} spins. The first term (the 1) in the expansion of the exponential is clearly independent of the values of the s' spins. The second term (H) is a function of the s' spins, but gives zero when the sum over the s' spins is performed because only a single factor of any s' ever appears, and $+1 - 1 = 0$. The third term ($H^2/2$) does contribute. If one writes out explicitly the form of $H^2/2$ one finds terms of the form $K^2 s'_1 \tilde{s} s'_2 = K^2 s'_1 s'_2$, where s'_1 and s'_2 denote two spins at nearest neighbour sites on the lattice of s' spins and \tilde{s} is the spin (in the other set) which lies between them. Now, in the corresponding expansion of the left hand side of Equation 9.2, we find terms of the form $K' s'_1 s'_2$, where K' is the nearest neighbour coupling for the s' spins. We conclude (with a little more thought than we detail here) that

$$K' = K^2 \tag{9.3}$$

Of course many other terms and couplings are generated by the higher orders of the high temperature expansion and it is necessary to include these if one wishes reliable values for the critical temperature and exponents. However, our aim here is to use this simple calculation to illustrate the RG method. Let us therefore close our eyes, forget about the higher order terms and show how the RGT Equation 9.3 can be used to obtain information on the phase transition.

The first point to note is that that mathematically Equation 9.3 has the fixed point $K^* = 1$; if $K = 1$ then the new effective coupling K' has the same value 1. Further, if K is just larger

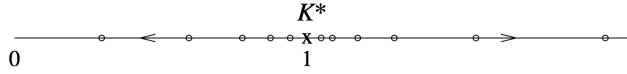


Figure 9.2: Coupling flow under the decimation transformation described in the text.

than 1, then K' is larger than K , i.e. further away from 1. Similarly, if K is less than 1, K' is less than K . We say that the fixed point is unstable: the flow of couplings under repeated iteration of Equation 9.3 is away from the fixed point, as illustrated in Figure 9.2. The physical significance of this is as follows: suppose that the original system is at its critical point so that the ratio of ξ to lattice spacing is infinite. After one application of the decimation transformation, the effective lattice spacing has increased by a factor of two, but this ratio remains infinite; the new system is therefore also at its critical point. Within the approximations inherent in Equation 9.3, the original system is an Ising model with nearest neighbour coupling K and the new system is an Ising model with nearest neighbour coupling K' . If these two systems are going to be at a common critically, we must identify $K' = K$. The fixed point $K^* = 1$ is therefore a candidate for the critical point K_c , where the phase transition occurs. This interpretation is reinforced by considering the case where the original system is close to, but not at, criticality. Then ξ is finite and the new system is further from critically because the ratio of ξ to lattice spacing is reduced by a factor of two. This instability of a fixed point to deviations of K from K^* is a further necessary condition for its interpretation as a critical point of the system. In summary then we make the prediction

$$K_c = J/k_B T_c = 1 \quad (9.4)$$

We can obtain further information about the behaviour of the system close to its critical point. In order to do so, we rewrite the transformation (Equation 9.3) in terms of the deviation of the coupling from its fixed point value. A Taylor expansion of the function $K' = K^2$ yields

$$\begin{aligned} K' &= (K^*)^2 + (K - K^*) \left. \frac{\partial K'}{\partial K} \right|_{K=K^*} + \frac{1}{2}(K - K^*)^2 \left. \frac{\partial^2 K'}{\partial K^2} \right|_{K=K^*} + \dots \\ K' - K^* &= 2(K - K^*) + (K - K^*)^2 \end{aligned}$$

where in the second line we have used the fact that the first derivative evaluates to $2K^* = 2$ and $(K^*)^2 = K^*$.

For a system sufficiently close to its critical temperature the final term can be neglected. The deviation of the coupling from its fixed point (critical) value is thus bigger for the new system than it is for the old by a factor of two. This means that the reduced temperature is also bigger by a factor of two:

$$t' = 2t$$

But ξ (in units of the appropriate lattice spacing) is smaller by a factor of 1/2:

$$\xi' = \xi/2$$

Thus, when we double t , we halve ξ , implying that

$$\xi \propto t^{-1}$$

for T close to T_c . Thus we see that the RGT predicts scaling behaviour with calculable critical exponents. In this simple calculation we estimate the critical exponent $\nu = 1$ for the square lattice Ising model. This prediction is actually in agreement with the exactly established value. The agreement is fortuitous- the prediction in Eq. refeq:Kc for K_c for K_c , is larger than the exactly established value by a factor of more than two. In order to obtain reliable estimates more sophisticated and systematic methods must be used.

The crude approximation in the calculation above produced a transformation, Equation 9.3, involving only the nearest neighbour coupling, with the subsequent advantages of simple algebra. We pay a penalty for this simplicity in two ways: the results obtained for critical properties are in rather poor agreement with accepted values, and we gain no insight into the origin of universality.

9.2 Universality and scaling

In order to expose how universality can arise, we should from the start allow for several different kinds of coupling J_a , and show how the systems with *different* J_a can have the *same* critical behaviour.

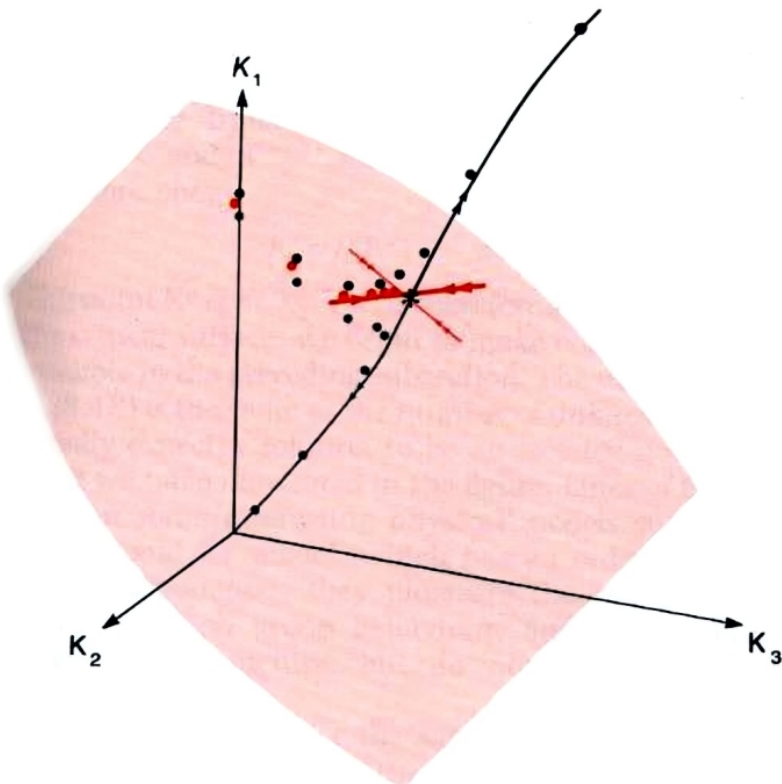


Figure 9.3: General flow in coupling space

Figure 9.3 is a representation of the space of all coupling strengths K_a in the energy function $H/k_B T$. This is of course actually a space of infinite dimension, but representing three of

these, as we have done, enables us to illustrate all the important aspects. First let us be clear what the points in this space represent. Suppose we have some magnetic material which is described by a given set of exchange constants $J_1, J_2, J_3 \dots$. As the temperature T varies, the coupling strengths $K_a = J_a/k_B T$ trace out a straight line, or ray, from the origin of the space in the direction $(J_1, J_2, J_3 \dots)$. Points on this ray close to the origin represent this magnet at high temperatures, and conversely points far from the origin represent the magnet at low temperatures. The critical point of the magnet is represented by a specific point on this ray, $K_a = J_a/k_B T, a = 1, 2, \dots$. The set of critical points on all of the possible rays forms a *surface*, the critical surface. Formally, it is defined by the set of all possible models (of the Ising type) which have infinite ξ . It is shown schematically as the shaded surface in Figure 9.3. (In the figure it is a two-dimensional surface; more generally it has one dimension less than the full coupling constant space, dividing all models into high and low temperature phases.)

Our immediate goal then is to understand how the RGT can explain why different physical systems near this critical surface have the same behaviour. Let us turn now to the schematic representation of the RG flow in Figure 9.3. Suppose we start with a physical system, with coupling strengths $K_a, a = 1, 2, \dots$. What the RGT does is generate a new point in the figure, at the coupling strengths $K_a^{(1)} = f_a(\mathbf{K})$; these are the couplings appearing in the effective energy function describing the coarse-grained system. If we repeat the transformation, the new energy function has coupling strengths $K_a^{(2)} = f_a(\mathbf{K})$. Thus repeated application of the transformation generates a flow of points in the figure: $\mathbf{K} \rightarrow \mathbf{K}^{(1)} \rightarrow \dots \rightarrow \mathbf{K}^{(n)}$ where the superscript (n) labels the effective couplings after n coarse-graining steps. If the change in coarse-graining scale is $b (> 1)$ at each step, the total change in coarse-graining scale is b^n after n steps. In the process, therefore, the ratio of ξ to coarse-graining scale is reduced by a factor of b^{-n} . The dots in Figure 9.3 identify three lines of RG flow starting from three systems differing only in their temperature. (The flow lines are schematic but display the essential features revealed in detailed calculations.)

Consider first the red dots which start from the nearest neighbour Ising model at its critical point. The ratio of ξ to coarse-graining scale is reduced by a factor b at each step, but, since it starts infinite, it remains infinite after any finite number of steps. In this case we can in principle generate an unbounded number of dots, $\mathbf{K}^{(1)}, \mathbf{K}^{(2)}, \dots, \mathbf{K}^{(n)}$, all of which lie in the critical surface. The simplest behaviour of such a sequence as n increases is to tend to a limit, K^* , say. In such a case

$$K_a^* = f_a(K^*) \quad a = 1, 2, \dots$$

This point $\mathbf{K}^* \equiv K_1^*, K_2^*, \dots$ is therefore a *fixed point* which lies in the critical surface.

By contrast, consider the same magnet as before, now at temperature T just greater than T_c , its couplings K_a , will be close to the first red dot (in fact they will be slightly smaller) and so will the effective couplings $K_a^{(1)}, K_a^{(2)}, \dots$ of the corresponding coarse-grained systems. The new flow will therefore appear initially to follow the red dots towards the same fixed point. However, the flow must eventually move away from the fixed point because each coarse-graining now produces a model further from criticality. The resulting flow is represented schematically by one set of black dots. The other set of black dots shows the expected flow starting from the same magnet slightly below its critical temperature.

We are now in a position to understand both universality and scaling within this framework. We will suppose that there exists a single fixed point in the critical surface which sucks in all flows starting from a point in that surface. Then any system at its critical point will exhibit large-length scale physics (large-block spin behaviour) described by the single set of fixed point coupling constants. The uniqueness of this limiting set of coupling constants is the essence of critical

point universality. It is, of course, the algebraic counterpart of the unique limiting spectrum of coarse-grained configurations, discussed in Section 8.5. Similarly the scale-invariance of the critical point configuration spectrum (viewed on large enough length scales) is expressed in the invariance of the couplings under iteration of the transformation (after a number of iterations large enough to secure convergence to the fixed point).

To understand the behaviour of systems near but not precisely at critically we must make a further assumption (again widely justified by explicit studies). The flow line stemming from any such system will, we have argued, be borne towards the fixed point before ultimately deviating from it after a number of iterations large enough to expose the system's noncritical character. We assume that (as indicated schematically in the streams of red and blue lines in Figure 9.3) the deviations lie along a single line through the fixed point, the direction followed along this line differing according to the sign of the temperature deviation $T - T_c$. Since any two sets of coupling constants on the line (on the same side of the fixed point) are related by a suitable coarse-graining operation, this picture implies that the large-length-scale physics of all near-critical systems differs only in the matter of a length scale. This is the essence of near-critical point universality.

Chapter 10

Dynamics of first order phase transitions: nucleation, growth and spinodal decomposition

10.1 Introduction to nucleation

In previous discussions, we considered first-order phase transitions but deferred a detailed analysis of the *dynamical* mechanism by which a system evolves from one phase to another. We now address this question explicitly.

Consider again the Ising model at a temperature $T < T_c$, where the system is initially prepared in the majority spin-up phase at zero external field, $H = 0$. We now examine the system's response to the application of a small negative external field $H < 0$, which lowers the free energy of the spin-down phase relative to the spin-up phase.

Despite the global free energy favoring the spin-down phase, the system does not undergo an instantaneous transition. This delay is a consequence of the free energy barrier associated with nucleating a region of the stable phase within the metastable one, as introduced in Section 5.2. The dynamical pathway of the phase transition proceeds via *nucleation* of localized regions—referred to as *droplets*—of the stable (spin-down) phase embedded within the metastable (spin-up) background. Once nucleated, these droplets may grow over time and ultimately coalesce to transform the system to the stable phase.

The nucleation of a droplet of the stable phase of size n spins entails a competition between bulk and interfacial contributions to the free energy. The bulk free energy gain is linear in n , given by $-nH$, due to the alignment of spins with the external field. However, this gain is offset by an interfacial free energy cost arising from broken bonds at the boundary between phases. For the Ising model, each broken bond contributes an energy cost of $+2J$, so the total interfacial energy scales with the perimeter (in 2D) or surface area (in 3D) of the droplet. This interfacial contribution is referred to as the *surface tension*, and constitutes a true free energy cost: it includes not only the energetic penalty from broken bonds but also an entropic contribution due to the configurational degrees of freedom associated with the droplet shape.

The resulting competition between the extensive free energy gain and the sub-extensive interfacial cost leads to a free energy barrier for droplet formation. Only fluctuations that produce a droplet larger than a critical size n_c will grow; smaller droplets will shrink. This framework is formalized in *classical nucleation theory*, which provides a quantitative description of the nucle-

ation rate, critical droplet size, and the associated activation energy barrier.

10.2 Classical Nucleation Theory: Homogeneous Nucleation

We now present the framework of **classical nucleation theory** (CNT) for the case of *homogeneous nucleation*, in which the nucleation of the stable phase occurs spontaneously and uniformly throughout the bulk of the metastable phase, without the aid of impurities, defects, or surfaces.

Let us consider a droplet of the stable (spin-down) phase of radius R embedded within the metastable (spin-up) background. The total change in free energy $\Delta F(R)$ associated with forming such a droplet consists of two competing contributions:

1. **Bulk free energy gain:** The interior of the droplet consists of $V \sim R^d$ spins aligned with the external field $H < 0$, leading to a volume free energy change

$$\Delta F_{\text{bulk}}(R) = -|\Delta f| R^d,$$

where $|\Delta f| \propto |H|$ is the free energy density difference between the metastable and stable phases, and d is the spatial dimensionality of the system.

2. **Interfacial free energy cost:** The boundary between the two phases has a surface area scaling as R^{d-1} , and incurs a free energy cost proportional to the *surface tension* σ :

$$\Delta F_{\text{surface}}(R) = \sigma S_d R^{d-1},$$

where S_d is a geometrical factor (e.g., $S_2 = 2\pi$ in 2D and $S_3 = 4\pi$ in 3D).

The total free energy change is therefore given by

$$\Delta F(R) = \sigma S_d R^{d-1} - |\Delta f| V_d R^d,$$

where V_d is another dimension-dependent constant. This expression (Figure 10.1) exhibits a characteristic maximum at a critical droplet radius R_c , obtained by extremizing $\Delta F(R)$ with respect to R :

$$\frac{d\Delta F}{dR} = 0 \quad \Rightarrow \quad R_c = \frac{(d-1)\sigma S_d}{d|\Delta f| V_d}.$$

The corresponding free energy barrier for nucleation is

$$\Delta F_c = \Delta F(R_c) = \frac{(d-1)^{d-1}}{d^d} \cdot \frac{(S_d)^d \sigma^d}{(|\Delta f|)^{d-1} (V_d)^{d-1}}.$$

This barrier must be surmounted by thermal fluctuations in order for a critical nucleus to form and grow. The nucleation rate per unit volume is given (in the Arrhenius approximation) by

$$I \sim I_0 \exp \left(-\frac{\Delta F_c}{k_B T} \right),$$

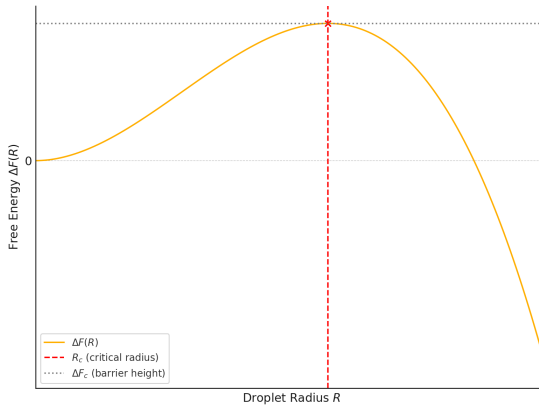


Figure 10.1: Free energy barrier $\Delta F(r)$ for nucleation of a spherical droplet as a function of radius R (schematic)

where I_0 is a prefactor determined by microscopic kinetics, and k_B is Boltzmann's constant.

10.2.1 Interpretation and Scaling Behavior

Several key features emerge from this analysis:

- **Barrier scaling:** The nucleation barrier $\Delta F_c \sim \sigma^d / |\Delta f|^{d-1}$ diverges as $H \rightarrow 0$, reflecting the increasing stability of the metastable phase near the coexistence point.
- **Critical radius:** The critical droplet size $R_c \sim \sigma / |\Delta f|$ also diverges as $|\Delta f| \rightarrow 0$, indicating that larger fluctuations are required to initiate nucleation close to the coexistence line.
- **Dimensional dependence:** Both ΔF_c and R_c exhibit strong dependence on the spatial dimension d , with nucleation becoming increasingly suppressed in higher dimensions due to the dominance of interfacial cost.

In summary, homogeneous nucleation in a first-order transition is governed by a delicate balance between surface tension and bulk free energy gain. Only droplets exceeding a critical size can overcome the barrier and initiate a transition. This sets an intrinsic timescale for the dynamics of phase transformation, which can become extremely long near coexistence due to the exponentially small nucleation rate.

10.3 Domain growth

Following successful nucleation of a supercritical droplet, the system enters a regime where the global transformation is driven by the deterministic growth of domains of the stable phase. Such *domain growth* involves more atoms or molecules attaching to these nuclei, causing them to expand into larger structures (e.g., growing crystals or droplets).

Growth rate depends on factors like temperature, concentration, and the availability of building blocks.

The shape and structure of the final phase often depend on how growth occurs (e.g., slow growth may form perfect crystals; rapid growth may be irregular).

10.4 Spinodal decomposition

Previously we have considered a scenario in which we move our system to a statepoint just inside the coexistence region so that the original phase remains metastable. We then wait for a fluctuation that yields a critical nucleus and subsequent growth.

Now imagine that rather than positioning the system just inside the coexistence region we move immediately to a state point well inside the coexistence region (cf. Figure 10.2) such that there is no metastable minimum in the free energy. Then there is no nucleation and growth, rather the system is *unstable* and immediately starts to phase separate at all points in the system. This so called *spinodal decomposition*.

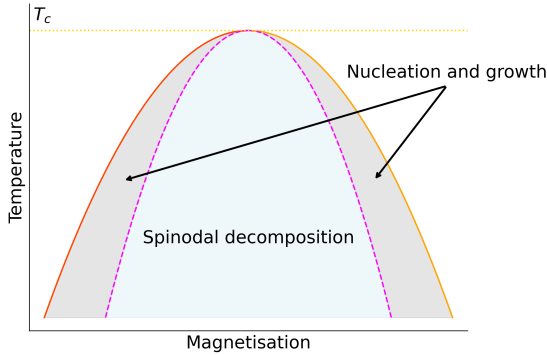


Figure 10.2: Schematic phase doagram showing the regions in which one observes nucleation and growth, or spinodal decomposition

The nature of spinodal decomposition and late-time domain growth depends sensitively on whether the order parameter is conserved or not.

10.4.1 Non-Conserved Order Parameter Dynamics (Model A)

In systems with a non-conserved order parameter, such as the Ising model with single spin flip (so called Glauber) dynamics, the order parameter can relax locally without constraint. This leads to curvature-driven motion of interfaces.

The typical domain size $L(t)$ grows algebraically with time:

$$L(t) \sim t^{1/2},$$

corresponding to a dynamic exponent $z = 2$. The growth is driven by reduction of the total interfacial area—regions of high curvature (small domains) shrink and are absorbed by larger, flatter ones.

Let us assume that domain walls move with velocity proportional to curvature:

$$v \sim \frac{1}{L}$$

Then with the typical domain size being $L(t)$ it follows that

$$\frac{dL}{dt} \sim \frac{1}{L}$$

Integrating both sides yields the $t^{1/2}$ domain growth law.

It turns out that the detailed evolution of the coarse-grained order parameter field $\phi(\mathbf{r}, t)$ is governed by the **Allen–Cahn equation**:

$$\frac{\partial \phi}{\partial t} = -\frac{\delta F[\phi]}{\delta \phi},$$

where $F[\phi]$ is a coarse-grained Ginzburg–Landau free energy functional:

$$F[\phi] = \int d^d x \left[\frac{1}{2} (\nabla \phi)^2 + V(\phi) \right],$$

with $V(\phi)$ typically a double-well potential such as $V(\phi) = \frac{1}{4}(\phi^2 - 1)^2$.

10.4.2 Conserved Order Parameter Dynamics (Model B)

For systems with a conserved order parameter, such as phase separation in binary alloys or the Ising model with spin-swap (so called ‘Kawasaki’) dynamics, the order parameter (e.g., composition or particle number) must be conserved locally. This imposes a diffusive constraint on the dynamics.

The domain size again grows algebraically, but with a different exponent:

$$L(t) \sim t^{1/3},$$

corresponding to a dynamic exponent $z = 3$.

A chemical potential difference drives diffusion and is given by

$$\Delta \mu \sim \frac{\sigma}{L}$$

(again due to curvature, where σ is surface tension)

Now the flux is proportional to the chemical potential gradient (Fick’s law):

$$\text{Flux} \sim -\nabla \mu \sim \frac{\Delta \mu}{L} \sim \frac{\sigma}{L^2}$$

and the rate of change of domain size is proportional to this flux:

$$\frac{dL}{dt} \sim \frac{1}{L^2} \quad \Rightarrow \quad L(t) \sim t^{1/3}$$

It turns out that the detailed dynamics are described by the **Cahn–Hilliard equation**, a continuity equation of the form:

$$\frac{\partial \phi}{\partial t} = \nabla^2 \left(\frac{\delta F[\phi]}{\delta \phi} \right),$$

reflecting that the order parameter can only evolve via diffusion of its conjugate chemical potential. This leads to the slow transport of material across domains and a more sluggish coarsening process compared to the non-conserved case.

10.4.3 Schematic of Domain Growth in 2D Ising model

Here are schematic illustrations of domain growth for:

- Non-conserved dynamics (Model A): Domains coarsen rapidly, with smoother and larger regions due to free relaxation of the order parameter.
- Conserved dynamics (Model B): Coarsening is slower and domains are more intricate, reflecting the constraint of local conservation.

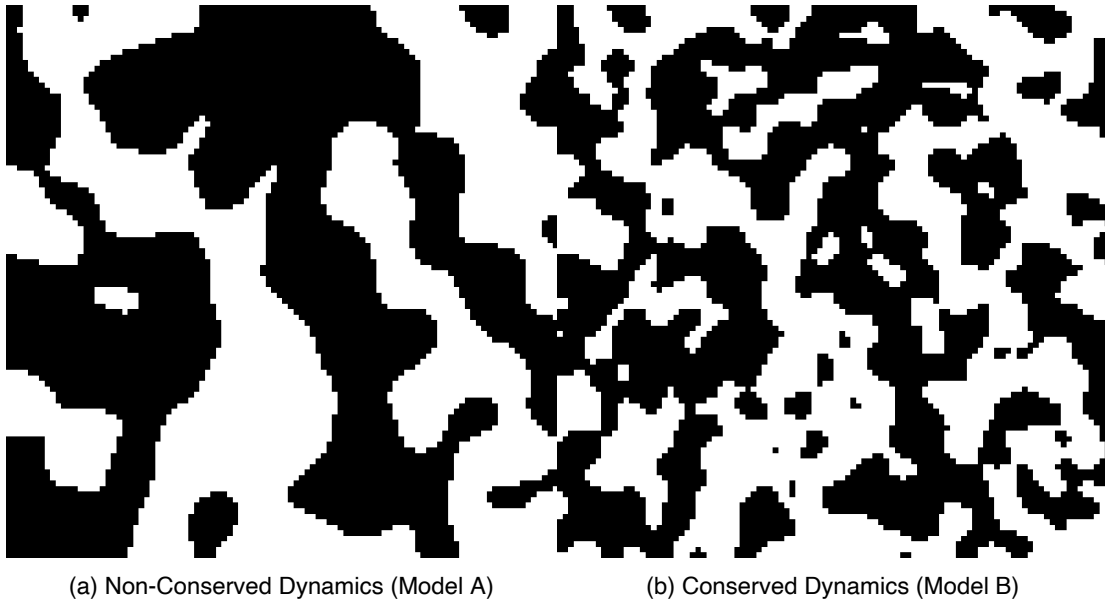


Figure 10.3: Schematic illustrations of domain morphology resulting from spinodal decomposition or late-time domain growth for non-conserved and conserved dynamics.

10.4.4 Dynamics Scaling Hypothesis

At late times, both conserved and non-conserved systems exhibit dynamic scaling: the statistical properties of the domain morphology become self-similar under rescaling of lengths by $L(t)$.

For example, the equal-time two-point correlation function satisfies

$$C(r, t) = f\left(\frac{r}{L(t)}\right),$$

where $f(x)$ is a time-independent scaling function. Plots of $C(r, t)$ collapse when plotted as a function of $r/L(t)$.

The structure factor $S(k, t)$, which is the Fourier transform of the correlation function, is experimentally accessible eg via X-ray or neutron scattering, and also obeys dynamic scaling:

$$S(k, t) = \int d^d r e^{-i\vec{k}\cdot\vec{r}} C(r, t).$$

Substituting the scaling form of $C(r, t)$ into this expression, and changing variables to $\vec{u} = \vec{r}/L(t)$, gives:

$$S(k, t) = L(t)^d \int d^d u e^{-i\vec{k}\cdot L(t)\vec{u}} f(u) = L(t)^d g(kL(t)),$$

with $g(x)$ a universal scaling function dependent on the dynamical class and dimensionality.

10.4.5 Summary of Growth Laws

Dynamics Type	Conservation Equation Type	Growth Law	Dynamic Exponent	
Model A (e.g. Glauber)	No	Allen–Cahn	$L(t) \sim t^{1/2}$	$z = 2$
Model B (e.g. Kawasaki)	Yes	Cahn–Hilliard	$L(t) \sim t^{1/3}$	$z = 3$

Remarks: The domain growth exponents $1/z$ are robust under many conditions, but can be modified in the presence of disorder, long-range interactions, or hydrodynamic effects.

In both the model A and model B cases, the system coarsens until it reaches equilibrium, characterized by a uniform macroscopic phase and the complete elimination of interfaces.

The approach to equilibrium is algebraically slow (described by power laws) due to the scale-free nature of domain dynamics.

More about the scientists mentioned in this chapter:

[John Cahn](#)

Chapter 11

Introduction to stochastic processes

Many natural phenomena are stochastic — they involve randomness in their evolution over time.

In classical physics, this randomness may arise from our lack of knowledge about microscopic details. For example, in a gas, we do not know the precise positions and velocities of each particle, so their collisions with the container walls appear random.

In quantum mechanics, stochasticity is even more intrinsic. The fundamental objects are probability amplitudes, and outcomes are inherently probabilistic.

To describe these systems effectively, we use a coarse-grained probabilistic description, which tracks the likelihood of different outcomes rather than precise trajectories. One of the key tools in this approach is the master equation.

11.1 The Master Equation

Consider a system in microstate i with energy E_i . It can transition to neighboring microstates j , where the energy difference $|E_j - E_i|$ is small (within δE).

Let ν_{ij} be the **rate** at which the system jumps from state i to state j . Over an infinitesimal time interval dt , the probability p_i changes as:

$$dp_i = \left[-p_i \sum_j \nu_{ij} + \sum_j \nu_{ji} p_j \right] dt$$

This expression contains two terms:

- A *loss term*: the system leaves state i at rate ν_{ij} ,
- A *gain term*: the system arrives in state i from other states j at rate ν_{ji} .

The master equation becomes:

$$\frac{dp_i}{dt} = - \sum_j \nu_{ij} p_i + \sum_j \nu_{ji} p_j$$

This is a linear first-order differential equation for the vector of probabilities $\{p_i\}$.

Alternatively, in matrix form:

$$\frac{d\mathbf{p}}{dt} = W\mathbf{p}$$

where W is the **rate matrix** with entries:

- $W_{ij} = \nu_{ji}$ for $i \neq j$,
- $W_{ii} = -\sum_{j \neq i} \nu_{ij}$.

This structure ensures probability conservation: the total probability $\sum_i p_i = 1$ remains constant in time.

The master equation is first order in time and does not have time reversal symmetry so describes an irreversible process. This irreversibility arises from the coarse-graining process that throws away information about underlying microphysics which is described by Newton's equations and which are time reversible. Only by doing so is the entropy allowed to increase which is required by the second law of thermodynamics for an irreversible process. Consequently the increase of entropy is linked to our knowledge about the system rather than anything it is doing internally in a manner that may appear dubious. Can it be possible that macroscopic and reproducible phenomena such as heat flow depend on how we handle information? Perhaps yes since the division between work and heat is somewhat arbitrary. Were we able to track all the particle positions there would be no need to talk about heat energy or heat flow.

11.2 From the Master Equation to the Diffusion Equation

Now consider the situation where the state index i corresponds to a position in space, $x_i = ia$, ie a one-dimensional lattice with lattice spacing a , and transitions only occur between neighboring lattice sites.

We assume:

- Transition rates are symmetric: $\nu_{i,i+1} = \nu_{i,i-1} = \nu$,
- The spacing $a \rightarrow 0$ in the continuum limit.

The master equation becomes a finite-difference equation:

$$\begin{aligned}\frac{dp_i}{dt} &= \sum_j \nu_{ij}(p_j - p_i) \\ \frac{dp_i}{dt} &= \nu(p_{i-1} - p_i) + \nu(p_{i+1} - p_i) \\ \frac{dp_i}{dt} &= \nu(p_{i+1} + p_{i-1} - 2p_i)\end{aligned}$$

We now define a continuous variable $x = ia$, and a probability density $p(x, t)$ such that $p_i(t) \approx p(x, t)$.

Using Taylor expansions:

$$p(x \pm a, t) = p(x, t) \pm a \frac{\partial p}{\partial x} + \frac{a^2}{2} \frac{\partial^2 p}{\partial x^2} + \dots$$

Substituting into the master equation gives:

$$\frac{\partial p}{\partial t} = \nu a^2 \frac{\partial^2 p}{\partial x^2}$$

Defining the diffusion constant $D = \nu a^2$, we obtain the **diffusion equation**:

$$\frac{\partial p}{\partial t} = D \frac{\partial^2 p}{\partial x^2}$$

The diffusion equation describes the evolution of the probability density of a particle with diffusion constant (sometimes called diffusivity) given by $D = \nu a^2$. The dimensions of D are $[\text{length}]^2 / [\text{time}]$. Typically, after expansion, we set the lattice spacing a to 1. Additionally, the diffusion equation can describe many non-interacting diffusing particles. In this case, we replace p with ρ , representing the density or concentration of particles, and use the normalization $\int dx \rho = M$, where M is the number of particles.

The diffusion equation, much like the master equation from which it originates, explicitly violates time-reversal symmetry, thus permitting entropy to increase.

The solution of the diffusion equation for an initial condition where the particle is initially localized at the origin (formally, $p(x, 0) = \delta(x)$) is a Gaussian:

$$p(x, t) = (4\pi Dt)^{-1/2} \exp \left[-\frac{x^2}{4Dt} \right]$$

We explicitly see the arrow of time by examining this Gaussian solution at various times t . As t increases, the Gaussian “bell-shaped” curve spreads out. Its width grows according to $\langle x^2 \rangle^{1/2} \sim t^{1/2}$. This is known as “diffusive scaling,” and it implies that, after time t , a particle will typically be found at a distance roughly proportional to $t^{1/2}$ from its starting point. Conversely, exploring a region of size L typically requires a time of order $O(L^2)$.

The evolution of the solution to the 1d diffusion equation in a spatial region $x = [0, 1]$ as a function of times are shown in the movie below. The diffusion constant is $D = 0.01$. The movie corresponds to a particle initialised at $x = 0.5$. One sees how the probability density spreads out over the range as time increases. This can be used to model the diffusion of particles down a concentration gradient as you will see in the next part of the course.

[Movies/diffusion_evolution.mp4](#)

```
import numpy as np
import matplotlib.pyplot as plt
import matplotlib.animation as animation
import os

# Parameters
L = 1.0          # Length of the domain
T = 1.0          # Total time
nx = 400         # Number of spatial points
```

```

nt = 2000      # Number of time steps
D = 0.1        # Diffusion coefficient

# Discretization
dx = L / (nx - 1)
dt = T / nt

# Stability condition auto-adjust
if D * dt / dx**2 > 0.5:
    print("Adjusting dt and nt to satisfy stability condition...")
    dt = 0.4 * dx**2 / D
    nt = int(T / dt)
    dt = T / nt # Recalculate dt exactly

nt = int(nt / 50) # Artificial slowdown for animation

print(f"Using dt = {dt:.4e}, nt = {nt}")

# Initialize x and u
x = np.linspace(0, L, nx)

# Initial condition: smooth narrow Gaussian
sigma = 0.01
u = np.exp(-(x - L/2)**2 / (2 * sigma**2))

# Normalize initial condition
u /= np.sum(u) * dx

# Setup figure
plt.rcParams.update({
    "text.usetex": True,
    "font.family": "serif"
})

fig, ax = plt.subplots()
line, = ax.plot(x, u)

# Compute peak height for setting y-axis
peak_height = 1 / (np.sqrt(2 * np.pi) * sigma)
ax.set_ylim(0, peak_height * 1.05)

ax.set_xlabel(r'$x$', fontsize=20)
ax.set_ylabel(r'$p(x,t)$', fontsize=20)

ax.tick_params(axis='both', which='major', labelsize=14)

# Tiny time counter text
time_text = ax.text(0.85, 0.05, '', transform=ax.transAxes, fontsize=10, verticalalignment='bottom')

# Function to update the plot
def update(frame):
    global u

```

```

unew = np.copy(u)
unew[1:-1] = u[1:-1] + D * dt / dx**2 * (u[2:] - 2*u[1:-1] + u[:-2])
u = unew

# Normalize at every step
u /= np.sum(u) * dx

line.set_ydata(u)
current_time = frame * dt
time_text.set_text(r'$t=%4f$' % current_time)
return line, time_text

ani = animation.FuncAnimation(fig, update, frames=nt, interval=100, blit=True)

# Save the animation as a movie
Writer = animation.writers['ffmpeg']
writer = Writer(fps=15, metadata=dict(artist='Me'), bitrate=1800)
ani.save("../Movies/diffusion_evolution.mp4", writer=writer)

plt.show()

```

11.3 Consequences of time reversal symmetry

As we have seen by introducing a type of coarse graining, the master equation violates time reversal symmetry of the underlying Newtonian dynamics. Remarkably however, the fact that the underlying microphysics is actually time reversal symmetric has several deep consequences which survive the coarse graining procedure. These results are some of the cornerstones of nonequilibrium thermodynamics.

11.3.1 Detailed balance

Recall from year 2 Statistical Mechanics that for a system in equilibrium, the principle of equal a-priori probabilities of microstates holds. Therefore

$$\nu_{ij} p_i^{eq} = \nu_{ji} p_j^{eq}$$

Hence, on average, the actual rate of quantum jumps from i to j (the left-hand side) is the same as from j to i . This is a stronger statement than the master equation, which asserts only that there is overall balance between the rate of jumping into and out of state i in equilibrium. The result above is known as the *principle of detailed balance*.

This principle is powerful because it applies not only to individual states but also to any grouping of states.

Exercise: Show that for two groups of states, A and B , the overall rate of transitions from group A to group B is balanced, in equilibrium, by those from B to A :

$$\nu_{AB} p_A^{eq} = \nu_{BA} p_B^{eq}$$

Hence, detailed balance arguments can be extended to subsystems within a large isolated system, and even to systems that are not isolated. However, in such cases, the principle is far from obvious, because once states are grouped together:

$$\nu_{AB} \neq \nu_{BA}, \quad p_A \neq p_B$$

(This can be easily demonstrated, for example, by considering two groups that contain different numbers of states with similar energies.) Nonetheless, the detailed balance relation holds, in equilibrium, in the general form above.

11.3.2 Computer simulation

In computer simulation, good results will be obtained if one accurately follows the microscopic equations of motion. This is the *molecular dynamics (MD)* method which we now outline.

Molecular dynamics

Molecular Dynamics (MD) involves a system of classical particles interacting through specified interparticle forces. The motion of these particles is determined by numerically integrating Newton's equations of motion. In MD simulations, averages of state variables are obtained as time averages over trajectories in phase space. Typically, the forces acting between particles are conservative, ensuring that the total energy E remains constant. This conservation implies that the motion is restricted to a $(2dN - 1)$ -dimensional surface in phase space, denoted by $\Gamma(E)$.

A central aspect of MD is the averaging of observables. For a given observable A , its average is computed as the time average along the trajectory. Mathematically, this is expressed as:

$$\langle A(\{\mathbf{p}_i\}, \{\mathbf{r}_i\}) \rangle = \frac{1}{\tau} \int_{t_0}^{t_0 + \tau} dt A(\{\mathbf{p}_i(t)\}, \{\mathbf{r}_i(t)\})$$

This formula represents the integral of the observable over a time interval τ , normalized by the length of that interval.

The practical steps of an MD simulation start with generating an initial random configuration of particle positions $\{\mathbf{r}_i\}$ and momenta $\{\mathbf{p}_i\}$. The system's equations of motion are then iteratively solved using a suitable algorithm to allow it to reach equilibrium. After equilibration, a production run is performed over many time steps to collect meaningful data. Finally, relevant averages, such as pressure or kinetic energy, are calculated from the collected data.

Monte Carlo

However, to obtain the equilibrium properties of the system, it may be much faster to use a dynamics which is nothing like the actual equations of motion.

At first sight, this looks very dangerous; however, if one can prove that in the required equilibrium distribution, the artificial dynamics obey the principle of detailed balance, then it is (almost) guaranteed that the steady state found by simulation is the true equilibrium state.

The best known example is the *Monte Carlo method*, in which the dynamical algorithm consists of random jumps. The jump rates ν_{AB} for all pairs of states (A, B) take the form:

$$\nu_{AB} = \nu_0 \quad \text{if } E_B \leq E_A$$

$$\nu_{AB} = \nu_0 e^{-\beta(E_B - E_A)} \quad \text{if } E_B \geq E_A$$

where ν_0 is a constant.

Exercise: Show that this gives the canonical distribution in steady state.

🔥 Solution

To show that this jump rate rule gives the canonical distribution in steady state, we assume the system reaches a steady-state probability distribution P_A for state A and apply the condition of detailed balance.

Detailed balance requires:

$$P_A \nu_{AB} = P_B \nu_{BA}$$

Assume the canonical distribution:

$$P_A = \frac{1}{Z} e^{-\beta E_A}, \quad P_B = \frac{1}{Z} e^{-\beta E_B}$$

Now consider two cases for ν_{AB} and ν_{BA} :

Case 1: $E_B \leq E_A$

Then:

$$\nu_{AB} = \nu_0, \quad \nu_{BA} = \nu_0 e^{-\beta(E_A - E_B)}$$

Substitute into the detailed balance condition:

$$P_A \nu_0 = P_B \nu_0 e^{-\beta(E_A - E_B)}$$

Cancel ν_0 :

$$P_A = P_B e^{-\beta(E_A - E_B)}$$

Use canonical form:

$$\frac{1}{Z} e^{-\beta E_A} = \frac{1}{Z} e^{-\beta E_B} e^{-\beta(E_A - E_B)} = \frac{1}{Z} e^{-\beta E_A}$$

Verified.

Case 2: $E_B > E_A$

Then:

$$\nu_{AB} = \nu_0 e^{-\beta(E_B - E_A)}, \quad \nu_{BA} = \nu_0$$

Substitute:

$$P_A \nu_0 e^{-\beta(E_B - E_A)} = P_B \nu_0$$

Cancel ν_0 :

$$P_A e^{-\beta(E_B - E_A)} = P_B$$

Again using canonical form:

$$\frac{1}{Z} e^{-\beta E_A} e^{-\beta(E_B - E_A)} = \frac{1}{Z} e^{-\beta E_B} = P_B$$

Verified.

Hence, in both cases the detailed balance condition is satisfied with the canonical distribution, and the steady state is indeed the canonical distribution.

Chapter 12

The Langevin Approach

12.1 The Random Walk and the Langevin equation

The concept of a random walk and its continuum limit – diffusion – introduced in the previous chapter, expresses the time evolution of the probability distribution $p(x, t)$ for a particle's position x by the diffusion equation:

$$\frac{\partial p}{\partial t} = D \frac{\partial^2 p}{\partial x^2},$$

which is a standard example of a so called *Fokker-Planck* equation, which is second-order in space and first-order in time.

In contrast, the *Langevin equation* provides a stochastic differential equation for the particle's trajectory $x(t)$. To understand it, consider the random hopping motion of a particle on a 1d lattice over a small time increment Δt :

$$x(t + \Delta t) = x(t) + \Delta x(t)$$

Here, $\Delta x(t)$ is a random displacement. If the lattice spacing is a , we define the step statistics as:

$$\Delta x(t) = \begin{cases} +a & \text{with probability } \nu \Delta t \\ -a & \text{with probability } \nu \Delta t \\ 0 & \text{with probability } 1 - 2\nu \Delta t \end{cases}$$

This defines a discrete-time, discrete-space random walk. The average and variance of the step are easily derived using binomial statistics:

- Mean: $\langle \Delta x \rangle = 0$
- Variance: $\langle (\Delta x)^2 \rangle = 2a^2 \nu \Delta t = 2D \Delta t$

The steps $\Delta x(t)$ are uncorrelated across time.

To take the continuum limit, we let both $a \rightarrow 0$ and $\Delta t \rightarrow 0$ in such a way that:

$$a \propto \sqrt{\Delta t}$$

In this limit, we obtain the **Langevin equation**:

$$\dot{x}(t) = \eta(t)$$

where $\eta(t) \equiv \frac{\Delta x(t)}{\Delta t}$ is a stochastic noise satisfying:

$$\langle \eta(t) \rangle = 0$$

$$\langle \eta(t)\eta(t') \rangle = \Gamma\delta(t-t')$$

This $\eta(t)$ is known as white noise — it has zero mean and is uncorrelated at different times. Γ measures its amplitude.

The Langevin equation tells us that the velocity $\dot{x}(t)$ is purely driven by noise. We can formally integrate it:

$$x(t) - x_0 = \int_0^t \eta(t') dt'$$

Taking ensemble averages:

- Mean displacement:

$$\langle x(t) - x_0 \rangle = 0$$

- Mean square displacement:

$$\langle [x(t) - x_0]^2 \rangle = \int_0^t \int_0^t \langle \eta(t')\eta(t'') \rangle dt' dt'' = \Gamma \int_0^t dt' = \Gamma t$$

Comparing this with the diffusion equation result, we identify:

$$\Gamma = 2D$$

Hence, the Langevin description yields the same physical behavior — not just the mean-square displacement but also the full probability distribution $p(x, t)$ — as the diffusion (Fokker-Planck) equation. This equivalence arises from the fact that the integral of many small, independent random steps leads to a Gaussian distribution, in agreement with the solution of the diffusion equation.

For more details, see: *Stochastic Processes in Physics and Chemistry* by N.G. van Kampen (North Holland, 1981).

12.2 Brownian Motion

Let us now examine Brownian motion, originally observed as the erratic motion of colloidal particles suspended in a fluid. These particles undergo constant collisions with surrounding (smaller) fluid molecules, which results in seemingly random movement.

From a coarse-grained perspective — where we do not track each individual collision — this appears as motion under random forces. This statistical treatment introduces irreversibility at the macroscopic level, even though the underlying molecular dynamics are reversible.

The Langevin equation provides a way to model this behavior. For a particle of mass m in one dimension, Langevin proposed the equation:

$$m\ddot{x} = -\gamma\dot{x} + f(t)$$

Here:

- $-\gamma\dot{x}$ is a frictional damping force, where γ is the damping coefficient.
- $f(t)$ is a random force due to molecular collisions.

Often, the mobility is defined as $\mu = 1/\gamma$ — note that this is unrelated to chemical potential.

12.2.1 Noise Properties

In principle the random forces are correlated in time since the molecular collisions which cause them are correlated and have some definite duration.

Let us assume that there is some correlation time t_c over which $\langle f(t_1)f(t_2) \rangle = g(t_1 - t_2)$ decays rapidly as shown in the sketch below:

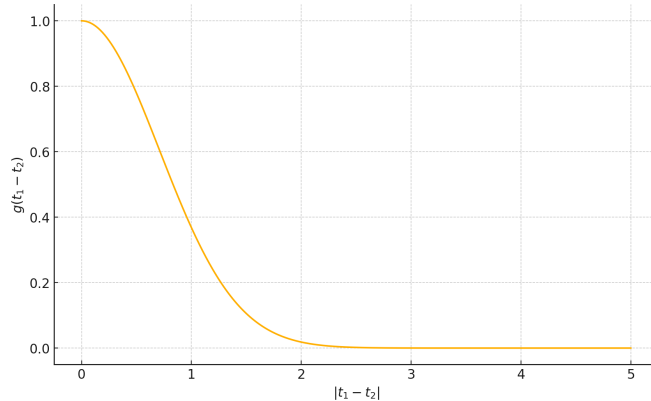


Figure 12.1: Sketch of $g(t_1 - t_2)$ against $|t_1 - t_2|$

Then as long as we consider timescales $\gg t_c$ we can safely replace $g(t_1 - t_2)$ by a delta function. Thus we can make the approximation of white noise

$$\langle f(t) \rangle = 0$$

$$\langle f(t_1)f(t_2) \rangle = \Gamma \delta(t_1 - t_2)$$

12.2.2 Solving the Langevin Equation (velocity)

Let's set $m = 1$ for simplicity and solve the equation:

$$\dot{v} + \gamma v = f(t)$$

We apply an integrating factor:

$$\frac{d}{dt} [ve^{\gamma t}] = e^{\gamma t} f(t)$$

Integrating both sides:

$$v(t) = v_0 e^{-\gamma t} + \int_0^t e^{-\gamma(t-t')} f(t') dt'$$

Taking the average:

$$\langle v(t) \rangle = v_0 e^{-\gamma t}$$

Thus:

- At short times: ($\gamma t \ll 1$): $\langle v \rangle \approx v_0$ ie. friction is negligible.
- At long times: ($\gamma t \gg 1$): $\langle v \rangle \rightarrow 0$ ie. the system loses memory of the initial velocity.

12.2.3 Mean-square velocity

We now compute:

$$\langle v(t)^2 \rangle = v_0^2 e^{-2\gamma t} + \Gamma \int_0^t e^{-2\gamma(t-t')} dt' = v_0^2 e^{-2\gamma t} + \frac{\Gamma}{2\gamma} (1 - e^{-2\gamma t})$$

Implying that at

- Short times: $\langle v^2 \rangle \approx v_0^2$
- Long times: $\langle v^2 \rangle \rightarrow \Gamma/(2\gamma)$

At equilibrium, the equipartition theorem gives:

$$\frac{1}{2}m\langle v^2 \rangle = \frac{1}{2}k_B T$$

Using this to identify Γ :

$$\Gamma = 2\gamma k_B T$$

This important result relates the noise strength to the damping and temperature — they have the same microscopic origin (molecular collisions).

12.2.4 Mean-square displacement

We now integrate $v(t)$ again to get position $x(t)$ (with $m = 1$):

Using the result above and substituting $\Gamma = 2\gamma k_B T$, we find:

$$\langle [x(t) - x_0]^2 \rangle = \frac{(v_0^2 - k_B T)}{\gamma^2} (1 - e^{-\gamma t})^2 + \frac{2k_B T}{\gamma} \left[t - \frac{1 - e^{-\gamma t}}{\gamma} \right]$$

Limiting behaviours:

- Short times: ($\gamma t \ll 1$):

$$\langle [x(t) - x_0]^2 \rangle \approx v_0^2 t^2$$

(corresponding to *ballistic motion*)

- Long time ($\gamma t \gg 1$):

$$\langle [x(t) - x_0]^2 \rangle \approx \frac{2k_B T}{\gamma} t$$

(corresponding to *diffusive motion*)

The effective diffusion constant is:

$$D = \frac{k_B T}{\gamma}$$

This is the **Einstein relation**, connecting the rate of diffusion to temperature and damping. It is useful as it allows an explicit expression for the diffusion constant if one knows γ . A famous example is a sphere: the equation for fluid flow past a moving sphere may be solved and yields $\gamma = 6\pi\eta a$ where a is the radius of the sphere and here η is the fluid viscosity. This gives

$$D = \frac{6\pi\eta a}{kT}$$

which is the **Stokes-Einstein** formula for the diffusion constant of a colloidal particle.

12.2.5 External Forces and Mobility

Now consider a charged particle with charge q under an external electric field E . The Langevin equation becomes:

$$m\dot{v} = -\gamma v + qE$$

At long times, the particle reaches a steady drift velocity:

$$\langle v \rangle = \frac{qE}{\gamma} = \frac{qED}{k_B T}$$

Defining the mobility μ by $\langle v \rangle = \mu qE$, we get the **Nernst-Einstein relation**:

$$\mu = \frac{D}{k_B T}$$

This relation connects the response of a system to an external perturbation (mobility) with its internal fluctuations (diffusivity).

12.2.6 Molecular Dynamics simulation of Brownian motion for a colloid particle in a liquid suspension

Movies/brownian_colloid.mp4

```
import numpy as np
import matplotlib.pyplot as plt
import matplotlib.animation as animation
from numba import njit

# Parameters
n_fluid = 300
box_size = 20.0
n_steps = 10000
sigma_f = 1.0
sigma_c = 10.0
epsilon = 0.05
mass_f = 1.0
mass_c = 2.0
dt = 1e-5
dt_e = 1e-5

# Echo the parameter values
print("Simulation Parameters:")
print(f"n_fluid = {n_fluid}")
print(f"box_size = {box_size}")
print(f"n_steps = {n_steps}")
print(f"sigma_f = {sigma_f}")
print(f"sigma_c = {sigma_c}")
print(f"epsilon = {epsilon}")
print(f"mass_f = {mass_f}")
print(f"mass_c = {mass_c}")
print(f"dt = {dt}")

# Derived quantities

sigma_f6 = sigma_f ** 6
sigma_f12 = sigma_f ** 12
sigma_cf = 0.5 * (sigma_f + sigma_c)
sigma_cf6 = sigma_cf ** 6
sigma_cf12 = sigma_cf ** 12

np.random.seed(42)

# Safe initialization to avoid overlaps with colloid and other fluid particles
def initialize_fluid_positions(n_fluid, box_size, sigma_f, sigma_c, colloid_pos, min_dist_factor=0.85):
    min_dist_ff = min_dist_factor * sigma_f
    min_dist_cf = min_dist_factor * 0.5 * (sigma_f + sigma_c)
    positions = []
    max_attempts = 20000

    for _ in range(n_fluid):
        for attempt in range(max_attempts):
            trial = np.random.rand(2) * box_size
```

```

too_close = False

# Check distance to colloid center
if np.linalg.norm(trial - colloid_pos[0]) < min_dist_cf:
    too_close = True

# Check distances to already placed fluid particles
for existing in positions:
    if np.linalg.norm(trial - existing) < min_dist_ff:
        too_close = True
        break

    if not too_close:
        positions.append(trial)
        break
else:
    raise RuntimeError("Failed to place a fluid particle without overlap after many attempts.")

return np.array(positions)

colloid_pos = np.array([[box_size / 2, box_size / 2]])
fluid_pos = initialize_fluid_positions(n_fluid, box_size, sigma_f, sigma_c, colloid_pos)
fluid_vel = (np.random.rand(n_fluid, 2) - 0.5)
colloid_vel = np.zeros((1, 2))

@njit
def compute_forces_numba(fluid_pos, colloid_pos, sigma_cf6, sigma_cf12, sigma_f6, sigma_f12, epsilon, box_size):
    forces_f = np.zeros_like(fluid_pos)
    force_c = np.zeros_like(colloid_pos)

    for i in range(n_fluid):
        # Fluid-colloid interaction
        rij = fluid_pos[i] - colloid_pos[0]
        rij -= box_size * np.round(rij / box_size)
        dist2 = np.dot(rij, rij)
        if dist2 < (2.5 ** 2) * ((sigma_cf6 ** (1/6)) ** 2) and dist2 > 1e-10:
            r2 = dist2
            r6 = r2 ** 3
            r12 = r6 ** 2
            fmag = 48 * epsilon * ((sigma_cf12 / r12) - 0.5 * (sigma_cf6 / r6)) / r2
            fvec = fmag * rij
            forces_f[i] += fvec
            force_c[0] -= fvec

        for j in range(i + 1, n_fluid):
            rij = fluid_pos[i] - fluid_pos[j]
            rij -= box_size * np.round(rij / box_size)
            dist2 = np.dot(rij, rij)
            if dist2 < (2.5 ** 2) * ((sigma_f6 ** (1/6)) ** 2) and dist2 > 1e-10:
                r2 = dist2
                r6 = r2 ** 3
                r12 = r6 ** 2
                fmag = 48 * epsilon * ((sigma_f12 / r12) - 0.5 * (sigma_f6 / r6)) / r2

```

```

        fvec = fmag * rij
        forces_f[i] += fvec
        forces_f[j] -= fvec

    return forces_f, force_c

fluid_history = []
colloid_history = []
forces_f, force_c = compute_forces_numba(fluid_pos, colloid_pos, sigma_cf6, sigma_cf12, sigma_f6, sigma_f12,
n_equilibration = 2000 # Number of steps to equilibrate before tracking

# Equilibration phase (no history recorded)

for step in range(n_equilibration):
    fluid_pos += fluid_vel * dt_e + 0.5 * forces_f / mass_f * dt**2
    colloid_pos += colloid_vel * dt_e + 0.5 * force_c / mass_c * dt**2
    fluid_pos %= box_size
    colloid_pos %= box_size
    new_forces_f, new_force_c = compute_forces_numba(fluid_pos, colloid_pos, sigma_cf6, sigma_cf12, sigma_f6, sigma_f12)
    fluid_vel += 0.5 * (forces_f + new_forces_f) / mass_f * dt_e
    colloid_vel += 0.5 * (force_c + new_force_c) / mass_c * dt_e
    forces_f = new_forces_f
    force_c = new_force_c
    # if step < 10: # Log only the first few steps
    #     force_mag = np.linalg.norm(force_c[0])
    #     print(f"Step {step:3d} | Colloid Pos: {colloid_pos[0]} | Vel: {colloid_vel[0]} | |F|: {force_mag:.3f}")

# Production phase (history recorded)

for step in range(n_steps):
    fluid_pos += fluid_vel * dt + 0.5 * forces_f / mass_f * dt**2
    colloid_pos += colloid_vel * dt + 0.5 * force_c / mass_c * dt**2
    fluid_pos %= box_size
    colloid_pos %= box_size
    new_forces_f, new_force_c = compute_forces_numba(fluid_pos, colloid_pos, sigma_cf6, sigma_cf12, sigma_f6, sigma_f12)
    fluid_vel += 0.5 * (forces_f + new_forces_f) / mass_f * dt
    colloid_vel += 0.5 * (force_c + new_force_c) / mass_c * dt
    forces_f = new_forces_f
    force_c = new_force_c
    if step % 10 == 0:
        fluid_history.append(fluid_pos.copy())
        colloid_history.append(colloid_pos.copy())

fig, ax = plt.subplots()
# Calculate figure and plot scale parameters
fig_width_inch = fig.get_size_inches()[0]
dpi = fig.dpi
axis_length_pt = fig_width_inch * dpi
marker_scale = 0.1 # Scale factor for visibility
fluid_marker_size = (marker_scale * axis_length_pt / box_size) ** 2
colloid_marker_size = 0.7*(marker_scale * sigma_c / sigma_f * axis_length_pt / box_size) ** 2
fluid_scatter = ax.scatter([], [], s=fluid_marker_size, c='blue')

```

```

colloid_scatter = ax.scatter([], [], s=colloid_marker_size, c='red')
trajectory, = ax.plot([], [], 'r--', linewidth=1, alpha=0.5)
ax.set_xlim(0, box_size)
ax.set_ylim(0, box_size)
ax.set_xticks([])
ax.set_yticks([])
ax.set_xticklabels([])
ax.set_yticklabels([])
ax.set_aspect('equal')
colloid_traj = []

def init():
    empty_offsets = np.empty((0, 2))
    fluid_scatter.set_offsets(empty_offsets)
    colloid_scatter.set_offsets(empty_offsets)
    trajectory.set_data([], [])
    return fluid_scatter, colloid_scatter, trajectory

def update(frame):
    fluid_scatter.set_offsets(fluid_history[frame])
    colloid_scatter.set_offsets(colloid_history[frame])
    colloid_traj.append(colloid_history[frame][0])
    traj_array = np.array(colloid_traj)
    trajectory.set_data(traj_array[:, 0], traj_array[:, 1])
    return fluid_scatter, colloid_scatter, trajectory

ani = animation.FuncAnimation(fig, update, frames=len(fluid_history), init_func=init, blit=True, interval=1)
ani.save("brownian_colloid.mp4", writer="ffmpeg", fps=30)
print("Simulation complete. Video saved as 'brownian_colloid.mp4'.")

```

More about the scientists mentioned in this chapter:

[Paul Langevin](#)

[Robert Brown](#)

[Albert Einstein](#)

[Walther Nernst](#)

[George Stokes](#)

Chapter 13

Dynamics of Fluctuations

This section is here for your interest but is not considered examinable.

In equilibrium, the principle of **detailed balance** implies microscopic reversibility — there are no net probability currents. As a result, time evolution is symmetric: fluctuations are time-reversal invariant. Recall the dynamic correlation matrix introduced in Section 2.2

$$\langle x(\tau)y(\tau+t) \rangle = M_{xy}(t)$$

of which $M_{xx}(t)$ is the diagonal.

Therefore:

$$M_{xx}(t) = \langle x(\tau)x(\tau+t) \rangle = \langle x(\tau)x(\tau-t) \rangle = M_{xx}(-t)$$

For the cross-correlation M_{xy} , we have:

$$M_{xy}(-t) = \langle y(\tau-t)x(\tau) \rangle = \langle y(\tau)x(\tau+t) \rangle$$

(using time translation invariance of the equilibrium state). Combining this with the previous symmetry, we find:

$$M_{xy}(t) = M_{yx}(t)$$

This means the dynamic correlation matrix is symmetric in its indices — a non-trivial consequence of microscopic time-reversal symmetry.

13.1 Linear Response Theory and the Fluctuation-Dissipation Theorem

Now suppose we gently perturb the system. For example, we might apply a small thermodynamic force f_x that couples to a fluctuating variable x — like a weak magnetic field h acting on a local magnetization.

(Formally, this means adding a perturbation $-f_x x$ to the Hamiltonian.)

A typical experimental protocol applies the perturbation from $t = -\infty$ and switches it off at $t = 0$. For $t > 0$, the average response of another variable y is observed to decay:

$$\langle y(t) \rangle_f = R_{yx}(t) f_x$$

Here, $R_{yx}(t)$ is the **response function** describing how y responds to a small force applied to x at earlier times (for $t \geq 0$).

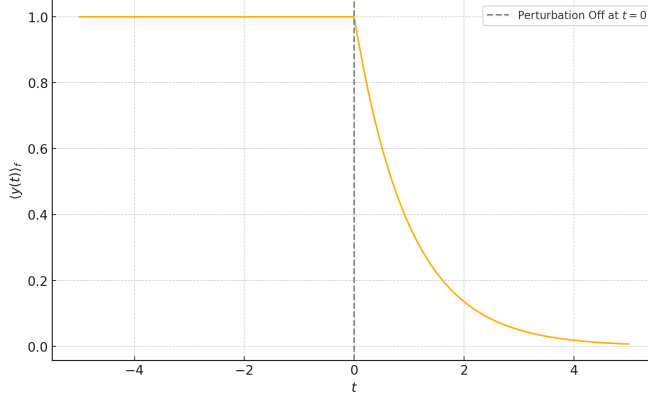


Figure 13.1: Effect of perturbation on a quantity which is zero in equilibrium

The key idea is this: If the perturbation is small enough, its effects are indistinguishable from those of a spontaneous fluctuation. So, the decay of the response function should mirror the decay of the correlation function of naturally occurring fluctuations.

This is the essence of the **fluctuation-dissipation theorem**:

$$k_B T R_{yx}(t) = M_{yx}(t)$$

This powerful result says that the system's response to a small disturbance is directly related to the correlation of fluctuations in thermal equilibrium.

The factor $k_B T$ ensures both sides of the equation have the same physical dimensions.

Note: We skip the full proof, which requires formal machinery from classical mechanics (e.g., Poisson brackets) or quantum mechanics (density matrices). For more, see the final chapter of Chandler.

13.2 Onsager's Theorem

Now, recall from the previous section that the correlation matrix is symmetric:

$$M_{xy}(t) = M_{yx}(t)$$

Combining this with the fluctuation-dissipation theorem gives:

$$R_{xy}(t) = R_{yx}(t)$$

This result is known as **Onsager's reciprocal relation**. It states that the response of variable x to a force acting on y is the same as the response of y to a force acting on x — provided the system is in equilibrium.

This is a deep and subtle consequence of microscopic reversibility, and Onsager's real contribution was realizing such a connection could exist. (Onsager also solved the 2D Ising model analytically and won the Nobel Prize in Chemistry in 1968.)



(a) Lars Onsager



(b) Onsager's gravestone and one-up-man-ship with colleague John Kirkwood

Figure 13.2: Norwegian Physicist and Nobel Laureate, [Lars Onsager](#)

Part II

Complex disordered systems

Chapter 14

Entropy matters

Most of the matter around us does not simply fit within the idealised pictures of crystalline solids or simple liquids: examples include colloids, polymers, surfactants, liquid crystals, foams, gels, and biological materials such as proteins, DNA, and cell membranes.

This means that cellular **life itself** (the very constituents that make us) obeys to principles that go beyond the standard patterns of conventional solid-state physics.

This branch of physics is called **soft condensed matter physics**, or **macromolecular physics**, or the physics of **complex fluids**. Specifically, *soft matter* refers to an area of condensed matter focused on systems that can be *easily deformed*.

In this course, we will emphasize the fact that many such systems are not crystalline: thermal noise and disordered configurations play a key role in their phase behavior, and hence we think of them as **complex disordered systems**.

While we often think about problems in physics as a matter of energy minimisation, in soft-matter physics a key role is played by the **fluctuations**. Typically (but not exclusively) these are **thermal fluctuations**. This means that **entropy** and not only the energy from the interactions plays a key role.

This is because soft matter systems are typically composed of **many microscopic constituents** in contact with an **environment**. The appropriate description of the **macroscopic state** of such systems is therefore **statistical** and uses the language of **statistical mechanics**. The relevant **energy**, therefore, is the free energy of the statistical ensemble representative of the system under consideration. For example, in the canonical ensemble, this is the Helmholtz free energy

$$F = U - TS$$

where U is the internal energy, T the temperature and S is the entropy of the system. Therefore, in a broader sense, soft matter is the physics of those systems for which the internal energy and the entropy are on comparable scales.

In other words, **fluctuations of the internal energy** are on the same scale as **thermal fluctuations**:

$$\Delta U \sim k_B T$$

where k_B is the Boltzmann constant and ΔU indicates standard deviations from the average internal energy.

The Physics of Entropy

Soft matter physics is fundamentally the physics of **entropy**. Unlike traditional systems where interaction energy minimization dominates, in soft matter, entropy plays a crucial role in determining the structure, dynamics, and behaviour of the system. The interplay between entropy and intermolecular energy leads to the rich and diverse phenomena observed in soft matter systems.

14.1 Systems and definitions

14.1.1 Elementary constituents and energy scales

Soft matter covers a wide spectrum of deformable systems. Each is constituted of many parts. Each is deformable because the interactions amongst such parts are **weak** compared to the perturbing forces (e.g. thermal fluctuations or mechanical loading).

In hard condensed matter, the elementary constituents are the atoms themselves, eventually with their subatomic particles. Between atoms, the scale of the interaction energies is in the 0.1 to 10 eV: for example the carbon-carbon covalent bond is approximately 3.6 eV.

The main units of soft matter are not atoms. They are instead themselves aggregates of atoms such as:

- **colloids**, micrometer- to nanometer-sized particles dispersed in a fluid.
- **polymers**, macromolecules composed of long chains such as DNA, proteins, plastics
- **surfactants**, macromolecules with polar head and tails that lead to the spontaneous formation of structures such as bilayers (e.g. the cellular membrane).

Amongst such units, the dominating forces of soft matter are much weaker than in hard condensed matter:

- Van der Waals forces are of the order of 0.001-0.01 eV
- weak interactions such as hydrogen-bonds are typically in the 0.01-0.2 eV range
- the thermal energy at room temperature is $k_B T \approx 0.025\text{eV}$ (check it for yourself)

At the **microscopic** level, all these interactions have essentially one source: the electrostatic force. However, this information is practically of no use when we want to understand how the units of soft matter come together to give rise to **macroscopic** properties of soft matter systems, such as their elastic properties, their viscosities, their plasticity. In fact, the emphasis on the atomistic details of the various units is fundamentally misleading: atomistically very different objects (e.g. colloids and micelles) can in fact share very similar macroscopic behaviours.

Therefore, theories of soft matter leverage the concept of **coarse-graining**, rooted in the renormalisation group notions explored earlier. Coarse-graining means integrating out the unimportant degrees of freedom and only describing the units in terms of a few important parameters. For example, instead of taking a full atomistic representation of the DNA we may want to focus on the fact that structurally it is a long chain with specific bending energies: we may want to include the fact that it is formed by a double helix but we may not want to specifically construct every single atom in the sugar chain that forms the backbone. An example of DNA coarse graining is provided by the successful model [oxDNA](#) (see picture below):

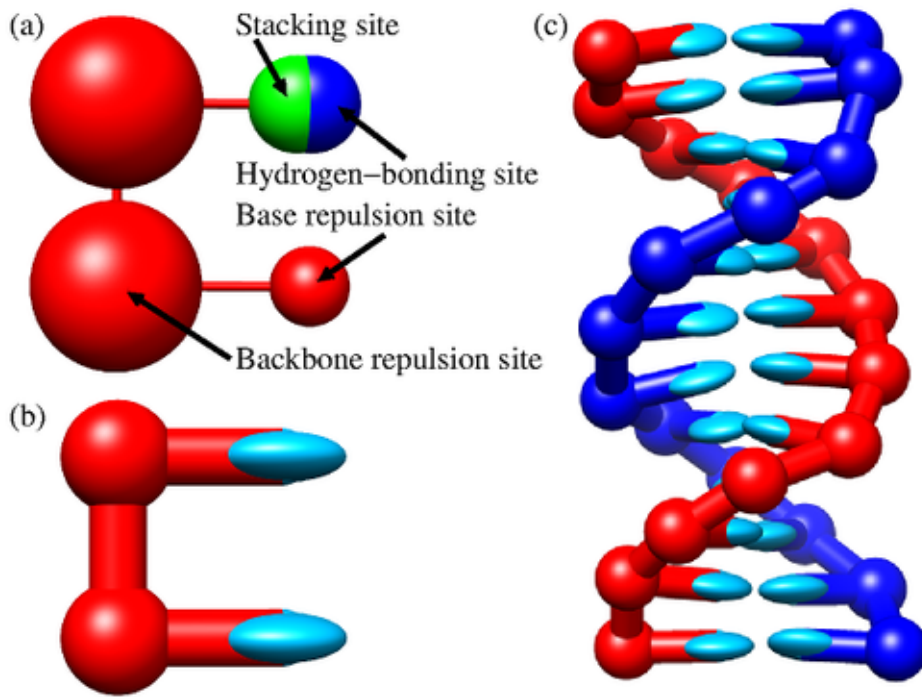


Figure 14.1: oxDNA model: (a) Base structure on one strand; (b) planarity of the bonding; (c) an example of the resulting double strand.

i Coarse graining

Coarse graining is often motivated by intuition, experimental insights or a simple desire of simplification. It allows for a multi-scale description of the problem which permits to describe large systems and long time scales.

Nonetheless, coarse-graining can also be made mathematically rigorous. For example, rigorous coarse graining in statistical mechanics can be performed by projecting the dynamics onto a relevant and an irrelevant (fluctuating) part, in the so called [Mori-Zwanzig formalism](#) (Mori 1965).

14.1.2 Classes of systems

In our exploration of soft matter we will focus on six main classes of systems which display different physics:

- colloidal dispersions
- polymeric systems
- liquid crystals
- surfactant aggregates
- arrested systems
- active matter

Colloidal dispersions

Colloidal dispersions are systems where small particles, typically in the nanometer to micrometer range, are dispersed in a continuous medium (a solvent). Prototypical colloids are **spherical**

particles of various sizes (e.g. as those present in paint) but colloidal science has achieved a high degree of sophistication, with colloidal particles with various different shapes and interactions.

Colloids are often thought as **big atoms**: they exhibit Brownian motion, can form ordered structures (colloidal crystals), and display phase transitions similar to atomic systems. However, their larger size and slower dynamics make them ideal for studying phenomena that are difficult to observe in atomic systems.

Polymeric systems

Polymer physics is a field on its own. Polymers are macromolecules composed of repeating structural units (monomers) connected by covalent bonds. Their unique properties arise from their string-like structure and the interplay between entropic and energetic contributions.

Polymers can be classified into two main categories:

- **Synthetic polymers**, including plastics (e.g., polyethylene, polystyrene) and synthetic rubbers.
- **Biopolymers**, such as polymers like DNA, RNA, and proteins.

Compared to colloids, polymers have distinctive characteristics common to all chain-like molecules, such as their topological constraints due to the fact that two polymers cannot cross each other (a phenomenon known as *polymer entanglement*).

Liquid crystals

When we take soft matter units that are highly anisotropic (e.g. elongate in particular directions) thermal fluctuations and high packing lead to equilibrium states with a degree of order that is intermediate between the complete disorder of a liquid and the long-ranged, three-dimensional order of a crystal.

Such states are referred to as **liquid crystal** and can be described successfully with continuum free energy theories that take into account the symmetries of the order parameters.

Components that form liquid crystals are called **mesogens** and include highly anisotropic organic macromolecules (as used in liquid crystal displays), rod-like molecules or polymeric aggregates, as well as disk-shaped molecules and particles(such as triphenylene and derivatives).

Surfactant aggregates

When two distinct fluid phases are put into contact, a free energy cost per unit area ensues: this is the surface tension. It is possible to control the tension by introducing molecules that sit at the interface between the two phases, called **surfactants**.

Hence, surfactants are molecules which contain chemical groups with different affinities (they are **amphiphilic**). A key example is the case of phospholipids, which possess both hydrophilic (water-preferring) heads and hydrophobic (water avoiding) tails. As surfactants sit at the interface they are able to **self-assemble** and separate different fluid phases, forming equilibrium bilayers and vesicles that are ubiquitous in cell biology.

Arrested systems

We have stressed that the thermal energy is distinctive of soft matter systems. It would be then natural to assume that as we reduce the temperature, we should converge readily to the solid state physics of crystalline solids. In fact, on the way to low temperatures, the lack of long-range order of most soft-matter systems has important consequences: many such systems find

themselves trapped in states that are not corresponding to the global energy minimum (i.e. the crystal) and instead display non trivial mechanisms of structural relaxation. These systems are disordered a bit like liquids, but share various mechanical properties, such as emergence rigidity, elasticity and plasticity.

Examples of arrested systems include:

- **Glasses**, such as silica glass or metallic glasses, where the system is kinetically trapped in a disordered state.
- **Gels**, which are networks of interconnected particles or polymers that span the entire system, providing rigidity despite being mostly liquid.

These systems are arrested as their relaxation towards equilibrium is so slow that is longer than any observable timescales. This makes them fundamentally **out-of-equilibrium** systems, escaping from an ordinary description in terms of equilibrium statistical mechanics.

Active matter

Active matter refers to systems composed of units that consume energy to generate motion or mechanical stresses. Unlike passive systems, active matter is inherently out of equilibrium due to the continuous energy input at the microscopic level. Examples include:

- **Biological systems**, such as bacterial colonies, cell tissues, and flocks of birds.
- **Synthetic systems**, like self-propelled colloids or active gels.

The study of active matter focuses on understanding how individual activity leads to emergent collective behaviors, such as swarming, clustering, or pattern formation, often described using hydrodynamic theories or agent-based models.

Chapter 15

Colloids

```
#| echo: false
#| autorun: true
# modifying the path to add the code folder
import sys
sys.path.insert(0, 'src')
```

15.1 Kinds of colloids

Colloids are mixtures where one substance is dispersed throughout another. They consist of particles that are larger than typical molecules but small enough to remain suspended without settling. Examples include milk, fog, and paint.

Colloids can be classified based on the state of the **dispersed phase** and the **dispersion medium**. Depending on the particular mixture, one can obtain a wide variety of soft materials, with unique mechanical, optical, and thermal properties.

Dispersion Phase	Dispersion Medium
Solid	Solid <i>Solid suspension:</i> pigmented plastics, stained glass, ruby glass, opal, pearl
Liquid	<i>Solid emulsion:</i> bituminous road paving, ice cream
Gas	<i>Solid foam:</i> zeolites, expanded polystyrene, 'silica gel'

Clearly, colloidal materials form an incredibly diverse class, and surround us in our everyday lives. Here are some visual examples from the table above:

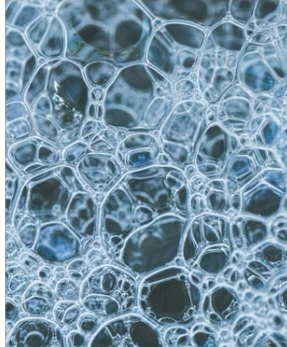
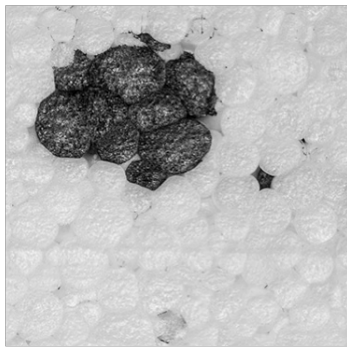


Figure 15.1: First row: opal, paint, smoke. Middle row: ice-cream (*gelato*), milk, fog. Bottom row: expanded polystyrene and foam. Source: unsplash.com

The [IUPAC definition of colloids](#) is based on the idea that the particles are dispersed in a medium, creating a *subdivision* at the **colloidal scale**: approximately 1nm to $1\mu\text{m}$.

The small sizes of colloids means that they are constantly subject to the collisions with the atom/molecules/particle of the medium, triggered by thermal fluctuations. Due to this, the colloids undergo [Brownian motion](#). For each particle, the amount of energy received from the medium is of the order of $k_B T$ (the reference energy scale of thermal soft matter). This energy can be compared with the potential energy to produce a dimensionless number, the

gravitational Péclet number

$$\text{Pe}_g = \frac{\Delta m g R}{k_B T}$$

where R is the radius of the colloid respectively, g is the acceleration due to gravity, and Δm is the *buoyant mass*, which for a spherical colloid is expressed as $\Delta m = \frac{4\pi}{3} \Delta\rho R^3$, with $\Delta\rho$ being the density difference between the particle and the dispersion medium (the *solvent*). We have a colloidal suspension only when $\text{Pe}_g \lesssim 1$, i.e. when Brownian motion is only marginally perturbed by the effects of gravity.

15.2 Stability of colloids and colloid-colloid interactions

A colloidal dispersion is said to be **stable** if it is able to remain dispersed and Brownian for a long time (typically, significantly longer than the experimental observation time). Unstable colloids undergo aggregation or sedimentation due to the dominance of attractive forces or gravity.

For example, consider a colloidal suspension like milk. Milk is an emulsion where fat droplets are dispersed in water and stabilised by proteins. If lemon juice (an acid) is added, the dispersion medium (water) changes, the pH drops, and the emulsion is *destabilised*. This causes the proteins to coagulate, leading to the separation of curds (solid) and whey (liquid).



Figure 15.2: Curds and whey resulting from the destabilisation of milk, a colloidal emulsion. (Wikimedia)

It is clear from this example that the nature of the dispersed phase and the dispersed medium ultimately determine the stability of colloidal dispersions. What ultimately matters for the stability is whether the colloids have a propensity to aggregate or not. This propensity is quantified in terms of **colloidal interactions**.

15.2.1 Fundamental and effective forces

At the colloidal scales, only two kinds of fundamental forces are relevant: gravity and electro (and occasionally magneto) static forces. As we have seen above, when a system is truly colloidal, gravitational contributions are assumed to be small, so in effect for a non magnetic colloid (which is the vast majority of colloidal systems) only electrostatic forces are fundamentally important.

However, colloidal dispersions consist of large particles carrying many charges both in the dispersed phase and the surrounding medium, arranged disorderly at the atomic scale. This makes a microscopic description of all charges and the resulting electrostatic fields not only unfeasible but also ineffective for understanding colloidal systems in terms of key characteristics such as particle size, density, and spatial distribution. The fundamental issue is the one of time-scales: the motion of colloids is much slower than the motion of individual ions or molecules. Over such longer timescales, many interactions at the **microscopic** atomistic scale take place and we can think of taking averages to extract **macroscopic, effective** interactions at the colloidal scale ¹.

This is especially important due to **quantum fluctuations**: the uncertainty principle means that electron clouds around atoms are not fixed but exhibit intrinsic fluctuations in their charge distribution. Perturbative approaches allow us to capture the effective forces resulting from such fluctuations.

There are many examples of such effective forces (Lekkerkerker, Tuinier, and Vis 2024). One you may already know is the Van der Waals interaction. For colloids, we have additional relevant forces, such as the double layer interaction and the depletion interaction. We detail them here below.

15.2.2 Van der Waals interaction

The London-van der Waals **dispersion forces** arise from the interaction between **instantaneous dipoles** in overall neutral atoms or molecules. We know from classical electrostatics that static dipoles interact via the dipole-dipole interaction, with a potential strength which decays like $1/r^3$, where r is the separation between two dipoles.

More in general, neutral atom or molecules have electronic clouds that are fluctuating and not symmetrically distributed, creating a **temporary dipole**. Such instantaneous dipole **induces** a dipole in a neighboring atom or molecule by distorting its electron cloud.

The interaction energy between two dipoles μ_1 and μ_2 separated by a distance r is proportional to:

$$U \propto -\frac{\mu_1 \mu_2}{r^3}$$

The dipole moments fluctuate due to quantum mechanical effects. The average interaction energy is derived using perturbation theory and is proportional to the polarisabilities α_1 and α_2 of the two particles:

$$U(r) = -\frac{C}{r^6}$$

where $C \propto \alpha_1 \alpha_2$ depends on the polarisabilities and ionization energies of the particles.

The resulting r^{-6} dependence is also referred to as the **London dispersion force**, which can be derived within quantum-mechanical perturbation theory (London 1937).

¹This is clearly an instance of the idea of **coarse graining** that we have introduced [earlier](#).

We can then assume to take two identical spherical colloids of radius R at distance h and that every volume element of such spheres interacts with the London dispersion force (see the semi-classical approach of Hamaker Hamaker (1937) for illustration). Integrating over all volume elements yields the colloidal spheres **Van der Waals attractive potential** in the form

$$W_{wdW}(h) = -\frac{A - H}{g} f(h/R)$$

where A_H is the **Hamaker constant** and $f(h/R)$ is

$$f(h/R) = \left[\frac{2R^2}{h^2 - 4R^2} + \frac{2R^2}{h^2} + \ln \left(\frac{h^2 - 4R^2}{h^2} \right) \right]$$

i Sketch of a derivation of colloid-colloid Van der Waals potential

Each volume element in one sphere interacts with each in the other sphere via:

$$\phi(r) = -\frac{C}{r^6}$$

So the total interaction energy is:

$$U(h) = -C \iint \frac{1}{|\mathbf{r}_1 - \mathbf{r}_2|^6} dV_1 dV_2$$

Let:

- Sphere 1 be centered at $(0, 0, 0)$,
- Sphere 2 be centered at $(0, 0, h)$,
- $\mathbf{r}_1 = \mathbf{r}$, $\mathbf{r}_2 = \mathbf{r}'$

Then $|\mathbf{r}_1 - \mathbf{r}_2| = |\mathbf{r} - \mathbf{r}'|$, and the integral becomes:

$$U(h) = -C \iiint_{|\mathbf{r}| \leq R} \iiint_{|\mathbf{r}' - h\hat{z}| \leq R} \frac{1}{|\mathbf{r} - \mathbf{r}'|^6} d^3\mathbf{r} d^3\mathbf{r}'$$

Hamaker evaluated this by integrating over the **densities of interacting atoms** with number density ρ in both spheres. The result:

$$U(h) = -\rho^2 C \iint \frac{1}{|\mathbf{r}_1 - \mathbf{r}_2|^6} dV_1 dV_2$$

Defining the **Hamaker constant**:

$$A_H = \pi^2 \rho^2 C$$

So,

$$U(h) = -\frac{A_H}{\pi^2} \iint \frac{1}{|\mathbf{r}_1 - \mathbf{r}_2|^6} dV_1 dV_2$$

This six-dimensional integral can be evaluated analytically for spheres, yielding:

$$U(h) = -\frac{A_H}{6} \left[\frac{2R^2}{h^2 - 4R^2} + \frac{2R^2}{h^2} + \ln \left(\frac{h^2 - 4R^2}{h^2} \right) \right]$$

```
#| autorun: true
import numpy as np
import plotting
# parameters: change them to explore the interaction!
R = 5.0 # Radius of the colloid
A_H = 1e-20 # Hamaker constant (in Joules)
h = np.linspace(2.01 * R, 10+R*2, 1000) # Separation distance (h > 2R)
# Van der Waals potential
def van_der_waals_potential(h, R, A_H):
    f_h_R = (2 * R**2 / (h**2 - 4 * R**2)) + (2 * R**2 / h**2) + np.log((h**2 - 4 * R**2) / h**2)
    return -A_H * f_h_R

# compute potential
W_vdW = van_der_waals_potential(h, R, A_H)
# convenience plotting function, you can use matplotlib if you prefer
plotting.simple_plot(h,W_vdW)
```

Van der Waals interactions are considered to be **short-range** forces in the sense that their decay rate(e.g. London's $1/r^6$) is much faster than Coulombic interactions ($1/r$). Importantly, since their origin resides in the fluctuation of charges on the colloids, their strength is *not additive*: simply summing all the pairwise interactions does not fully accurately account for man-body effects. We often rely on such two-body approximations, but we should be aware that they are a simplified scenario.

15.2.3 Double-layer interaction

Colloids are often charged. The solution they are immersed also has an **inhomogeneous** distribution of ions: there will be

- **co-ions** (same charge as the colloid) that will be pushed away from the colloid surface, while
- **counter-ions** (opposite charge) will accumulate at the surface.

These two different concentrations of oppositely charged ions form what is called a **double layer** and its property (such as its width) are obviously controlled by the number of ions in the solvent, which can be tuned by adding or removing, for example, salts.

Suppose we now have two colloids of the same size and charges in the solvent. Th charges in their double layers will interact giving rise to a **repulsive interaction**. This interaction is referred to as **screened-Coulomb** (as the electrostatic interaction is *screened by the presence of the ions* or **double layer repulsion**. We are not going to derive it, but it can be shown that, for a colloid of radius R in solvent with salt density n_s it can approximated by an exponential decay

$$W_{DR}(h) = B \frac{R}{\lambda_B} \exp(-h/\lambda_D)$$

where λ_D is called the **Debye length**

$$\lambda_D = \sqrt{\frac{1}{8\pi\lambda_B n_s}}$$

while λ_B is the **Bjerrum length**, which is itself derived from the characteristic distance at which two elementary charges have energy $k_B T$ ²

$$\lambda_B = \frac{e^2}{4\pi\epsilon_0\epsilon_r k_B T}$$

The coefficient B is a material properties that depend on the surface potential. We are not going more into the details of these features, which are important for the design of colloidal experiments.

From our point of view, what matters is that identical colloids in solution appear to have two interactions of opposite sign

- a van der Waals components, typically attractive and emergent from induced dipole -dipole interactions emerging from quantum fluctuations of the electronic clouds
- a double layer component, repulsive in nature, and resulting from the electrostatic repulsions induced by ions and counterions

The **sum** of the two gives rise to the **DLVO** (Derjaguin–Landau–Verwey–Overbeek) **interaction** which is an elementary model for colloid stability and aggregation.

```
#| autorun: true

import numpy as np
import matplotlib.pyplot as plt

R = 1.0 # Radius of the colloid (micron)
h = np.linspace(2.01 * R, 2+R*2, 1000) # Separation distance (h > 2R)
# Van der Waals attractive potential
def van_der_waals_potential(h, R, A_H):
    f_h_R = (2 * R**2 / (h**2 - 4 * R**2)) + (2 * R**2 / h**2) + np.log((h**2 - 4 * R**2) / h**2)
    return -A_H * f_h_R
# double layer repulsive potential
def double_layer(h, R,B,ns ):
    lambdaB = 0.0007 # typical Bjerrum length for water at 25 degrees (micron)
    lambdaD = np.sqrt(1/(8*np.pi*lambdaB*ns))
    print("Debye length of", lambdaD)
    return B*R/lambdaB*np.exp(-h/lambdaD)

#| caption: "DLVO potential [press ctrl/cmd [ENTER] to run]"
#| autorun: true
# parameters: CHANGE them to explore the interaction!

A_H = 1.0 # Hamaker constant (kBT)
B = 50.0 # double layer energy scale
salt_ns = 2000 # salt concentration (particles/micron^3)

# compute potentials
W_vdW = van_der_waals_potential(h, R, A_H)
W_DR = double_layer(h, R, B,salt_ns)
```

²As you see, scaling by $k_B T$ is a recurrent feature of soft matter.

```
DLVO = W_vdW+W_DR
```

```
import plotting
plotting.multi_plot(h, W_vdW, W_DR,DLVO,
    xlabel="h [μm]", ylabel="Interaction strength [kBT]")
# nicer cliping
ylim = max(DLVO.max(),0.5)
plt.ylim(-ylim*1.1, ylim*1.1)
plt.show()
```

! Activity

Modify the script above and test graphically that:

1. When the salt concentration is low, the double layer repulsion dominates the DLVO interaction
2. There are salt concentrations where two minima occur in the DLVO potential: one at very close distance (dominated by the Van der Waals attraction) and one, much shallower, at intermediate distances comparable to $2(R + \lambda_D)$. This minimum can lead to weak aggregation of colloids
3. Large salt concentrations depress the DLVO maximum altogether and eventually the Van der Waals interaction dominates.

15.2.4 Steric interactions and depletion interactions

We have seen that quantum fluctuations from the uncertainty principle can be recast via a semi-classical approach into effective short-range interactions (van-der Waals). Another fundamental quantum principle – Pauli's **exclusion principle** – is also at the source of key effective interactions that can be understood in a semi-classical picture. Indeed, the main consequence of the exclusion principle is that since electrons cannot occupy the same quantum state, there are minimal distances below which atoms cannot be brought together.

This simply means that as we take a pair of atoms, below a certain distance they **repel** each other with very strong forces, even in the absence of double layer interactions. These **repulsive interactions** can be approximated in various ways: their strength depends on the details of the atoms and hence, in the case of colloids, on the details of the materials composing the colloids. We call these excluded volume interactions **steric interactions**³.

These fundamentally repulsive interactions mean that that, in a system with N colloids, an additional $N + 1$ colloid does not have access to the entire configuration space: there is a large **excluded volume** due to the presence of the other colloids.

What is intriguing of these interactions is that, even if they are purely repulsive, they can collectively give rise to effective attractive interactions: **attraction through repulsion**.

15.2.4.1 A simple example: particles in a one-dimensional line (*hard rods*)

As an introductory example, let us consider a very simple, idealised system of purely repulsive objects. Let us confine them along a one dimensional line, bounded by hard (repulsive and impenetrable) walls separated by the distance L . Assume the objects to be N spheres of diameter d , or (equivalently) *hard rods* of length d . They cannot overlap so, once they are placed along the line, their order cannot change.

³From the Greek στερεός, “solid, three-dimensional”.

What we want to know is how these hard objects, that interact solely via repulsive interactions, distribute themselves along the line. The problem is a classic of statistical mechanics and thanks to its one-dimensional nature can be addressed extensively using analytical methods.

Here we take a more algorithmic approach, and directly sample the probability density distribution $\rho(x)$ of finding a particle center at position x .

To do so, we do the following:

i Algorithm

1. position the particles in a valid configuration (no overlaps with other particles or the walls)
2. pick a particle at random
3. move it slightly along the line
4. test the if the new position is valid (no overlaps)
5. if valid, accept the move otherwise, reject
6. go back to (2)

This very simple algorithm is based on a **trial** move and an **accept/rejection** step. This is the heart of a very popular molecular simulation method, named **Metropolis Monte-Carlo Chain method**.

Here below you have a very simple implementation in python.

```
#| caption: "1D hard particles [press ctrl/cmd [ENTER] to run]"
import numpy as np
import matplotlib.pyplot as plt

#number of particles
N = 18
# particle diameter
d = 1.0
# box size
L = 24.0
# maximum displacement and number of steps
delta, steps = 0.5, 100000
# initial configuration
pos = np.linspace(d, L - d, N)

def valid(p):
    "Check that consecutive (sorted) particles are non-overlapping"
    return np.all(p >= d/2) and np.all(p <= L-d/2) and np.all(np.diff(p) >= d)

positions_samples = []

for step in range(steps):
    i = np.random.randint(N)
    move = np.random.uniform(-delta, delta)
    new_pos = pos.copy()
    new_pos[i] += move
    # sprting allows ot only check for consecutive particles
    new_pos.sort()
    if valid(new_pos):
        pos = new_pos
```

```

if step % 100 == 0:
    positions_samples.extend(pos)

plt.hist(positions_samples, bins=128, range=(0, L), density=True)
plt.xlabel("Position [d]")
plt.ylabel("Probability density")
plt.title("Histogram of particle positions")
plt.show()

```

The code should produce a final probability distribution along the x axis. The main control parameter here is the **packing fraction**, i.e. $\phi = \frac{dN}{L}$, the coverage of the line. If you take high values for the packing fraction you will observe an interesting effect: the distribution $\rho(x)$ displays distinctive modulations. Surely, these reflect the layering of the particles along the line, due to their hard-core interactions. However, the oscillations are even more interesting as we observe that the particles are more likely to be found near the walls than away from them.

Reflect on this point. In the complete absence of any attractive interactions, we find that the hard particles are *preferentially* located close to the walls. It is *as if* the walls exerted an *attractive force* capable of pulling the particles close to them. In reality, the force is purely statistical in nature. It is merely the result of the **entropic** advantage that the **entire** system acquire when the particles are closer to the walls: simply put, if the first (and last) particles are close to the walls, there is more space for the particles in the middle, hence a larger number of configurations and hence larger **configurational entropy**.

Even if the force is statistical, it is not less real: in this simplified case, it leads to the layering of the density profile. Its generalisation to less idealised conditions leads to a family of forces that are essential for the aggregation of soft matter which are called **depletion interactions**.

15.2.5 Asakura-Oosawa depletion potential

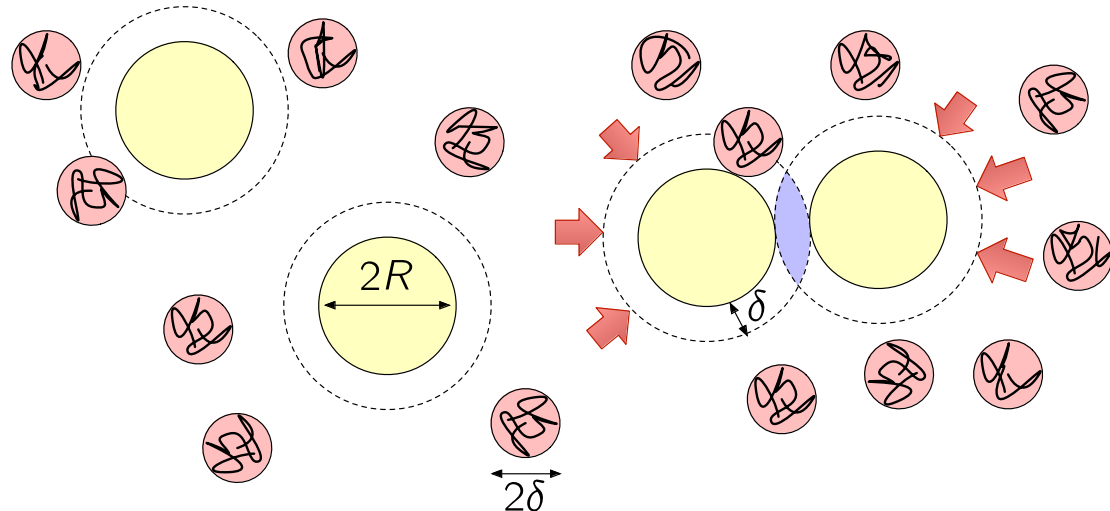


Figure 15.3: Mixture of colloids (yellow) and polymers (squiggly lines inside red circles). The depletion layers are as thick as the polymer radius (red circles) and are indicated with the dashes around the colloids. When the two layers do not overlap, the osmotic pressure due to the polymers on the colloids is balanced. When there is overlap, there is a region inaccessible to the polymers (purple) and the pressure is unbalanced, leading to aggregation.

The simple unidimensional scenario can be extended to a more interesting situation of hard-core colloidal particles dispersed in a medium where other smaller, repulsive particles (e.g. coiled polymers) are also dispersed. It is not important at this stage to know the details of such polymeric structures. We will ignore their internal structure and we will also ignore their mutual interactions. We will only consider for the moment how they interact with the colloids and how this mediates an interaction *between* the colloids. We call these idealised polymers *penetrable hard spheres*.

This assumption yields a great simplification: the polymers, on their own, are an ideal gas. Their chemical potential is given by

$$\mu = k_B T \ln \eta_b \quad (15.1)$$

We assume also to work in an ensemble at fixed volume V , temperature T and chemical potential μ : this is the **grand canonical ensemble**. This means that we imagine that there is some ideal reservoir with which we can exchange polymers in order to maintain the chemical potential constant.

The grand potential for such ideal polymers is given by

$$\Omega = -k_B T e^{\mu/k_B T} V_{\text{accessible}}$$

where $V_{\text{accessible}}$ is the accessible volume. In the absence of the colloids, the entire volume V is accessible.

Let's imagine to introduce two colloids at separation r . For all $r > 2(R + \delta) = R_d$, the accessible volume is $V_{\text{accessible}}^\infty = V - 2V_{\text{exclusion}}$, where R_d is the **depletion radius** and $V_{\text{exclusion}}$ is the inaccessible region due to the colloid-polymer interaction around each colloid:

$$\begin{aligned} V_{\text{exclusion}} &= V_{\text{outer}} - V_{\text{inner}} \\ &= \frac{4\pi}{3} ((R + \delta)^3 - R^3) \end{aligned}$$

Changing the separation between the two colloids but maintaining $r > 2R_d$ does not change the grand potential: there is no free energy advantage and hence no effective interaction.

Instead, it is only when we take the colloids closer than $2R_d$ that we see a free energy difference. When $r < 2R_d$ (and, obviously, $r > 2R$) an overlap region is formed (the lens-shaped region of the figure above). Its volume can be calculated simply from geometrical considerations and it is

$$V_{\text{overlap}}(r) = \frac{4\pi}{3} R_d^3 \left[1 - \frac{3}{4} \frac{r}{R_d} + \frac{1}{16} \left(\frac{r}{R_d} \right)^3 \right] \quad (15.2)$$

The new accessible volume is

$$V_{\text{accessible}}' = V - 2V_{\text{exclusion}} + V_{\text{overlap}}$$

The interaction between the two colloids resulting from the free energy advantage is called **potential of mean force** $W(r)$. It is expressed as

$$\begin{aligned} W_{AO}(r) &= \Omega(r) - \Omega^\infty = -k_B T e^{m/k_B T} (V_{\text{accessible}}(r) - V_{\text{accessible}}(\infty)) \\ &= -k_B T e^{m/k_B T} [V - 2V_{\text{exclusion}} + V_{\text{overlap}}(r) - (V - 2V_{\text{exclusion}})] \\ &= -k_B T e^{m/k_B T} V_{\text{overlap}}(r) \end{aligned}$$

We can now re-use the ideal polymer chemical potential definition Equation 15.1 and the gemoetrical expression for V_{overlap} in Equation 15.2 to finally write the **Asakura-Oosawa** potential

$$W_{\text{AO}}(r) = -\frac{4\pi\eta_b k_B T}{3} (R+\delta)^3 \left[1 - \frac{3}{4} \frac{r}{R+\delta} + \frac{1}{16} \left(\frac{r}{R+\delta} \right)^3 \right] \quad 2R \leq r < 2R+\delta$$

taking $q = \delta/R$ (the polymer-to-colloid size ratio), so $R + \delta = R(1 + q)$ and $r/(R + \delta) = r/[R(1 + q)]$ the AO potential can also be rewritten as:

$$W_{\text{AO}}(r) = -\frac{4\pi\eta_b k_B T}{3} [R(1+q)]^3 \left[1 - \frac{3}{4} \frac{r}{R(1+q)} + \frac{1}{16} \left(\frac{r}{R(1+q)} \right)^3 \right] \quad 2R \leq r < 2R(1+q)$$

```
#| caption: "Asakura-Oosawa potential [press ctrl/cmd [ENTER] to run]"
#| autorun: true

import numpy as np
import matplotlib.pyplot as plt

# Parameters (change to explore)
R = 1.0          # Colloid radius
delta = 0.2       # Polymer radius
eta_b = 0.1       # Polymer concentration (dimensionless)
kBT = 1.0         # Set kBT=1 for reduced units

# Depletion radius
Rd = R + delta

# r values: from contact (2R) up to 3(R+delta)
r = np.linspace(2*R, 3*Rd, 500)

def AO_potential(r, R, delta, eta_b, kBT):
    Rd = R + delta
    # Only defined for 2R <= r < 2Rd
    W = np.zeros_like(r)
    mask = (r >= 2*R) & (r < 2*Rd)
    x = r[mask] / Rd
    W[mask] = - (4 * np.pi * eta_b * kBT / 3) * Rd**3 * (1 - 0.75 * x + 0.0625 * x**3)
    return W

W_AO = AO_potential(r, R, delta, eta_b, kBT)

plt.plot(r, W_AO)
plt.gca().set(xlabel="Separation $r/R$ ", ylabel="$W_{\text{AO}}(r)$", title="Asakura-Oosawa Depletion Potential")
plt.show()
```

i Force-based derivation of the AO interaction

When the colloids are so close the polymers cannot enter the lens-shaped region between the two colloids. This gap leads therefore to an *uniform* distribution of polymers which results in an pressure difference: the outer polymers push the colloids together, producing an effective attractive force. Such pressure resulting from an uncompensated concentration gradient is called **osmotic**.

The lens-shaped overlap region between the two colloids consists of two identical spherical caps, each subtending an angle θ_0 at the center of the colloid. From the given geometry, the angle is such that

$$\cos \theta_0 = \frac{r}{2R_d}.$$

The uncompensated pressure acts on such surface.

For symmetry reasons, only the forces along the axis connecting the two spheres contribute to the total force. For a given angle θ the components is proportional to $P \cos \theta$ where P is the pressure exerted by the ideal gas of polymers is simply $P = \eta_b kT$ where η_b is the polymer concentration. The surface element on which this pressure acts for a small increment $d\theta$ is

$$dS = 2\pi R_d^2 \sin \theta d\theta$$

. Integrating over the range $[0, \theta_0]$ yields the total force F_d

$$\begin{aligned} F_d(r) &= -2\pi \eta_b k_B T R_d^2 \int_0^{\theta_0} \sin \theta \cos \theta d\theta \\ &= -\pi R_d^2 \eta_b k_B T \left[1 - \left(\frac{r}{2R_d} \right)^2 \right] \end{aligned}$$

Notice the negative sign, chosen to reflect the fact that the force is attractive.

Integrating the force yields the interaction potential.

i Summary of main colloid-colloid interactions

Interaction Type	Description	Range
Van der Waals	Attractive forces arising from induced dipoles between particles.	Short-range
Double Layer	Electrostatic repulsion due to overlapping electrical double layers around charged particles.	Long-range
DLVO	Combination of van der Waals attraction and double layer repulsion.	Short and long range
Depletion	Typically attractive interactions emerging from purely entropic interactions	Short range

15.3 Colloids as big atoms

Colloids can be viewed as “big atoms”: they are large particles suspended in a medium, exhibiting thermal motion and interactions in various ways analogous to atoms, but at much larger length and time scales. As we have seen above, the interactions can have statistical or even quantum-mechanical origins, but are ultimately cast in a classical form that is amenable to a classical treatment. At the same time, the large scales of colloids mean that via dedicated microscopy techniques one is able to identify individual colloids, study their arrangements in detail, and follow their dynamics.

As mentioned earlier, there is a huge variety of colloids and a vast literature characterising their properties but also producing theoretical and computational models.

Here we focus on the most elementary model of a colloid. The simplest such example is the purely repulsive hard-sphere colloid. While an idealisation, quasi-hard-sphere colloids can be prepared in the laboratory by various techniques (see Royall et al. (2024)). This includes by synthesizing spheres of bundled polymers (you will learn about polymers in the next chapter) such as polymethyl methacrylate (PMMA), but also simply silica (small sphere of non-crystalline SiO_2) micron-sized beads carefully treated to screen and minimize the electrostatic interactions that would lead to DLVO-like contributions.

15.3.1 The archetype: hard-spheres

A **hard-sphere** is an idealized particle model in which each particle is represented as a perfectly rigid sphere of fixed radius R and diameter $\sigma = 2R$. Hard spheres interact only through excluded volume: they cannot overlap, but otherwise experience no attraction or repulsion. The interaction potential $U(r)$ between two hard spheres separated by a center-to-center distance r is:

$$U(r) = \begin{cases} \infty & \text{if } r < \sigma \\ 0 & \text{if } r \geq \sigma \end{cases}$$

This model captures the essential physics of **excluded volume** which, as we said earlier, fundamentally emerges from Pauli’s exclusion principle (electrons cannot occupy the same quantum state so electronic clouds of different atoms *exclude* each other).

$r \leq 2R \Rightarrow U(r) = \infty$ forbidden Hard Sphere Potential

Phase behaviour of hard spheres

Since the interaction potential is only based on excluded volume, the energy of hard spheres is trivial: it is **always zero**. A naive interpretation of such trivial energetics may lead to conclude that nothing interesting happens to a collection of hard spheres, since they always are at their energy minimum (namely, zero). However, it is clear from the earlier discussion of depletion forces that the interaction energy is only a part of the picture for systems subject to thermal fluctuations: indeed, for any $T > 0$, **entropic** contributions to the free energy are always present. In the specific case of a fixed number of hard spheres in a fixed volume, they are *the only* contribution to the free energy.

In this sense, hard-spheres are completely **entropy-driven** system. For a collection of identical (**monodisperse**) hard spheres the entropy is solely **configurational** and corresponds to the number of possible arrangements. This is constrained only by the accessible volume, of which we have seen an instance when considering the depletion interactions. Notice that changing the temperature does not really affect the statistics of the configurations: the Boltzmann factor

$e^{U(\mathbf{r}^N)/k_B T}$ is always 1 for all valid configurations. The only way we can change the state of the system is by varying the accessible volume. For a system of N identical hard spheres in a volume V this can only be done in two ways

- by adding more spheres (of the same kind)
- by varying the volume V

The two routes essentially amount to varying one single parameter, which is the **packing fraction** (also called, *volume fraction*) of the system, defined as

$$\phi = N \frac{v_{\text{sphere}}}{V} = \frac{\pi \sigma^6 N}{6V}$$

which can also be expressed in terms of the **number density** $\rho = N/V$ as $\phi = \pi \sigma^3 \rho / 6$.

To change the phase behaviour of hard spheres we have a **single control parameter**, ϕ meaning that (differently from fluids like water) we are bound to have **one-dimensional** phase diagram.

We explore the phase behaviour of hard spheres by considering different regimes of packing fraction.

Low packing fractions

The hard repulsion between hard spheres means that each sphere is surrounded by an excluded volume in which the center of other spheres cannot be placed. Since the distance of closest approach between two spheres is σ such **excluded volume** per particle is simply $v_{\text{ex}} = 4\pi\sigma^3/3$ and it is much larger than the volume per particle $v = V/N$. A collection of N hard spheres has a total excluded volume $V_{\text{ex}} \neq Nv_{\text{ex}}$ simply because the excluded volumes of individual particles can in general overlap, as we saw earlier with the case of depletion.

At very low densities, most hard spheres isolated. So, in this case, we can approximate the total excluded volume as $V_{\text{ex}} \approx Nv_{\text{ex}}$ so that the accessible volume (the volume not occupied by the spheres) is

$$V_{\text{accessible}} = V - Nv_{\text{ex}}$$

We use this to perform an appropriate statistical mechanical calculation for the Helmholtz free energy of system F , which we know is purely entropic $F = -TS$. The partition function \mathcal{Z} is

$$\mathcal{Z} = \frac{1}{N! \Lambda^{3N}} \int_{V_{\text{accessible}}} d\mathbf{r}_1 \dots d\mathbf{r}_N$$

where Λ is the thermal de Broglie wavelength

$$\Lambda = h / \sqrt{2\pi m k_B T},$$

and originates from the integration over the Maxwell-Boltzmann distribution of momenta for particles of mass m , while h is Planck's constant.

For hard spheres, the integral is over all configurations where no two spheres overlap (i.e., $|\mathbf{r}_i - \mathbf{r}_j| \geq \sigma$ for all $i \neq j$), and $V_{\text{accessible}}$ is the total accessible volume. The results is that

$$\mathcal{Z} = \frac{(V - Nv_{\text{ex}}/2)^N}{N! \Lambda^{3N}},$$

with the $1/2$ factor coming from the fact that we avoid double counting the excluded volume of pairs. The entropy is

$$S = k_B \ln \mathcal{Z} = k_B [N \ln(V - Nv_{\text{ex}}/2) - \ln N! - 3N \ln \Lambda]$$

From the partition function, we use Stirling's formula $\ln N! = N \ln N - N$ and obtain

$$S = k_B [N \ln(V - Nv_{\text{ex}}/2) - (N \ln N - N) - 3N \ln \Lambda]$$

which reads

$$S = Nk_B \left[\ln \left(\frac{V - Nv_{\text{ex}}/2}{N\Lambda^3} \right) + 1 \right]$$

The phase behaviour is encoded in the **equation of state** (the equation that links the three thermodynamics variables P, T and ϕ). To obtain it, we calculate the pressure

$$P = - \left(\frac{\partial F}{\partial V} \right)_{N,T} = T \left(\frac{\partial S}{\partial V} \right)_{N,T} = \frac{k_B T}{v - v_{\text{ex}}/2}$$

This expression can be simplified (do it as an exercise) to obtain the equation of state

$$Z_{\text{comp}} = \frac{PV}{Nk_B T} = \frac{1}{1 - 4\phi} \quad (\phi \ll 1)$$

also known as the **compressibility factor** Z_{comp} . Since ϕ is very small the expression is in fact

$$Z_{\text{comp}} = 1 + 4\phi + O(\phi^2)$$

This expression makes it apparent that the first term linear in ϕ is a *correction* to the ideal gas law. This is example (to very low order) of what is called the **virial expansion**. This, in general takes the form

The choice of the letter "Z" is unfortunate. Do not confuse the compressibility factor with the partition function!

$$Z_{\text{comp}} = 1 + B_2 \rho + B_3 \rho^2 + \dots$$

where B_2, B_3, \dots are the **virial coefficients** and for systems that are not hard spheres they depend also on the temperature, $B_2(T), B_3(T), \dots$. They are important as they encode the effects of **correlations**:

- B_2 accounts for pairwise correlations (how the presence of one particle affects the probability of finding another nearby),
- B_3 for three-body correlations, and so on.

Given an interaction potential the second virial coefficient B_2 can be calculated independently from the equation state

$$B_2(T) = -\frac{1}{2} \int_0^\infty \left(\exp \left(-\frac{U(r)}{k_B T} \right) - 1 \right) 4\pi r^2 dr$$

For hard spheres this results in

$$B_2 = \frac{2\pi}{3}\sigma^3$$

which is exactly what is predicted by the equation of state above, once you recognise that $\phi = \frac{\pi\sigma^3}{6}\rho$.

Higher-order coefficients become increasingly complex to compute and reflect more complex many-body correlations that can be established even if the interaction potential is purely two-body (as in the case of hard spheres). The higher order coefficients become more and more important as the packing fraction is increased. Eventually something surprising occurs at a sufficiently high volume fraction.

Exercise: check this calculation.

Dense packing: metastability and crystallisation

As we increase the packing fraction, the accessible (free) volume reduces rapidly. At some point, disordered packing of spheres are so tightly packed that thermal motion becomes extremely inefficient or even impossible. Such disordered (**random**) packing of spheres are described as **jammed**: they are so densely packed that they are no longer behaving like a fluid but they instead display some of the rigidity that we typically associate with solids. Such jammed configurations are indeed examples of **amorphous solids**. We will explore them more in detail in the chapter dedicated to arrested systems.

It is important to note, however, that the disordered packing at high volume fractions are not minima of the free energy. The densest possible packing of hard spheres is achieved by arranging them in a crystalline lattice. In three dimensions, the densest packings are the face-centered cubic (FCC) and hexagonal close-packed (HCP) structures, both of which have a maximum packing fraction of

$$\phi_{\max} = \frac{\pi}{3\sqrt{2}} \approx 0.74$$

This means that, at most, about 74% of the available volume can be filled by the spheres, with the remainder being empty space. This result was conjectured by Kepler in 1611 and proved rigorously only in 1998 (the [Kepler conjecture](#)).

In contrast, **random close packing** (the densest disordered arrangement of spheres) yields a lower packing fraction, typically around $\phi_{\text{rcp}} \approx 0.64$. Notice that this value is approximate and variations can be observed (due to randomness and, more importantly, to the method by which such packings are reached, i.e. the *compression protocol*). This means that the only way to compress spheres at very high packing has to lead (*spontaneously*) to the formation of crystals. We can indeed imagine to perform the following experiment:

- prepare a disordered assembly of colloidal hard spheres
- compress them gradually to high and higher packing fraction, taking care to monitor the systems so that time correlations decay and the system is at thermal equilibrium
- measure the resulting packing fraction

Experiments of this sort have been performed historically, leveraging for example the **slow sedimentation** of colloids, which on long time scales leads to the accumulation of dense packings of spheres. Such experiments reveal that beyond the so-called **freezing packing fraction** $\phi_f \approx 0.494$ the system spontaneously forms small regions of crystals mixed with the fluid. At a high **melting packing fraction** $\phi_m = 0.545$ the entirety of the system is then crystalline and its optical properties consequently change.



Figure 15.4: Phase behaviour of hard-sphere colloids from Pusey et al. (2009)

A simple **cell model** can help us rationalise what is taking place. When the spheres are packed within their FCC cell, they can move very little beyond their own diameter σ . Assume that the volume per particle again is v and the (geometrically constrained) close packed volume is v_{cp} .

The maximum displacement is

$$\delta = \frac{\sigma}{\sqrt{2}} \left(\left(\frac{v}{v_{cp}} \right)^{1/3} - 1 \right)$$

The corresponding free volume is then $v_f = \frac{4\pi}{3}\delta^3$ from which we can calculate the entropy

$$S = -Nk_B T \ln(v_f/\Lambda^3)$$

and the resulting pressure

$$P = \frac{Nk_B T}{v_{cp}} \frac{(v/v_{cp})^{-2/3}}{(v/v_{cp})^{1/3} - 1}$$

Rearranging and expressing everything in terms of packing fraction $\phi = \frac{\pi\sigma^3}{6v}$ yields

$$Z_{\text{comp}} = \frac{1}{1 - (\phi/\phi_{cp})^{1/3}}$$

What is notable here is that the expression we have obtained is a completely different functional form compared to the low density fluid regime. This is indicative of a **discontinuous, first-order** phase transition between the fluid and the crystalline phases. First order phase transitions are characterised by coexisting regions where the system can be found in partial fluid and partial crystalline state, as illustrated in the experiments above. This also means that we can prepare a disordered packing at very high density: this will not be its equilibrium state (global minimum of the free energy), but will still be stable for some (finite) time. This *local equilibrium state* is called a ***metastable state**.

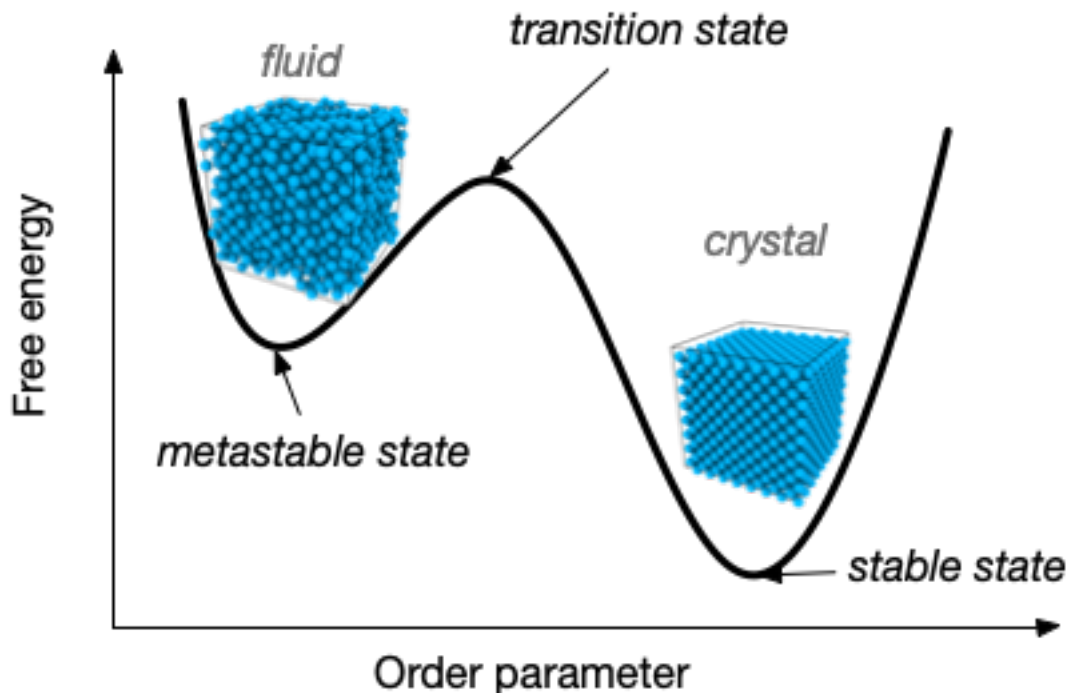


Figure 15.5: Schematic free energy for hard spheres compressed at high pressures: the fluid branch becomes metastable and the free energy minimum is located in the crystal phase

But where does the free energy advantage of the crystal over the disordered fluid come from? From the discussion above the answer is obvious: crystals can accommodate higher packings, meaning that they use the available volume more efficiently. This in fact means that (on average) every hard sphere has more available volume if it is arranged in the crystalline state compared to the fluid phase: the increased volume (available for thermal fluctuations and random particle displacements) is translated into an **increased entropy**. So, in fact the ordered, crystalline state has overall a higher entropy than the disordered fluid. This is an important instance in which the conventional storytelling, where entropy is just **disorder**, simply does not hold. As we have seen with depletion forces earlier, entropy can lead to structure: in the case of hard spheres, it is the only mechanism leading to structure, and such structure is the most orderly one we can think of: long-range, crystalline order.

The video below shows instead the results of a Monte-Carlo simulation at packing $\phi = 0.493$ for a small system of 32 particles. Small systems have enhanced fluctuations, and since the

overall packing fraction is very close to the freezing line, we see spontaneous freezing and unfreezing of the small system (wait until second 14 in the movie).

[figs/melt_freeze.mp4](#)

In conclusion, colloidal hard spheres have a one-dimensional phase diagram, that depends only on the packing fraction but with various distinct phases



Figure 15.6: Hard-spheres phase diagram

15.3.2 Beyond hard-spheres: simple liquids

A **simple liquid** is a system of particles interacting via short-range, spherically symmetric (isotropic) pair potentials. The most common model is the **Lennard-Jones (LJ) potential**, which captures both the short-range repulsion (due to Pauli exclusion) and longer-range van der Waals attraction:

$$U_{\text{LJ}}(r) = 4\epsilon \left[\left(\frac{\sigma}{r}\right)^{12} - \left(\frac{\sigma}{r}\right)^6 \right]$$

where ϵ sets the depth of the potential well (interaction strength) and σ is the particle diameter (distance at which $U = 0$). The r^{-12} term models steep repulsion, while r^{-6} describes the attractive tail.

The Lennard-Jones fluid exhibits rich phase behavior: at low temperatures and densities, it forms a gas; at intermediate conditions, a liquid; and at high densities, a solid. The LJ model is widely used to study atomic and molecular liquids, and serves as a reference for understanding real fluids and their phase transitions.

In the phase diagram below these different phases have been highlighted. It is clear that, compared to hard spheres which only display a fluid and a crystalline solid phase, systems like the Lennard-Jones fluid display an additional phase, the **liquid**. This phase emerges from the presence of the attractive well in the interaction potential. This allows for short-range attractive interactions that case a region of the phase diagram in the same class of universality of the **Ising model** and the **lattice gas**.

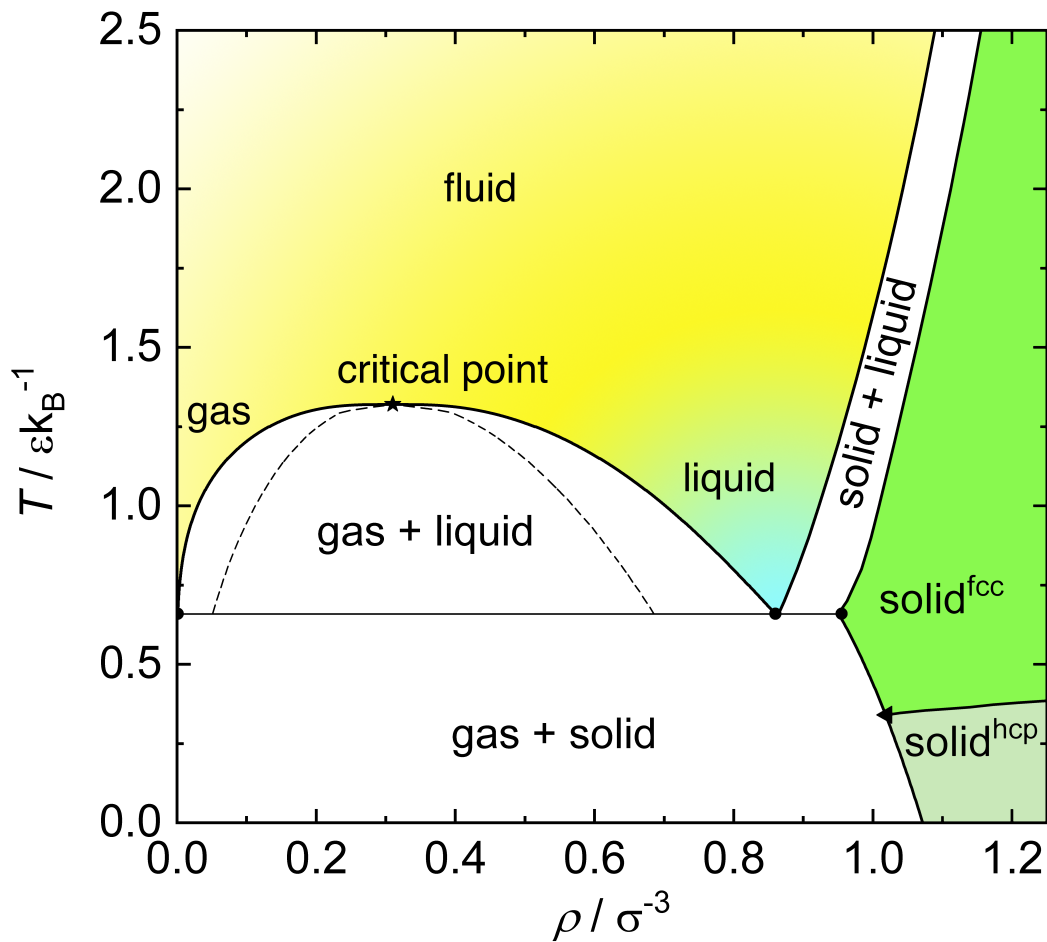


Figure 15.7: Phase diagram of the Lennard-Jones Fluid, adapted from Wikimedia.

The Lennard-Jones interaction has already been designed to model noble gases (e.g. Argon) but has over time been used to model many other systems due to its simplicity and computational convenience: in particular it is used to construct coarse-grained models of macromolecules, as well as colloids and nanoparticles. It belongs to a wider class of, classical, effective **pair-wise** interaction models extensively used to calculate properties and phase diagrams of a variety of condensed matter systems. This are useful because they allow one to, for example, long molecular simulations that are normally unreachable when considering atomistics and electronic density calculations.

The following table provides you with a few example potentials and their functional forms:

Potential Name	Mathematical Form	Typical Systems/Features
Lennard-Jones (LJ)	$U(r) = 4\epsilon \left[\left(\frac{\sigma}{r} \right)^{12} - \left(\frac{\sigma}{r} \right)^6 \right]$	Simple atomic fluids, coarse-grained molecular interactions
Hard Sphere	$U(r) = \begin{cases} \infty & r < \sigma \\ 0 & r \geq \sigma \end{cases}$	Colloids, granular materials, excluded volume

Potential Name	Mathematical Form	Typical Systems/Features
Yukawa (Screened Coulomb)	$U(r) = \epsilon \frac{e^{-\kappa r}}{r}$	Charged colloids, plasmas, electrolytes
Dipolar	$U(r) = \frac{\mu_0 \mu_1 \mu_2}{4\pi r^3} (1 - 3 \cos^2 \theta)$	Magnetic colloids, polar molecules

15.4 Characterisation of colloidal systems

When looking at colloidal systems, we typically focus on two main aspects of their physics:

- their **structural features**, characterised by the **spatial** correlations between their constituents
- their **dynamical features**, characterised by the mobility of single particles or groups of particles.

Here below, we briefly account of some main approaches to characterise these two dimensions.

15.4.1 Structural properties: the radial distribution function

Structural features of disordered (but also ordered) systems are described in terms of **correlation functions**. The underlying idea is that we are provided with an ensemble of stochastic variables (the positions of the colloids) which have a characteristic spatial distribution. For N particles we have an N -body probability distribution function $\rho_N(\mathbf{r}^N)$ which contains all the necessary statistical mechanical information to describe the thermodynamics of the system. However, this is very difficult to access directly. In experiments or theoretical calculations we typically only have access to some lower order *marginalisation* of the distribution, in terms of few-body distributions.

One of the simplest assumptions we can make when we describe a system is that its potential energy is expressed in terms of purely pairwise additive potential, meaning that

$$U_N(\mathbf{r}^N) = \sum_{i=1}^{N-1} \sum_{j=i+1}^N V(r_{ij}) = \frac{1}{2} \sum_{i \neq j} V(r_{ij})$$

where $V(r_{ij})$ is the pairwise, radial interaction potential that only depends on the distance between particle centres $r_{ij} = |\mathbf{r}_i - \mathbf{r}_j|$.

For systems with pairwise interactions, the natural spatial correlation function is a twobody correlation $g(\mathbf{r}_i, \mathbf{r}_j)$, where \mathbf{r}_i and \mathbf{r}_j are two randomly chosen particles. In the case of non-crystalline, disordered systems the correlation function has to be

- translationally invariant, so that it only depends on the difference $\mathbf{r}_i - \mathbf{r}_j$
- rotationally invariant, so that there is no angular component and hence only the distance $r_{ij} = |\mathbf{r}_i - \mathbf{r}_j|$ matters

This function $g(r)$ is called the **radial distribution function** and plays a crucial role in the characterisation of fluids, crystals, glasses and much more. For systems with twobody interactions only, it contains in principle all the thermodynamic information necessary to reconstruct the free energy, as one can write

$$\frac{F_{\text{ex}}}{k_B T} = 2\pi\rho N \int_0^\infty [g(r) \ln g(r) - g(r) + 1] r^2 dr + \frac{\rho N}{2k_B T} \int V(r) g(r) d^3r$$

where the first term represent the entropic contributions and the second term represents the energetic contribution.

But how is it calculated? very simply. You can think of constructing a histogram of the distances between all of the particles and suitably normalising such histogram by the density of the system. Mathematically this reads as

$$g(r) = \frac{1}{\rho N} \left\langle \sum_{i=1}^N \sum_{j \neq i} \delta(|\mathbf{r}_i - \mathbf{r}_j| - r) \right\rangle$$

where $\rho = N/V$ is the number density, and the angle brackets denote an ensemble average and δ is a Dirac delta function.

- For an **ideal gas**, $g(r) = 1$ everywhere (no correlations).
- For **hard spheres**, $g(r) = 0$ for $r < \sigma$ (no overlap), and $g(r)$ shows oscillations at higher r due to packing effects.

Notice that the radial distribution function is an instance of the more general class of pair-wise correlations that have been introduced earlier, see Section 2.2 and it is paired with its reciprocal space Fourier transform, the **structure factor**:

$$S(k) = 1 + \rho \int [g(r) - 1] e^{-ik \cdot r} dr$$

For isotropic systems, this reduces to:

$$S(k) = 1 + 4\pi\rho \int_0^\infty r^2 [g(r) - 1] \frac{\sin(kr)}{kr} dr$$

Experimentally, one can measure $S(k)$ can be measured using scattering techniques or $g(r)$ via direct imaging in colloidal systems. They provide insight into short-range order, local structure, and phase transitions in soft matter.

- ! The radial distribution function $g(r)$ has two possible interpretations
- It represents the probability density of finding a particle at distance r away from a reference particle *relative* to the probability density of an ideal gas at the same number density.
 - If a given reference particle is taken at the origin, then the local average density at distance r is $\rho g(r)$.

Here below we show two codes to calculate the radial distribution function for an ideal gas (which is trivial) and then for an assembly of hard spheres

```
#| caption: "Radial distribution function of an ideal gas [press ctrl/cmd [ENTER] to run]"
#| autorun: true
import numpy as np
import matplotlib.pyplot as plt
```

```

# Parameters
N = 500      # number of points, change this to check convergence
L = 10.0      # box size
bins = 50     # number of bins

# Generate random points (ideal gas)
positions = np.random.uniform(0, L, size=(N, 3))

def radial_distr(positions, L):
    N = len(positions)

    # Compute all pairwise distances with PBC
    diff = positions[:, np.newaxis, :] - positions[np.newaxis, :, :]
    diff = diff - L * np.round(diff / L)
    dists_matrix = np.sqrt(np.sum(diff**2, axis=-1))

    # Get upper triangular distances (each pair counted once)
    i, j = np.triu_indices(N, k=1)
    dists = dists_matrix[i, j]

    # Create histogram
    r_max = L/2
    r_edges = np.linspace(0, r_max, bins+1)
    hist, _ = np.histogram(dists, bins=r_edges)
    r_centers = 0.5 * (r_edges[:-1] + r_edges[1:])

    # Calculate g(r) with correct normalization
    rho = N / L**3  # number density
    dr = r_edges[1:] - r_edges[:-1]  # bin widths

    # Volume of spherical shell
    shell_volumes = 4 * np.pi * r_centers**2 * dr

    # For each particle, expected number of neighbors in shell = rho * shell_volume
    # Total expected pairs in shell = N * rho * shell_volume / 2
    # (divide by 2 because we count each pair once)
    expected_pairs = N * rho * shell_volumes / 2

    # g(r) = actual_pairs / expected_pairs
    g_r = hist / expected_pairs

    return r_centers, g_r

r, g = radial_distr(positions, L)
plt.plot(r, g, 'b-', drawstyle="steps-mid")
plt.axhline(y=1, color='r', linestyle='--', alpha=0.7, label='Ideal gas (g(r)=1)')
plt.xlabel("r")
plt.ylabel("g(r)")
plt.gca().set(xlim=(0, L/2), ylim=(0,2))
plt.legend()
plt.show()

```

We can compare this with arrangements of hard spheres

```
#| caption: "Radial distribution function for a hard sphere configuration [press ctrl/cmd [ENTER] to run]"
# now try with hard spheres, using a custom libarry you will find in the course pages
from src import hardspheres

sigma = 1.0
L = 5.*sigma #take a small value
phi = 0.2 # packing fraction
N = int(phi/(np.pi/6*sigma**3)*L**3)

# we run Monte-Carlo simulations of hard-spheres on the fly
freq = 5
nsteps = 100*N
trajectory, acceptance = hardspheres.Monte_Carlo_traj(N,L, sigma, nsteps,freq)
gs = []
for positions in trajectory:
    _r, _g = radial_distr(positions, L)
    gs.append(_g)
plt.plot(r, np.mean(gs, axis=0), 'b-', label=rf"Hard spheres, rf$\phi={phi}$")
plt.xlabel("r", ylabel="g(r)", ylim=(0,2))
plt.legend()
plt.show()
```

The radial distribution function is the central object of much of **liquid state theory**, which aims to predict the shape of the correlation functions (such as $g(r)$) from the sole knowledge of the interaction potential between the elementary particles (see Santos (2016) for a gentle introduction to the topic). In particular, one can imagine the correlations between two particles 1 and 2 in a fluid to have two possible origins

- a **direct** correlation between the two particles, mediated by direct interactions (e.g. collisions) between 1 and 2.
- an **indirect correlation**, mediated by other particles in the fluid

The $g(r)$ contains both direct and indirect correlations. We can assume that a suitable function $c(r)$ exists to express the direct correlations. In such case, for twobody interactions, we can write a hierarchy of equations via a central result of liquid state theory, the **Ornstein-Zernicke** (OZ) equation

$$h(r_{12}) = c(r_{12}) + \rho \int c(r_{13}) h(r_{32}) d\mathbf{r}_3 \quad (15.3)$$

where we defined the total correlation function as $h(r) = g(r) - 1$. The OZ equation is an integral equation. In Fourier space (assuming the isotropicity of a fluid) it becomes an algebraic equation

$$\tilde{h}(k) = \frac{\tilde{c}(k)}{1 - \rho \tilde{c}(k)}$$

Since both $h(r)$ and $c(r)$ an additional relationship is known called a **closure**. These constructed through physical arguments. A common one is the so-called Percus-Yevick closure

$$c(r) = [1 + h(r)] [1 - e^{\beta U(r)}]$$

where the pairwise interaction enters explicitly.

Solving the OZ equation with the Percus-Yevick closure produces realistic radial distribution functions in a wide range of packing fractions for hard spheres.

15.4.2 Dynamics: single vs collective displacements

We have seen [earlier](#) that if we are given a number of particles evolving microscopically according to the Langevin equation of drag γ and zero-mean noise η

$$m \frac{d\vec{v}}{dt} = -\gamma \vec{v} + \vec{\eta}(t)$$

then an *ensemble* of independent particles will follow the **diffusion equation**:

$$\frac{\partial \rho(\mathbf{r}, t)}{\partial t} = D \nabla^2 \rho(\mathbf{r}, t)$$

where $\rho(\mathbf{r}, t)$ is the probability of finding a particle at position \mathbf{r} at time t with diffusivity D . The diffusivity D is related to the microscopic Langevin equation parameters via the fluctuation-dissipation relation (or Einstein relation)

$$D = \frac{k_B T}{\gamma}$$

where k_B is Boltzmann's constant, T is temperature, and γ is the friction (drag) coefficient.

It is easy to show (see below) that in 1 dimension the general solution is

$$\rho(x, t) = \frac{1}{\sqrt{4\pi Dt}} \exp\left(-\frac{x^2}{4Dt}\right)$$

Solution of the diffusion equation using Laplace transform

The 1D diffusion equation is:

$$\frac{\partial \rho(x, t)}{\partial t} = D \frac{\partial^2 \rho(x, t)}{\partial x^2}$$

Suppose the initial condition is a delta function at the origin:

$$\rho(x, 0) = \delta(x)$$

Take the Laplace transform in time:

$$\tilde{\rho}(x, s) = \int_0^\infty \rho(x, t) e^{-st} dt$$

The Laplace transform of the time derivative:

$$\mathcal{L}\left[\frac{\partial n}{\partial t}\right] = s\tilde{\rho}(x, s) - \rho(x, 0)$$

So the transformed equation is:

$$s\tilde{\rho}(x, s) - \delta(x) = D \frac{\partial^2 \tilde{\rho}(x, s)}{\partial x^2}$$

Rearrange:

$$D \frac{\partial^2 \tilde{\rho}}{\partial x^2} - s\tilde{\rho} = -\delta(x)$$

For $x \neq 0$, the homogeneous equation:

$$D \frac{\partial^2 \tilde{\rho}}{\partial x^2} - s\tilde{\rho} = 0$$

General solution:

$$\tilde{\rho}(x, s) = Ae^{-\lambda|x|}, \quad \lambda = \sqrt{\frac{s}{D}}$$

The delta function at $x = 0$ gives a discontinuity in the derivative:

$$\left. \frac{\partial \tilde{\rho}}{\partial x} \right|_{x=0^+} - \left. \frac{\partial \tilde{\rho}}{\partial x} \right|_{x=0^-} = -\frac{1}{D}$$

Compute derivatives:

$$\frac{\partial \tilde{\rho}}{\partial x} = -A\lambda \operatorname{sgn}(x)e^{-\lambda|x|}$$

So at $x = 0^+$: $-A\lambda$, at $x = 0^-$: $A\lambda$. The jump is $-2A\lambda$.

Set equal to $-1/D$:

$$-2A\lambda = -\frac{1}{D} \Rightarrow A = \frac{1}{2D\lambda}$$

So:

$$\tilde{\rho}(x, s) = \frac{1}{2D\lambda} e^{-\lambda|x|} = \frac{1}{2\sqrt{Ds}} e^{-|x|\sqrt{\frac{s}{D}}}$$

Invert the Laplace transform (using tables or convolution theorem):

$$\rho(x, t) = \frac{1}{\sqrt{4\pi Dt}} \exp\left(-\frac{x^2}{4Dt}\right)$$

This is the fundamental solution (Green's function) of the diffusion equation.

The diffusion equation can also be read as a simple consequence of two requirements:

- continuity of the distribution of mass (no mass is lost during the transport), as expressed in the **continuity equation**

$$\frac{\partial \rho(\mathbf{r}, t)}{\partial t} + \nabla \cdot \mathbf{J}(\mathbf{r}, t) = 0$$

where the divergence $\nabla \cdot \mathbf{J}(\mathbf{r}, t)$ represents the net outflow of particles from a given region due to the flux \mathbf{J} .

- the flux of particles is assumed to be proportional to the gradient in the density (or concentration of the particles). This can be taken as an empirical assumption, a reasonable approximation (i.e. a perturbative approach) or a consequence of underlying Brownian dynamics. It is known as Fick's law:

$$\mathbf{J}(\mathbf{r}, t) = -D\nabla\rho(\mathbf{r}, t)$$

The diffusivity constant D is therefore central for the diffusion. It is possible to link the microscopic motion of the particles to the collective behaviour of the density distribution $\rho(x, t)$ by exploiting the connection provided by the **mean squared displacement**, which is simply the variance of the distribution $\rho(x, t)$ at time t .

As discussed earlier, in d dimensions this is equal to

$$\langle r(t)^2 \rangle - \langle r(t) \rangle^2 = 2dDt$$

Hence, measuring the average squared displacements is sufficient to recover the diffusivity and to reconstruct the distribution.

15.4.2.1 Diffusion and interactions

We have up to now considered the dilute (or non-interacting) limit, where collisions between the colloids are ignored. Let's now consider instead simple colloids (again, hard spheres) and their dynamics.

We are interested in the mean squared displacement $\langle r^2(t) \rangle$ as a function of time for different volume fractions. At low volume fractions, the particles undergo Brownian motion (random-walk diffusion) due to collisions with liquid molecules. The mean squared displacement (in three dimensions) is

$$\langle r^2(t) \rangle = 6D_0t$$

where the meaning of the subscript 0 will be apparent shortly.

For sufficiently dense hard spheres (e.g. above $\phi \sim 0.3$), however, different regimes are observed. At short times the particles diffuse with the short time (self) diffusion constant D_s . This is determined from the short time limit and is smaller than the D_0 measured for $\phi \rightarrow 0$. The motion of the particles (self diffusion) is still driven by collisions with the liquid molecules, but in addition the interactions between particles become significant.

While the particles are diffusing in their cages formed by their neighbours, the hydrodynamic interaction with the neighbours, transmitted through flows in the liquid, causes slowing down relative to the free diffusion at low concentrations. At intermediate times the particles encounter the neighbours and the interactions slow the motion down. To make further progress, the particle has to break out of the cage formed by its neighbours. Now the particles experience a further interaction, direct interactions (hard-sphere interactions), in addition to the hydrodynamic interactions. The long-time and long-ranged movement is also diffusive, i.e. we still have

$$\langle r^2(t) \rangle \propto t$$

when the particles undergo large-scale random-walk diffusion through many cages.

However, the motion is further slowed and a smaller diffusion constant relative to the motion in the short time limit is observed, the long time (self) diffusion constant D_L .

The slowing down due to collisions eventually dominates the physics of hard spheres at high densities. This is more broadly true also for generic dense colloidal suspensions, where the short range interactions dominate over other mechanisms of motion (including the hydrodynamics). Eventually, for very dense packings one observes the emergence of a new physical regime where relaxation becomes anomalous and non-diffusive: this is the glassy regime, which we will revisit in a following chapter.

15.4.3 Stokes-Einstein relation

Suppose that the particles are subjected to an external force F in the x direction, e.g. gravity. In thermal equilibrium the Maxwell-Boltzmann distribution is valid, i.e. the particle density $n(x)$ is given by

$$n(x) = n_0 \exp(-U(x)/k_B T) = n_0 \exp(-Fx/k_B T)$$

where we assumed a constant force F in the last equation. In the case of gravity $F = m_B g$ with m_B the buoyant mass. $n(x)$ results from the balance between the motion of the particles due to the external force setting up a concentration gradient, and the resultant diffusion given by Fick's law.

```
// | echo: false
{
  const width = 600;
  const height = 400;
  const numCircles = 300;

  let temperature = 300;      // Arbitrary scale
  let viscosity = 0.02;       // Arbitrary scale
  const particleRadius = 5; // pixels
  let timeStep = 1;

  const kB = 1; // reduced units
  let gravityFactor = 0.1;
  let gravity = 10 * gravityFactor;

  // Compute damping as velocity decay per timestep (Langevin friction)
  function computeDamping(viscosity, radius, dt) {
    const gamma = 6 * Math.PI * viscosity * radius; // friction coeff
    return Math.exp(-gamma * dt);
  }

  let damping = computeDamping(viscosity, particleRadius, timeStep);

  // Create SVG
  const svg = d3.create("svg")
    .attr("width", width)
    .attr("height", height)
    .style("border", "1px solid #ccc")
    .style("background", "#f9f9f9");

  // Initialize circles
  const circles = Array.from({ length: numCircles }, (_, i) => ({
    id: i,
    x: Math.random() * width,
    y: Math.random() * height * 0.3,
    vx: (Math.random() - 0.5) * 2,
    vy: (Math.random() - 0.5) * 2,
    radius: particleRadius,
    color: d3.interpolateYlOrBr(Math.random() * 0.5 + 0.25)
  }));
}
```

```

// Create circles in SVG
const circleElements = svg.selectAll("circle")
  .data(circles)
  .enter()
  .append("circle")
  .attr("r", d => d.radius)
  .attr("fill", d => d.color)
  .attr("opacity", 0.8)
  .attr("stroke", "#333")
  .attr("stroke-width", 1);

// Collision detection & response
function handleCollisions() {
  for (let i = 0; i < circles.length; i++) {
    for (let j = i + 1; j < circles.length; j++) {
      const c1 = circles[i];
      const c2 = circles[j];
      const dx = c2.x - c1.x;
      const dy = c2.y - c1.y;
      const dist = Math.hypot(dx, dy);
      const minDist = c1.radius + c2.radius;

      if (dist < minDist && dist > 0) {
        const overlap = minDist - dist;
        const nx = dx / dist;
        const ny = dy / dist;

        c1.x -= nx * overlap / 2;
        c1.y -= ny * overlap / 2;
        c2.x += nx * overlap / 2;
        c2.y += ny * overlap / 2;

        const dvx = c2.vx - c1.vx;
        const dvy = c2.vy - c1.vy;
        const vn = dvx * nx + dvy * ny;

        if (vn > 0) continue;

        const restitution = 1.0;
        const impulse = (-(1 + restitution) * vn) / 2;

        c1.vx -= impulse * nx;
        c1.vy -= impulse * ny;
        c2.vx += impulse * nx;
        c2.vy += impulse * ny;
      }
    }
  }
}

// Update damping when viscosity or timestep changes
function updateDamping() {
  damping = computeDamping(viscosity, particleRadius, timeStep);
}

```

```

}

// Animate function
function animate() {
  const diffusion = (kB * temperature) / (6 * Math.PI * viscosity * particleRadius);

  circles.forEach(c => {
    // Apply gravity
    c.vy += gravity * timeStep;

    // Diffusion random kick scaled by sqrt(2*D/dt)
    const diffusionForce = Math.sqrt(2 * diffusion / timeStep);
    c.vx += (Math.random() - 0.5) * diffusionForce;
    c.vy += (Math.random() - 0.5) * diffusionForce;

    // Apply damping
    c.vx *= damping;
    c.vy *= damping;

    // Update position
    c.x += c.vx * timeStep;
    c.y += c.vy * timeStep;

    // Boundary collision
    if (c.x - c.radius < 0) {
      c.x = c.radius;
      c.vx *= -1;
    }
    if (c.x + c.radius > width) {
      c.x = width - c.radius;
      c.vx *= -1;
    }
    if (c.y - c.radius < 0) {
      c.y = c.radius;
      c.vy *= -1;
    }
    if (c.y + c.radius > height) {
      c.y = height - c.radius;
      c.vy *= -1;
    }
  });
}

handleCollisions();

circleElements
  .attr("cx", d => d.x)
  .attr("cy", d => d.y);

diffusionDisplay.text(`Diffusion: ${diffusion.toFixed(4)}`);

}

// Start timer
const timer = d3.timer/animate);

```

```

// Controls container
const controls = d3.create("div")
  .style("margin-top", "10px")
  .style("padding", "10px")
  .style("background", "#f0f0f0")
  .style("border-radius", "8px")
  .style("width", `${width}px`);

// Slider factory
function createSlider(labelText, min, max, initial, step, onChange) {
  const container = controls.append("div")
    .style("margin-bottom", "10px")
    .style("display", "flex")
    .style("align-items", "center")
    .style("gap", "10px");

  container.append("label")
    .text(labelText)
    .style("min-width", "120px")
    .style("font-weight", "bold");

  const slider = container.append("input")
    .attr("type", "range")
    .attr("min", min)
    .attr("max", max)
    .attr("step", step)
    .attr("value", initial)
    .style("flex", "1");

  const valueDisplay = container.append("span")
    .text(initial.toFixed(step < 1 ? 4 : 0))
    .style("width", "50px")
    .style("text-align", "right")
    .style("font-family", "monospace");

  slider.on("input", function () {
    const val = +this.value;
    onChange(val);
    valueDisplay.text(val.toFixed(step < 1 ? 4 : 0));
  });

  return slider;
}

// Create sliders
createSlider("Gravity", -100, 100, gravity / gravityFactor, 10, v => gravity = v * gravityFactor);

createSlider("Temperature", 0, 1000, temperature, 10, v => temperature = v);

createSlider("Viscosity", 0.001, 0.1, viscosity, 0.001, v => {
  viscosity = v;
  updateDamping();
});

```

```

});

// createSlider("Time Step", 0.1, 5, timeStep, 0.1, v => {
//   timeStep = v;
//   updateDamping();
// });

// Diffusion display
const diffusionDisplay = controls.append("div")
  .style("margin-top", "10px")
  .style("font-family", "monospace")
  .style("font-weight", "bold")
  .text("");

// Reset button
controls.append("button")
  .text("Reset Positions")
  .style("margin-top", "10px")
  .style("padding", "6px 12px")
  .on("click", () => {
    circles.forEach(c => {
      c.x = Math.random() * width;
      c.y = Math.random() * height * 0.3;
      c.vx = (Math.random() - 0.5) * 2;
      c.vy = (Math.random() - 0.5) * 2;
    });
  });
}

// Start/Stop toggle
const startStopBtn = controls.append("button")
  .text("Stop")
  .style("margin-left", "10px")
  .style("padding", "6px 12px")
  .on("click", function () {
    if (timer._call) {
      timer.stop();
      this.textContent = "Start";
    } else {
      timer.restart/animate);
      this.textContent = "Stop";
    }
  });
}

// Container div
const container = d3.create("div");
container.node().appendChild(svg.node());
container.node().appendChild(controls.node());

return container.node();
}

```

In the case of gravity, this leads to a sedimentation equilibrium. (a) Flux due to external force, J_F

The velocity of a particle under an applied force F in a viscous fluid can be written as $v = F/\xi$ which defines the friction coefficient ξ . Hence

$$J_F = n(x)v = \frac{n(x)F}{\xi}$$

(b) Diffusive flux, J_D J_D is given by Fick's Law (see above):

$$J_D(x) = -D \frac{\partial n(x)}{\partial x}$$

Equating the two fluxes $J_F = J_D$ we get

$$\frac{n(x)F}{\xi} = -D \frac{\partial n(x)}{\partial x} = +D \frac{F}{k_B T} n(x)$$

The second equation is obtained by differentiating the Maxwell-Boltzmann distribution. This gives the relation between the diffusion and friction coefficients:

$$D = \frac{k_B T}{\xi} = \frac{k_B T}{6\pi\eta R}$$

The last equation applies to a spherical particle of radius R in a fluid of viscosity η , for which Stokes's Law gives $\xi = 6\pi\eta R$ (which applies only at low Reynold's number, $\rho Rv/\eta \ll 1$) resulting in the Stokes-Einstein (and Sutherland) relation.

- The Stokes-Einstein relation is a very deep result. It relates equilibrium fluctuations in a system to the energy dissipation when the system is driven off equilibrium. Here, the fluctuations in the fluid give rise to the diffusive motion of the suspended particle and D is therefore the 'fluctuation' part. A sheared fluid will dissipate energy because of its finite viscosity and thus η represents the dissipative part.
- More generally, Brownian motion sets a natural limit to the precision of physical measurements. Example from the [Feynman Lectures](#):

A mirror suspended on a torsion fibre reflects a spot of light onto a scale. The spot will jiggle due to the random impact of air molecules and the random motion of atoms in the quartz fibre. To reduce the jiggle, the apparatus has to be cooled. The relation between fluctuation and dissipation tells us where to cool. 'This depends upon where [the mirror] is getting its 'kicks' from. If it is through the fibre, we cool it ... if the mirror is surrounded by a gas and is getting hit mostly by collisions in the gas, it is better to cool the gas. As a matter of fact, if we know where the damping of the oscillations comes from, it turns out that that is always the source of the fluctuations. (Adapted from Feynman, Chapter 41)

! Check your understanding

- Colloids are mixtures with dispersed particles ($1 \text{ nm} - 1 \mu\text{m}$) that remain suspended due to Brownian motion.
- Stability of colloids depends on the balance between attractive (van der Waals) and repulsive (double layer) interactions.
- The DLVO theory combines van der Waals attraction and double layer repulsion to explain colloidal stability and aggregation.

- Entropic effects (e.g., depletion interactions) can induce effective attractions even in purely repulsive systems.
- Hard-sphere colloids are a fundamental model: their phase behavior is controlled by packing fraction, leading to fluid, crystalline, and metastable (jammed) states.
- The radial distribution function $g(r)$ characterizes spatial correlations and structure in colloidal systems.
- Dynamics of colloids are governed by Brownian motion, with diffusion slowed at higher densities due to interactions.
- The Stokes-Einstein relation links diffusion to temperature, viscosity, and particle size.
- Entropy can drive ordering (e.g., crystallization of hard spheres), showing that entropy is not always associated with disorder.
- Colloidal systems serve as accessible models for studying fundamental concepts in soft matter and statistical mechanics.

References

Chapter 16

Polymers

```
#| echo: false
#| autorun: true
# modifying the path to add the code folder
import sys
sys.path.insert(0, 'src')
```

16.1 General molecular properties

A polymer is a **large molecule** made up of many small, simple chemical units, joined together by chemical bonds. The basic unit of this sequence is called a **monomer**, and the number of units in the sequence is called the **degree of polymerisation**.

It is possible to have polymers containing over 10^5 units and there are naturally occurring polymers with a degree of polymerisation exceeding 10^9 . For example, polystyrene with a degree of polymerisation of 10^5 has a molecular weight of about 10^7 g/mol and, if fully stretched out, would be about $25 \mu\text{m}$ long.

Polymers play a central role in many fields, ranging from technology to biology. This is reflected in a huge number of different chemical structures. Given this manifold and the complexity of polymer molecules, the theories are astonishingly simple. This is possible because of the characteristic feature of polymers: The molecule itself is **very large** (compared to the individual units) and the macroscopic behaviour is dominated by this large-scale property of the molecule. Theories focus on such *large-scale* properties, whereas the small scale *fine structure* is typically resolved by computer simulations.

Polymers exist in very different architectures, such as

- **linear**: straight chains of repeating units (e.g., polyethylene).
- **branched**: polymers with a main chain and side chains (branches) attached. The branching affects properties like density and melting point (e.g., low-density polyethylene).
- **star**: polymers with multiple linear chains (arms) radiating from a central core. These structures can have unique properties like lower viscosity.
- **cross-linked**: polymers where chains are interconnected by covalent bonds, forming a network. This structure makes them rigid and heat-resistant (e.g., vulcanized rubber).

Furthermore, a large variation in the chemical structure may be achieved by combining different monomers (**copolymerisation**).

For simplicity, we will focus on **linear homopolymers**, i.e. with no branch points and with all identical subunits.

16.1.1 Example structures

Here below you can see the chemical structures of (sections) of a few common polymers. Hovering on the diagram should highlight the repeated units.

How to use the visualisers

Click on the  symbol to customise the visualisation:

- you should see a **State Tree** to your left
- click on the last item (highlighted in light blue, by default *Ball & Stick*)
- click on *Update 3D representation* and select a suitable *Type*. For example the **Cartoon** mode will correspond to the kind of coarse graining we will have in mind when talking about polymer chains.

Polystyrene (C_8H_8)_n

Poly(methyl methacrylate) (PMMA) ($C_5H_8O_2$)_n

This polymer is also known as acrylic, acrylic glass, or plexiglass. This a very common material also to fabricate colloids (PMMA particles).

Natural rubber (C_5H_8)_n

16.2 Models for the conformation of polymers

In order to understand the properties of most substances, we must consider a large assembly of molecules. In the case of polymers, however, the molecules themselves are very large and due to their flexibility they can take up an enormous number of configurations by rotation of chemical bonds. The shape of the polymer can therefore only be usefully described **statistically** and one need to use statistical mechanics to calculate the characteristics of even an isolated polymer.

To be able to investigate the properties of a **single polymer** and to neglect interactions between polymers, the polymer is placed in a very **dilute solution**. In this chapter, we will theoretically investigate the properties of an isolated, single polymer chain in solution (which in addition is linear and consists of only one kind of monomers).

16.2.1 Freely-jointed chain

Many polymers are highly flexible and are coiled up in solution. In a simple model we thus describe a polymer with two assumptions :

- it is composed of a **large number of segments** freely joined up
- all angles between segments are assumed to be **equally likely**.

The monomers are located at positions \mathbf{R}_j and connected by bonds $\mathbf{r}_j = \mathbf{R}_j - \mathbf{R}_{j-1}$ of length $|\mathbf{r}_j| = b_0$.

The **end-to-end vector** \mathbf{R} is then simply the vector linking the head to the tail of the chain:

$$\mathbf{R} = \mathbf{r}_1 + \mathbf{r}_2 + \cdots + \mathbf{r}_N = \sum_{j=1}^N \mathbf{r}_j.$$

At any instant, the configuration (arrangement) of the polymer is one realisation of an N-step random walk in three dimensions.

```
#| autorun: true
#| caption: "Example of freely-jointed chain as a random walk in 3d"

import numpy as np

# Play with the parameters (e.g. large and small N) and explore different conformations in 3D
# The color coding only maps the index of the monomer in the chain
def generate_free_polymer(N=100, b=1):
    # Generate random walk in 3D
    theta = np.arccos(2 * np.random.rand(N) - 1) # polar angle
    phi = 2 * np.pi * np.random.rand(N)           # azimuthal angle

    dx = b * np.sin(theta) * np.cos(phi)
    dy = b * np.sin(theta) * np.sin(phi)
    dz = b * np.cos(theta)

    x = np.concatenate([[0], np.cumsum(dx)])
    y = np.concatenate([[0], np.cumsum(dy)])
    z = np.concatenate([[0], np.cumsum(dz)])
    return x,y,z

# custom plotting
import sys

sys.path.append("./src")
import plotting
N, b = 100, 1
# Plot the end-to-end vector as a red arrow

x, y, z = generate_free_polymer(N, b)
fig = plotting.plotly_3d(x, y, z, name=f"{N}-step polymer")
fig = plotting.plot_vector([x[0],x[-1]], [y[0],y[-1]], [z[0],z[-1]], fig, name="end-to-end vector")
# ensure plotting works by encapsulating it in HTML
from IPython.display import HTML
HTML(fig.to_html(include_plotlyjs="cdn"))
```

End-to-end vector

In time, the various segments undergo Brownian motion and the polymer fluctuates between all possible configurations of the random walk. Rememebr however that it does this with fixed inter-monomer distance.

The mean squared end-to-end distance is then simply

$$\begin{aligned}\langle \mathbf{R}^2 \rangle &= \left\langle \left(\sum_{i=1}^N \mathbf{r}_i \right) \cdot \left(\sum_{j=1}^N \mathbf{r}_j \right) \right\rangle \\ &= \left\langle \sum_{i=1}^N \sum_{j=1}^N \mathbf{r}_i \mathbf{r}_j \right\rangle\end{aligned}$$

We can split the sum into the terms where $i = j$ and the rest. This yields in general

$$\langle \mathbf{R}^2 \rangle = Nb_0^2 + \langle \mathbf{r}_i \mathbf{r}_j \rangle$$

where the second term simply encodes the covariances between the (random) variables $\mathbf{r}_i, \mathbf{r}_j$. Since we assumed (in this simplistic case) that they are independent, only the first term remains for the free-jointed chain

$$\langle \mathbf{R}^2 \rangle = Nb_0^2$$

This is essentially the same result as for the mean squared displacement of a random walk, provided that we recognise that the number of monomers has taken the role played by time in the case of the walk. We had $\text{MSD} \propto t$ and here we have

$$\langle \mathbf{R}^2 \rangle \propto N$$

Since we formally inherit all the results holding for a random walk, we can also predict what happens to the distribution of possible end-to-end distances in the limit of long polymers, i.e. large N .

The mean squared end-to-end distance can be decomposed as

$$\langle \mathbf{R}^2 \rangle = \langle R_x^2 \rangle + \langle R_y^2 \rangle + \langle R_z^2 \rangle = 3\sigma^2 = Nb_0^2 \Rightarrow \sigma^2 = \frac{Nb_0^2}{3}$$

where σ is the variance per component.

We know that the random walk converges to a Gaussian distribution in 3d with each component having variance σ . Thus, for large N , the probability distribution for the end-to-end vector \mathbf{R} is

$$P(\mathbf{R}) = \left(\frac{3}{2\pi Nb_0^2} \right)^{3/2} \exp \left(-\frac{3\mathbf{R}^2}{2Nb_0^2} \right)$$

This means that, for long chains, the end-to-end distance is distributed as a 3D Gaussian, centered at zero, with variance proportional to N . Also, we can

Radius of gyration

While the end-to-end distance represents a well-defined quantity for a linear chain, we need a more versatile measure of the size for more complicated architectures, such as branched or star-shaped polymers. This is provided by the so called **radius of gyration**, a measure of the (average) extent of the polymer chain.

The radius of gyration is a generic quantity that can be measured from any point cloud. It is closely linked to the (co)-variance of the set of points.

We define the **center of mass** as the average position

$$\mathbf{R}_{\text{CM}} = \frac{1}{N} \sum_{j=1}^N \mathbf{R}_j$$

A general way to describe the spatial extent and shape of the polymer is to construct the **gyration tensor** (also called the configuration tensor):

$$\mathbf{S} = \frac{1}{N} \sum_{j=1}^N (\mathbf{R}_j - \mathbf{R}_{\text{CM}}) \otimes (\mathbf{R}_j - \mathbf{R}_{\text{CM}})$$

where \otimes denotes the outer product, and \mathbf{S} is a 3×3 symmetric matrix. The elements of \mathbf{S} are given by

$$S_{\alpha\beta} = \frac{1}{N} \sum_{j=1}^N (R_{j,\alpha} - R_{\text{CM},\alpha})(R_{j,\beta} - R_{\text{CM},\beta})$$

where $\alpha, \beta \in \{x, y, z\}$.

The **radius of gyration squared** is then simply the trace of this tensor:

$$R_g^2 = \text{Tr}(\mathbf{S}) = S_{xx} + S_{yy} + S_{zz}$$

The eigenvalues and eigenvectors of \mathbf{S} provide information about the principal axes and shape anisotropy of the polymer coil. The **tensor of gyration** corresponds to the **covariance matrix** of the positions \mathbf{R}_j .

The radius of gyration is directly proportional to the end-to-end vector.

$$\langle R_g^2 \rangle = \frac{1}{6} \langle R^2 \rangle$$

i Proof

The radius of gyration is

$$R_g^2 = \frac{1}{N} \sum_{j=1}^N (\mathbf{R}_j - \mathbf{R}_G)^2$$

We can rewrite it as

$$R_g^2 = \frac{1}{2N^2} \sum_{j=1}^N \sum_{k=1}^N (\mathbf{R}_j - \mathbf{R}_k)^2$$

and note that, from our previous result on the end-to-end distance, the mean squared distance between monomers j and k in a free jointed chain is

$$\langle (\mathbf{R}_j - \mathbf{R}_k)^2 \rangle = |j - k| b_0^2$$

So,

$$\langle R_g^2 \rangle = \frac{b_0^2}{2N^2} \sum_{j=1}^N \sum_{k=1}^N |j - k|$$

Evaluating the double sum gives:

$$\sum_{j=1}^N \sum_{k=1}^N |j - k| = \frac{N^3 - N}{3}$$

Thus,

$$\langle R_g^2 \rangle = \frac{b_0^2}{2N^2} \cdot \frac{N^3 - N}{3} = \frac{b_0^2}{6} \left(N - \frac{1}{N} \right)$$

For large $N \gg 1$:

$$\langle R_g^2 \rangle \approx \frac{1}{6} N b_0^2$$

16.2.2 Freely-rotating chain

In a polymer molecule the bond angles are usually restricted, which leads to a limited flexibility of the molecule. Let us consider the case of *n*-butane:



N-butane

The **valence angle** (also called the bond angle) is the angle formed between two adjacent chemical bonds originating from the same atom. In the context of polymers, it is the angle between two consecutive bonds along the polymer backbone. The value of the valence angle is determined by the chemical structure of the monomer and affects the flexibility and overall conformation of the polymer chain. For example, in *n*-butane, the C–C–C bond angle is about 112°. Still rotations about the C–C bond are possible.

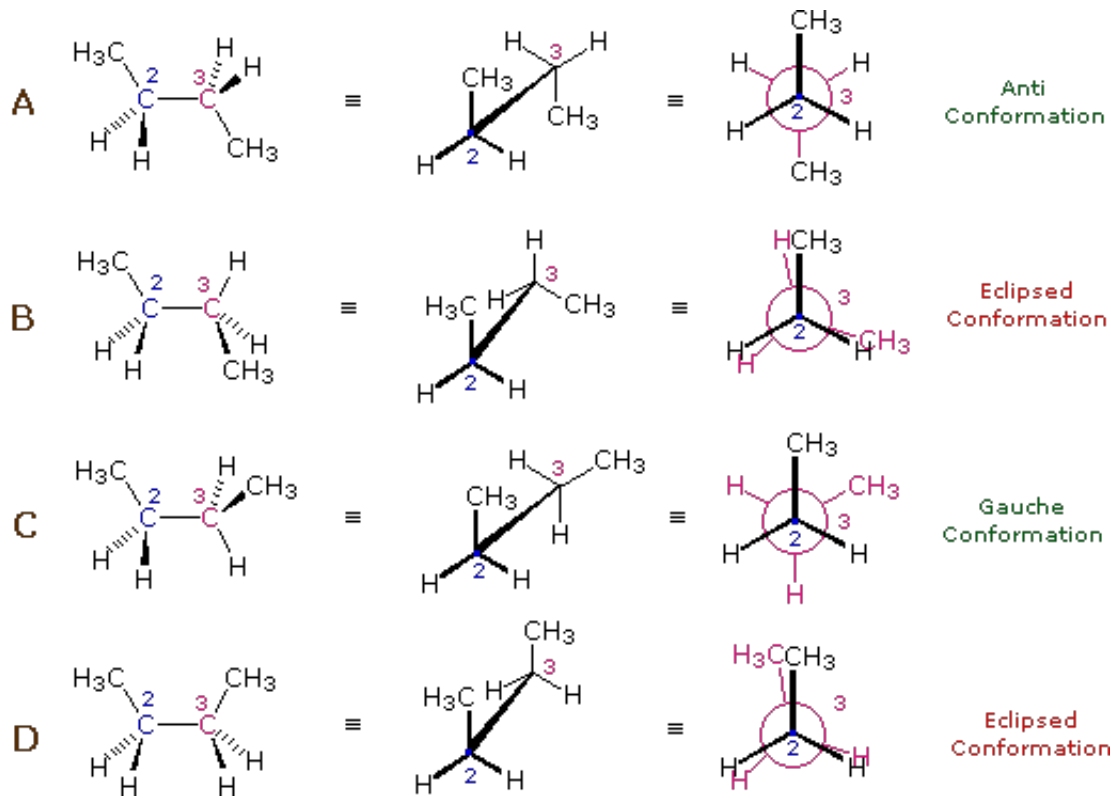


Figure 16.1: Four conformers of butane, from [LibreText Chemistry](#)

Indeed, the potential energy of a polymer configuration depends on the valence (dihedral) angle.

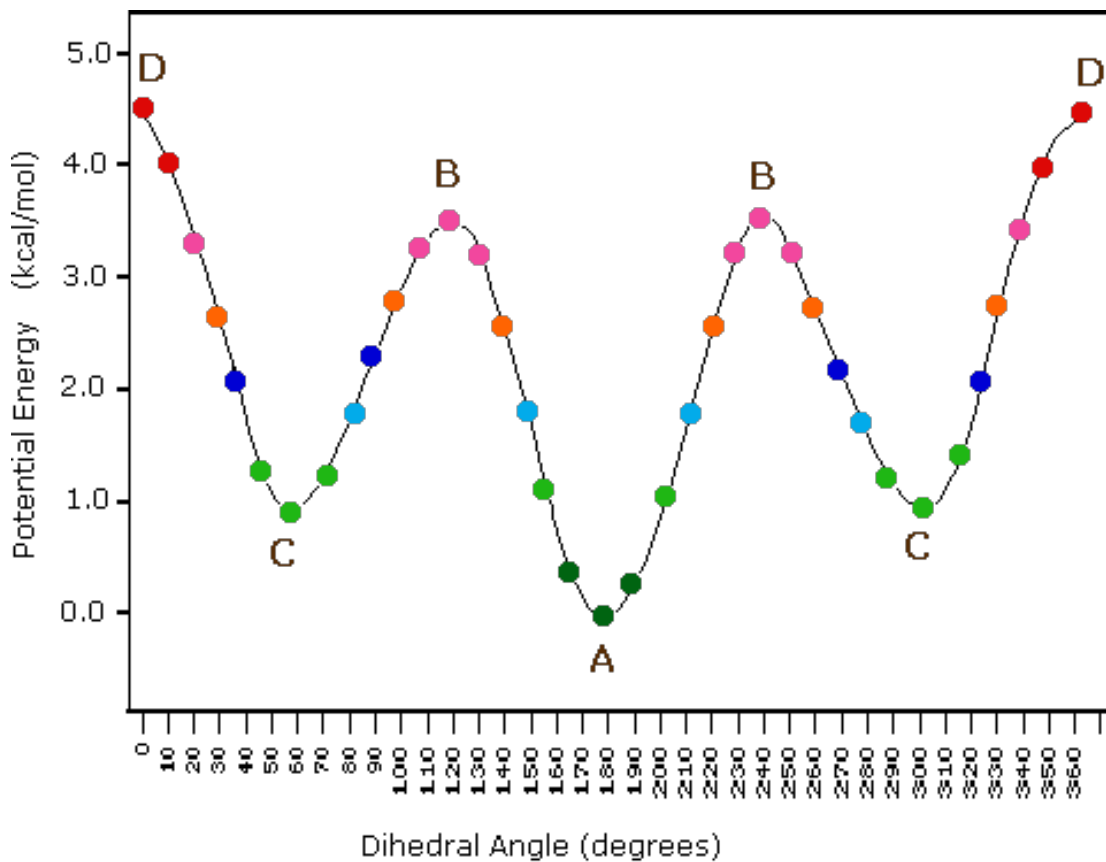
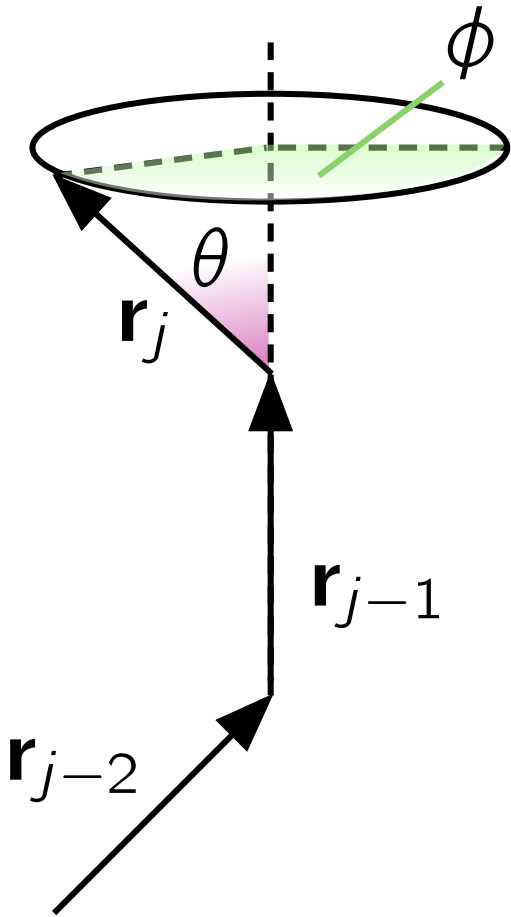


Figure 16.2: Potential energy of the above conformers

At low temperatures ($k_B T <$ configurational energy) the configuration will thus be predominantly of type **A** (an anti conformation). As the temperature is increased ($k_B T \sim$ config. energy), there will also be **C** (gauche) configurations and at high temperatures ($k_B T \gg$ config. energy), any angle will be possible.

This suggests that a good model of polymeric conformation can take fixed angles between bonds, but needs to include **free rotation about** the bonds. This model is called the **freely-rotating chain**.



We start with a fixed configuration of $\mathbf{r}_l, \mathbf{r}_2, \dots, \mathbf{r}_{j-1}$ and then add the next segment \mathbf{r}_j . While the bond angle θ is given by the chemistry of the molecule, the segment can still freely rotate about the axis defined by \mathbf{r}_{j-1} , i.e. φ can take any value $0 \leq \varphi \leq 2\pi$. If we average \mathbf{r}_j over φ , while keeping $\mathbf{r}_1, \mathbf{r}_2, \dots, \mathbf{r}_{j-1}$ fixed, only the component in \mathbf{r}_j direction remains:

$$\langle \mathbf{r}_j \rangle_{\mathbf{r}, \mathbf{r}_2, \dots, \mathbf{r}_{j-1} \text{ fixed}} = \cos \theta \mathbf{r}_{j-1}$$

For the calculation of $\langle R^2 \rangle$ we also need $\langle \mathbf{r}_j \cdot \mathbf{r}_k \rangle$, which we obtain by multiplying both sides with \mathbf{r}_k and taking the average: $\langle \mathbf{r}_j \mathbf{x}_k \rangle = \cos \theta \langle \mathbf{r}_{j-1} \mathbf{x}_k \rangle = \cos^2 \theta \langle \mathbf{r}_{j-2} \mathbf{x}_k \rangle = \dots = (\cos^{|j-k|} \theta) \langle \mathbf{r}_k \mathbf{x}_k \rangle = (\cos^{|j-k|} \theta) b_0^2 \$$

Since $\cos \theta < 1$, correlations between \mathbf{r}_j and \mathbf{r}_k decrease with increasing distance $|j - k|$ between the links and the orientations of distant links become uncorrelated.

The end-to-end distance $\langle R^2 \rangle$ of a freely-rotating chain is hence

$$\begin{aligned} \langle R^2 \rangle &= \sum_{j=1}^N \sum_{k=1}^N \langle \mathbf{r}_j \cdot \mathbf{r}_k \rangle = b_0^2 \sum_{j=1}^N \sum_{k=1}^N (\cos^{|j-k|} \theta) = Nb_0^2 + 2b_0^2 \sum_{j=1}^N \sum_{k=1}^{j-1} \cos^{|j-k|} \theta \\ &= Nb_0^2 + 2b_0^2 \sum_{j=1}^N \cos^j \theta \sum_{k=1}^{j-1} \cos^{-k} \theta \end{aligned}$$

where we used the same argument as above to deal with $|j - k|$. To calculate these two sums we consider the geometric progression:

$$S = \sum_{m=1}^M x^m = x + x^2 + \dots + x^M \quad \therefore xS = x^2 + x^3 + \dots + x^{M+1} \quad \therefore S - xS = x - x^{M+1}$$

$$\therefore S = \frac{x - x^{M+1}}{1 - x}$$

With the help of this formula we get

$$\begin{aligned} \langle R^2 \rangle &= Nb_0^2 + 2b_0^2 \sum_{j=1}^N \cos^j \theta \frac{\frac{1}{\cos \theta} - \frac{1}{\cos^j \theta}}{1 - \frac{1}{\cos \theta}} = Nb_0^2 + \frac{2b_0^2}{\cos \theta - 1} \left(\sum_{j=1}^N \cos^j \theta - \sum_{j=1}^N \cos \theta \right) \\ &= Nb_0^2 + \frac{2b_0^2}{\cos \theta - 1} \left(\frac{\cos \theta - \cos^{N+1} \theta}{1 - \cos \theta} - N \cos \theta \right) \end{aligned}$$

For large N this can be simplified

$$\langle R^2 \rangle \approx Nb_0^2 + \frac{2b_0^2}{1 - \cos \theta} N \cos \theta = Nb_0^2 \left(\frac{1 + \cos \theta}{1 - \cos \theta} \right) = CNb_0^2$$

with $C = (1 + \cos \theta)/(1 - \cos \theta)$.

To get a better idea of the effect of a fixed angle θ , i.e. going from a freely-jointed to a freely-rotating chain, we look at a few special (but not necessarily very realistic) cases:

$$1. \theta \rightarrow 0 \Rightarrow \cos \theta \rightarrow 1 - \frac{\theta^2}{2} \Rightarrow C = \frac{2 - \theta^2/2}{\theta^2/2} \approx \frac{4}{\theta^2} \quad (C \approx 500 \text{ for } \theta = 5^\circ)$$

$$\therefore \langle R^2 \rangle \gg Nb_0^2$$

This corresponds to a nearly straight chain, i.e., a rigid rod. The end-to-end distance is much larger than that of a flexible chain with the same number of segments.

2.

$$\theta \rightarrow \pi - \delta \Rightarrow \cos \theta \rightarrow -1 - \frac{\delta^2}{2} \Rightarrow C = \frac{\delta^2/2}{2 - \delta^2/2} \approx \frac{\delta^2}{4} \quad (C \approx 2 \times 10^{-3} \text{ for } \theta = 175^\circ)$$

$$\therefore \langle R^2 \rangle \ll Nb_0^2$$

This corresponds to the opposite limit, where the chain is compact and forms a globular, collapsed assembly. Examples include:

- polypeptides (the constituents of amino acids) with strong hydrophobic interactions (e.g. alanine, leucine, methionine)
- polystyrene in water
- chromatin (the genetic information *condensed* in the nucleus of cells)

$$3. \theta \rightarrow \pi/2 \Rightarrow \cos \theta \rightarrow 0 \Rightarrow C = 1$$

$$\therefore \langle R^2 \rangle = Nb_0^2$$

These are ideal conditions, where the random walk model of the free-jointed chain works exactly.

Again, we get $\langle R^2 \rangle \propto N$, which suggests that a long freely-rotating chain can be represented by an *effective* freely-jointed chain with N' segments of length b .

Real and effective chain must have the same actual length, i.e.

$$Nb_0 = N'b$$

This is another example of **coarse-graining**.

and the same end-to-end distance,

$$CNb_0^2 = N'b^2.$$

Solving these two equations gives $b = Cb_0$ and $N' = N/C$.

These constraints result in $b = Cb_0$ and $N' = N/C$. This has important consequences:

- All sufficiently long flexible chains have identical behaviour as regards their dimensions: the chemical details are hidden in N' and b .
- While individual monomer pairs are not totally flexible, groups of monomers are
- C represents the number of monomers over which the orientational correlation is lost
- b is the so called "**Kuhn**" **statistical segment length** and defines a related characteristic known as the "persistence length" $l_p = b/2$, also calculated directly via the correlation of bond vectors along the chain:

$$\langle \mathbf{r}_i \cdot \mathbf{r}_{i+n} \rangle = b_0^2 \langle \cos \theta \rangle^n = b_0^2 e^{-nb_0/l_p}$$

where b_0 is the bond length, θ is the angle between consecutive bonds, and n is the number of bonds separating the two segments.

For the freely-rotating chain,

$$l_p = -\frac{b_0}{\ln \langle \cos \theta \rangle}$$

For small angles, this simplifies to $l_p \approx \frac{b_0}{1 - \langle \cos \theta \rangle}$.

16.2.3 Excluded volume effects

The fact that two monomers **cannot occupy** the same space has consequences on different length scales.

- On a local length scale this prevents neighbouring monomers from coming too close together. This effect is taken into account in terms of a **restricted bond-angles**, which prevent them from overlapping.
- Non-overlap, i.e. excluded volume, of **distant monomers** along the chain has also to be taken into account and can have surprisingly large effects.

To estimate the importance of this effect, we consider the fraction of coil volume actually occupied by monomers:

$$V_N = NV_1 \sim Nb^3,$$

This visualisation doesn't strictly satisfy the equal length requirement we set out above, but satisfies the equal end-to-end vector for the sake of visualisation. The Kuhn length should be thought of as a *statistical* quantity and the coarse-grained chain as a polymer with the equivalent statistical properties to a chain of subunits of the original chain.

where V_1 is the volume of a monomer.

The overall volume occupied by the whole coil is

$$V_{\text{coil}} = \frac{4\pi}{3} \langle R_g^2 \rangle^{3/2} \sim \frac{4\pi}{3} N^{3/2} b^3$$

$$\therefore \frac{V_N}{V_{\text{coil}}} = \frac{Nb^3}{(4\pi/3)N^{3/2}b^3} \sim N^{-1/2}$$

This means that for $N = 10^4$ monomers occupy only about 1% of the whole coil volume.

The overall chain size as estimated by the radius of gyration $\langle R_g^2 \rangle^{1/2}$ is determined by the competition of two effects:

1. **Entropy** (and chain connectivity) favour a **compact chain** and avoid the more unlikely stretched configurations
2. Repulsive **excluded volume** interactions want to **expand the chain** to avoid overlap.

Based on this balance we will estimate the effect of excluded volume in a very hand-waving way. (Due to a fortuitous cancellation of errors introduced by various approximations, the result is practically identical to more rigorous treatments, which are very involved.)

We consider the Helmholtz function of a single chain, which is regarded as an assembly of particles with constant volume NV_1 at constant temperature T :

$$F = U - TS$$

The entropy S is given by

$$S = k_B \ln(\text{number of configurations})$$

where for a given end-to-end vector \mathbf{R} the number of configurations is expected to be proportional to

$$P(\mathbf{R}) = \left(\frac{3}{2\pi \langle R^2 \rangle} \right)^{3/2} e^{-\frac{3R^2}{2\langle R^2 \rangle}}$$

and hence

$$S \sim \frac{-3k_B R^2}{2Nb^2} + \text{terms indep. of } \mathbf{R}$$

The internal energy U includes the kinetic and potential energy. However, the kinetic energy is *independent of the configuration* and thus of \mathbf{R} and we only have to consider the potential energy.

To estimate the potential energy, we disregard the connectivity of the chain and calculate the interaction energy of a ‘segment gas’ confined in a volume R^3 . The probability of a monomer to lie in this volume is given by the fraction of total coil volume occupied by monomers, which we estimated above to be NV_1/R^3

Thus the probability of monomer-monomer contacts is $N^2 V_1 / R^3 \sim N^{1/2}$. With an energy ε of a monomer-monomer contact, the potential energy $U \sim \varepsilon N^2 V_1 / R^3$. We thus obtain

$$F = \frac{\varepsilon N^2 V_1}{R^3} + \frac{3k_B T R^2}{2Nb^2} + \text{terms indep. of } R$$

which can be minimized with respect to R , i.e. $dF/dR = 0$, yielding

$$R^5 = \frac{\varepsilon V_1 b^2}{k_B T} N^3 \sim \frac{\varepsilon}{k_B T} N^3 b^5$$

$$\therefore R \sim N^{3/5} b$$

Simulations give a very similar scaling, $R \sim N^{0.588}$. The chain can no longer be modelled by a random walk, but has to be described by a **self-avoiding random walk**. The distribution of end-to-end distances is also not Gaussian. Note that the exponent $3/5$ here is an example of a critical exponent (though not in exactly the same sense that you saw when studying magnets and fluids). Inclusion of excluded volume effects changes the universality class of the scaling of the chain length and radius of gyration with N compared to the Gaussian chains that we looked at previously.

Although the difference between an exponent of 0.5 (as is characteristic for the freely jointed and freely-rotating chains, i.e. a random walk) and 0.6 (excluded volume chain, i.e. self-avoiding random walk) seems small, it has a large effect at large N . For example, for $N = 10^4$, $R = N^{0.5} b = 100b$, while $R = N^{0.6} b = 251b$, which corresponds to a swelling of the chain by a factor of 2.5.

This is an example of the importance of accurate scaling exponents and how they can impact our predictions.

16.3 Good, poor and theta solvents

So far we only considered monomer-monomer interactions, which we assumed to be purely repulsive, and neglected the influence of the solvent.

However, the type of solvent has a great effect on the polymer size. If there is a high affinity with the solvent ('good solvent') the polymer swells, while it will shrink in a 'poor solvent'.

Solvent affinity refers to how strongly the solvent molecules interact with the polymer (or monomer) molecules compared to how they interact with themselves or with other monomers. Mathematically, this is captured by the interaction energy ε_{sp} (solvent-monomer), compared to the average of solvent-solvent (ε_{ss}) and monomer-monomer (ε_{pp}) interactions.

We consider a **lattice model**, where each lattice site has z nearest neighbours and there are N_s solvent molecules and N_p monomers, with N_{sp} solvent-monomer contacts.

The energies of interaction are

- ε_{ss} for the solvent-solvent
- ε_{pp} for monomer-monomer
- ε_{sp} for solvent-monomer interactions.

Then the energy of mixing ΔU_{mix} is given by

$$\Delta U_{\text{mix}} = U - (U_S + U_p)$$

where energy of pure solvent is

$$U_s = \frac{zN_s \varepsilon_{ss}}{2}$$

and the energy of pure polymer is

$$U_p = \frac{zN_p \varepsilon_{pp}}{2}$$

resulting in an energy of solution

$$U = N_{sp} \varepsilon_{sp} + \frac{(zN_s - N_{sp}) \varepsilon_{ss}}{2} + \frac{(zN_p - N_{sp}) \varepsilon_{pp}}{2}$$

Hence we obtain for the **energy of mixing**

$$\Delta U_{\text{mix}} = N_{sp} \left[\varepsilon_{sp} - \frac{1}{2} (\varepsilon_{ss} + \varepsilon_{pp}) \right]$$

which can be either positive or negative:

- **Good solvent:** $\varepsilon_{sp} < \frac{1}{2} (\varepsilon_{ss} + \varepsilon_{pp}) \quad \therefore \Delta U_{\text{mix}} < 0$

This is the case of a ‘good solvent’, because the monomers prefer to be near the solvent molecules. Excluded volume effects then expand the chain.

- **Poor solvent:** $\varepsilon_{sp} > \frac{1}{2} (\varepsilon_{ss} + \varepsilon_{pp}) \quad \therefore \Delta U_{\text{mix}} > 0$

This is the case of a ‘poor solvent’, because the monomers prefer to be near to each other (and similarly for the solvent molecules). The attraction between the different monomers offset the excluded volume effect.

The importance of the attractions generally depends on temperature. At very high temperatures the coil is expanded and the solvent quality is good. In contrast, at very low temperatures, the solvent quality is poor, attraction dominates, the coil collapses and phase separation is observed. In between these two limits, there is a temperature, the so-called theta temperature θ , where the coil has ideal dimensions and the effects of excluded volume and attraction cancel each other. The solvent at $T = \theta$ is called a ‘theta solvent’. The stronger the attractions the higher θ will be, while for weak attractions θ is low. A full treatment of the coil expansion is rather involved and has to take into account excluded volume, attractions, configurational entropy and entropy of mixing. You can read more about the theta condition in Jones (2002).

! Check your understanding

- A polymer has characteristic features on different length scales.
- On a very global length scale, it has a molar mass M and an overall size which can be characterised by the root mean square end-to-end distance $\langle R^2 \rangle^{1/2}$ or radius of gyration $\langle Rg^2 \rangle^{1/2} \propto N^\nu \propto M^\nu$, where $\nu = 1/2$ for a freely-jointed or freely-rotating chain (random walk) and $\nu = 3/5$ for an excluded volume chain (self-avoiding random walk).
- On a smaller length scale the behaviour will be dominated by the finite flexibility or *persistence* of the chain, which is characterised by the Kuhn length b . The chain will essentially behave like a stiff rod on this length scale. This rod typically has a constant mass per length, M/L , and thus $M\alpha L$.
- Finally, the local cross-sectional structure will be observed on an even smaller length

scale.

16.4 Concentrated polymer solutions

Up to now we considered a single polymer in a very dilute solution. Now we increase the concentration in steps until we reach bulk polymers.

The most important regimes of concentration are:

- **Dilute regime**

The polymer coils are well-separated on average. Call c the concentration expressed as mass per unit volume, then it satisfies

$$\frac{c}{M} N_A \times \frac{4\pi}{3} R_g^3 \ll 1$$

- **Overlap concentration c^***

Overlap occurs when the volume fraction of coils reaches unity and thus

$$\frac{c^*}{M} N_A \frac{4\pi}{3} R_g^3 \sim 1 \quad \therefore c^* = \frac{3M}{4\pi N_A R_g^3}$$

using $Rg = \langle Rg^2 \rangle^{1/2} = BM^\nu$ gives

$$c^* = \frac{3}{4\pi N_A B^3} M^{1-3\nu}$$

For example, polystyrene with $M = 10^6 \text{ g mol}^{-1}$ in a good solvent ($\nu = 0.6$) and $B = 0.028 \text{ nm} \left(\text{g mol}^{-1} \right)^{-0.6}$ leads to $c^* = 0.29 \text{ kg m}^{-3} = 0.29 \text{ mg/ml}$. With the density of polystyrene $\rho = 1050 \text{ kg m}^{-3}$, the volume fraction of monomers is $c^*/\rho = 0.28 \times 10^{-3}$. c^* can be very small for large polymers.

- **Semi-dilute**

The concentration is larger than the overlap concentration c^* , but still much smaller than the bulk density. The coils interpenetrate and entangle, but the solution is still mostly solvent

- **Concentrated**

In this case the concentration is very close to the bulk density and the polymer monomers occupy a significant fraction of the total volume.

- **Bulk polymers**

A **bulk polymer** refers to a polymeric material in which the polymer chains occupy a significant fraction of the total volume, with little or no solvent present. In this regime, the properties of the material are dominated by polymer-polymer interactions rather than polymer-solvent interactions. Bulk polymers can be amorphous, semi-crystalline, or crystalline, and their mechanical, thermal, and optical properties are determined by the arrangement and mobility of the polymer chains.

Bulk polymers are divided into two main classes, characterised by whether they are cross-linked or not. There are elastomers or rubbers with a low degree of cross-linking and thermosets

with a high degree of cross-linking. We will investigate the behaviour of rubbers in the next chapter. The second class are thermoplastics, which are not cross-linked. Most everyday plastic products are thermoplastics. We will briefly discuss their behaviour upon cooling, which shows similarities to the behaviour of colloids. At high temperature the free energy is dominated by the entropic terms. The melt resembles a random assembly of mobile, intertwined, flexible coils with a density similar to the density of the corresponding monomer liquid. Upon cooling the potential energy takes over and the bonds are restricted in their rotation leading to configurations which are more straightened out. Below the melting temperature T_m , a crystal is the lowest free energy state. Crystallisation, however, requires significant ordering of the initially random melt and is only possible if cooling occurs slow enough. If the melt is rapidly cooled below the glass transition temperature $T_g (< T_m)$, then instead of a crystal a glass is formed, which represents an amorphous metastable, but long-lived state. Although the polymers can still vibrate, they can no longer move. Solid thermoplastics are frequently a mixture of crystalline and amorphous structures.

References

Chapter 17

Liquid crystals

Ordered phases of matter are typically characterised by spatial correlations, which can be **positional or orientational** in nature.

Positional order is the regular arrangement of particle positions in space, often forming a repeating lattice structure. Orientational order refers to the angular alignment of the neighbours of a particle, influenced for example by the anisotropy of the particle itself (e.g. rods tending to align with other rods).

In crystalline phases, both positional and orientational order are long-ranged, meaning that the arrangement and orientation of particles are correlated over macroscopic distances. In contrast, simple liquids exhibit only very short-range (positional and orientational) correlations.

Liquid crystals represent an intermediate case, where orientational order can persist over long distances while positional order remains short-ranged or absent.

17.1 Anisotropic particles

The decoupling between orientational and translational degrees of freedom is favoured by individual microscopic units (particles) that already have preferential axis of symmetry, i.e. anisotropic particles. Anisotropic particles have shapes that are not spherically symmetric, such as rods, ellipsoids, or plates. Their interactions depend not only on the distance between particles but also on their relative orientations.

There are many kinds of anisotropic particles. The table below contains a non-exhaustive list.

Particle Shape	Description	Example Materials	Typical Applications
Rods	Cylindrical, length > width	Gold nanorods, Tobacco virus	Photothermal therapy, plasmonics
Ellipsoids	Elongated or flattened spheroids	Hematite ellipsoids	Anisotropic optics, directed self-assembly
Plates/Discs	Flat, disk-like shapes	Graphene oxide, clay platelets	Barrier materials, viscosity control
Polyhedra	Multi-faceted, highly symmetric shapes	Gold nanocubes, silica polyhedra	Photonic crystals, catalysis

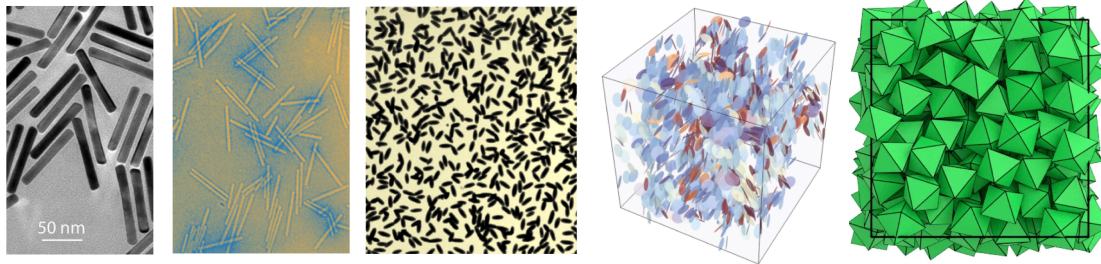


Figure 17.1: Various assemblies of anisotropic particles. Left to right: Golden nanorods (from [Stanford Advanced Materials](#)), tobacco virus rods (adapted from Knapp and Lewandowski (2001)), ellipsoidal silica-coated hematite particles (adapted from Sánchez-Ferrer et al. (2010)), hard platelets in the isotropic phase (from Atashpendar, Ingenbrand, and Schilling (2020)), and an arrangement of octahedra simulated using hard particle Monte Carlo with [hoomdblue](#)

17.2 Liquid crystal phases

The additional orientational degrees of freedom makes opens up the possibilities of phases that do not normally exist for spherical, isotropic particles. We progress from the most disordered to the most ordered phase:

- **Isotropic fluid:** this phase is not very different from the ordinary fluid phase of spherical particles. There is no long-range positional or orientational order and all correlations decay rapidly and on short lengthscales.
- **Nematic phase:** still without translational order, the constituents arrange themselves spontaneously in a preferential, average direction, called the **director**. Since there is no positional order, the transition from isotropic to nematic can only be detected by taking into account the *relative orientations* between the constituents, as the individual centres of mass are as disordered in the nematic as they are in the isotropic. If the particles are themselves chiral (i.e., the particle differs from its mirror image) the director tends to form a helix due to the propensity of te molecules to align at some angle between each other. This leads to so called chiral nematic phase (also known as **cholesteric**).
- **smectic phase:** in this phase, particles not only align along a common direction (as in the nematic phase) but also exhibit partial translational order. The centers of mass of the particles tend to form well-defined layers, with orientational order within each layer. However, within a layer, the positions of the particles remain disordered, similar to a liquid. Smectic phases can be further classified (e.g., smectic A, smectic C) depending on the relative orientation of the director with respect to the layer normal.
- **Columnar phase:** here, anisotropic particles (often disc-like) stack into columns, which then arrange themselves into a two-dimensional lattice. There is long-range positional order in two directions (within the plane perpendicular to the columns) and orientational order along the column axis.
- **Crystal:** the most ordered phase, where both positional and orientational order are long-ranged in all directions, forming a true three-dimensional periodic lattice.

Phase	Positional Order	Orientational Order
Isotropic fluid	No	No
Nematic	No	Yes (long-range)
Chiral nematic	No	Yes (helical)
Smectic	Yes (1D: layered)	Yes (within layers)
Columnar	Yes (2D: columns)	Yes (along columns)

Phase	Positional Order	Orientational Order
Crystal	Yes (3D: lattice)	Yes (long-range)

17.3 Orientational correlations and the isotropic/nematic transition

While for the spherical colloids we focused on positional correlation functions like the radial distribution function, for anisotropic particle we need to quantify orientational correlations.

Suppose we have N rod-like particles, each with an orientation angle θ_i (in 2D) or a unit vector \mathbf{u}_i (in 3D). We want to determine the director, i.e. the average direction of the long molecular axes of all molecules in the liquid crystal.

The rods are head-tail symmetric, so, we cannot truly distinguish which one is the head or the tail (e.g. an orientation of θ in 2D is the same as an orientation of $\theta + \pi$). We cannot therefore just take the average of the vectors to extract the common orientation of the various vectors, otherwise we would incur into a cancellation.

Instead, we construct a second moment tensor called the **alignment tensor**

$$\mathbf{Q} = \frac{d}{2} \left\langle \mathbf{u}_i \otimes \mathbf{n}_i - \frac{1}{d} \mathbf{I} \right\rangle$$

where d is the dimensionality. The removed $\frac{1}{d} \mathbf{I}$ term ensures that the tensor is traceless and does not include isotropic components.

The analysis of the tensor yield the main characteristics of the orientation of the system: - the largest eigenvalue of \mathbf{Q} is the **scalar nematic order parameter** \mathcal{S} - the eigenvector corresponding to the largest eigenvalues is called the **director** \mathbf{n} and corresponds to the main collective orientation of the system.

In two dimensions, the director is simply characterised by the angle ψ expressed as

$$\psi = \frac{1}{2} \text{atan2}(\sin 2\theta_i, \cos 2\theta_i).$$

and the nematic order parameter is simply

$$\mathcal{S} = \sqrt{\langle \cos 2\theta_i \rangle^2 + \langle \sin 2\theta_i \rangle^2}$$

while in three dimensions this gives

$$\mathcal{S} = \frac{1}{2} \langle 3 \cos^2 \theta_i - 1 \rangle$$

(the expression for the director in 3d requires explicit diagonalisation).

Notice that \mathcal{S} is not the entropy S !
These commonly used symbols should not be confused.

i Derivation of 2D director

For the purpose of illustrating how the calculations for the director are carried out, we provide a detailed example in two-dimensions.

In two dimensions, each particle has an orientation unit vector

$$\mathbf{u}_i = \begin{pmatrix} \cos \theta_i \\ \sin \theta_i \end{pmatrix},$$

and the alignment tensor is defined as

$$\mathbf{Q} = \langle \mathbf{u}_i \otimes \mathbf{u}_i \rangle = \begin{pmatrix} \langle \cos^2 \theta_i \rangle & \langle \cos \theta_i \sin \theta_i \rangle \\ \langle \cos \theta_i \sin \theta_i \rangle & \langle \sin^2 \theta_i \rangle \end{pmatrix}.$$

Using double-angle trigonometric identities,

$$\cos^2 \theta = \frac{1 + \cos 2\theta}{2}, \quad \sin^2 \theta = \frac{1 - \cos 2\theta}{2}, \quad \cos \theta \sin \theta = \frac{1}{2} \sin 2\theta,$$

we rewrite \mathbf{Q} as

$$\mathbf{Q} = \frac{1}{2} \begin{pmatrix} 1+C & D \\ D & 1-C \end{pmatrix},$$

where

$$C = \langle \cos 2\theta_i \rangle, \quad D = \langle \sin 2\theta_i \rangle.$$

To find the eigenvalues λ , solve

$$\det(\mathbf{Q} - \lambda \mathbf{I}) = 0,$$

which yields the largest eigenvalue

$$\lambda_{\max} = \frac{1}{2} + \frac{S}{2},$$

with the scalar nematic order parameter

$$\mathcal{S} = \sqrt{C^2 + D^2}.$$

Where $\mathcal{S} \rightarrow 1$ indicates strong alignment and $\mathcal{S} \rightarrow 0$ indicates isotropic order.

The director \mathbf{n} is the eigenvector corresponding to λ_{\max} , satisfying

$$(\mathbf{Q} - \lambda_{\max} \mathbf{I}) \mathbf{v} = 0,$$

which gives

$$\mathbf{Q} - \lambda_{\max} \mathbf{I} = \frac{1}{2} \begin{pmatrix} C-S & D \\ D & -C-S \end{pmatrix}.$$

The eigenvector is

$$\mathbf{v} \propto \begin{pmatrix} 1 \\ \frac{S-C}{D} \end{pmatrix}.$$

Normalizing \mathbf{v} gives the director \mathbf{n} .

The director angle ψ is given by

$$\tan \psi = \frac{S - C}{D}.$$

This simplifies to

$$\tan \psi = \frac{D}{S + C}.$$

Using the double-angle formula,

$$\psi = \frac{1}{2} \operatorname{atan2}(D, C).$$

The angle ψ represents the director's orientation modulo π .

17.4 Landau-de Gennes mean field theory

Let us consider the uniaxial 3D case, which is the most commonly discussed case (this focuses on nematic order, excluding cholesteric and smectic order) and attempt to construct a Landau theory centred on the order parameter in the spirit of what we saw in Section 5.5. If the system is uniaxial, then the order is characterized by a single director and the \mathbf{Q} must be symmetric and traceless with a preferred axis \mathbf{n} .

The tensorial order parameter can be rewritten leveraging that the scalar order parameter is an eigenvalue of the director. i.e. $\mathbf{Q}\mathbf{n} = S\mathbf{n}$. The result is that

$$\mathbf{Q} = S \left(\mathbf{n} \otimes \mathbf{n} - \frac{1}{d} \mathbf{I} \right)$$

for some scalar value S (the order parameter between 0 for the isotropic and 1 for the nematic). If we choose now the z axis along \mathbf{n} we can write this explicitly as

$$\mathbf{Q} = S \begin{pmatrix} -\frac{1}{3} & 0 & 0 \\ 0 & -\frac{1}{3} & 0 \\ 0 & 0 & \frac{2}{3} \end{pmatrix}$$

with $S = \frac{3}{2} \langle (\mathbf{u} \cdot \mathbf{n})^2 - \frac{1}{3} \rangle$ as defined earlier.

We can now make an extra step by considering how to express the scalar order parameter in terms of the **probability distribution** $p(\Omega)$ of finding a rod with pair of polar angles $\Omega = (\theta, \phi)$ in a coordinates system with polar axis along \mathbf{n} (which is the reference frame we have just chosen). The infinitesimal probability is $p(\Omega)d\Omega$.

As often in physics, we need to make a symmetry observation, and remark that the nematic phase has full **cylindrical symmetry** around the director. This means that, for us $p(\Omega) = p(\theta, \phi)$ is in fact independent of The azimuthal angle ϕ and only depends on the deviation from the director θ .

We also note that the expression for the nematic order parameter satisfies head-tail symmetry bt employing the first non-trivial **Legendre polynomial**, $P_2(\cos \theta)$ as

$$S = \frac{3}{2} \left\langle (\mathbf{u} \cdot \mathbf{n})^2 - \frac{1}{3} \right\rangle = \frac{1}{2} \langle 3 \cos^2 \theta - 1 \rangle = \langle P_2(\cos \theta) \rangle$$

In terms of the probability distribution this is

$$\mathcal{S} = 2\pi \int_0^\pi P_2(\cos \theta) p(\theta) \sin \theta d\theta$$

The Landau free energy density for the isotropic-nematic transition is constructed by scalar combinations of the tensor \mathbf{Q} . The idea is to expand the **free energy density** f around the transition and write it as

$$f = f_0 + \frac{A}{2} Q_{ij} Q_{ji} - \frac{B}{3} Q_{ij} Q_{jk} Q_{ki} + \frac{C}{4} (Q_{ij} Q_{ij})^2$$

or in more compact form

$$f = f_0 + \frac{A}{2} \text{tr } \mathbf{Q}^2 - \frac{B}{3} \text{tr } \mathbf{Q}^3 + \frac{C}{4} (\text{tr } \mathbf{Q}^2)^2$$

where we stop the construction to terms of **fourth order** in \mathbf{Q} and A, B, C are temperature dependent coefficients.

We note that given our definitions above the following identities hold

$$\text{Tr}(\mathbf{Q}^2) = \frac{2}{3} S^2 \quad , \quad \text{Tr}(\mathbf{Q}^3) = \frac{2}{9} S^3$$

so that

$$f = f_0 + \frac{A}{3} S^2 - \frac{2B}{27} S^3 + \frac{C}{9} S^4$$

We can follow the scheme used for Landau phase transitions and obtain the so-called **Landau-de Gennes theory** result

$$f - f_0 = \frac{a}{3} (T - T^*) S^2 - \frac{2b}{27} S^3 + \frac{c}{9} S^4.$$

This has the form of standard Landau free energy (combinations of power of S up to the power of 4 with real coefficients that depend on the temperature). It can be shown that this corresponds to a first order phase transition without critical point (because the isotropic and nematic phase have different symmetry) with transition temperature

$$T_{NI} = T^* + \frac{b^2}{27ac}$$

where T^* is a material dependent temperature, identifying where the quadratic term of the free energy vanishes, and where the isotropic phase becomes unstable (spinodal).

We can expand A, B, C around the reference temperature T^* as

$$A(T) = a (T - T_*) + \dots$$

and at zeroth order for both B and C as
 $B(T) = b + \dots$,
 $C(T) = c + \dots$,
with $a, b, c > 0$
to preserve the most relevant terms.

17.5 Maier-Saupe theory

The Landau-de Gennes theory illustrates how the simple existence of a suitably defined nematic order is compatible with the construction of a theory that predicts a first order phase transition. A complementary approach is to consider the minimal physical ingredients that lead to the transition itself. As in the case of the colloids, we have essentially two classes

1. attractive interactions that can favour the new symmetries (e.g. the nematic order)
2. entropic contributions that make it easier to pack the rods in the new symmetry (i.e. when they are aligned)

Phenomenologically, we can put these two together assuming a form for the energetic and entropic contributions to write down a free energy of the following form

$$f = f_0 - u \frac{S^2}{2} + k_B T \int_0^\pi p(\theta) \ln(4\pi p(\theta)) \sin \theta d\theta$$

where the 4π term assumes that $p(\theta)$ is correctly normalised on the sphere and $\sin \theta d\theta$ is the usual Jacobian. The two terms above identify two simple contributions:

- an energetic contribution that is a simple quadratic function of the order parameter (more order, lower energy, with the isotropic phase paying the highest cost). Near the isotropic phase the free energy needs to be even due to the head-tail symmetry.
- a generic entropic contribution of the form $k_B \int p(\theta) \ln p(\theta) d\theta$ using the [Gibbs entropy formula](#).

The minimization of the free energy with respect to $p(\theta)$, under the normalization constraint $\int_0^\pi p(\theta) \sin \theta d\theta = 1$, is performed using a Lagrange multiplier λ . The variational problem is:

$$\delta \left[f + \lambda \left(\int_0^\pi p(\theta) \sin \theta d\theta - 1 \right) \right] = 0$$

Taking the functional derivative with respect to $p(\theta)$ and setting it to zero yields:

$$\frac{\delta f}{\delta p(\theta)} + \lambda \sin \theta = 0$$

Plugging in the expression for f and simplifying, we obtain the solution:

$$p(\theta) = \frac{1}{Z} \exp(\lambda P_2(\cos \theta)) = \frac{1}{Z} \exp\left(\frac{uS}{k_B T} P_2(\cos \theta)\right)$$

where S is the nematic order parameter to be determined self-consistently, and Z is the normalization constant (partition function):

$$Z = \int_0^\pi \exp\left(\frac{uS}{k_B T} P_2(\cos \theta)\right) \sin \theta d\theta$$

This is the Maier-Saupe self-consistent equation for the orientational distribution in the mean-field theory of nematic liquid crystals. In the code below, we can see how this leads to a non

trivial energy profile which corresponds to the emergence of a ordered state (a minimum at high S) corresponding to the nematic phase.

The transition is **weakly-first** order, as two separate basins of stability (separated typically by a small barrier) are formed.

```
#| autorun: true
#| caption: "Free energy profile of the Maier-Saupe model for various values of the coupling parameter u"

import numpy as np
import matplotlib.pyplot as plt

for u in np.linspace(1,10,10):
    = np.linspace(0.1, 100.0, 1000)
    thetas = np.linspace(0, np.pi, 100)
    T = 1.0 ## CHANGE T TO SEE WHAT HAPPENS: CAN YOU EXPLAIN WHY?
    legendre_weight = (1.5 * np.cos(thetas)**2 - 0.5) * np.sin(thetas)
    S = []
    F = []
    for l in :
        p_theta = np.exp(l *legendre_weight) # p( ; )
        p_theta /= np.trapezoid(p_theta * np.sin(thetas), thetas) # Normalize p()
        S_l = np.trapezoid(p_theta * legendre_weight, thetas)
        f = -0.5*u*S_l**2+T*np.trapezoid(p_theta * np.log(4*np.pi*p_theta)*np.sin(thetas), thetas)
        S.append(S_l)
        F.append(f)
    S = np.array(S)
    F = np.array(F)
    plt.plot(S,F-F[0], label=str(u))
plt.legend(frameon=False, title="u")
plt.gca().set(xlabel="Order parameter S", ylabel="free energy density / kBT" )
plt.show()
```

These profiles are example of simple **free energy landscapes**. We will see more about this later in Section 19.1.

17.5.1 Lattice model: the Lebwohl-Lasher model

The Lebwohl-Lasher model is a lattice model designed to capture the orientational ordering of anisotropic particles, such as those found in nematic liquid crystals and is a lattice version of the Maier-Saupe mean field model. In this model, each lattice site i is associated with a unit vector \mathbf{n}_i representing the local orientation (the “director”) of a particle at that site.

The Hamiltonian of the Lebwohl-Lasher model is given by:

$$H = -\epsilon \sum_{\langle i,j \rangle} \left[\frac{3}{2}(\mathbf{n}_i \cdot \mathbf{n}_j)^2 - \frac{1}{2} \right]$$

where: - $\epsilon > 0$ is the coupling constant favoring alignment, - the sum $\langle i, j \rangle$ runs over all pairs of nearest-neighbor sites, - $(\mathbf{n}_i \cdot \mathbf{n}_j)^2$ measures the degree of alignment between neighboring directors.

This Hamiltonian favors parallel (or antiparallel) alignment of neighboring directors, capturing the essential physics of the isotropic-nematic transition in liquid crystals.

In two dimensions, the Lebwohl-Lasher model is similarly defined, but the directors \mathbf{n}_i are restricted to lie in the plane. Each director can be represented by a unit vector $\mathbf{n}_i = (\cos \theta_i, \sin \theta_i)$, where θ_i is the orientation angle at site i .

The Hamiltonian in 2D becomes:

$$H = -\epsilon \sum_{\langle i,j \rangle} \left[\frac{3}{2} \cos^2(\theta_i - \theta_j) - \frac{1}{2} \right]$$

where the sum is over nearest-neighbor pairs on a 2D lattice. This model captures the essential features of orientational ordering and the isotropic-nematic transition in two-dimensional systems.

```
#| autorun: true
#| define:
#|   - snapshots
import numpy as np
import matplotlib.pyplot as plt

def p2(x):
    return 0.5 * (3 * x * x - 1)

def delta_energy(theta, i, j, new_angle, epsilon):
    L = theta.shape[0]
    old_angle = theta[i, j]
    dE = 0.0
    neighbors = [((i+1) % L, j), ((i-1) % L, j), (i, (j+1) % L), (i, (j-1) % L)]
    for k in range(4):
        ni, nj = neighbors[k]
        cos_old = np.cos(old_angle - theta[ni, nj])
        cos_new = np.cos(new_angle - theta[ni, nj])
        dE += -epsilon * (p2(cos_new) - p2(cos_old))
    return dE

L = 64 # lattice size
epsilon = 1.0 # coupling
T = 1.0 # CHANGE THIS VALUE TO EXPLORE DIFFERENT REGIMES
steps = 20*L*L #MC sweeps

# Initialize lattice with random angles [0, pi) (nematic symmetry)
theta = np.random.uniform(0, np.pi, size=(L, L))
# preassign random numbers for efficiency
rands = np.random.randint(0, L, (steps,2))
new_angles = np.random.uniform(0, np.pi, steps)
rs = np.random.uniform(0, 1, size=steps)
snapshots= []

for step in range(steps):
    i, j = rands[step]
    new_angle = new_angles[step]
    dE = delta_energy(theta, i, j, new_angle, epsilon)
    if dE < 0 or rs[step] < np.exp(-dE / T):
        theta[i, j] = new_angle
    if step % 100 == 0:
        print(f"Step {step}: Energy = {dE}, Angle = {new_angle}, Random = {rs[step]}")
```

```

if step%100==0:
    snapshots.append(theta.copy())

plt.matshow(theta, cmap='hsv', vmin=0,vmax = np.pi)
plt.colorbar(label="angle $\backslash\theta$")
plt.show()

```

! Activity

Modify the script above to check the following

1. The high temperature regime ($T \gg 0.5\pi$) is mostly disordered (isotropic)
2. The low temperature regime forms larger and larger patches with coherent orientations
3. Define and plot a global nematic order parameter. The global nematic order parameter S is defined as:

$$S = \langle \cos(2(\theta - \psi)) \rangle$$

where ψ is the director (average orientation), which in 2D is

$$\psi = \frac{1}{2}\text{atan}2(\langle \sin(2\theta) \rangle, \langle \cos(2\theta) \rangle)$$

17.6 Splay, twist and bend

In the continuum limit, the nematic liquid crystal can be characterised in terms of the deformation of a vector field $\mathbf{n}(\mathbf{r})$ which represents the director at every point \mathbf{r} (a *local* director, resulting from the average over a large number of particles in a single volume).

The Frank free energy density for distortions of the director field is

$$f = \frac{1}{2}K_1(\nabla \cdot \mathbf{n})^2 + \frac{1}{2}K_2[\mathbf{n} \cdot (\nabla \times \mathbf{n})]^2 + \frac{1}{2}K_3[\mathbf{n} \times (\nabla \times \mathbf{n})]^2$$

where: - K_1 is the splay elastic constant, - K_2 is the twist elastic constant, - K_3 is the bend elastic constant.

Each term in the Frank free energy penalizes a specific type of distortion: splay, twist, or bend. The total elastic free energy is found by integrating f over the entire sample volume. This formulation is named after Charles Frank, a pioneer in the study of crystal dislocations (which are defects in crystalline solids) and what we call today soft matter at the University of Bristol, for whom the Frank lecture theatre is named.

The formulation allows one to model the behaviour of liquid crystals with finite element methods on much larger scales than the typical size of the elementary constituents. It also allows to phenomenologically add more deformation modes, to include for example the description of chirality.

17.7 Topological defects

The continuum limit description of liquid crystals allows us to enhance their description with the notion of **topological defects**.

Topological defects are singularities in the director field that can not be removed by a continuous deformation of the director field: they are **topologically protected**. We can see this with a few examples in 2d by drawing lines of the director (remember that the head-tail symmetry means that the lines do not have any preferential direction but indicate local orientation):

These topological defects are places where the orientation changes discontinuously and are also called **disclinations**.

In two dimensions, the disclinations are characterized by a topological charge (or strength) s , defined by the total rotation of the director around a closed loop enclosing the defect:

$$\Delta\theta = 2\pi s$$

Common disclination strengths in nematic liquid crystals are $s = \pm\frac{1}{2}$ and $s = \pm 1$. For example, a $+1/2$ disclination corresponds to a director field that rotates by $+\pi$ as one encircles the defect, while a $-1/2$ disclination rotates by $-\pi$.

When two disclinations of opposite charges meet, they **annihilate**. This means the defects can cancel each other out, restoring uniform orientational order in the region. The annihilation of defect pairs is a key mechanism by which nematic liquid crystals relax toward equilibrium after being disturbed. This is because the idealised equilibrium state should in principle be free of any such defects, as they cost energy: they deform the director field on long distances, leading to a deformation cost, and they also engender a complete loss of orientational order at the singularity point, which costs energy by itself.

In three dimensions, disclinations are line defects rather than point defects. These line defects represent regions where the orientational order of the director field is singular along a curve, rather than at isolated points. The topology and dynamics of disclination lines in 3D nematic liquid crystals are richer and more complex than in 2D, allowing for phenomena such as defect loops, entanglements, and reconnections. Disclination lines can form closed loops, terminate at surfaces, or interact with other defects, and play a crucial role in the response of liquid crystals to external fields, boundary conditions, and during phase transitions.

The classification of disclination in 3D involves the rotation group **SO(3)*** (that generalises the construction we have seen in two dimensions) and are more complex in general. They include **lines**, **closed loops**, point-like features (**hedgehogs** and **monopoles**) and complex **textures**.

You can read more about liquid crystal's defects and their coupling to the material properties in Jones (2002).

References

Chapter 18

Surfactants

```
#| echo: false
#| autorun: true
# modifying the path to add the code folder
import sys
sys.path.insert(0, 'src')
```

18.1 Hydrophobicity and amphiphiles

The hydrophobic interaction between solutes is a statistical force mediated by water (the solvent). Traditional explanations focus on the role played by hydrogen bonds (an attractive interaction due to the difference in electronegativity between oxygen and hydrogen in water) and the structure of water around solutes.

Polar molecules have regions with partial positive and negative charges due to differences in electronegativity between atoms, resulting in an uneven distribution of electrons. This allows them to interact strongly with water (hydrophilic) and other polar substances.

Apolar (or nonpolar) molecules, instead, have a more even distribution of electrical charge, lacking distinct poles. They do not mix well with water and tend to aggregate with other nonpolar substances.

In this chapter we discuss the behaviour of a special class of molecules. In these molecules one end contains a *hydrophilic* (literally, *water-loving*) part, while the other end is *hydrophobic* (*water-fearing*). For their nature, they are called **amphiphilic** (loving both) molecules, which reflects their structure, or **surfactants** (from *SURFace ACTive AGENT*), which refers to their behaviour in solution.

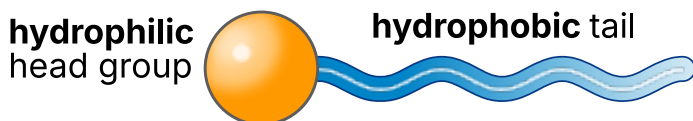


Figure 18.1: Schematic model of a surfactant (adapted).

For very small solutes (a few atoms) the traditional picture of hydro-phobicity/philicity is that the energetic advantage due to hydrogen bonding favors configurations that minimally disrupt the local structure of water, and this means that multiple apolar solutes tend to come together to minimise such disruption since they cannot form such bonds. However, for larger molecules (such as large proteins or longer macromolecular chains) interfaces between the bulk water and the solutes are formed, to which we can associate characteristic density fluctuations and surface tensions. Phase separation between a local vapor-like layer and the bulk water becomes then important and aggregation due to hydrophobicity becomes very much a many-body effect. This is an active topic of current research (even by some of us, see Wilding and Turci (2025)) and demonstrates how even very foundational concepts in soft matter remain to be explored.

In the rest of the chapter, we will look mostly phenomenologically at the structure of surfactants and how they collectively come together to form meso-scale structures via the process of **self-assembly**, and assume that there exist solvent-mediated interactions such as hydrophobicity that control the free energies of these assemblies.

A few chemical structures are shown below. They illustrate that the hydrophobic tail usually consists of hydrocarbon chains of different lengths

SDS (dodecyl sulfate)

In SDS (sodium dodecyl sulfate) the head is the hydrophilic sulfate group ($-\text{OSO}_3^-$), which is negatively charged and water-attracting while the tail is the long hydrophobic 12-carbon alkyl chain (dodecyl group), which is water-repelling.

Cholesterol

In cholesterol the head is the small polar hydroxyl (-OH) group and the tail is the nonpolar hydrocarbon isoctyl side chain at the opposite end.

In general, the hydrophilic head might either be positively or negatively charged, zwitterionic (with both charges but overall neutral) or uncharged.

The hydrocarbon chains are insoluble in water. The molecules are thus preferentially located at the surface, which allows the hydrophilic head to be surrounded by water and the hydrophobic chains to avoid contact with water. There is always an equilibrium between surfactants at the surface and in the bulk of the solution. The coverage of the surface leads to a reduction of the surface tension with increasing surfactant concentration.

18.2 Self-assembled structures

Self-assembly is a fundamental property of surfactant molecules in solution. It is also a highlight feature of soft-matter systems: under the influence of thermal fluctuations (typically mediated by a solvent), the constituents of soft matter systems self-organise into more complex, meso or macroscopic structures. This is typically due to driving thermodynamic forces that make initially uniform systems find (local or global) minima of their free energy which distinctive structural features. In this sense, soft matter systems explore **free energy landscapes** whose complexity is tuned by the strength of thermal fluctuations.

In many ways, we have already seen various forms of self assembly: crystallisation of colloids is itself self-organised but so is also the phase transition between the gasous and the liquid phase, or the isotropic-nematic transition in liquid crystals.

Full phase separation, though, is much more demanding than self assembly: in full phase separation we eventually attain the (global) free energy minimum corresponding to the equilibrium

state prescribed by the chosen thermodynamic variables (e.g. temperature and pressure). The notion of self assembly emphasises instead the propensity of the constituents to aggregate, to form structures at intermediate scales, structures which can often be only very **locally stable**, and whose existence may rely not only on the structure of the energy landscape but also on the **kinetics** of the constituents, such as their diffusion mechanism.

In the case of surfactants, we need to consider that these molecules are often very small—typically just a few nanometers in length. This small size means that thermal fluctuations play a significant role in their behavior, and their assembly is rapid due to their fast diffusion. For example, for an approximately spherical surfactant of size R in a viscous medium its diffusivity is given by the Stokes-Einstein relation (see)

$$D = \frac{k_B T}{6\pi\eta R}$$

where D is the diffusion coefficient, k_B is Boltzmann's constant, T is temperature, η is the viscosity of the solvent, and R is the radius of the particle. Compared to a colloidal particle of 20nm, a single SDS surfactant molecule of approximately 2nm in size will be approximately 1000 times faster.

This leads to fast local equilibration and constant exchange between monomers and aggregates. As a result, the structures formed by surfactants are not static but exist in a dynamic equilibrium, with lifetimes and sizes that depend sensitively on temperature, concentration, and solvent conditions.

Due to their amphiphilic nature, surfactants spontaneously organise into ordered structures without external guidance, but driven by forces such as hydrophobicity, described above.

As a result, surfactants minimize the system's free energy by forming a variety of aggregates such as **micelles**, **vesicles**, or bilayers. The specific structure formed depends on the molecular geometry of the surfactant and the solution conditions. Self-assembly is in many cases reversible and fundamentally dynamic process, with aggregates constantly forming and dissociating in equilibrium with monomers in solution.

18.2.1 Aggregation: general case

Suppose we have a system where solvent particles are dispersed in a solvent and tend to aggregate due to their mutual interactions. Suppose that we know the quantity ϵ_N representing the free energy change when a specific particle is taken from the bulk and added to an aggregate of size N .

Call μ_1 the chemical potential of isolated particles and aggregates of size N respectively. In equilibrium, they must be equal, with value μ .

Let's focus on an aggregate of size N . We can express μ in terms of

- the interaction energy from being in the aggregate (ϵ_N)
- the (translational) entropy of the aggregate as a whole ($\propto \text{numberofaggregates} \times \ln \text{numberofaggregates}$)

Assume an overall volume fraction of surfactants ϕ . Call the volume fraction of surfactants in an aggregate with N molecules X_N , so that $\sum_N X_N = \phi$. The numbers of aggregates of size N is then simply X_N/N . This means that we can write the uniform chemical potential as

$$\mu = \epsilon_N + \frac{k_B T}{N} \ln \frac{X_N}{N}$$

we can rewrite this as

$$X_N = N \exp \left(\frac{N(\mu - \epsilon_N)}{k_B T} \right)$$

we can eliminate μ by evaluating the expression for $N = 1$ and plugging it back to get

$$X_N = N X_1^N \exp \left(\frac{N(\epsilon_1 - \epsilon_N)}{k_B T} \right)$$

Obviously, the equation show that one has a large fraction of the solutes in an aggregated state only if there is a free energy advantage at forming aggregates, i.e. $\epsilon_1 > \epsilon_N$.

This means that knowing the form of ϵ_N allows us to predict the aggregation behaviour. For example, imagine we have an aggregate with N particles of total radius $r \approx (Nv)^{1/3}$ where v is the volume of a single particle. Then ϵ_N is the free energy per particle of the aggregate of size N , $G_N = \text{bulk free energy} + \text{surface free energy}$. Assuming a surface tension γ we can then write

$$\epsilon_N = \frac{G_N}{N} = \epsilon_\infty + \frac{1}{N} \gamma r^2 = \epsilon_\infty + \gamma \left(\frac{v^2}{N} \right)^{1/3}$$

which is a **monotonically decreasing** function of N . By defininit $\alpha k_B T = \gamma v^{2/3}$ we can extract a relation between X_N and X_1 parametrised solely by α , i.e.

$$\text{number of aggregates of size } N \text{ per unit volume} = \frac{X_N}{N} \sim (X_1 e^\alpha)^N$$

This should be read as follows: if we have very few isolated particles at a certain thermodynamic condition, then $X_1 e^\alpha < 1$ and the exponential factor $(X_1 e^\alpha)^N$ becomes vanishingly small for large N , leaving us with very few large aggregates. On the contrary, as X_1 approaches $e^{-\alpha}$ from below, we reach the critical point where $X_1 e^\alpha = 1$, and aggregates of all sizes become equally probable. Since ϵ_N is rapidly decreasing in N , this means that above a critical value of overall packing fraction ϕ , the system cannot remain in a homogeneous state. Instead, it undergoes phase separation into a dilute phase of isolated monomers (with X_1 pinned at $e^{-\alpha}$) in coexistence with a dense phase consisting of one or very few aggregates of very large (effectively infinite) size.

The volume fraction ϕ at which this occurs is called **critical aggregation concentration**, or CAC.

18.2.2 Aggregation: the surfactant case

For amphiphilic molecules like surfactants, the free energy change ϵ_N associated with adding a molecule to an aggregate is not a monotonically decreasing function of N . Instead, ϵ_N typically exhibits a minimum at a characteristic aggregation number N^* . This reflects the fact that aggregates (such as micelles) of a particular size are thermodynamically favored: too-small aggregates cannot sufficiently shield the hydrophobic tails from the solvent, while too-large aggregates become energetically unfavorable due to packing constraints or headgroup repulsion. See Jones (2002) for a expanded discussion of this.

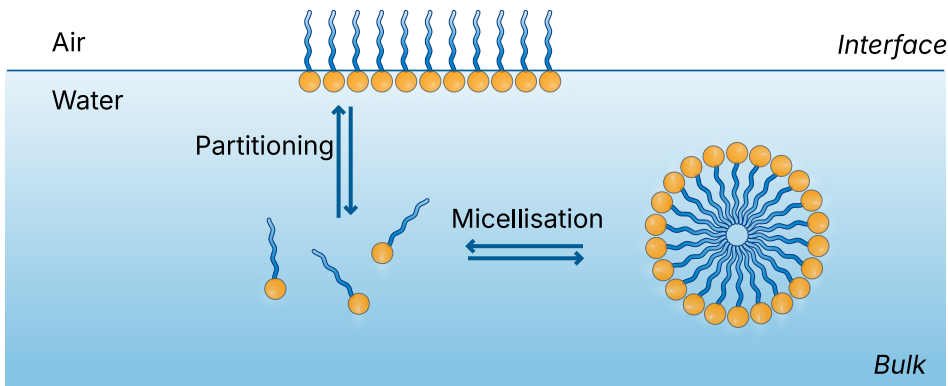


Figure 18.2: Surfactants in solution: normally, this is done in water in the presence of an interface with air. Due to their nature as amphiphiles, the surfactants typically sit at the air-water interface in a dynamical, equilibrium process that exchanges monomers between the bulk and the surface. The bulk surfactants, when the concentration is larger than a critical value, also self-assemble into micellar structures, which are at equilibrium with the isolated single surfactants.

Mathematically, this means that the distribution X_N of aggregates as a function of N is sharply peaked around N^* , leading to a well-defined aggregate size in solution. The equilibrium is then characterized by a coexistence of monomers and aggregates of size N^* , with very few intermediate-sized clusters. This is in contrast to the general case discussed above, where the aggregate size distribution can be broad or even diverge near a phase separation threshold.

This behavior underlies the concept of the **critical micelle concentration (CMC)**: below the CMC, almost all surfactant molecules are present as monomers; above the CMC, additional surfactant molecules predominantly form micelles of size N^* , while the monomer concentration remains nearly constant.

Above the critical micellar concentration surfactants self-assemble in solution spontaneously into larger structures. (In the following we will consider aqueous solutions, although the arguments also apply to other polar or non-polar (organic) solvents.) This allows the hydrophobic parts to crowd together while being ‘shielded’ by the hydrophilic heads. The density of the hydrophobic cores is very similar to the density of fluid hydro-carbons and the random arrangements of the chains resemble closely a fluid structure.

The surfactant assemblies are not held together by chemical bonds, but only by weak interactions ($\lesssim kT$). Their existence and properties are thus determined by a delicate balance between different effects, such as the transfer of hydrophobic chains into the core, interactions between the head group and the entropy of mixing. Small changes in control parameters, for example temperature, salt concentration or pH, thus have large effects on the characteristics of the surfactant aggregates. Nevertheless, for given conditions, they have very well-defined properties (shape, size etc.).

18.2.3 Shape of surfactant assemblies

Surfactants spontaneously self-assemble into a variety of different structures. We use packing considerations to understand and predict the shape of surfactant aggregates, leveraging what

we have learned on colloids, polymers and liquid crystals.

We construct a geometric model where a surfactant molecule is described using the following parameters:

- **optimal headgroup area a_0** : As discussed in the previous section, this depends on a delicate balance of forces and is thus not only controlled by the chemistry of the surfactant molecule, but also depends on different control parameters of the solution, such as salt concentration, pH or temperature. **-volume v of the hydrophobic part**: The hydrophobic part usually consists of hydrocarbon chains and for saturated hydrocarbons the volume v can be approximated by $v \approx (27.4 + 26.9n) \times 10^{-3} \text{ nm}^3$ where n is the number of carbon atoms.
- **critical chain length l_c** : The maximum effective length of the hydrophobic chains is called the critical chain length l_c , which has to be shorter than the fully extended molecular length of the chain l_{\max} . For saturated hydrocarbons the critical length can be estimated using $l_c \leq l_{\max} \approx (0.154 + 0.1265n)\text{nm}$. The critical chain length heavily depends on the detailed chemical structure of the molecule, for example on the presence of double bonds or branching, as well as the temperature.

The structure which will be adopted is determined by a balance between entropy, which favours small aggregates, and energy considerations: A certain shape or size might only be possible by imposing a headgroup area $a > a_0$, which is energetically not favourable. We will now establish the criteria for the different shapes.

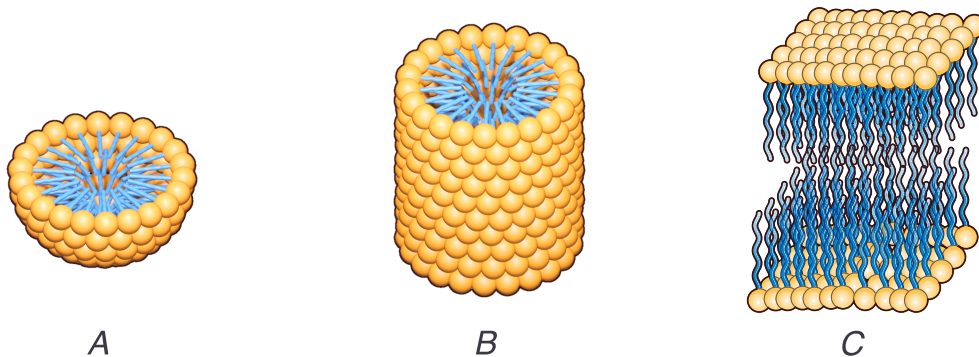


Figure 18.3: Different types of self assembled structures: (A) spherical micelles, (B) cylindrical micelles and (C) bilayers.

A. Spherical micelle

For a spherical micelle with aggregation number N , the total volume and surface area are given by

$$\begin{aligned} Nv &= \frac{4\pi}{3}R^3 \\ Na_0 &= 4\pi R^2 \\ \therefore \frac{v}{a_0} &= \frac{R}{3} < \frac{l_c}{3} \end{aligned}$$

where we used the fact that the radius R cannot be larger than the critical chain length l_c . We thus obtain for the critical packing parameter P

$$P = \frac{v}{a_0 l_c} < \frac{1}{3}$$

B. Cylindrical micelles

For a cylindrical micelle the total volume and surface area are given by $Nv = \pi R^2 L Na_0 = 2\pi RL \therefore \frac{v}{a_0} = \frac{R}{2} < \frac{l_c}{2}$ again using $R < l_c$.

We thus obtain for the critical packing parameter $P \frac{1}{3} < \frac{v}{a_0 l_c} < \frac{1}{2}$

Below the lower limit spherical micelles are formed.

C. Bilayers

For a bilayer the total volume and surface area are given by

$$\begin{aligned} Nv &= AD \\ Na_0 &= 2A \\ \frac{v}{a_0} &= \frac{D}{2} < l_c \quad (\text{using } D < 2l_c) \end{aligned}$$

We thus obtain for the critical packing parameter $P \frac{1}{2} < \frac{v}{a_0 l_c} < 1$ Below the lower limit cylindrical micelles are formed.

18.3 A simple on-lattice model for micelle formation

Aggregation of surfactants has been studied in various ways, including numerical simulations. One can employ extremely realistic, all-atom molecular dynamics to glean the microscopic details or construct more coarse-grained, statistical mechanics models using for example on lattice interactions.

Here below you can find a Javascript implementation of a lattice-gas-like model where surfactants are represented by chains of 3 sites on a lattice, with one site for the solvophilic head and two for the solvophobic tail. Each lattice site is occupied by either an amphiphile segment or a solvent molecule.

There are only nearest-neighbor interactions and the hamiltonian is simply

$$H = n_{HH}E_{HH} + n_{TS}E_{TS} + n_{HS}E_{HS} + \sum_i E_c$$

where n_{HH} , n_{TS} and n_{HS} are the total number of head-head, tail-solvent and head-solvent bonds, E_{HH} , E_{TS} and E_{HS} are the head-head, tail-solvent and head-solvent interaction energies and E_c is the energy associated with the conformation of the i th molecule. The model has been discussed in detail in Care (1987).

The model is simplified by setting the head-head interaction to zero, the tail-solvent interaction hydrophobic $E_{TS} > 0$, the head-solvent hydrophilic $E_{HS} < 0$ and the chain completely flexible, $E_c^i = 0$.

```

///| echo: false
viewof temperature = Inputs.range([0.01, 2], {step: 0.05, label: "Temperature (kT)", value: 0.5})

///| echo: false
viewof numChains = Inputs.range([3, 300], {step: 10, label: "Number of Chains", value: 100})

///| code-fold: true
// This is ObservableJS code
// You can run at observablehq.com or convert it to an equivalent (and faster?) Python version if you like
viewof simulation = {
    // --- Parameters ---
    const width = 40, height = 40;
    const chainLength = 3;
    const chainsToCreate = numChains;
    const T = temperature;
    // const numChains = 10;
    const E_TS = 1.0;      // tail-solvent energy (solvophobic)
    const E_HS = -1.5;     // head-solvent energy (solvophilic)
    // const T = 0.1;        // temperature (kT units)

    // --- Initialize grid and chains ---
    let grid = Array.from({length: width}, () => Array(height).fill(null));
    let chains = [];

    // Periodic boundary helper
    function mod(n, m) { return ((n % m) + m) % m; }

    function getNeighbors(x, y) {
        return [
            {x: mod(x - 1, width), y: y},
            {x: mod(x + 1, width), y: y},
            {x: x, y: mod(y - 1, height)},
            {x: x, y: mod(y + 1, height)}
        ];
    }

    function placeChains() {
        for (let id = 0; id < numChains; id++) {
            for (let tries = 0; tries < 100; tries++) {
                let x = Math.floor(Math.random() * width);
                let y = Math.floor(Math.random() * height);
                if (grid[x][y]) continue;

                let chain = [{x, y, type: 'head'}];
                grid[x][y] = {id, type: 'head'};
                let ok = true;

                for (let i = 1; i < chainLength; i++) {
                    let last = chain[chain.length - 1];
                    let nbs = getNeighbors(last.x, last.y).filter(p => !grid[p.x][p.y]);
                    if (nbs.length === 0) { ok = false; break; }
                    let next = nbs[Math.floor(Math.random() * nbs.length)];
                    chain.push({...next, type: 'tail'});
                }
            }
        }
    }
}

```

```

        grid[next.x][next.y] = {id, type: 'tail'};
    }

    if (ok) { chains.push({id, segments: chain}); break; }
    else { chain.forEach(p => grid[p.x][p.y] = null); }
}
}

function energy(seg) {
    let solventNbs = getNeighbors(seg.x, seg.y).filter(p => !grid[p.x][p.y]).length;
    return seg.type === 'head' ? solventNbs * E_HS : solventNbs * E_TS;
}

function attemptMove(chain) {
    const forward = Math.random() < 0.5;
    const tail = forward ? chain.segments[0] : chain.segments.at(-1);
    const head = forward ? chain.segments.at(-1) : chain.segments[0];
    const options = getNeighbors(head.x, head.y).filter(p => !grid[p.x][p.y]);

    if (options.length === 0) return;
    const next = options[Math.floor(Math.random() * options.length)];

    const dE_old = energy(tail);
    grid[tail.x][tail.y] = null;
    const dE_new = energy({...next, type: tail.type});
    grid[tail.x][tail.y] = {id: chain.id, type: tail.type};

    const deltaU = dE_new - dE_old;
    const accept = deltaU < 0 || Math.random() < Math.exp(-deltaU / T);

    if (accept) {
        grid[tail.x][tail.y] = null;
        grid[next.x][next.y] = {id: chain.id, type: tail.type};
        if (forward) {
            chain.segments.shift();
            chain.segments.push({...next, type: tail.type});
        } else {
            chain.segments.pop();
            chain.segments.unshift({...next, type: tail.type});
        }
    }
}

// --- Visualization ---
const svg = d3.create("svg")
    .attr("viewBox", `0 0 ${width} ${height}`)
    .style("width", "400px")
    .style("height", "400px")
    .style("border", "1px solid #ccc");

const g = svg.append("g");

```

```

function draw() {
  const data = chains.flatMap(c => c.segments);
  g.selectAll("circle")
    .data(data, d => `${d.x}-${d.y}`)
    .join("circle")
    .attr("cx", d => d.x + 0.5)
    .attr("cy", d => d.y + 0.5)
    .attr("r", 0.45)
    .attr("fill", d => d.type === "head" ? "blue" : "red");
}

// --- Main Loop ---
placeChains();
draw();

let running = true;
const button = html`<button> Pause</button>`;
button.onclick = () => {
  running = !running;
  button.textContent = running ? " Pause" : " Resume";
};

(async () => {
  while (true) {
    if (running) {
      for (let i = 0; i < chains.length; i++) {
        const c = chains[Math.floor(Math.random() * chains.length)];
        attemptMove(c);
      }
      draw();
    }
    await new Promise(r => setTimeout(r, 50));
  }
})();

return html`<div>${button}<br>${svg.node()}</div>`;
}

```

References

Chapter 19

Arrested states

In these chapters we have been considering systems implicitly (or explicitly) in thermal equilibrium with a surrounding environment. This is typically some kind of dispersion medium (a solvent). But we also been more demanding: we have required that the dispersed phase (the colloids, the polymers the anisotropic particles of liquid crystals) have explored exhaustively their free energy options and that they are truly in some macrostate corresponding to a global, stable thermal equilibrium state.

Equilibrium signifies time reversibility.

Many fluids, whether simple liquids like argon or complex liquids such as colloids and polymers, can be **rapidly cooled** (quenched) to temperatures well below their equilibrium freezing point without crystallization occurring on experimental timescales. In thermodynamic terms this is interpreted as a failure of the system to reach its true equilibrium (minimum free energy) state, namely the ordered crystalline phase. At these low temperatures, the dynamics slows down and the large scale structures remain disordered as the parent fluids. This slow dynamics is however characterised by a continuous drift away from equilibrium, with all of the characteristics of the systems (slowly) evolving during time as the system **ages**.

These **relaxation dynamics** are examples of **nonequilibrium processes**: the system spontaneously relaxes under the competing constraints of its kinetic rules (typically, diffusion mechanisms) and from the shape of its free energy profile.

In this chapter we are going to consider two paradigmatic cases of such nonequilibrium dynamics

- **glasses**, where the system falls out of equilibrium due to a dramatic slowing down of dynamics as temperature decreases or density increases, leading to a rigid but disordered structure.
- **physical gels**, where the system forms a disordered, arrested state due to the formation of a percolating network of reversible bonds (e.g., hydrogen bonds or van der Waals interactions) between particles.

At equilibrium, the entropy change ΔS of a system between two times t_1, t_2 or equivalently the entropy production $\frac{dS}{dt}$ are zero. Hence the transformation between t_1 and t_2 has to be reversible.

What is distinctive of both gels and glasses is that they are both examples of amorphous materials that behave like solids: they lack long-range atomic order yet resist deformation like crystalline solids. Indeed one can calculate properties that are distinctive of solids for both gels and glasses, including:

- **Elastic moduli** (such as the shear modulus G and bulk modulus K): Both gels and glasses exhibit a finite shear modulus, meaning they can sustain a static shear stress without flowing, unlike liquids.

- **Yield stress:** They can support a certain amount of stress before yielding or flowing, a property absent in equilibrium fluids.
- **Vibrational density of states:** Amorphous solids display a characteristic “boson peak” in their vibrational spectrum, distinct from the phonon modes of crystals.

These features highlight that rigidity and solidity do not require crystalline order; amorphous materials like gels and glasses can be mechanically solid while remaining structurally disordered. Indeed, the border between solidity and fluidity has been questioned in recent research work, emphasizing how this depends on observational timescales and the notion of metastability, see Sausset, Biroli, and Kurchan (2010).

19.1 Energy landscapes

The **free energy landscape** is a conceptual framework used to describe the multitude of possible configurations (microstates) of a system and their associated free energies. Each point in this high-dimensional landscape corresponds to a particular arrangement of all the particles in the system, and the height at that point represents the free energy of that configuration. In particular, the landscapes is characterised by the presence of free energy **minima** (valleys) which correspond to stable or metastable states—configurations where the system tends to reside and local maxima (barrier) between the valleys, representing the so-called **transition states**.

Various minima can be clustered together when their energies are relatively close, i.e. when the barriers that separate them are of the order of the energy from thermal fluctuations $k_B T$. These clusters of minima are known as **(meta)-basins** and are very important for amorphous systems: the same system at the same temperature can display similar macroscopic characteristic not because these reflect the properties of one particular minimum, but because they are the result of local averaging within a given metabasin.

In the context of supercooled liquids and glasses, the landscape is rugged, with many local minima separated by high barriers. At high temperatures, the system can easily hop between minima (exploring many configurations), but as the temperature decreases, it becomes trapped in deeper minima, leading to slow dynamics and eventual dynamical arrest (glass formation).

Similarly, in the case of gels, the free energy landscape is also rugged, but the system becomes arrested due to the formation of a percolating network of reversible bonds. Instead of being trapped in deep minima solely by energetic barriers (as in glasses), the system’s dynamics are constrained by the connectivity of the network. The system can only relax if enough bonds break and reform to allow large-scale rearrangements, which becomes increasingly unlikely as the network spans the system. Thus, the arrested state in gels is associated with the system being confined within a region of the landscape corresponding to networked, mechanically stable configurations, separated from other regions by high barriers related to breaking the network connectivity.

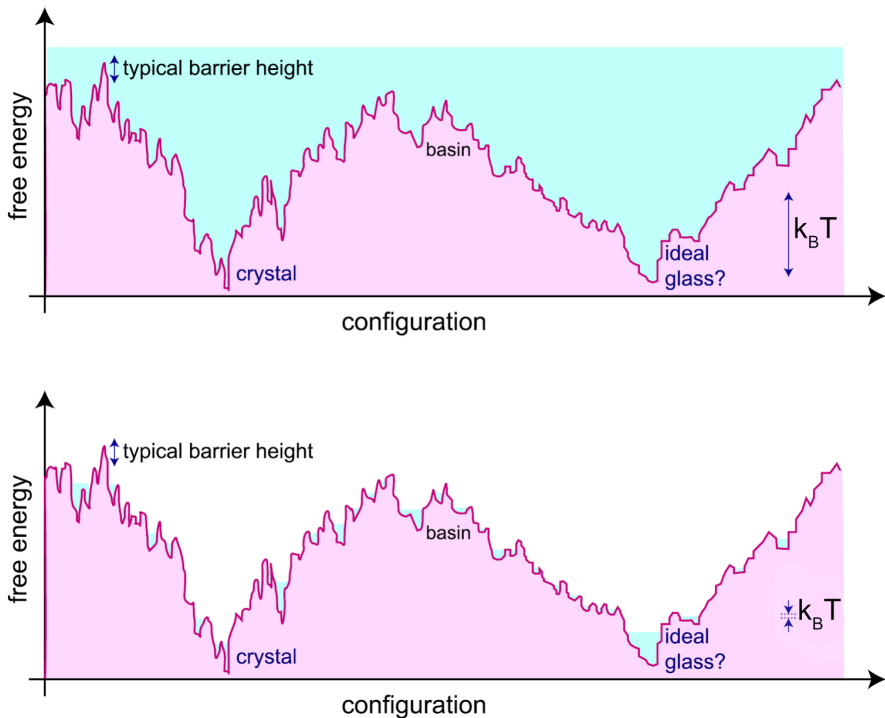


Figure 19.1: The free energy landscape for supercooled liquids, adapted from Royall et al. (2018).

The free energy landscape is helpful as it suggests ways to enumerate distinct conformations of a disordered system: the various metabasins can be in principle enumerated. Their number N_{minima} allows us to define a **configurational entropy**:

$$S_{\text{conf}} = k_B \ln N_{\text{minima}}$$

How is this different from the total entropy? In principle, the total entropy S can be obtained from thermodynamic relations, for example as an integral over the pressure:

$$S(T) = S(T_0) + \int_{T_0}^T \frac{1}{T'} \left(\frac{\partial P}{\partial T'} \right)_V dV$$

or, more commonly for liquids and glasses at constant volume,

$$S(T) = S(T_0) + \int_{T_0}^T \frac{C_V(T')}{T'} dT'$$

where C_V is the heat capacity at constant volume and T_0 is a reference temperature. For a fluid like a gas, only the total entropy is well defined. Even for a liquid at high temperature this is the case, because there are no meaningful metabasins in the free energy profile.

It is only as we decrease the temperature further that the metabasins can be defined (via *coarse-graining*). These reference conformations can be used to split the total entropy into two contributions

$$S = S_{\text{conf}} + S_{\text{vib}}$$

where S_{vib} is the vibrational entropy around the reference conformations, and is mainly due to thermal fluctuations. In this sense, we are describing the thermodynamics of a disordered system in a way closer to what we would do for a crystal, where the reference conformations are provided by the crystalline packings (e.g. FCC, HCP, BCC etc.).

19.2 Glasses

19.2.1 Glass formation

How are glasses formed? The figure below illustrates the standard route. First of all, one selects systems for which crystal formation (via nucleation and growth) is **hindered** (or in other words, **frustrated**): this can be because of the overall composition (silicate glasses, i.e. e window glasses, have many components) or because of competing interactions (binary mixtures may have interactions between the A and B components that favour mixing without crystallisation).

Then, for a chosen composition, one cools down the liquid across the temperature where in principle (if given enough time) the system would crystallise (dubbed T_m). The liquid becomes a so-called **supercooled liquid** which is a state of local equilibrium that has access to many disordered basins, but not the crystalline one (see energy landscape picture above).

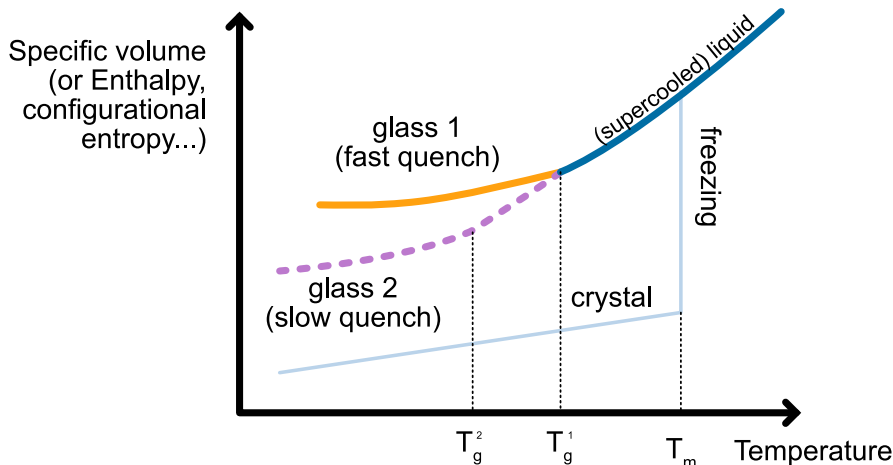


Figure 19.2: Standard picture of glass formation: a (local) equilibrium state (the supercooled liquid) is cooled at a certain cooling rate R . The cooling rate is fast enough to avoid crystallization (freezing) at T_m . At the glass transition temperature T_g the structural relaxation time of the system exceeds the observation timescale and the system falls off equilibrium. The experimental glass transition temperature is not unique and depends on the protocol: fast cooling rate lead to higher glass transition temperatures.

As we keep on cooling the supercooled liquid to lower and lower temperature, the molecules or constituents move more and more slowly, so that the diffusivity is progressively reduced. This slowing down is typically characterized in terms of autocorrelation functions of the density.

A common way to quantify this is through the (self-part) **intermediate scattering function** $F_s(q, t)$, which measures how density fluctuations at a given wavevector q decay over time:

$$F_s^{\text{self}}(q, t) = \left\langle \frac{1}{N} \sum_{j=1}^N e^{i\mathbf{q} \cdot [\mathbf{r}_j(t) - \mathbf{r}_j(0)]} \right\rangle$$

At high temperatures, $F_s(q, t)$ decays rapidly, indicating fast relaxation. As temperature decreases, the decay becomes much slower, often exhibiting a two-step relaxation: a rapid initial drop (the “ β -relaxation”) followed by a long plateau and then a slow final decay (the “ α -relaxation”). The time at which $F_s(q, t)$ decays to a certain fraction (e.g., $1/e$) defines the **structural relaxation time** τ_α , which represents the typical time for a particle to move over a lengthscale $\sim 2\pi/q$.

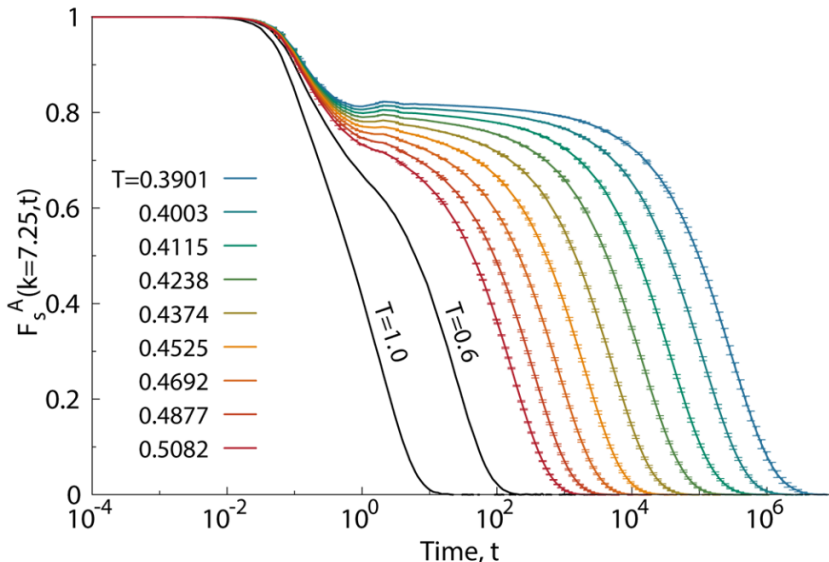


Figure 19.3: Intermediate scattering functions for molecular dynamics simulations of a standard glassformer (a coarse grained metallic binary mixture) for various reduced temperatures. From Coslovich, Ozawa, and Kob (2018). One can identify the initial relaxation (β) followed by a long plateau which is itself followed by the complete relaxation (α). Notice the logarithmic scale of the horizontal axis (in reduced time units).

As the supercooled liquid gets colder and colder, the relaxation time increases rapidly, eventually of many orders of magnitude. At some *experimentally determined* temperature the relaxation time is larger than the observation time, i.e.

$$\tau_\alpha > t_{\text{obs}}$$

This means that it is impossible to take time averages to estimate thermodynamic properties of the system, because the system does not satisfy any longer the minimal requirement of the ergodic hypothesis. This **failure of ergodicity** means that the system effectively falls **out of equilibrium**, because it does not explore all relevant microstates within the available time. The system has become a **glass**. The temperature at which this clearly non-ordinary (and non-thermodynamic!) transition occurs is called the **experimental glass transition temperature** T_g .

The intermediate scattering function $F_s(q, t)$ can be decomposed into two contributions:

- **Self part**
 $F_s^{\text{self}}(q, t)$: Measures the correlation of each particle with its own initial position. It captures single-particle dynamics (how far a particle moves from where it started).
- **Collective part**
 $F_s^{\text{coll}}(q, t)$: Measures correlations between different particles, reflecting how density fluctuations evolve collectively. The collective part is given by

$$F_s^{\text{coll}}(q, t) = \frac{1}{N} \left\langle \sum_{j,k=1}^N e^{i\mathbf{q} \cdot [\mathbf{r}_j(t) - \mathbf{r}_k(t)]} \right\rangle$$

In glassy systems, the self part is sensitive to particle mobility (e.g., caging and hopping), while the collective part describes how groups of particles rearrange together. Both are important for understanding relaxation and dynamical

A key feature of the glass transition is that there is no unique glass transition temperature T_g : the transition temperature itself depends on how fast we are cooling the liquid down. It is a **protocol dependent** property. We can understand this by referring back to the energy landscape: at high temperatures, the system has enough thermal energy to explore many minima in the landscape, hopping over barriers with ease. As the temperature decreases, the barriers become increasingly difficult to cross within the available observation time. If the cooling is slow, the system can equilibrate and find deeper minima, resulting in a lower T_g . If the cooling is fast, the system becomes trapped in higher-energy, shallower minima, and T_g is higher. Therefore, the glass transition is not a sharp thermodynamic phase transition, but a kinetic phenomenon determined by the interplay between the system's relaxation time and the timescale of the experimental protocol.

19.3 Viscosity and relaxation times

The structural relaxation time extracted from correlation functions such as the intermediate scattering function is proportional to a macroscopic property, the **viscosity**

$$\tau_\alpha \propto \eta$$

and hence the viscosity at the glass transition increases rapidly (diverges) like τ_α .

i Relationship between viscosity and structural relaxation time

The proportionality between viscosity η and the structural relaxation time τ_α can be understood using linear response theory and the Green-Kubo relations.

The viscosity is given by the Green-Kubo formula as an integral of the stress autocorrelation function:

$$\eta = \frac{1}{k_B T V} \int_0^\infty \langle \sigma_{xy}(0) \sigma_{xy}(t) \rangle dt$$

where σ_{xy} is the off-diagonal component of the stress tensor.

In supercooled liquids and glasses, the decay of the stress autocorrelation function is governed by the same slow structural relaxation processes that control τ_α . Thus, the integral is dominated by timescales of order τ_α , leading to:

$$\eta \sim G_\infty \tau_\alpha$$

where G_∞ is the instantaneous (high-frequency) shear modulus.

This proportionality holds in the regime where the relaxation is dominated by structural rearrangements (i.e., near the glass transition), and is supported by both experiments and simulations. Therefore, the dramatic increase in viscosity as the glass transition is approached directly reflects the growth of the structural relaxation time.

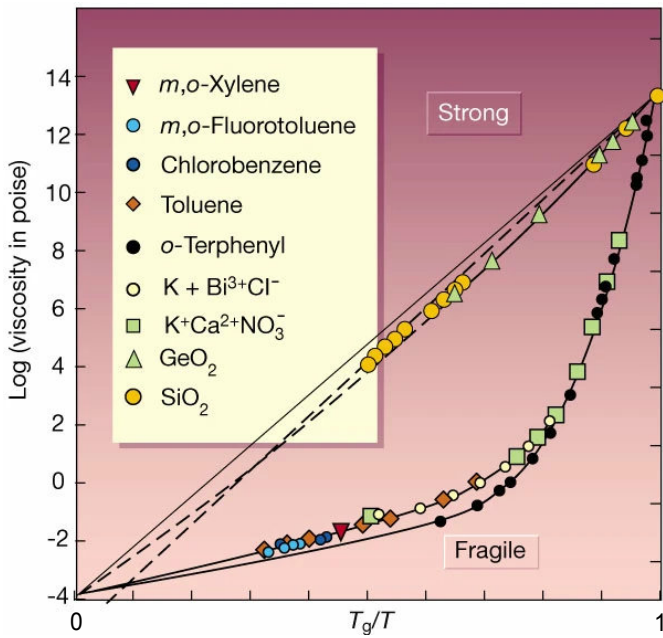


Figure 19.4: Viscosity as a function of the inverse temperature scaled by the experimental glass transition temperature (Angell plot). One observes an increase of several orders of magnitude between the high temperature and the low temperature regime. Also one can distinguish different classes of glassformers, conventionally termed as *strong* and *fragile*. Adapted from Debenedetti and Stillinger (2001).

This dramatic increase in relaxation time is a hallmark of glassy dynamics and underlies the kinetic arrest observed in glasses.

Presently, we do not have a single unified theory of the glass transition: there is no universal law capable to predict the viscosity (or the relaxation times) of glassy systems from specific microscopic parameters. To date, the origin of the glass transition remains one of the [major unsolved problems condensed matter physics](#).

First steps are typically phenomenological: glasses are classified as **strong** or **fragile** based on how their viscosity (or relaxation time) increases as temperature decreases toward the glass transition temperature T_g . We have seen earlier in Section 10.2 that activated process are often governed by what are called Arrhenius laws, with a rate $R \propto \exp[-\Delta E/k_B T]$ where ΔE is an energy barrier. Viscosity curves can be fitted by empirical models inspired the activated picture:

- **Strong glasses** (e.g., silica, SiO₂) follow an Arrhenius law :

$$\eta(T) = \eta_0 \exp\left(\frac{E_A}{k_B T}\right)$$

where E_A is an activation energy. The plot of $\log \eta$ vs $1/T$ is a straight line.

- **Fragile glasses** (e.g., o-terphenyl, many polymers) show super-Arrhenius behavior, often described by the Vogel-Fulcher-Tamman (VFT) equation:

$$\eta(T) = \eta_0 \exp\left(\frac{B}{T - T_0}\right)$$

where B and T_0 are empirical parameters. The plot of $\log \eta$ vs $1/T$ is highly curved.

The distinction is visualized in the so-called **Angell plot**, where strong glasses show nearly linear behavior, while fragile glasses show a dramatic upturn as $T \rightarrow T_g$.

These models are suggestive of a **thermodynamic** origin of the glass transition. Indeed, it is possible to think to think of the emerging barrier E_A and B as the result of some free energy expression from the sampling of the energy landscapes in various basins.

19.3.1 Connection between VFT and configurational entropy: the Adam-Gibbs model

A key theoretical link between the dramatic slowdown of dynamics (as described by the VFT law) and the underlying thermodynamics is provided by the **Adam-Gibbs model**, details in Bouchaud and Biroli (2004).

This model proposes that the structural relaxation time τ_α is controlled by the **configurational entropy** S_{conf} , which counts the number of distinct amorphous basins available to the system.

The Adam-Gibbs relation reads:

$$\tau_\alpha(T) = \tau_0 \exp\left(\frac{A}{TS_{\text{conf}}(T)}\right)$$

where A is a constant. As temperature decreases, S_{conf} drops, leading to a rapid increase in τ_α . If S_{conf} vanishes at a finite temperature T_K (the so-called Kauzmann temperature), the relaxation time diverges, reproducing the VFT form:

$$\tau_\alpha(T) \sim \exp\left(\frac{B}{T - T_0}\right)$$

with $T_0 \approx T_K$. Thus, the Adam-Gibbs model provides a thermodynamic interpretation of the VFT law, connecting the kinetic slowdown to the loss of configurational entropy as the glass transition is approached.

19.3.2 Alternative perspective: Dynamical facilitation and the parabolic law

While thermodynamic models like Adam-Gibbs relate the glass transition to configurational entropy, a radical alternative approach is the **dynamical facilitation theory**, see Chandler and Garrahan (2010) for more details. This framework emphasizes that glassy slowdown arises from the dynamics themselves, rather than underlying thermodynamic changes.

In dynamical facilitation, mobility is sparse at low temperatures: regions of the system can only relax if they are adjacent to already mobile regions—mobility “facilitates” further mobility. This leads to hierarchical, cooperative dynamics without invoking a thermodynamic singularity.

A schematic illustration:

- At high T , mobile regions are abundant and relaxation is fast.
- As T decreases, mobile regions become rare, and relaxation requires the creation and propagation of mobility, which is a rare event.
- The relaxation time grows rapidly due to the need for cooperative rearrangements.

This scenario predicts a **parabolic law** for the relaxation time:

$$\log \tau_\alpha(T) \sim J^2 \left(\frac{1}{T} - \frac{1}{T_0}\right)^2$$

where J is an energy scale and T_0 is an onset temperature. Unlike the VFT law, the parabolic law does not diverge at finite T but still captures the super-Arrhenius growth of relaxation times.

Interestingly, both the two perspective fit the viscosity data well within their regimes of validity (and recent research suggests that close to the glass transition temperature the microscopic mechanisms resemble dynamical facilitation).

Here below is a visual representation of the time evolution of the magnitude of the displacement field in a model of glass governed by dynamical facilitation, see Hasyim and Mandadapu (2024) for more details.

[./figs/pnas.2322592121.sm04.mp4](#)

19.4 Physical gels

The word *gel* signifies many different things to different scientific communities. In the context of soft matter physics, a physical gel is typically understood as a system in which the constituent particles or polymers are connected via reversible, non-covalent bonds to form a percolating network that spans the entire sample. This network imparts solid-like mechanical properties to the material, even though the underlying structure remains disordered and fluid-like on a microscopic scale.

Physical gels differ from chemical gels, where the network is formed by irreversible covalent bonds. In physical gels, the bonds can break and reform dynamically, have an energy of order $1k_B T$, allowing the system to respond to external stresses and sometimes to self-heal. Examples include gelatin desserts, agarose gels, and certain colloidal suspensions where attractive interactions lead to network formation, see Zaccarelli (2007) for a comprehensive review.

The transition from a fluid to a gel state is often associated with the appearance of a system-spanning cluster, which can be described using concepts from **percolation theory**. The mechanical rigidity of the gel arises when this cluster forms, leading to a dramatic increase in viscosity and the emergence of an elastic response.

Percolation

Percolation is the study of an apparently innocent mathematical problem: take a square grid of $L \times L$ sites and randomly label N of them; how does the likelihood of forming a cluster that spans across the grid (i.e. *percolates*) depend on the probability $p = N/L^2$ of having a labelled square?

The problem is interesting for its various applications across domains of science as diverse as networks formation, transport, material science, epidemiology and ecology. It is amenable to an analytical treatment and can be solved via direct simulations. Percolation is a classic example of a phase transition and critical phenomena. The probability p_c at which a spanning cluster first appears is called the **percolation threshold**. For a large 2D square lattice, $p_c \approx 0.5927$. Below p_c , only small, disconnected clusters exist; above p_c , a giant connected component spans the system. The transition is **continuous**, i.e. second order.

Analytically, percolation is tractable and exhibits universal critical exponents near p_c , making it a cornerstone of statistical physics and network theory.

You can play with percolation on a squared lattice with the code below.

```

#| autorun: true
import numpy as np
import matplotlib.pyplot as plt
from scipy.ndimage import label

def sample_percolation(
    L = 50,  # grid size
    p = 0.2  # occupation probability
):
    # Generate random grid
    grid = np.random.rand(L, L) < p

    # Label clusters
    structure = np.array([[0,1,0],[1,1,1],[0,1,0]], dtype=int)
    labeled, num_features = label(grid, structure=structure)

    # Find largest cluster
    sizes = np.bincount(labeled.ravel())
    sizes[0] = 0  # background is label 0
    largest_label = sizes.argmax()

    # Mask for largest cluster
    mask = labeled == largest_label

    return grid, mask

# sample
p = 0.2
L = 120
grid, mask = sample_percolation(L,p)
# Plot
plt.figure(figsize=(6, 6))
# Show all clusters in gray
plt.imshow(grid, cmap='gray', interpolation='none')

plt.imshow(np.ma.masked_where(~mask, mask), cmap='autumn', alpha=0.8, interpolation='none')
plt.axis('off')
plt.title(f'Percolation in 2D (p={p})\nLargest cluster highlighted in red')
plt.show()

```

```
#| autorun: true

ps = np.linspace(0.1, 1.0, 50)
L = 500
largest_sizes = []
repeats = 3
for p in ps:
    grid, mask = sample_percolation(L, p)
    sizes = []
    for r in range(repeats):
        sizes.append(mask.sum() / (L * L)) # Fraction of sites in largest cluster
    largest_sizes.append(np.mean(sizes))

plt.figure(figsize=(7, 4))
plt.plot(ps, largest_sizes, marker='o')
plt.xlabel('Occupation probability $p$')
plt.ylabel('Fraction in largest cluster')
plt.title('Percolation transition in 2D')
plt.show()
```

The following table illustrates that various values of the critical percolation probability are known for various lattices, either exactly or via simulation. Notice that this non-universal feature, the critical p_c , decreases with increasing dimensionality: at higher dimensions, the connectivity is naturally higher and so a comparatively smaller fraction of the system is required in order to find a percolating path.

Lattice Type	Dimension	Coordination z	p_c^{site}	p_c^{bond}
Square	2	4	0.592746	0.5
Triangular	2	6	0.5	0.347296
Honeycomb	2	3	0.697043	0.652703
Kagome	2	4	0.6527	0.5244
Union Jack	2	8	0.379	0.429
Cubic	3	6	0.3116	0.2488
FCC	3	12	0.199	0.120
BCC	3	8	0.245	0.180
Diamond	3	4	0.43	0.389
Hypercubic (4D)	4	8	0.197	0.160
Hypercubic (5D)	5	10	0.141	0.118
Hypercubic (6D)	6	12	0.109	0.094
Hypercubic (7D)	7	14	0.091	0.079
Hypercubic (8D)	8	16	0.078	0.069

Instead, other properties of percolation are **universal**: these are the critical exponents of observables on the lattice, and do not depend on the lattice detail, such as the probability to find a site in a percolating cluster $P_\infty(p) \propto (p - p_c)^\beta$

Dimension d	β (Percolation)
2	5/36 ≈ 0.1389
3	≈ 0.41
4	≈ 0.65
5	≈ 0.81
6	≈ 0.96
≥6 (Mean-field)	1

In the case of physical gels, percolation is a required ingredient for mechanical stability: in the absence of a large spanning percolating network, it is not possible for the gel to sustain external stresses or even self-generated stresses such as its own weight under gravity.

19.4.1 Colloid-polymer mixtures as an example

A way to realise robust physical gels in experiments is to use colloid-polymer mixtures, which we have seen previously when we talked about depletion. When the colloids are significantly larger than the polymers, the resulting depletion interaction is attractive and very short ranged: it is a so-called **sticky** interaction, ideally suited to form robust physical bonds where the colloids cluster in a nonequilibrium, branched, dense phase.

The resulting phase diagrams differ significantly from the ones of simple liquids (e.g., Lennard-Jones interactions): the liquid-gas coexistence curve (the binodal) becomes metastable.

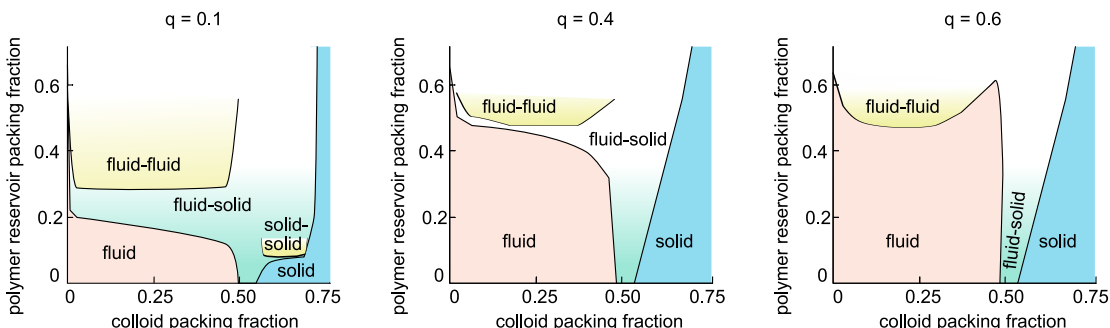


Figure 19.5: Phase diagrams of colloid-polymer mixtures for different values of the size ratio parameter $q = \sigma_{\text{polymer}}/\sigma_{\text{colloid}}$. Left: very small size ratio make the gas-liquid binodal (enclosing the yellow fluid-fluid region) metastable to gas-solid phase separation. Centre: as we increase the size ratio, the liquid pocket at high density starts developing. Right: for almost equal sizes the phase diagram is reminiscent of the one of simple fluids (e.g. Lennard-Jones) after noticing that the polymer reservoir packing fraction plays a role inverse to the temperature. Adapted from Dijkstra, Brader, and Evans (1999).)

Given the very short range of the interactions, models of colloid-polymer mixtures can approximate the Asakura-Oosawa potential (see Section 15.2.5) using even simpler pair-wise interactions. For example, for Monte-Carlo simulations and theoretical calculations one often uses the **square-well** model,

The square-well potential $U(r)$ is defined as:

$$U(r) = \begin{cases} \infty & r < \sigma \\ -\epsilon & \sigma \leq r < \lambda\sigma \\ 0 & r \geq \lambda\sigma \end{cases}$$

where σ is the particle diameter (hard core), ϵ is the well depth (attractive strength), and λ controls the range of the attraction.

For molecular dynamics one often employs the so-called **Morse potential**, which combines fast exponentially decaying tails and a repulsive core in a simple analytical form

$$U_{\text{Morse}}(r) = D [e^{-2\alpha(r-r_0)} - 2e^{-\alpha(r-r_0)}]$$

where D is the well depth, α controls the range (steepness) of the potential, and r_0 is the equilibrium bond distance.

Pair correlations

In many situation, pair-wise correlation functions are sufficient to capture gel formation. Both the radial distribution function and the structure factor are able to describe gel formation, but they focus (and are accurate) in different regimes:

The radial distribution function $g(r)$ has best statistics at short distances, capturing the features of the clusters that form the branched network.

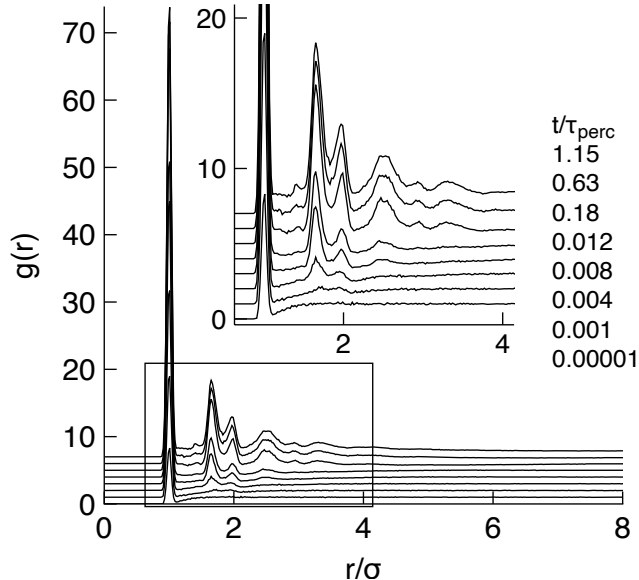


Figure 19.6: The changes in the radial distribution function $g(r)$ as time evolves and the frozen structure of a simulated colloidal gel emerges. The system is at an overall dilute concentration, so clusters appear as very sharp peaks at short distances, and their structure in terms of nearest and second-nearest neighbour shells are reflected in the first few peaks. From Griffiths, Turci, and Royall (2017)

In gels near the percolation threshold, the structure factor $S(q)$ exhibits **scale-free (power-law) behavior** at low q :

$$S(q) \sim q^{-D_f}$$

where D_f is the **fractal dimension** of the gel network. This power-law regime reflects the absence of a characteristic length scale in the structure—clusters are **self-similar** over a range of sizes.

- For q much smaller than the inverse cluster size, $S(q)$ flattens (finite-size effects).
- For intermediate q , $S(q) \sim q^{-D_f}$, indicating fractal geometry.
- For large q , $S(q)$ reflects local (non-fractal) structure.

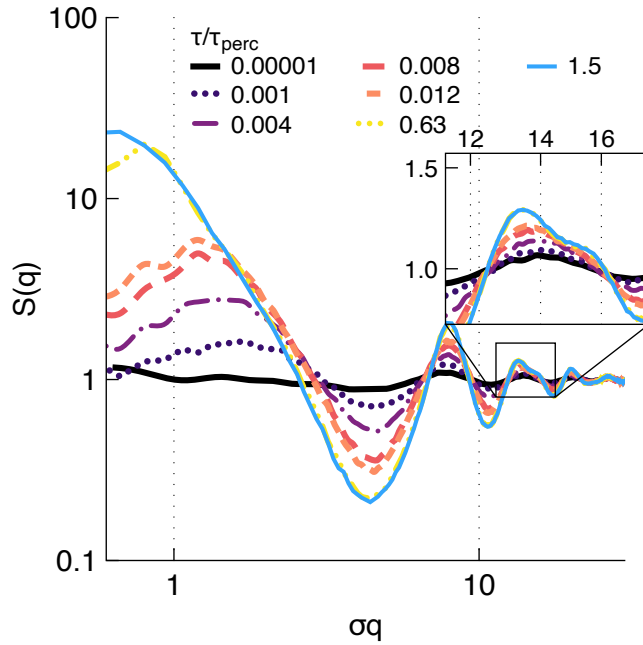


Figure 19.7: The same changes of the previous figures as seen in changes in the structure factor $S(q)$ as time evolves and the frozen structure of a colloidal gel emerges. At small q , a characteristic power law behaviour emerges, while at higher q the mistructure changes are subtly captured by the reorganisation or splitting of the peaks.

The exponent D_f is related to the spatial scaling of mass with size in the fractal cluster: $M(R) \sim R^{D_f}$. Typical values for percolation clusters in 3D are $D_f \approx 2.5$.

Thus, by analyzing the low- q behavior of $S(q)$, one can extract the fractal dimension and confirm scale-free, self-similar structure in gels.

i Measuring fractal dimensions: the box-counting algorithm

Fractal dimensions are in practice quite tricky to measure. A common method is the **box-counting algorithm**:

1. Overlay a grid of boxes of size ℓ over the structure (e.g., a cluster or network).
2. Count the number $N(\ell)$ of boxes that contain any part of the structure.
3. Repeat for different box sizes ℓ .
4. Plot $\log N(\ell)$ versus $\log(1/\ell)$. For a fractal, this plot is linear over some range,

and the slope gives the fractal dimension D_f :

$$N(\ell) \sim \ell^{-D_f}$$

This method is widely used for experimental images and simulation data to estimate the fractal dimension of clusters, aggregates, or networks.

Below, illustrate this using a known fractal, the [Sierpinski carpet](#), whose fractal dimensions is exactly $D_f = \log 8 / \log 3 \approx 1.8929$

<https://www.youtube.com/watch?v=QOa2qhDdywc>

19.4.2 Arrested spinodal scenario

But how do physical gels come about? A viable scenario is the so-called **arrested spinodal decomposition** scenario. Here, a system is rapidly quenched into a region of its phase diagram where it would normally phase separate into two distinct phases (e.g., a dense and a dilute phase) via spinodal decomposition. However, before the phase separation can complete, the dynamics of the dense regions slow down dramatically—often due to glassy or jamming behavior—leading to a dynamically arrested, bicontinuous structure.

This process is relevant for colloid-polymer mixtures, protein solutions, and some polymer blends. The resulting gels are characterized by a network-like structure that reflects the early stages of spinodal decomposition, “frozen in” by the arrest of particle motion.

For the arrested spinodal scenario to hold, the system evolves following these steps:

- The system is quenched inside the spinodal region, where spontaneous fluctuations grow.
- Domains of different densities form, but the dense domains become dynamically arrested before macroscopic phase separation completes.
- The final structure is a bicontinuous, percolating network with solid-like mechanical properties.

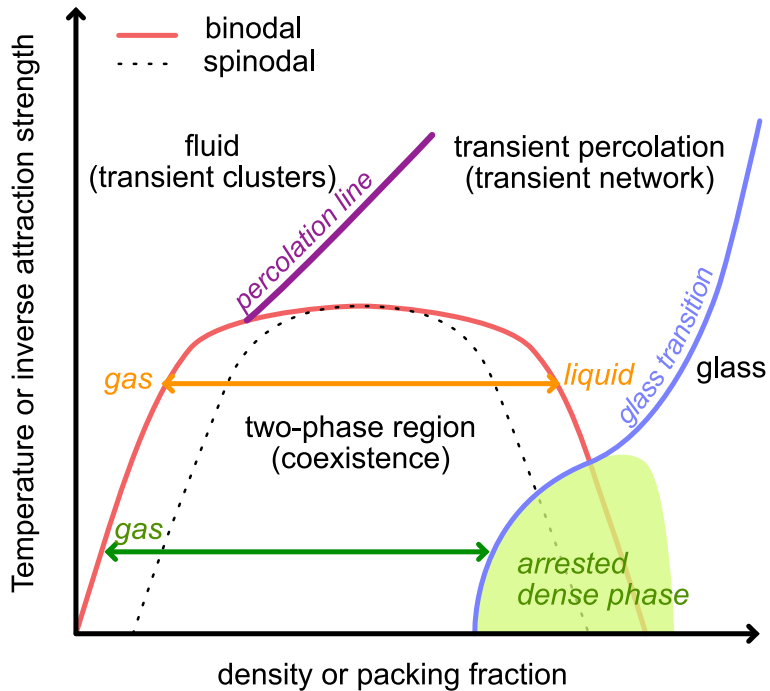


Figure 19.8: The arrested spinodal scenario mapped on the phase diagram of the dispersed particles (e.g. colloids), adapted from Zaccarelli (2007). We distinguish various lines: the liquid-gas coexistence (binodal) in red, the spinodal line (where phase separation is unstable) black dashed, the percolation line (across which a percolating cluster can be detected), the glass transition line (a dynamical line, where the relaxation time of the system exceeds a conventional threshold, e.g. 100 seconds). If a system is cooled rapidly down from the fluid to the coexistence region, two scenarios are possible: the fluid spontaneously phase separates into two equilibrium phases (liquid and gas, orange horizontal line); or, the cooling is so rapid that proper equilibrium phases cannot be formed and the system separates into a disordered arrested dense phase and a vapor phase (green horizontal line). This second scenario corresponds to physical gel formation via spinodal decomposition.

For more details, see Zaccarelli (2007).

Chapter 20

Active matter

20.1 Beyond thermal systems

All the systems we have considered up to now are composed of naturally occurring or synthetic molecules (or atoms) that far are composed of naturally occurring or synthetic molecules (or atoms) that so now are composed of naturally occurring or synthetic molecules (or atoms) that far are composed of naturally occurring or synthetic molecules (or atoms) that we have considered up to now are composed of naturally occurring or synthetic molecules (or atoms) which interact via conservative forces (potentials) and are subject to thermal fluctuations. Essentially, energy is either stored in the system as potential energy or exchanged with the environment as heat, leading to equilibrium dynamics governed by the laws of thermodynamics and statistical mechanics. In these systems, the random motion of particles arises from thermal noise, and the system eventually relaxes to a Boltzmann distribution.

However, many systems in nature and technology are driven out of equilibrium by continuous energy consumption at the microscopic scale. These are known as **active matter** systems. Here, each constituent (such as a bacterium, a synthetic microswimmer, or a molecular motor) converts energy from its surroundings into a variety of mechanisms:

- motion
- sensing
- processing
- growth and deformation

This is what is typically performed by many living organisms: by consuming energy **locally** (hence dissipating heat) they perform some function. Here we focus on of the most fundamental kinds of functions which is **motion**. A bacterium uses energy to propel itself into space, explore it and eventually interact with the environment, including other bacteria.

We could, at this stage, say that these interactions and the behaviour emerging from them are inherently *biological* and governed solely by mechanisms that transcend the physical correlations (behavioural science). As physicists, we do not negate the existence of such dimensions (especially when communication and sensing are involved) but aim to run a different research programme: we want to **gauge** the level of biological surprise¹, as nicely put by Andrea Cavagna, a complex system physicist.

To do so we need to understand how systems that dissipate energy locally to produce self-propelled motion can lead to the emergence of non-trivial phase behaviour and how this differs

¹Andrea Cavagna, a complex system physicist, describes “biological surprise” as the extent to which observed behaviour cannot be explained by physical interactions alone.

from systems that are either at thermal equilibrium (e.g. colloidal fluids) or are slowly relaxing towards it (e.g. glasses and gels).

The field of research that studies such systems is called physics of **active matter** and in this chapter we will describe some reference model systems and main results.

20.2 Life-inspired motion: *run and tumble*

The run-and-tumble model describes the motion of active particles, such as bacteria, that alternate between two types of movement: “runs” (straight-line motion) and “tumbles” (random reorientation). This model captures the behavior of microorganisms like *E. coli*.

<https://www.youtube.com/watch?v=b9P8uPkeKmc>

Figure 20.1: Swimming Escherichia coli bacteria with fluorescently-labeled flagellar filaments, showing individual run-and-tumble events with flagellar filaments unbundling, cells turning, and flagellar filaments rejoining the bundle. The details of the experimental procedure are given in Turner, Ryu, and Berg (2000).

```
//| code-fold: true
//| fig-cap: "Non-interacting run and tumble particles."
viewof simulation = {
    const n = 100, W = 1000, H = 300, dt = 0.5, v0 = 1.5;

    const tumbleSlider = Inputs.range([0.01, 1.0
    ], {step:0.01, value:0.1, label:"Tumble rate"});
    const button = html`<button>Pause</button>`;
    let running = true;
    button.onclick = () => {
        running = !running;
        button.textContent = running ? "Pause" : "Resume";
    };

    let state = Array.from({length: n}, () => ({
        x: Math.random() * W,
        y: Math.random() * H,
        theta: Math.random() * 2 * Math.PI
    }));
}

// Each particle gets a trace array
let traces = Array.from({length: n}, () => []);

// Reset traces when tumble rate changes
let lastLambda = tumbleSlider.value;
tumbleSlider.addEventListener("input", () => {
    traces = Array.from({length: n}, () => []);
    lastLambda = tumbleSlider.value;
});

function step(state, ) {
    return state.map((p, i) => {
        if (Math.random() < * dt) p.theta = Math.random() * 2 * Math.PI;
```

```

// Predict next position
let nx = p.x + v0 * Math.cos(p.theta) * dt;
let ny = p.y + v0 * Math.sin(p.theta) * dt;

// Bounce at left/right walls
if (nx < 0) {
    p.x = 0;
    p.theta = Math.PI - Math.random() * Math.PI; // random angle pointing right
} else if (nx > W) {
    p.x = W;
    p.theta = Math.PI + Math.random() * Math.PI; // random angle pointing left
} else {
    p.x = nx;
}

// Bounce at top/bottom walls
if (ny < 0) {
    p.y = 0;
    p.theta = (Math.random() * Math.PI); // random angle pointing down
} else if (ny > H) {
    p.y = H;
    p.theta = Math.PI + (Math.random() * Math.PI); // random angle pointing up
} else {
    p.y = ny;
}

// Add current position to trace
traces[i].push([p.x, p.y]);
// Limit trace length for performance
if (traces[i].length > 200) traces[i].shift();
return p;
});
}

const container = html`<div></div>`;
container.append(tumbleSlider, button);
const svg = d3.select(container).append("svg")
    .attr("width", W)
    .attr("height", H)
    .style("background", "#f8f8f8");

while (true) {
    const  = tumbleSlider.value;
    if (running) state = step(state, );
    svg.selectAll("*").remove();

    // Draw traces
    traces.forEach(trace => {
        if (trace.length > 1) {
            svg.append("path")
                .attr("d", d3.line()(trace))
                .attr("stroke", "#90caf9")
    
```

```

        .attr("stroke-width", 1)
        .attr("fill", "none");
    });
}

// Draw particles
svg.selectAll("circle")
    .data(state)
    .enter().append("circle")
    .attr("cx", d => d.x)
    .attr("cy", d => d.y)
    .attr("r", 3)
    .attr("fill", "#1976d2");

svg.selectAll("line")
    .data(state)
    .enter().append("line")
    .attr("x1", d => d.x)
    .attr("y1", d => d.y)
    .attr("x2", d => d.x + 10 * Math.cos(d.theta))
    .attr("y2", d => d.y + 10 * Math.sin(d.theta))
    .attr("stroke", "#1976d2")
    .attr("stroke-width", 1.2);

yield container;
await Promises.delay(16);
}
}

```

The model is designed to encode a **minimal set of ingredients** that make the characteristic trajectories of the bacteria quite different from an ordinary random walk. We can formulate this kind of model via a simple algorithm.

1. **Run Phase:** During a run, the particle moves in a straight line with constant velocity v_0 :

$$\mathbf{r}(t + \Delta t) = \mathbf{r}(t) + v_0 \hat{\mathbf{n}}(t) \Delta t$$

where:

- $\mathbf{r}(t)$ is the position of the particle at time t ,
- v_0 is the constant speed,
- $\hat{\mathbf{n}}(t)$ is the unit vector indicating the direction of motion.

2. **Tumble Phase:** During a tumble, the particle randomly reorients. The new direction $\hat{\mathbf{n}}(t)$ is chosen from a uniform distribution over the unit sphere (in 3D) or circle (in 2D).

We can imagine a schematic algorithm: - Initialize the particle's position $\mathbf{r}(0)$ and direction $\hat{\mathbf{n}}(0)$. - For each time step Δt : - With probability $\lambda \Delta t$, perform a tumble (randomize $\hat{\mathbf{n}}$). - Otherwise, update the position using the run equation. - Repeat for the desired simulation duration.

Here, λ is the tumble rate, which determines the frequency of reorientation events.

The mean squared displacement (MSD) of run-and-tumble particles exhibits a characteristic three-phase behavior:

1. Ballistic regime (short times):

At very short times, before the first tumble occurs, particles move in straight lines at constant speed. The MSD grows quadratically with time:

$$\langle \Delta r^2(t) \rangle \sim v_0^2 t^2$$

2. Diffusive regime (long times):

At times much longer than the average run time ($t \gg 1/\lambda$), the direction of motion has been randomized many times, and the motion becomes diffusive:

$$\langle \Delta r^2(t) \rangle \sim 2D_{\text{eff}} t$$

where $D_{\text{eff}} = \frac{v_0^2}{2\lambda}$ in 2D.

At intermediate timescales, the MSD transitions smoothly from ballistic to diffusive behavior. This crossover is a hallmark of persistent random walks like run-and-tumble dynamics.

```
#| autorun: true
import numpy as np
import matplotlib.pyplot as plt

# Parameters
N = 300           # number of particles
v0 = 1.0          # speed
lambda_tumble = 0.1 # tumble rate
dt = 0.01         # time step
T = 1000          # total time
steps = int(T/dt)

# Arrays to store positions
x = np.zeros((N, steps))
y = np.zeros((N, steps))
theta = np.random.uniform(0, 2*np.pi, N)

# Simulate run-and-tumble
for t in range(1, steps):
    tumble = np.random.rand(N) < lambda_tumble * dt
    theta[tumble] = np.random.uniform(0, 2*np.pi, tumble.sum())
    x[:, t] = x[:, t-1] + v0 * np.cos(theta) * dt
    y[:, t] = y[:, t-1] + v0 * np.sin(theta) * dt

# Compute MSD
msd = np.mean((x - x[:, 0:1])**2 + (y - y[:, 0:1])**2, axis=0)
time = np.arange(steps) * dt

# Plotting
plt.figure(figsize=(9,4))
t_ballistic = 1 / (10 * lambda_tumble)
t_crossover = 1 / lambda_tumble
t_diffusive = 10 / lambda_tumble
# Plot
plt.loglog(time, msd, label="Simulated MSD")
plt.loglog(time, (v0*time)**2, '--', label=r"Ballistic: $v_0^2 t^2$")
plt.loglog(time, 2*(v0**2/(2*lambda_tumble))*time, '--', label=r"Diffusive: $2D_{\text{eff}} t$")
```

```

plt.xlim(1*dt,time.max())
plt.tick_params(axis='both', labelsize=8, pad=15)
plt.tight_layout()

plt.xlabel("Time $t$")
plt.ylabel(r"MSD $\langle \Delta r^2(t) \rangle$")
plt.legend(frameon=False)

plt.show()

```

20.3 Coloured noise

Coloured noise introduces temporal correlations into the random forces acting on a particle, unlike white noise, which is uncorrelated. This is often modeled using an Ornstein-Uhlenbeck process for the noise term.

In the context of active matter, coloured noise can be used to describe the dynamics of active particles, where the noise term $\eta(t)$ evolves as:

$$\frac{d\eta(t)}{dt} = -\frac{\eta(t)}{\tau_c} + \sqrt{\frac{2D_c}{\tau_c}}\xi(t),$$

where:

- τ_c is the correlation time of the noise,
- D_c is the noise strength,
- $\xi(t)$ is a Gaussian white noise term with zero mean and unit variance.

The particle's velocity $\mathbf{v}(t)$ is then given by:

$$\mathbf{v}(t) = v_0 \hat{\mathbf{n}}(t) + \eta(t),$$

where $\hat{\mathbf{n}}(t)$ is the direction of self-propulsion.

The coloured noise description of active matter is a generalisation of the run and tumble dynamics. The run phase corresponds to the persistence of $\hat{\mathbf{n}}(t)$ over time, governed by the correlation time τ_c , whereas the tumble phase is analogous to a rapid decorrelation of $\hat{\mathbf{n}}(t)$, which can be modeled by resetting $\eta(t)$ or introducing a large noise term.

20.4 Active Brownian particle and motility-induced phase separation

Active Brownian particles (ABPs) are a minimal model for self-propelled colloids, such as Janus particles, which move due to chemical reactions at their surfaces. For example, a colloid half-coated with platinum can catalyze the decomposition of hydrogen peroxide in solution, generating local gradients that propel the particle forward.

The ABP model captures the essential physics of these systems. Each particle moves with a constant speed in a direction that undergoes rotational diffusion. This leads to persistent motion at short times and diffusive behavior at long times, similar to the run-and-tumble model but with continuous reorientation.

The dynamics of an ABP can be described by the following equations:

1. **Translational Motion:** The position $\mathbf{r}(t)$ of the particle evolves as:

$$\frac{d\mathbf{r}(t)}{dt} = v_0 \hat{\mathbf{n}}(t) + \sqrt{2D_t} \xi(t),$$

where:

- v_0 is the self-propulsion speed,
- $\hat{\mathbf{n}}(t)$ is the unit vector indicating the particle's orientation,
- D_t is the translational diffusion coefficient,
- $\xi(t)$ is a Gaussian white noise term with zero mean and unit variance.

2. **Rotational Motion:** The orientation $\hat{\mathbf{n}}(t)$ undergoes rotational diffusion, described by:

$$\frac{d\hat{\mathbf{n}}(t)}{dt} = \sqrt{2D_r} \eta(t),$$

where:

- D_r is the rotational diffusion coefficient,
- $\eta(t)$ is a Gaussian white noise term with zero mean and unit variance.

In 2D, the orientation $\hat{\mathbf{n}}(t)$ can be expressed in terms of an angle $\theta(t)$:

$$\hat{\mathbf{n}}(t) = (\cos \theta(t), \sin \theta(t)),$$

and the rotational dynamics reduce to:

$$\frac{d\theta(t)}{dt} = \sqrt{2D_r} \eta_\theta(t),$$

where $\eta_\theta(t)$ is a scalar Gaussian white noise term.

We can analyse this a little more in detail by considering the characteristic features of the displacements of (dilute or noninteracting) active Brownian particles.

20.4.1 Mean squared displacement of Active Brownian Particles

Indeed, it can be shown. (see below) that the mean squared displacement for active Brownian particles displays three regimes:

$$MSD(\tau) = [4D_T + 2v^2\tau_R] \tau + 2v^2\tau_R^2 (e^{-\tau/\tau_R} - 1).$$

where: - $D_{\text{eff}} = \frac{v_0^2}{2D_r}$ is the effective long-time diffusion coefficient,

This clearly shows that there are three main regimes:

- a very short time diffusive regime $MSD(\tau) \propto 4D_T \tau$
- an intermediate regime around the reorientation time τ_R where $MSD(\tau) = 4D_T \tau + 2v^2\tau^2$ leading to **super-diffusive** motion (ballistic)
- a final regime where the reorientation has taken place and where a new diffusive regime is reached where the MSD is proportional to time, i.e. $MSD(\tau) = [4D_T + 2v^2\tau_R] \tau$ but with a new diffusion constant.

Note

We derive the MSD expression for 2d Active Brownian particles.

We first integrate the velocity

$$\mathbf{r}(\tau) - \mathbf{r}(0) = v \int_0^\tau \hat{\mathbf{n}}(s) ds + \sqrt{2D_T} \int_0^\tau \eta(s) ds.$$

Since $\eta(t)$ is independent from $\hat{\mathbf{n}}(t)$,

$$\langle \Delta r^2(\tau) \rangle = v^2 \left\langle \left| \int_0^\tau \hat{\mathbf{n}}(s) ds \right|^2 \right\rangle + 4D_T \tau,$$

using $\langle |\int \eta(s) ds|^2 \rangle = 2dD_T\tau$ with dimension $d = 2$.

We first need to evaluate the orientation correlation integral.

Write the first term as a double integral:

$$\left\langle \left| \int_0^\tau \hat{\mathbf{n}}(s) ds \right|^2 \right\rangle = \int_0^\tau ds \int_0^\tau ds' \langle \hat{\mathbf{n}}(s) \cdot \hat{\mathbf{n}}(s') \rangle.$$

For 2D rotational diffusion, the orientation correlation is exponential:

$$\langle \hat{\mathbf{n}}(s) \cdot \hat{\mathbf{n}}(s') \rangle = e^{-|s-s'|/\tau_R}.$$

We calculate the following double integral

$$I(\tau) = \int_0^\tau ds \int_0^\tau ds' e^{-|s-s'|/\tau_R}.$$

Use symmetry: the integrand depends only on $|s - s'|$. Express as

$$I(\tau) = 2 \int_0^\tau ds \int_0^s ds' e^{-(s-s')/\tau_R} = 2 \int_0^\tau ds \int_0^s du e^{-u/\tau_R},$$

where we set $u = s - s'$.

Integrate over u :

$$\int_0^s e^{-u/\tau_R} du = \tau_R (1 - e^{-s/\tau_R}).$$

So

$$I(\tau) = 2\tau_R \int_0^\tau (1 - e^{-s/\tau_R}) ds = 2\tau_R \left[\tau - \int_0^\tau e^{-s/\tau_R} ds \right].$$

By integrating the exponential we get

$$\int_0^\tau e^{-s/\tau_R} ds = \tau_R (1 - e^{-\tau/\tau_R}).$$

Hence

$$I(\tau) = 2\tau_R [\tau - \tau_R (1 - e^{-\tau/\tau_R})] = 2\tau_R \tau - 2\tau_R^2 (1 - e^{-\tau/\tau_R}).$$

Putting it all together,

$$\langle \Delta r^2(\tau) \rangle = v^2 I(\tau) + 4D_T\tau = v^2 [2\tau_R\tau - 2\tau_R^2(1 - e^{-\tau/\tau_R})] + 4D_T\tau,$$

or equivalently

$$\boxed{\langle \Delta r^2(\tau) \rangle = (4D_T + 2v^2\tau_R)\tau + 2v^2\tau_R^2(e^{-\tau/\tau_R} - 1).}$$

```
#| autorun: true
- $\tau_p = 1/D_r$ is the persistence time.

**Short times ($t \ll \tau_p$):**
The motion is ballistic:
$$
\langle \Delta r^2(t) \rangle \approx v_0^2 t^2
$$

**Long times ($t \gg \tau_p$):**
The motion is diffusive:
$$
\langle \Delta r^2(t) \rangle \approx 4 D_{\text{eff}} t
$$

This crossover from ballistic to diffusive behavior is a hallmark of persistent random walks such as ABPs.

import numpy as np
import matplotlib.pyplot as plt

# Parameters
N = 300          # number of particles
v0 = 1.0         # self-propulsion speed
Dr = 0.1         # rotational diffusion coefficient
Dt = 0.0         # translational diffusion coefficient (set to 0 for pure ABP)
dt = 0.01        # time step
T = 1000         # total time
steps = int(T/dt)

# Arrays to store positions
x = np.zeros((N, steps))
y = np.zeros((N, steps))
theta = np.random.uniform(0, 2*np.pi, N)

# Simulate ABP
for t in range(1, steps):
    # Rotational diffusion
    theta += np.sqrt(2*Dr*dt) * np.random.randn(N)
    # Translational motion
    x[:, t] = x[:, t-1] + v0 * np.cos(theta) * dt + np.sqrt(2*Dt*dt) * np.random.randn(N)
    y[:, t] = y[:, t-1] + v0 * np.sin(theta) * dt + np.sqrt(2*Dt*dt) * np.random.randn(N)

# Compute MSD
msd = np.mean((x - x[:, 0:1])**2 + (y - y[:, 0:1])**2, axis=0)
```

```

time = np.arange(steps) * dt

# Theoretical curves
tau_p = 1 / Dr
D_eff = v0**2 / (2*Dr)
msd_ballistic = (v0*time)**2
msd_diffusive = 4*D_eff*time

plt.figure(figsize=(9,4))
plt.loglog(time, msd, label="Simulated MSD")
plt.loglog(time, msd_ballistic, '--', label=r"Ballistic: $v_0^2 t^2$")
plt.loglog(time, msd_diffusive, '--', label=r"Diffusive: $4D_{\mathrm{eff}} t$")
plt.xlim(1*dt, time.max())
plt.tick_params(axis='both', labelsize=8, pad=15)
plt.tight_layout()
plt.xlabel("Time $t$")
plt.ylabel(r"MSD $\langle \Delta r^2(t) \rangle$")
plt.legend(frameon=False)
plt.show()

```

20.4.2 Interacting ABPs and motility induced phase separation

When the active Brownian particles are actually interacting with each other, they can give rise to an exceptional nonequilibrium phenomenon of self organisation called **motility-induced phase separation** (MIPS).

The idea is to consider purely repulsive particles (i.e hard spheres) obeying the ABP dynamics. This means that, in equilibrium (i.e. in the absence of self-propulsion) no liquid-gas phase separation is possible (see Section 15.3.1).

However, as we reduce the rotational diffusion, the persistent motion becomes more important, the system becomes more out of equilibrium and new physics comes to play.

In particular, the collision between particles are no longer leading to quick decorrelation: on the contrary, head-to-head collisions between the particles mean that there is a finite residence time for a pair of particles to stay in each other neighborhoods. This effect is amplified by multiple collisions, leading to many-body caging effects that promote density heterogeneities in the fluid.

The result is striking: for sufficiently low rotational diffusions, the fluid of active Brownian particles spontaneously phase separates into a dilute and a dense phase, akin to the gas and liquid phase of equilibrium systems. Before reaching this regime, the fluid also displays a critical like phenomenology, with enhanced fluctuations terminating at a critical point.

This has been examined in detail in computer simulations, both in two dimensional systems and in three dimensional systems (where the physics is even richer and presents parallels with the situation of colloid-polymer mixtures due to the very short range nature of the effective interactions between active particles).

Chapter 21

Problems

21.1 Relaxation time in atomic fluids

Spherical colloidal particles of radius 30 nm and density 1.35 g cm^{-3} are suspended in water (temperature 25°C , density 1.0 g cm^{-3} , viscosity $1.0 \times 10^{-3} \text{ Pa s}$). Calculate the average distance from the origin along a given axis travelled by a particle in 1 minute due to Brownian motion and sedimentation, respectively. What are the displacements after 1 hour?

21.2 Equipartition

The equipartition theorem states that in thermal equilibrium each generalised co-ordinate which occurs in the total system energy only as a quadratic term contributes $(1/2)k_B T$ to the mean energy of the system. Use the theorem to estimate the typical time it takes atoms (or small molecules) in an atomic liquid to move distances of the order of their own size, i.e. estimate the relaxation time.

21.3 Gravitational length

- Find the typical length scale ('gravitational length') of the distribution of polystyrene particles (density $\rho_p = 1.05 \times 10^3 \text{ kg m}^{-3}$) of radius 50 nm and $1\mu\text{m}$ respectively, suspended in water (density $\rho_w = 1.00 \times 10^3 \text{ kg m}^{-3}$, viscosity $1.0 \times 10^{-3} \text{ Pa s}$) at room temperature. Hint: The gravitational length is the height at which the concentration falls to $1/e$ of its greatest value.
- If a container of height $H = 4 \text{ cm}$ contains a dilute suspension of these particles at an average concentration of n_a particles per unit volume, what are the actual concentrations (in terms of n_a) at the top and bottom of the sample when sedimentation equilibrium has been reached.
- If the above sample is shaken up to give an initially uniform concentration and then left undisturbed, estimate how long it will take the concentration profile to reach its equilibrium state (A surprisingly long time!)

21.4 Peclet number

A definition of a colloid is a particle small enough that its Brownian motion is not dominated by gravity. Thus if the particle is raised a distance equal to its radius, the increase in its gravitational potential energy must be less than the thermal energy $(3/2)k_B T$. Another measure of the relative importance of the effects of Brownian motion and gravity, is the Peclet number $\text{Pe} = \tau_R/\tau_{\text{sed}}$. Here τ_R is the time taken by a particle to diffuse a distance equal to its radius, and τ_{sed} is the time taken by it to sediment the same distance. When $\text{Pe} \ll 1$, Brownian motion dominates; when $\text{Pe} \gg 1$, gravity dominates. Show that the condition $\text{Pe} < 1$ is more or less equivalent to the definition of a colloid given above.

21.5 Diffusion equation

Prove by direct substitution that $n(x, t) = C(4\pi Dt)^{-1/2} \exp(-x^2/4Dt)$ is indeed a solution to the 1 D diffusion equation $\partial n/\partial t = D\partial^2 n/\partial x^2$. Discuss the meaning of the constant C .

21.6 Mean square displacement

Starting from the diffusion equation, deduce the mean square displacement, $\langle x^2 \rangle = 2Dt$, without using the full solution to the diffusion equation. Note that $n(x, t)$ is the number density, from which the probability density of finding a particle in the region $[x, x + dx]$ during the time interval $[t, t + dt]$, can be obtained by normalising with $\int n(x, t)dx = N$ (the total number of particles). Having this in mind, the mean square displacement is $\langle x^2(t) \rangle = \frac{\int_{-\infty}^{\infty} x^2 n(x, t) dx}{\int_{-\infty}^{\infty} n(x, t) dx} = \frac{1}{N} \int_{-\infty}^{\infty} x^2 n(x, t) dx$. Hint: Multiply both sides of the 1D diffusion equation by x^2 and integrate by parts over x to get an o.d.e for $\langle x^2 \rangle$ with t as the independent variable.

21.7 Relaxation time in colloidal suspensions

Use $\langle r^2 \rangle = 6Dt$ and the Stokes-Einstein relation to show that the time τ_R for a particle to diffuse its own radius R , scales as R^3 . The relaxation time τ_R is a good estimate for the time taken to return to equilibrium after a disturbance. Estimate τ_R for a suspension of spheres of radius $R \approx 1\mu\text{m}$, i.e. at the upper limit of the colloidal size range.

21.8 Colloidal crystals

Colloidal crystals are observed for volume fractions ϕ between 0.545 and 0.74. Show that the upper limit of $\phi = 0.74$ corresponds to the closest packing in a fcc crystal. What is the average distance between the colloidal particles for the lower limit $\phi = 0.545$? Hint: to get the average consider a simple cubic lattice of the same volume fraction

21.9 Lagrange's expression for the radius of gyration

For N equal point masses at positions $\{\underline{R}_j\}$, the radius of gyration is defined by $R_g^2 = \frac{1}{N} \sum_{j=1}^N (\underline{R}_j - \underline{R}_G)^2$ where $\underline{R}_G = \frac{1}{N} \sum_{j=1}^N \underline{R}_j$ is the position of the centre of mass. Show that

$$R_g^2 = \frac{1}{2N^2} \sum_{j=1}^N \sum_{k=1}^N (\underline{R}_j - \underline{R}_k)^2$$

Hint: Note that $\frac{1}{N} \sum_{j=1}^N 1 = 1$

21.10 Mean length

Calculate the mean end-to end length of a freely jointed polymer consisting of 10^5 monomers of length 4.322. How does the end-to-end length change if the valence angle of the chain is fixed at 108° ?

21.11 Real data

Light scattering measurements on dilute solutions of polystyrene, of different molar masses M , at the theta temperature give the following results for the mean square radius of gyration $\langle R_g^2 \rangle$:

$M (10^6 \text{ g mol}^{-1})$	4.04	1.56	1.20	1.06	0.626	0.394
$\langle R_g^2 \rangle$ (nm 2)	3260	1210	928	770	484	305

- (a) Show that these results are consistent with $\langle R_g^2 \rangle^{1/2} = BM^{1/2}$ ($M = NM_M$ where N is the number of monomers in the chain and M_M is the molar mass of one monomer; $M_M = 100 \text{ g mol}^{-1}$) and estimate the value of B .
- (b) Given that the 'size' of a styrene monomer is about $b_0 = 0.23 \text{ nm}$, calculate the factor C which represents the effect of restricted bond angles in $\langle R^2 \rangle = CNb_0^2$. From C , calculate the bond angle θ which would apply if polystyrene can be represented by a freely-rotating chain. [Remember $\langle R_g^2 \rangle = \frac{1}{6} \langle R^2 \rangle$]
- (c) Calculate $\langle R_g^2 \rangle^{1/2}$ for a polystyrene chain of molar mass $1 \times 10^7 \text{ g mol}^{-1}$ at the theta temperature.
- (d) For the chain of (c), estimate the fraction of the volume $(4\pi/3) \langle R_g^2 \rangle^{3/2}$ which is actually occupied by styrene monomers (assume that the density of styrene when polymerised is about 1 g cm^{-3}). What is the overlap concentration c^* (in mass per volume)? How do you expect c^* to change upon an increase (decrease) in temperature?

21.12 Micelles

The volume of a linear hydrocarbon chain with n carbon atoms is given by $v = (27.4 + 26.9n) \times 10^{-3} \text{ nm}^3$, and its critical chain length is $l_c = (0.154 + 0.1265n) \text{ nm}$. An amphiphile has an anionic head group with an optimum head group area in aqueous solution of $a_0 = 0.65 \text{ nm}^2$. (i) What shape micelles are formed by amphiphiles with linear hydrocarbon chains having $n = 10$? (ii) What is the average size and aggregation number of each micelle?

21.13 Viscosity

For polystyrene, the variation of viscosity with temperature follows the Vogel-Fulcher law $B = 710$ and $T_0 = 50^\circ\text{C}$. Plot the function η/η_0 in the temperature range $80 - 150^\circ\text{C}$. By what factor does the viscosity and relaxation time vary between the temperatures of $100 - 140^\circ\text{C}$?

21.14 The glass transition

For polystyrene, a relaxation time associated with configurational rearrangements, τ_{config} , follows a Vogel-Fulcher law,

$$\tau_{\text{config}} = \tau_0 \exp\left(\frac{B}{T - T_0}\right)$$

Where τ_0 , $B = 710$ and $T_0 = 50^\circ\text{C}$ are constants. A value of the experimental glass transition temperature is measured with an experiment carried out at an effective timescale $\tau_{\text{exp}} = 1000$ s and found to be 101.4°C . (a) Another experiment is carried out at an effective timescale of 10^5 s. What is the value of the glass transition temperature obtained from this experiment? (b) On what timescale must an experiment be carried out if it is to measure a glass transition temperature within 10°C of the Vogel-Fulcher temperature T_0 . Is this practically possible?

Part III

Experimental techniques

Appendix A

Revision guide

In addition to having worked through and being familiar with all the questions on the problem sheets, you are expected to:

- Know the relationship between the free energy of a system and its partition function. Be able to differentiate the free energy to obtain thermodynamic observables and fluctuation relations for the heat capacity and magnetic susceptibility.
- Know the forms of the singularities exhibited by key observables on the approach to criticality and be able to define the exponents $\alpha, \beta, \gamma, \delta$ and ν .
- Be able to draw the phase diagrams of magnetic and fluid systems and define the critical exponents. You should know the key differences between first and second order phase transitions.
- Understand the isomorphism between the Ising model and lattice gas.
- **Ising model:** Write down the Hamiltonian of the Ising model and be familiar with its properties in $d = 1, 2, 3$. Derive the Ising model free energy in $d = 1$ both in zero magnetic field (kink method) and in a finite field (Transfer matrix method).
- **Mean field theory:** Show that the effective Hamiltonian

$$H_{\text{eff}} = H + qJm$$

and derive the equation

$$m = \tanh(\beta H_{\text{eff}}).$$

From this, find the behaviour of m and χ near T_c . Know the form of the spin-spin correlation function in mean field theory and use it to calculate the behaviour of the heat capacity near criticality. Describe the shortcomings of mean field theory and explain the underlying reasons.

- **Landau theory:** Given the Landau free energy, sketch and interpret the form of the free energy as a function of magnetisation for a range of temperatures around T_c . Derive the values of the critical exponents $\beta, \delta, \gamma, \alpha$. Understand the genesis of first order phase transitions and metastability within Landau theory and the importance of symmetry considerations.
- **Scaling theory:** Recast a generalised homogeneous function as a power law in one variable. Applying this to the free energy, deduce scaling forms for key observables and relationships between the scaling variables and the critical exponents. Deduce scaling laws relating the critical exponents. Describe experimental tests of scaling and its utility in the context of computer simulations of critical phenomena.

- **Renormalization Group:** Describe the main purpose and features of the RG formalism in the real-space (block variable) approach. Describe the relevance of the RG to scaling phenomena and universality. Know which essential qualitative features of a system delineate universality classes.
- **Classical nucleation theory:** Understand that in first-order phase transitions, like in the Ising model under a small external field, or a slightly oversaturated gas, a free energy barrier must be overcome for the stable phase to nucleate within the metastable phase. Describe in qualitative and mathematical terms how nucleation involves the formation of a critical-sized region of the new phase, which can then grow to complete the transition, with the balance between bulk energy gain and surface energy cost determining the critical size. Describe mathematically how growth dynamics after nucleation depend on factors like interface motion and external driving forces, shaping the overall evolution from the metastable to the stable phase.
- **Stochastic processes:** Understand that many natural processes are stochastic, meaning their evolution over time involves inherent randomness, either from lack of microscopic detail (in classical physics) or intrinsic probabilistic nature (in quantum mechanics). Describe such systems, using coarse-grained probabilistic methods, focusing on the likelihood of different outcomes instead of exact trajectories, ie. the master equation. Derive macroscopic behaviors like diffusion by analyzing the balance of transition rates between states. Understand that the Langevin approach models particle motion using a stochastic differential equation, offering a trajectory-based view complementary to the probability-focused diffusion (Fokker-Planck) equation. Describe mathematically how in the Langevin equation, random forces and friction combine to determine particle displacements over small time intervals, capturing the randomness inherent in Brownian motion. Derive key statistical quantities such as the mean square displacement and the form of the diffusion constant and damping constant. By analyzing the statistics of these random steps, one can derive the diffusion equation as the continuum limit of the random walk.
- **Dynamics of fluctuations:** Understand and describe mathematically how fluctuations of thermodynamic variables, like local magnetization or density, can be analyzed through their time correlations when the system is in thermal equilibrium. Describe the role of the two-time correlation function $M_{xx}(t)$, which measures how a fluctuation at one time is related to a fluctuation at a later time. Describe how in equilibrium, this correlation depends only on the time difference and typically decays exponentially with a characteristic correlation time t_c .

Note that some of the above items were mainly covered in the problem sheets.

Appendix B

Mindmaps - Linking concept and methods

- Atashpendar, Arshia, Tim Ingenbrand, and Tanja Schilling. 2020. "Shape, Geometric Percolation, and Electrical Conductivity of Clusters in Suspensions of Hard Platelets." *Phys. Rev. E* 101 (March): 032706. <https://doi.org/10.1103/PhysRevE.101.032706>.
- Bouchaud, Jean-Philippe, and Giulio Biroli. 2004. "On the Adam-Gibbs-Kirkpatrick-Thirumalai-Wolynes Scenario for the Viscosity Increase in Glasses." *The Journal of Chemical Physics* 121 (15): 7347–54. <https://bris.on.worldcat.org/oclc/110636005>.
- Care, Christopher M. 1987. "Cluster Size Distribution in a Monte Carlo Simulation of the Micellar Phase of an Amphiphile and Solvent Mixture." *Journal of the Chemical Society, Faraday Transactions 1: Physical Chemistry in Condensed Phases* 83 (9): 2905–12. <https://pubs.rsc.org/en/content/articlehtml/1987/f1/f19878302905>.
- Chandler, David, and Juan P Garrahan. 2010. "Dynamics on the Way to Forming Glass: Bubbles in Space-Time." *Annual Review of Physical Chemistry* 61 (1): 191–217. <https://bris.on.worldcat.org/oclc/4761088692>.
- Coslovich, Daniele, Misaki Ozawa, and Walter Kob. 2018. "Dynamic and Thermodynamic Crossover Scenarios in the Kob-Andersen Mixture: Insights from Multi-CPU and Multi-GPU Simulations." *The European Physical Journal E* 41: 1–11. <https://bris.on.worldcat.org/oclc/7634416384>.
- Debenedetti, Pablo G, and Frank H Stillinger. 2001. "Supercooled Liquids and the Glass Transition." *Nature* 410 (6825): 259–67. <https://www.nature.com/articles/35065704>.
- Dijkstra, Marjolein, Joseph M Brader, and Robert Evans. 1999. "Phase Behaviour and Structure of Model Colloid-Polymer Mixtures." *Journal of Physics: Condensed Matter* 11 (50): 10079. <https://bris.on.worldcat.org/oclc/4843512718>.
- Griffiths, Samuel, Francesco Turci, and C Patrick Royall. 2017. "Local Structure of Percolating Gels at Very Low Volume Fractions." *The Journal of Chemical Physics* 146 (1). <https://pubs.aip.org/aip/jcp/article/146/1/014501/313344/Local-structure-of-percolating-gels-at-very-low>.
- Hamaker, Hugo C. 1937. "The London—van Der Waals Attraction Between Spherical Particles." *Physica* 4 (10): 1058–72. <https://www.sciencedirect.com/science/article/pii/S0031891437802037>.
- Hasyim, Muhammad R, and Kranthi K Mandadapu. 2024. "Emergent Facilitation and Glassy Dynamics in Supercooled Liquids." *Proceedings of the National Academy of Sciences* 121 (23): e2322592121. <https://www.pnas.org/doi/abs/10.1073/pnas.2322592121>.
- Jones, Richard AL. 2002. *Soft Condensed Matter*. Vol. 6. Oxford University Press. <https://bris.on.worldcat.org/oclc/48753186>.

- Knapp, Elisabeth, and Dennis J Lewandowski. 2001. "Tobacco Mosaic Virus, Not Just a Single Component Virus Anymore." *Molecular Plant Pathology* 2 (3): 117–23.
- Lekkerkerker, Henk NW, Remco Tuinier, and Mark Vis. 2024. *Colloids and the Depletion Interaction*. Springer Nature. <https://bris.on.worldcat.org/oclc/1428319704>.
- London, Fritz. 1937. "The General Theory of Molecular Forces." *Transactions of the Faraday Society* 33: 8b–26.
- Mori, Hazime. 1965. "Transport, Collective Motion, and Brownian Motion." *Progress of Theoretical Physics* 33 (3): 423–55. <https://bris.on.worldcat.org/oclc/8091001741>.
- Pusey, PN, E Zaccarelli, C Valeriani, E Sanz, Wilson CK Poon, and Michael E Cates. 2009. "Hard Spheres: Crystallization and Glass Formation." *Philosophical Transactions of the Royal Society A: Mathematical, Physical and Engineering Sciences* 367 (1909): 4993–5011. <https://bris.on.worldcat.org/oclc/8582157462>.
- Royall, C Patrick, Patrick Charbonneau, Marjolein Dijkstra, John Russo, Frank Smallenburg, Thomas Speck, and Chantal Valeriani. 2024. "Colloidal Hard Spheres: Triumphs, Challenges, and Mysteries." *Reviews of Modern Physics* 96 (4): 045003. <https://journals.aps.org/rmp/abstract/10.1103/RevModPhys.96.045003>.
- Royall, C Patrick, Francesco Turci, Soichi Tatsumi, John Russo, and Joshua Robinson. 2018. "The Race to the Bottom: Approaching the Ideal Glass?" *Journal of Physics: Condensed Matter* 30 (36): 363001. <https://bris.on.worldcat.org/oclc/1098708850>.
- Sánchez-Ferrer, Antoni, Mathias Reufer, Raffaele Mezzenga, Peter Schurtenberger, and Hervé Dietsch. 2010. "Inorganic–Organic Elastomer Nanocomposites from Integrated Ellipsoidal Silica-Coatedhematite Nanoparticles as Crosslinking Agents." *Nanotechnology* 21 (18): 185603.
- Santos, Andrés. 2016. "A Concise Course on the Theory of Classical Liquids." *Lecture Notes in Physics* 923: 064601–4. <https://bris.on.worldcat.org/oclc/949904359>.
- Sausset, F, G Biroli, and J Kurchan. 2010. "Do Solids Flow?" *Journal of Statistical Physics* 140: 718–27. <https://bris.on.worldcat.org/oclc/5649060652>.
- Turner, Linda, William S Ryu, and Howard C Berg. 2000. "Real-Time Imaging of Fluorescent Flagellar Filaments." *Journal of Bacteriology* 182 (10): 2793–2801.
- Wilding, Nigel B., and Francesco Turci. 2025. "Origin of the Inverse Temperature Dependence of Hydrophobic Attraction." *Phys. Rev. Res.* 7 (June): L022079. <https://doi.org/10.1103/66lz-1yw9>.
- Zaccarelli, Emanuela. 2007. "Colloidal Gels: Equilibrium and Non-Equilibrium Routes." *Journal of Physics: Condensed Matter* 19 (32): 323101. <https://doi.org/10.1088/0953-8984/19/32/323101>.